Title
TURBULENCE MODELING OF SINGLE AND TWO PHASE CURVED CHANNEL FLOWS

Author
Pourahmadi, F.

Publication Date
1982-05-01

Lawrence Berkeley Laboratory
UNIVERSITY OF CALIFORNIA

Materials & Molecular Research Division

TURBULENCE MODELING OF SINGLE AND TWO PHASE CURVED CHANNEL FLOWS

Farzad Pourahmadi
(Ph.D. thesis)

May 1982

Prepared for the U.S. Department of Energy under Contract DE-AC03-76SF00098

DISCLAIMER

LBL-13808

TURBULENCE MODELING OF SINGLE AND TWO PHASE CURVED CHANNEL FLOWS

Farzad Pourahmadi

(Ph.D. thesis)

Department of Mechanical Engineering
Lawrence Berkeley Laboratory
University of California
Berkeley, California 94720

May 1982

This work was supported by the Director, Office of Energy Research, Office of Basic Energy Sciences, Materials Sciences Division of the U.S. Department of Energy under Contract No. DE-AC03-76SF00098.

This report was printed from originals provided by the author.

TABLE OF CONTENTS

Abstract v

Dedications. vii

Acknowledgments. viii

Nomenclature ix

1. Introduction 1

2. Single Particle Motion and Turbulence Interactions 12

2.1 Equation of motion for a single solid particle. 12
2.2 Solutions to the equation of motion 25
2.3 Interaction of a single particle with turbulent flow. . . 31

3. Transport Equations for Turbulent Two-Phase Flows. 34

3.1 Continuum model for a cloud of particles. 35
3.2 Conservation equations for two-phase turbulent flows. . . 41

3.2.1 Mass conservation equations. 42
3.2.2 Momentum balance equations 46
3.2.3 Transport equations for the mean kinetic energy of the phases 54
3.2.4 Transport equation for the fluid turbulent kinetic energy (k) 55
3.2.5 Transport equation for the particulate turbulent kinetic energy (k_p). 57
3.2.6 Transport equation for dissipation rate of fluid turbulent kinetic energy (ε). 63

3.3 Boundary conditions for the fluid phase 71
3.4 Boundary conditions for the particulate phase 82

4. Second-Order Closure for Fluid-Particle Correlation Terms. . . 87

4.1 The correlation $\overline{u_{f_i} u_{p_i}}$ (k equation) 88
4.2 Particle turbulent kinetic energy (k_p). 97
4.3 Fluid-particle velocity correlation coefficient (R_{f-p}). . 99
4.4 Fluid-particle interaction length scale (L_{f-p}). 99
4.5 The correlation $\overline{\partial u_{f_i}/\partial x_j \; \partial u_{p_i}/\partial x_j}$ (ε equation). 100

TABLE OF CONTENTS (continued)

5. Diffusion Processes in Two-Phase Flows 118

5.1 Diffusion by turbulent drag 119
5.2 Brownian diffusion for solid particles. 136
5.3 Diffusion of solid particles by Bernoulli forces. 138

6. Single-Phase Flow Modeling, Erosion Model and Numerical Method 140

6.1 Computation of single-phase curved channel flows. 140
6.2 Erosion wear model and related considerations 142
6.3 Numerical method. 144

6.3.1 Grid system. 144
6.3.2 Derivation of finite-difference equations. 145
6.3.3 Solution of the finite-difference equations. . . . 150

7. Two-Phase Flow Results and Discussion. 154

7.1 Straight channel/pipe flow results. 155
7.2 Curved channel flow and erosion results 164

8. Conclusions and Recommendations. 179

References 183

Figure Captions. 194

Figures 198

Appendix I. Conservation equations for turbulent two-phase flows. 242

Appendix II. Prediction of curved channel flow with an extended k-ε model of turbulence 258

Appendix III. Detailed derivation of general C_μ function in single-phase flow. 304

LBL-13808

TURBULENCE MODELING OF SINGLE AND TWO PHASE CURVED CHANNEL FLOWS

Farzad Pourahmadi

Department of Mechanical Engineering
Lawrence Berkeley Laboratory
University of California
Berkeley, California 94720

ABSTRACT

A theoretical analysis of steady turbulent flow with small solid particulates in suspension has been conducted based on the continuum hypothesis for both phases. The analysis provides the basis for a two-dimensional numerical model capable of predicting dilute two-phase flows. The numerical procedure requires the solution of fully elliptic coupled transport equations for both phases. The turbulence characteristics of the fluid phase are predicted using a two equation (k-ε) model of turbulence and involves the calculation of the fluid turbulent kinetic energy (k) and its rate of dissipation (ε).

Due to their appearance in the modeled equations for k, ε and particulate phase momentum, algebraic relations describing fluid-particle interactions and the particulate phase turbulent kinetic energy (k_p) are derived from the instantaneous Lagrangian equation of motion for the particulates. Modeled forms of the fluid-particle velocity and velocity gradient correlations appearing in the transport equations are shown to conform with expected limiting behavior.

While the particulate phase mean motion is presumed to respond to fluid flow changes via the Stokes viscous drag, in the vicinity of solid walls the solid phase is assumed to behave like a rarefied gas flow; i.e., particles are allowed to "slip" at the wall.

The analysis shows the existence of two mechanisms for the dissipation of fluid turbulent kinetic energy. The first corresponds to direct viscous dissipation by small scales of motion in the single phase. The second, however, is due to the presence of the particulate phase which, through interaction with the fluid, provides a second sink for turbulent kinetic energy. Further, it is found that the presence of particles provides an additional mechanism for transorming mean kinetic energy from both the fluid and the particle phases to their respective turbulent kinetic energy components.

The numerical model has been rigorously tested by reference to single and two-phase flow experimental data in confined flows. In general, predictions of the mean flow and of the turbulence quantities for both phases are in good agreement with the available experimental data. The inclusion of a model for erosive wear has allowed the prediction of erosion on the concave wall in developing curved channel flow. Both the longitudinal position of maximum erosion and the relative amount of wear as a function of Reynolds number for different particle/fluid characteristics are well predicted by the numerical procedure.

To Mojdeh, to my mother, and to my father

in loving appreciation of
all they have done for me.

ACKNOWLEDGMENTS

I wish to express my sincere gratitude to Professor J.A.C. Humphrey for his continued advice, guidance, and encouragement during the course of this investigation. His friendship has indeed been of enormous value to me during my doctoral study in Berkeley.

Special thanks are due to Professor M. Holt for his constant encouragement and support, since the early stages of my research activities.

I also wish to thank Professor W.C. Webster for kindly reviewing this dissertation; Mr. Alan Levy, of Lawrence Berkeley Laboratory, for his continued funding of the research; Valerie Kelly for her excellent skill in word processing and editing the manuscript; Gloria Pelatowski for drawing the figures; and all my friends who have helped me in different ways.

Finally, I am greatly indebted to my family. I would like to thank my father and mother for their immeasurable support, invaluable encouragement, and for giving me the opportunity for higher education; my wife, Mojdeh, who has shared my life, for her gentle patience, constant encouragement, and infinite moral support, and my sister and brother for their kindness. My family have all been a constant source of inspiration to me and therefore have immensely contributed to this achievement in my life.

This work was supported by the Director, Office of Energy Research, Office of Basic Energy Sciences, Materials Sciences Division of the U.S. Department of Energy under Contract No. DE-AC03-76SF00098.

NOMENCLATURE

C_f	friction coefficient
C_T	constant in the expression for fluid Lagrangian integral time scale
C_μ	constant in Prandtl-Kolmogorv relation
D	pipe diameter
d_p	particle diameter
$\dot{E}$	erosion rate
E_{L_f}	fluid Lagrangian energy spectrum
E_{L_p}	particle Lagrangian energy spectrum
g	gravity acceleration
k	fluid phase turbulent kinetic energy
k_p	particulate phase turbulent kinetic energy
k_B	Boltzman constant
L_m	particle momentum equilibration length
L_E	Eulerian integral length scale
L_{f-p}	fluid-particle interaction length scale
L_{p-p}	particle mean free path
ℓ_p	average interparticle distance
M	Mach number
m_p	mass of a single particle
m_f	mass of fluid displaced by a single particle
p_1	wall hardness
P	instantaneous pressure
P	time-averaged pressure
p	fluctuating pressure

q_p	magnitude of particle impingement velocity
R	straight pipe radius
R_i	curved channel inner wall radius of curvature
R_o	curved channel outer wall radius of curvature
R_c	curved channel average radius of curvature
R_{f-p}	fluid-particle correlation coefficient
R_E	fluid Eulerian correlation coefficient
R_{L_f}	fluid Lagrangian auto-correlation
R_{L_p}	particle Lagrangian auto-correlation
Re	flow Reynolds number
Re_p	particle Reynolds number
T	time scale of energy containing eddies
T_L	fluid Lagrangian integral time scale
T'	flow temperature
t	time
U_{f_i}	instantaneous fluid phase velocity in i direction
U_{p_i}	instantaneous particulate phase velocity in i direction
U_{f_i}	time-averaged fluid phase velocity in i direction
U_{p_i}	time-averaged particulate phase velocity in i direction
u_{f_i}	fluctuating fluid phase velocity in i direction
u_{p_i}	fluctuating particulate phase velocity in i direction
U_r	instantaneous slip velocity between the phases
$U_{p_{w_i}}$	particulate wall velocity in i direction
x_i	spatial coordinate in i direction
y	distance from pipe/channel wall

α	instantaneous particulate volume concentration
$\overline{\alpha}$	time-averaged particulate volume concentration
α'	fluctuating particulate volume concentration
β_{imp}	particle angle of impingement on the wall
σ_ϵ	ϵ-Prandtl number
σ_k	k-Prandtl number
Δ	channel width
Δ_{p_w}	deformation rate for the particulate phase at the wall
δ_{ij}	Kronecker delta
ϵ	dissipation rate of fluid turbulent kinetic energy
ϵ_D	Drag dissipation
η	Kolmogorov length scale
κ	Von Karman constant
Λ	Length scale of energy containing eddies
Λ_f	fluid Eulerian integral length scales
Λ_{L_f}	fluid Langrangian integral length scales
λ_E	fluid Eulerian Taylor microscale in isotropic turbulence
λ_f	fluid Taylor microscale in streamwise direction
λ_g	fluid Taylor microscale in lateral direction
μ	fluid dynamic viscosity
ν	fluid kinematic viscosity
ν_{t_f}	fluid eddy viscosity
ν_{t_p}	particulate eddy viscosity
$\nu_{t_f}^{(\alpha)}$	fluid turbulent diffusivity for the transport of the scalar α

$\nu_{t_p}^{(\alpha)}$	particulate turbulent mass diffusivity
ν_{B_p}	particulate diffusion coefficient due to Brownian motion
ρ_f	fluid density in the presence of particulate phase
ρ_p	particulate density in the presence of fluid phase
$\tilde{\rho}_f$	fluid density
$\tilde{\rho}_p$	particle density
τ	Kolmogorov time scale
τ_m	particle response time
ψ	particle response parameter, ratio of particle response time to time scale of the mean motion

subscripts

f	fluid phase
in.	value at the inlet
max	corresponding to the maximum value across the curved channel width
p	particulate phase
∞	free stream condition

CHAPTER 1

INTRODUCTION

The Practical Problem

Processes associated with two-phase turbulent flow have today a very significant influence on human life. Two-phase flows cover a very wide spectrum of applications in many areas, ranging from numerous engineering applications to a variety of processes associated with natural flows. The dispersion of dust and pollutant particulates in the atmosphere, the transport of silt ad fine mineral particles by rivers, the erosion of pipeline components in coal liquefaction/ gasification systems, and also the erosion of gas turbine blades and internal walls of nozzles in solid-propellant rockets are but a few examples of the diversified processes which arise due to the motion of two-phase turbulent flows. Other engineering examples of these types of flows of strong relevance to this work are: fluidized beds, pneumatic conveying, settling tanks, sand blasting, the flow of slurries and fibers and the flows occurring in cyclone separators and electrostatic precipitators.

The flows of particle-laden fluids in coal liquefaction/ gasification pipeline systems, in rocket nozzles and over gas turbine blades cause erosion of the wall materials and can result in serious damage and possible catastrophic failures of these systems, both from the safety and economical points of view. For coal liquefaction/ gasification systems the problem of erosive wear is quite severe at

pipe bends, tee junctions and impinging jet surfaces. The successful design and determination of optimum operation conditions of such systems requires analysis and prediction of the fluid mechanical characteristics of the turbulent flows in the components comprising the systems.

Earlier works and modeling approaches

In the course of reviewing the literature on two-phase fluid-particulate flows, the variety of investigations and the range of complexity of the analyses is amazingly large. Many significant contributions have been cited in the books by Soo [1967] and Boothroyd [1971], and in the review given by Torobin and Gauvin [1959], [1960] and [1961]. The motion of the dispersed particulate phase in the continuous fluid phase has been analyzed by both Lagrangian and Eulerian methods. In the Lagrangian approach, the dynamics of a single particle are analyzed by following the motion of the particle with prescribed set of initial conditions. In the Eulerian approach, the two-phase flow is considered as two interacting continua, with a different set of boundary conditions for each phase. The success of either approach for prediction of the flow variables of interest, depends on the appropriate inclusion and accurate modeling of the various and relatively complex physical processes represented in the governing equations. The occurrence of fluid turbulence, and the associated solid phase turbulence, implying complex interaction and exchange mechanisms between the two phases, can be fairly significant and requires proper modeling.

Continuum-type approaches can be generally divided into two categories. In the first, the two-phase flows are treated as separate, interacting continua, in which, for the particulate phase, a diffusional mode of transport, as well as convection, is conceived. In this respect, the following investigations are noteworthy: Soo [1968], Drew [1976b], Hinze [1962] for laminar flow, and Hinze [1972], Drew [1976a], Nagarajan [1972] and Soo [1962a] for turbulent flow. In another approach, the two-phase flow is treated as a single continuum in which fluid variables are redefined to include the presence of the dispersed particulate phase. The formulation of this approach is given by Wallis [1969] and Hinze [1962] and is common in two-phase, gas/liquid flows with mass exchange between the phases. Wallis [1969] has shown that for such an approach to be valid, the assumption of dynamical and thermal equilibrium between the phases must be made which is approximately valid only for very small particles and low flow velocities.

In the Lagrangian approach, the motion of a single particle is considered and the relevant variables are calculated along the particle trajectory. Early approaches based on Lagrangian equations of motion are due to Glauert [1940], Langmuir and Blodgett [1946] and Brun and Mergler [1953] in relation to the impingement of rain-drops on aircraft surfaces for the analysis of ice formation on aircraft wings. Other more recent investigations using this approach are those due to Laitone [1979a], Yeung [1977] and Abuaf and Gutfinger [1974].

The influence of turbulence

In the presence of turbulence, the problem of measuring and/or predicting two-phase flows becomes even more complicated. A successful prediction of turbulent two-phase flow requires a thorough understanding and proper modeling of the important turbulence-related processes involved. It is clear that a detailed analysis requires the understanding of the fundamentals of fluid and particulate phase turbulence, including fluid-particle interactions which are significant. In this regard the investigation of Baw and Peskin [1971] can be mentioned. In that study, the particle effects on the fluid turbulence energy spectrum were analyzed and the results showed an increased reduction in the spectrum value with an increase in wave-number compared to the pure fluid spectrum. In a related work, Owen [1969] has shown a reduction in fluid turbulence intensity with increase in particle concentration which was not shown by Soo et al. [1960] who noticed no effect due to the presence of particles. An increase in dissipation rate of turbulent kinetic energy with particulate concentration has been reported by Kada and Hanratty [1960], Owen [1969] and Hino]1963]. In the last two investigations, a decrease in eddy diffusivity with particle concentration was observed which is in contrast with the results given by Kada and Hanratty.

A review of the fundamental problems arising in turbulent two-phase flows is given by Peskin [1975]. The particle effects on fluid mean velocity have been investigated by Soo [1964], Peskin [1963] and Peskin and Dwyer [1965] in pipe flow. The results show a flattening of

fluid velocity by solid particles even at small concentrations of the particulate phase. Soo et al. [1960] have shown a decrease in Lagrangian integral scale with an increase in particulate concentration. The investigations for measurement of various two-phase flow properties in channel/pipe flows are listed in Table (7.1) of Chapter 7. Other works for the same configurations are due to Soo [1969], Soo and Regalbuto [1960], Eichorn et al. [1964], Soo et al. [1964], Soo and Tung [1971], McCarthy and Olson [1968] and Reddy and Pei [1969]. Measurements in two-phase turbulent jet flows are due to, Melville and Bray [1977], Goldschmidt and Eskinazi [1966], Popper et al. [1974], Hedman and Smoot [1975] and Yuu et al. [1978].

Despite the lack of detailed fundamental knowledge, required for the formulation and modeling of two-phase turbulent flows, the need to predict flows of industrial interest has stimulated the analysis for obtaining solutions for these flows. Drew [1975] has modeled the problem of turbulent sediment transport over the flat bottom of a stirring tank in which the mixing length hypothesis was used. Nagarajan and Murgatroyd [1971] have presented an analytical model for two-phase turbulent flow in a fully-developed pipe flow. The assumption of a linear variation of the turbulent shear stress in the radial direction, the neglect of all but the dissipation and production terms in the turbulence kinetic energy equation, and the introduction of several empirical and configuration-dependent coefficients make the solution obtained too specific for a general application. In a related work, the effects due to gravity and electrostatic effects were later

included by Nagarajan [1972]. Based on the single-continuum model approach, Kramer and Depew [1972a] developed a calculation model for fully developed two-phase turbulent pipe flows. To obtain a solution, they expressed velocity fields in terms of various empirical coefficients and in addition an assumption of linear mixing length was made. Yuu et al. [1978] developed a solution for two-phase turbulent jet flows. In their calculations, Yuu et al. substituted empirical relations for the fluid mean velocities in the Lagrangian equations for the motion of the particles.

Smith et al. [1980) have presented a two-dimensional model in which the fluid variables have been obtained using a two-equation (k-ε) model of turbulence, without considering particle effects on fluid turbulence. The particle Lagrangian equations are solved for a representative number of particle trajectories. The particle velocity is assumed to be composed of convective and turbulent diffusive components. The first component is obtained from a particle Lagrangian equation of motion and the diffusion velocity is approximated by a gradient-type diffusion of particle mean concentration, the derivation of which is based on empirical information. The treatment of particles in this way has lead to great simplifications in the calculation of particle variables, however, no rigorous justification for this type of approach is presented by the authors. In addition, collision effects between neighboring solid particles were also excluded in the above approach making it valid only for cases of extremely dilute mixtures.

Danon et al. [1977] have presented a turbulence model for two-phase turbulent flows which is based on a set of parabolic conservation equations. In their model the particulate phase mean velocity is not solved directly but is assumed to be equal to the fluid velocity. Furthermore, in order to avoid complex particulate-wall interaction effects, the model was applied to axi-symmetric free jet flows. The fluid Reynolds stresses were modeled using fluid turbulent length scale and fluid turbulent kinetic energy concepts. For the turbulent length scale, an algebraic relation was assumed which remained constant in the lateral directions, and the fluid turbulent kinetic energy was obtained from a parabolic conservation equation in which particulate interaction effects with the fluid were included. However, the closure relation for the fluid-particle correlation term was assumed to be of an exponential form and was not rigorously derived. Finally, for obtaining better agreement with the data for turbulent kinetic energy, the dissipation and production terms were assumed to have a linear variation with particulate concentration. This assumption, however, resulted in the introduction of two new empirical constants which were dependent on particle size and were "tuned" to match the experimental data.

Genchev and Karpuzov [1980] proposed a turbulence model for fluid-particle flows in which the effect of particles in the turbulence transport equations were considered. The assumptions of uniform particulate concentration and equivalence of particle-phase mean velocity to the fluid velocity simplified the problem by making it

possible to discard the governing equations for particulate phase concentration and momentum. These assumptions, of course, have limited the range of applicability of the model with respect to the flow and particulate conditions. In the Genchev and Kapuzov model, the closure for fluid Reynolds stresses is based on an eddy viscosity concept proposed by Harlow and Nakayama [1967] in which the transport equations for fluid turbulent kinetic energy and a turbulent length scale are solved. Despite the inclusion of particle effects in the fluid turbulence transport equations, the fluid-particle correlation terms were assumed to be negligible in comparison with their fluid-fluid counterparts. This simplified the modeling problem even further by avoiding the need to account for the complex fluid-particle correlation terms. As argued by the authors, this assumption is valid if the particle response time becomes much larger than the time scale characteristic of the mean fluid mean motion. However, the last assumption regarding time scales is in conflict with the earlier assumption regarding equal fluid and particulate mean velocities. For the equal velocity condition the particle response time must be much smaller than the mean fluid motion time scale. Thus, the assumption which makes it possible to avoid the complexity of the fluid-particle interaction terms raises a serious inconsistency in the model. Finally, the authors applied their turbulence model to the case of fully-developed pipe flow, with no experimental data provided in order to evaluate the capabilities and limitations of their model.

Summary and Conclusions

As discussed above, the various calculation methods for two-phase turbulent flows, have generally embodied numerous simplifying assumptions in order to obtain a solution for the flow field variables. Furthermore, in the majority of the investigations, the particulate phase effects on the fluid turbulence structure have not been considered. In the few investigations where such effects have been incorporated, further simplifications in the governing turbulence equations were necessary and various empirical coefficients were introduced. The latter are, in general, a function of flow conditions. These calculation schemes can, therefore, yield results which are strictly valid for the flow conditions for which they were formulated and are not readily extended to encompass more general flow conditions and configurations.

The purpose of this work is to analyze two-phase flow turbulence in depth and, as a resuslt, to develop a more generalized turbulence model for the computation of turbulent two-phase flows of engineering interest. The model of interest is based on the two-equation (k-ε) model of turbulence for single-phase flows with universal constants. The governing equations for particulate and fluid phase velocities are taken in their fully-elliptic forms in order not to preclude the possibility of predicting flow recirculation. In the momentum balance equations, the interactive effects of the two phases are considered and, in addition, the particulate phase momentum exchange with the solid walls is included. The inclusion of the latter effect enhances

further the capability of the present model for predicting wall-bounded flows which are of great importance in engineering.

The influence of the particulate phase on the fluid turbulence is included in the present model through terms which arise in a detailed derivation of the transport equations for the turbulent kinetic energy and the rate of turbulent kinetic energy dissipation of the fluid. The analysis of two-phase turbulence based on these equations, as well as the transport equations for the mean kinetic energies, reveals various mechanisms for the exchange of kinetic energy between the mean and turbulent motion of the fluid and the particulate phases. The various fluid-particulate correlation terms in the equations for fluid turbulent kinetic energy and its dissipation rate are rigorously modeled using the governing equation for the particulate-phase fluctuating velocity. Ultimately, the numerical model developed in this investigation will be used to predict various two-phase flow quantities as well as erosive wear by a dilute mixture of solid particulates in a curved two-dimensional channel. The tested and validated calculation procedure can be viewed as a relatively inexpensive and very valuable tool for conducting two-phase flow and erosive wear "experimentation"; not only in curved channels, but in other shapes such as sharp bends, tees, backward- and forward-facing steps, axisymmetric contractions and expansions, and curved solid objects immersed in a free flow, to name a few.

While the computational tool developed in the remainder of this text is more economical than experimentation, it can not be looked upon as a substitute for experiments. The foundations of the model depend on critical experimentation and validation of the model requires appropriate test data, for checking purposes. Notwithstanding, in many systems of engineering interest, especially newly conceived ones, often the data required to characterize the system is not available, and to conduct an experiment is prohibitively expensive or time consuming. In such cases the tool provided here is of most use. While in absolute terms calculations of an unknown two-phase flow may not be verifiable, relative comparisons of parametric effects are still extremely useful for altering and/or optimizing the system characteristic and performance. It is in this spirit that the present study has been motivated.

CHAPTER 2

SINGLE PARTICLE MOTION AND TURBULENCE INTERACTIONS

The following chapter consists of three sections. In Section 2.1 the general equation for the motion of a single particle in viscous flow is presented, and the various contributing terms are discussed. In Section 2.2 existing solutions for the equation of motion for turbulent flow are analyzed. The interaction with turbulence will be discussed in Section 2.3.

2.1 Equation of Motion for a Single Solid Particle

The motion of a single particle suspended in viscous fluid is complicated due to the interaction of various forces which make a mathematical description of the particle motion extremely difficult to obtain. Owing to this complexity, it is common to introduce simplifying assumptions which make mathematical solutions possible, even if only for the special flow cases to which the assumptions apply.

The original derivation of an equation of motion for a single particle suspended in viscous flow is due to Basset [1888], Boussinesq [1903], and Oseen [1927].

The equation was further generalized by Tchen [1947] to include effects due to a possible unsteady state and the surrounding viscous fluid. Tchen's derivation has also been reviewed by Hinze [1975] and Soo [1967].

The general equation of motion for a single particle in turbulent flow as given by Tchen [1947] is:

$$m_p \frac{dU_{p_i}}{dt_p} = 3\pi\mu d_p(U_{f_i} - U_{p_i}) + m_f \frac{dU_{f_i}}{dt} + \frac{1}{2} m_f \left(\frac{dU_{f_i}}{dt} - \frac{dU_{p_i}}{dt_p}\right)$$

(a) (b) (c)

$$+ \frac{3}{2} d_p^2 \sqrt{\pi\tilde{\rho}_f\mu} \int_{-\infty}^{t} \frac{\frac{dU_{f_i}}{dt'} - \frac{dU_{p_i}}{dt'}}{(t-t')^{1/2}} dt' + m_p g \left(1 - \frac{\tilde{\rho}_f}{\tilde{\rho}_p}\right) \frac{\partial x_i}{\partial x_g} + F_{e_i}$$

(d) (e) (f)

(2.1.1)

where;

$$\frac{d}{dt_p} \equiv \frac{\partial}{\partial t} + U_{p_j} \frac{\partial}{\partial x_j}$$

and

$$\frac{d}{dt} \equiv \frac{\partial}{\partial t} + U_{f_j} \frac{\partial}{\partial x_j}$$

and furthermore;

m_p mass of the particle

m_f mass of the fluid occupied by the particle

x_g represents the coordinate in the direction of gravity.

In Eq. (2.1) the following assumptions are made;

1 - The particle is considered to be rigid and spherical. The Reynolds number, based on the particle diameter and slip velocity, is to be small compared to unity.

2 - The turbulence is homogeneous and stationary.

3 - The particle size is small compared to the smallest length scale characteristic of the turbulence, i.e., the Kolmogorov length scale, η.

Equation (2.1) states that the time rate of change of particle momentum is equal to the sum of forces acting on the particle, these forces are described below.

a) Viscous drag force

This force represents the main contribution to particle motion in most viscous fluid-particle flows and is caused by the non-zero velocity difference between the particle and the neighboring fluid (the "slip" velocity). The assumption of a rigid, spherical particle eliminates the need to consider deformation and directionality dependent effects. Non-spherical dependent effects in particle geometry have been discussed by Boothroyd [1971].

The assumptions 1 and 2 above lead to a simplification of the equation of motion, since the linear Stokes viscous drag relation can then be incorporated. The particle Reynolds number is defined as:

$$Re_p \equiv \frac{\Delta U_r d_p}{\nu} \qquad (2.1.2)$$

with

$$\Delta U_r = \left| U_f - U_p \right| \ .$$

For $Re_p < 0.1$, the drag coefficient can be expressed as; Schlichting [1968]:

$$C_D = \frac{24}{Re_p} \ . \qquad (2.1.3)$$

The inclusion of this relation in the equation of motion simplifies it considerably since Eq. (2.1.3) represents a linear drag law in terms of slip velocity.

The assumption 3 above implies a simple shear around the particle and excludes the possibility of complex effects on fluid drag due to various small eddies randomly distributed around the larger particle.

If the Stokes' viscous drag is assumed to be the only driving force in steady uniform fluid flow, from Eq. (2.1.1) one obtains:

$$\frac{dU_{p_i}}{dt} = \frac{U_{f_i} - U_{p_i}}{\tau_m} \qquad (2.1.4)$$

with the solution:

$$\Delta U_{r_i}(t) = \Delta U_{r_i}(0)\ e^{-t/\tau_m} \qquad (2.1.5)$$

where:

$$\Delta U_{r_i} = \left| U_{p_i} - U_{f_i} \right| \ .$$

In Eq. (2.1.2), the parameter τ_m has dimension of time and is defined as;

$$\tau_m = \frac{\tilde{\rho}_p \, d_p^2}{18\mu} \qquad (2.1.6)$$

Throughout the analysis related to particle motion, the parameter τ_m will be extensively considered. It is a measure of particle's inertial response time to variations in neighboring fluid velocity, and is commonly referred to as the "particle momentum equilibration time" or "particle response time." Thus, relatively large values of τ_m are associated with large, dense particles which require longer times for dynamical adjustment to changes in the immediate flow. In contrast, small, less dense particles have short dynamical response times.

Mathematically, from Eq. (2.1.5) τ_m is defined as the time period during which particle relative velocity (ΔU_r) will reduce to e^{-1} of its initial value at $t = 0$. Based on τ_m a "momentum equilibration length" can also be defined as, Marble [1963];

$$L_m \equiv \tau_m U_{f_o} \quad . \qquad (2.1.7)$$

Characteristic of a particle's responsive traveling distance. In Eq. (2.1.7), U_{f_o} represents the characteristic velocity of mean fluid motion.

b) Pressure gradient force

The pressure gradient in the flow exerts a net force on the particle and is approximately related to the fluid velocity as given by Tchen [1947]:

$$\frac{\partial p}{\partial x_i} = \tilde{\rho}_f \frac{dU_{f_i}}{dt} \quad . \tag{2.1.8}$$

However, it has been argued that due to viscous effect, the pressure gradient term should actually be substituted from the Navier-Stokes equations, Corrsin and Lumley [1956]:

$$\frac{\partial p}{\partial x_i} = \tilde{\rho}_f \frac{dU_{f_i}}{dt} - \mu \nabla^2 U_{f_i} \quad , \tag{2.1.9}$$

with the implication of no particle effects on fluid motion. However, for particle sizes smaller then the Kolmogorov length scale associated with the neighboring fluid element, a relatively uniform fluid velocity around the particle can be assumed to exist with negligible viscous effects, as argued by Hinze [1975].

The motion of fluid around relatively small particle has been approximated as steady potential flow with linear variation as in Soo [1975]. Further substitution of this linear form in the viscous drag term (a) of Eq. (2.1.1) results in an additional term which cancels the pressure gradient term (b) when the Reynolds number based on free stream velocity is unity. In a related analysis the same linear velocity function is used to obtain the same result for any value of the Reynolds number, Soo [1976].

The latter analysis is based on the inclusion of the force balancing the rate of change in fluid momentum around the particle.

For the case of invisid flow around the particle as can be shown from Eq. (2.1.8), the ratio of the pressure gradient force to particle inertia force becomes proportional to the fluid to particle density ratio if the particle and its neighboring fluid element possess nearly equal accelerations. Therefore, under such a condition in gas-solid flows, the effect of the pressure gradient term becomes negligible compared to the inertia. However, the assumption of equal accelerations is, apparently, not valid in the regions of excess gas acceleration like shock waves.

c) The "apparent mass" force

The apparent, or virtual, mass term represents a resisting force on the accelerating particle due to a non-zero relative acceleration between the particle and its neighboring fluid elements. As shown by Milne-Thomson [1968] it is equal to;

$$F_i = C_A m_f \left(\frac{dU_{f_i}}{dt} - \frac{dU_{p_i}}{dt_p} \right) \qquad (2.1.10)$$

with $C_A = 0.5$ for spherical particles. However for values of Re_p beyond the valid range of Stokes drag law, C_A becomes an empirical constants as indicated by Odar [1966]. The apparent mass force is usually broken up into it's particle and fluid acceleration terms as defined by Eq. (2.1.10). The particle acceleration contribution to this term can be combined with the

inertia term on the LHS of Eq. (2.1.1). The fluid acceleration contribution can be incorporated into the pressure gradient term. Therefore, the particle response time with apparent mass effects included can be re-written as:

$$\tau_{m_1} = (\tilde{\rho}_p + 0.5\ \tilde{\rho}_f)\ \frac{d_p^2}{18\mu}$$

d) Basset force

The unsteady viscous effect associated with fluid-particle interaction results in the Basset force. In general, this force represents the deviation of the total viscous drag from the steady component and is, therefore, associated with the changes in flow pattern around the particle during the unsteady motion. The term shows a dependency on the history of particle-fluid relative accelerations. For a spherical particle the force is expressed as, Basset [1888]:

$$F_i = C_H \frac{d_p^2}{4} (\pi \tilde{\rho}_f \mu)^{1/2} \int_{t_o}^{t} \frac{\frac{dU_{f_i}}{dt} - \frac{dU_{p_i}}{dt_p}}{(t-t')^{1/2}}\ dt' \qquad (2.1.11)$$

where t_o is the initial time of particle motion. Also for C_H, Bassett theoretically obtained:

$$C_H = 6$$

However, for $Re_p > 0.1$, C_H becomes an empirical constant.

The influence of unsteady flow patterns around a particle, when falling in a quiescent fluid, have been investigated by Hughes and Gilliland [1952]. The analysis shows small deviations from Stokes drag law when the ratio $\tilde{\rho}_p/\tilde{\rho}_f$ becomes large, i.e., $O(10^3)$, while rather large deviations are observed when the ratio becomes small, i.e., $o(10^{-4})$.

The investigation of Hjemfelt and Mockros [1966] shows the significance of pressure gradient, apparent mass and Basset force on the amplitude ratio and phase shift angle of the fluid-particle oscillatory motion. Their analysis is based on a linearized equation of motion obtained by Tchen [1947] which will be discussed in Section 2.2. In general, the analysis shows no significant contributions by these forces at high Stokes number corresponding to the low frequency region of the fluid oscillatory motion.

The Stokes number is defined as:

$$N_s \equiv \sqrt{\frac{\nu}{\omega d_p^2}} \tag{2.1.12}$$

with ω, representing the frequency of the fluid motion past the particle, proportional to the ratio of the velocity scale to the length scale of the turbulence in the vicinity of the particle.

For the case of $\tilde{\rho}_p/\tilde{\rho}_f = O(1)$, typical of liquid-solid flows, contributions by the pressure gradient term to the fluid-particle amplitude ratio and phase shift angle become important for values of $N_s \lesssim 0.40$ and $N_s \lesssim 0.82$, respectively.

For the case when $\tilde{\rho}_p/\tilde{\rho}_f = 0(10^3)$, typical of gas-solid flows, the analysis shows less significant overall contributions by all three pressure gradient, apparent mass and Basset forces. This is especially the case for changes induced in the amplitude ratio. However, from among the three forces, the Basset force shows the largest influence on the amplitude ratio. For values of the phase shift angle the effect of the pressure gradient force becomes significant when,

$$\omega \gtrsim \frac{\nu}{d_p^2} \quad .$$

The maximum error induced by dropping the Basset term from the force balance on a spherical particle is approximately 16% for:

$$\omega \approx .25 \frac{\nu}{d_p^2}$$

The analysis of Hinze [1975] for gas-solid systems, also shows a non-significant contribution by the Basset force for:

$$\omega \approx \frac{\nu}{d_p^2} \quad .$$

e) Buoyancy force

Buoyancy force is caused by the fluid-particle density difference and affects particle momentum in the direction of gravity.

f) External forces

The term F_{e_i} in Eq. (2.1.1) represent the forces caused by anything other than fluid like electrostatic force.

Lift forces:

Under certain flow conditions, solid particles experience lateral lift forces which move them away from wall regions in, for instance, straight channel or pipe flows. In general, such lift forces are generated by the combination of particle rotation and fluid shear. The particle rotation in a fluid-particle flow can be attributed to various effects among which are the fluid shear, particle-particle collision and particle-wall collision.

For a spherical particle with an angular velocity $\vec{\Omega}_p$ in potential flow the lift force is, Rubinow and Keller [1961]:

$$\vec{F}_{L_1} = \frac{\pi d_p^3}{8} \tilde{\rho}_f (\vec{U}_r \times \vec{\Omega}_p) \qquad (2.1.13)$$

with;

$$\vec{U}_r = \vec{U}_f - \vec{U}_p$$

as the relative velocity vector.

The lift force so defined in usually referred to as the "Magnus" lift and requires a knowledge of the particle angular velocity in order to be determined. Evaluation of $\vec{\Omega}_p$ in a flow is not simple. However, for small, short response time particles in shear flow, $\vec{\Omega}_p$ can be approximated by assuming it is equal to the neighboring fluid rotation. Thus:

$$\left|\vec{\Omega}_p\right|_k \simeq \frac{\partial U_{f_i}}{\partial x_j} \varepsilon_{ijk} \qquad (2.1.14)$$

where ε_{ijk} is the third-order alternating tensor.

As an example, in the case of simple shear flows with all velocity gradients equal to zero except that along a normal to the wall:

$$\left|\Omega_p\right|_2 \simeq \frac{1}{2} \frac{dU_{fx_1}}{dx_2} , \qquad (2.1.15)$$

and from Eq. (2.1.13) for this case the lift force is:

$$F_{L_1} = \frac{\pi d_p^3}{16} U_{rx_1} \frac{dU_{fx_1}}{dx_2} . \qquad (2.1.16)$$

Equation (2.1.16) shows the same functional dependency on fluid variables as presented by Owen [1969].

The lift force given by Eq. (2.1.13) is applicable to the case of inviscid flow only and does not include viscous effects. Therefore, it is not to be used in low particle Reynolds number viscous dominated flows. However, the adoption of such a lift force as an approximation in a viscous flow shows that the effects on the particle motion are, at least, one order of magnitude smaller than those due to the viscous drag when the particle motion in the small-scale, dissipative eddies is considered, Hinze [1972]. Evaluation of the lift force with the viscous effects considered for a spherical particle requires a solution of the Navier-Stokes equations in the vicinity of the particle. It has been shown that by neglecting non-linear inertia terms at low Reynolds numbers the resulting linear momentum equation is not capable of

producing a net lift force on the particle in the direction of the normal to the relative velocity as shown by Cox and Mason [1971] and Lumley [1957]. This result is in contradiction with the experimental observation of Segre and Silberberg [1962] who have observed the migration of neutrally buoyant particles away from the wall to an equilibrium dimensionless radial position equal to 0.6 in Poiseuille flow. The transverse force associated the particle migration is therefore attributed to fluid inertial effects with the conclusion that such effects are not to be neglected, but should be incorporated in the derivation of the lift force.

Using perturbation methods, Saffman [1965] has derived the viscous affected lift force. The result is applicable in uniform shear low Reynolds number flows with the first term of the series obtained as:

$$F_{L_2} = 81.2\ \mu\ U_r\ \frac{d_p^2}{4}\left(\frac{1}{\nu}\ \frac{dU_{fx_1}}{dx_2}\right)^{1/2} \qquad (2.1.17)$$

which is usually referred to as the Saffman lift force. The assumptions are that:

$$\frac{U_r d_p}{2\gamma}\ ,\ \frac{d_p^2}{4\nu}\ \frac{dU_{fx_1}}{dx_2}\ ,\ \frac{\Omega d_p^2}{4\nu} \ll 1 \qquad (2.1.18)$$

and also:

$$\frac{dU_{fx_1}}{dx_2} \gg \frac{2U_r}{d_p} \qquad (2.1.19)$$

where Ω represents the particle's angular velocity.

The ratio of Saffman lift force to the Stokes drag is;

$$\frac{F_{L_2}}{F_D} = 4.3\left[\frac{d_p^2}{4\nu}\left(\frac{dU_{f_1}}{dx_2}\right)\right]^{1/2} \qquad (2.1.20)$$

The expression in the brackets is much smaller than unity according to the second assumption in Eq. (2.1.18). For the ratio in Eq. (2.1.20) to be small, the particle size should satisfy the condition:

$$d_p \ll 0.5\left(\frac{1}{\nu}\frac{dU_{f_1}}{dx_2}\right)^{-1/2} \qquad (2.1.21)$$

Therefore, for the lift force to be neglected with respect to the Stokes drag, the particle size should be small compared to a characteristic dimension of the near-wall flow region where velocity gradients, due to viscous effects, are steep.

2.2 Solutions to the Equation of Motion

Equation (2.1.1) describing the motion of a particle in turbulent flow is complex in its full differential form, and an exact solution is difficult to obtain. The greatest difficulty is due to the complicated nature of fluid-particle interactions which appear through the inclusion of various fluid-induced accelerating and decelerating forces. Equation (2.1.1) in its general form is a non-linear integro-differential equation for the motion of a single particle in Lagrangian coordinates. The non-linearity is due to the condition that the particle does not generally remain in the vicinity of its initial

neighboring fluid element. As a consequence, the i^{th} component of the fluid velocity encountered by the particle at time (t) will be:

$$U_{f_i} \left[\vec{x}_p(\vec{\xi}_p,t) \; ; \; t\right] \quad ,$$

instead of the velocity:

$$U_{f_i} \left[\vec{x}_f(\vec{\xi}_f,t) \; ; \; t\right] \quad ,$$

with $\vec{\xi}_p$ and $\vec{\xi}_f$ representing initial vectorial positions of the particle and fluid element which are coincident at t = 0.

The fluid velocity encountered by the particle depends on the position at time t. By further manipulations, Eq. (2.1.1) becomes a second order differential equation in terms of the particle position with the solution depending on the particle initial position, the particle response time and also on a complete description of the turbulent flow field. Such a description, if available, is statistical and will result in a statistical description of particle motion. However, the non-linearity as defined above, requires a description of turbulent flow field along the <u>particle trajectory</u>. In other words, since the particle does not follow the same fluid element in general, the probability of the particle being in a specified location at a certain time is also required.

This non-linearity does not exist in, for instance, Brownian motion, where the particle motion driving mechanism is provided by the random collision with other particles independently of particle position as shown by Peskin [1959].

The first solution for the Basset-Boussinesq-Oseen equation of single particle motion is due to Tchen [1947]. In addition to the assumptions following Eq. (2.1.1), Tchen assumed that the particle remained in the neighborhood of its original fluid element. The latter assumption produces identical values for the diffusion coefficients of the particle and its neighboring fluid element. It has been argued that, Hinze [1975], for the particle to remain in the vicinity of the same fluid element, the particle displacement relative to the initial neighboring fluid must remain smaller than the local characteristic fluid length scale, during a time period shorter than the local time scale.

For a conservative estimate, such local length and time scales can be taken as the Kolmogorov length and time scales, η and τ. This implies that:

$$\left| \frac{U_{f_i} - U_{p_i}}{U_{f_i}} \right| \ll 1 \qquad (2.2.1)$$

and the assumption of the fluid and particle following the same trajectory results in:

$$\frac{d}{dt_p} \equiv \frac{d}{dt} \qquad (2.2.2)$$

which removes the non-linearity in Eq. (2.1.1) and simplifies the problem of finding a solution.

The requirement for linearization is that, Soo [1967];

$$\frac{d_p^2}{4\nu} \frac{\partial U_{f_i}}{\partial x_i} \ll 1 \qquad (2.2.3)$$

The condition expressed by Eq. (2.2.3) can be obtained by comparing linear and non-linear terms in Eq. (2.1.1) after some algebraic rearrangement.

Furthermore, removal of the viscous second-order term in Eq. (2.1.1) introduced by the pressure gradient term requires that, Soo [1967]:

$$U_{p_k} \frac{\partial U_{f_i}}{\partial x_k} \gg \nu \frac{\partial^2 U_{f_i}}{\partial x_j \partial x_j} \qquad (2.2.4)$$

which means that if the time scale for particle inertial effects is substantially smaller than that characterizing viscous flow effects, the particle "sees" an essentially inviscid fluid element in its vicinity. The conditions Eq. (2.2.3) and Eq. (2.2.4) have been shown by Levich and Kuchanov [1967] to be equivalent to the respective conditions:

$$\frac{d_p^2}{4\nu} \ll 1 \qquad (2.2.5)$$

$$Re_L^{1/4} \gg 1 \qquad (2.2.6)$$

The solution of Tchen [1947] for Eq. (2.1.1) includes all the assumptions mentioned above regarding linearization and also the removal of the fluid viscous terms. In that analysis a stationary solution was obtained with the initial time set to $(-\infty)$. Tchen's solution is significant in that it has subsequently been followed by many investigations. Hinze [1975] obtained a solution by taking Fourier integrals of fluid and particle velocities and substituting in the linear equation of motion. The results are similar to those obtained by Tchen for the particle diffusivity. A similar approach has been followed by Hjelmfelt and Mockros [1966]. Finally, a solution has been obtained by Chao [1964] which is based on the Fourier transport, linearized form of the equation of motion with the same results.

In order to facilitate further the analysis of the dynamics of a particle in turbulent flow it is appropriate to focus on a more simplified equation of motion. In the absence of significant external forces, it can be assumed that the drag force gives the major contribution to the particle motion and on this basis produce a rigorous analysis for solid particle motion. Therefore, following this argument one would obtain from Eq. (2.1.1):

$$\frac{dU_{p_i}}{dt} + \frac{U_{p_i}}{\tau_m} = A_i(t) \qquad (2.2.7)$$

where:

$$A_i(t) = \frac{U_{f_i}[\vec{x}_p(\vec{\xi}_p,t);t]}{\tau_m} \qquad (2.2.8)$$

in turbulent flow. For the cases where diffusion mechanisms other than turbulence are present, the term $A_i(t)$ in Eq. (2.2.7) should be substituted appropriately. This has been discussed by Peskin [1959] in case of Brownian diffusion and diffusion under Bernouli forces. By integration of Eq. (2.2.7) with Eq. (2.2.8) substituted one obtains, Lumley [1957]:

$$x_{p_i}(\vec{\xi}_p,t) = \int_0^t g(t-\eta)\, U_{f_i}[\vec{x}_p(\vec{\xi}_p,\eta);\eta]\, d\eta + x_{p_{io}} \qquad (2.2.9)$$

In general, the solution to Eq. (2.2.7) is, Peskin [1959]:

$$x_{p_i}(\vec{\xi}_p,t) = \frac{1}{\tau_m} \int_0^t g(t-\eta)\, A_i[x_{p_j}(\vec{\xi},\eta),\eta]\, d\eta + x_{p_{io}} \qquad (2.2.10)$$

where:

$$g(t-\eta) = 1 - e^{-(t-\eta)/\tau_m} \qquad (2.2.11)$$

represents the response function which becomes identical to unity in the case of particles with $\tau_m = 0$. This implies that the turbulent dispersion of fluid elements is a special case of the dispersion of solid particles for the case of $\tau_m = 0$.

Furthermore, using Eq. (2.2.9) for the derivation of the particle mean square displacement, it has been shown by Peskin [1959] that G. I. Taylor's theory of "diffusion by continuous movements," Taylor [1921], is a special case of solid particle diffusion when $\tau_m = 0$ and the solid particle becomes indistinguishable from its neighboring fluid elements.

2.3 Interaction of a Single Particle with Turbulent Flow

For further analysis of the dynamics of a single particle suspended in turbulent flow, a comparison between the particle response time and the characteristic time of turbulent eddies surrounding the particle should be made. For a particle much larger than neighboring eddies, the particle dynamics are affected through modifications to viscous resistance drag rather than by the direct action of inertial forces on the eddies themselves. For a particle to be responsive to the smallest eddies, its response time (τ_m) should be comparable to that of the Kolmogorov time scale, $\tau = (\nu/\varepsilon)^{1/2}$, which is a characteristic time scale in the high wave number part of the turbulence spectrum.

Hence, for a responsiveness of the particles to eddies in this part of the spectrum, the ratio:

$$\frac{\tau_m}{\tau} \simeq 0.06\left(\frac{\tilde{\rho}_p}{\tilde{\rho}_f} + 0.05\right)\left(\frac{d_p}{\eta}\right)^2 \qquad (2.3.1)$$

should be small compared to unity.

In Eq. (2.3.1), η is Kolmogroff's length scale and τ_m also includes the effects due to apparent mass. Therefore, for the particle to be responsive to the viscous dominated, small eddies in liquid-solid systems, where $\tilde{\rho}_p/\tilde{\rho}_f = O(1)$, the particle size should be of the order, or smaller than the eddy size. However, in gas-solid flows, with $\tilde{\rho}_p/\tilde{\rho}_f = O(10^3)$, the particle should be at least one order of magnitude smaller than the eddies.

In high Reynolds number flows, turbulent eddies are characterized by their turbulent kinetic energy, k, and dissipation rate of kinetic energy, ε, the typical time and length scales are, respectively:

$$L = A_1 \frac{k^{3/2}}{\varepsilon}$$

and;

$$T = A_2 \frac{k}{\varepsilon}$$

in which A_1 and A_2 are constants.

Hence, for a particle with response time (τ_m) to respond to the eddies in this range:

$$\frac{\tau_m}{T} = \frac{0.06\ A_1^2}{A_2} \left(\frac{\tilde{\rho}_p}{\tilde{\rho}_f} + 0.05 \right) \left(\frac{d_p}{L} \right)^2 \left[\frac{(k^{1/2})\ (k^{3/2}/\varepsilon)}{\nu} \right] \qquad (2.3.2)$$

should be small compared to unity.

In Eq. (2.3.2), the last bracket contains the local Reynolds number which is large. The particle to eddy size ratio should compensate the high Reynolds number effect to give a small value for the time ratio. As above, a higher density ratio requires a smaller particle size.

In the case of energy containing eddies characterized by the velocity scale $\tilde{u}_f$ and length scale Λ, the time scale of the eddies are;

$$T = \frac{\Lambda}{\tilde{u}_f} \ ,$$

therefore the ratio of the time scales is:

$$\frac{\tau_m}{T} = 0.06\left(\frac{\tilde{\rho}_p}{\tilde{\rho}_f} + 0.05\right)\frac{d_p^2}{\Lambda^2}\frac{\tilde{u}_f\Lambda}{\nu} \qquad (2.3.3)$$

which should be smaller than unity. Hence, it requires that, Hinze [1972]:

$$\frac{d_p}{\Lambda} < 0.2\left[\frac{\tilde{u}_f\Lambda}{\nu}\left(\frac{\tilde{\rho}_p}{\tilde{\rho}_f} + 0.5\right)\right]^{-1/2} \qquad (2.3.4)$$

for the particle to respond to the large energy-containing eddies. However, from Tennekes and Lumley [1972]:

$$\frac{\lambda_\varepsilon}{\Lambda} \simeq B_1\, Re_\lambda^{-1} \qquad (2.3.5)$$

with $B_1 = O(10)$.

Thus Eq. (2.3.4) becomes

$$\frac{d_p}{\lambda_\varepsilon} < 0.6\left(\frac{\tilde{\rho}_p}{\tilde{\rho}_f} + 0.5\right)^{-1/2}$$

requiring particle sizes two orders of magnitude smaller for the cases of gas-solid flows, when compared to liquid-solid flows for equivalent flow conditions.

CHAPTER 3

TRANSPORT EQUATIONS FOR TURBULENT TWO-PHASE FLOWS

In the previous chapter the dynamics of a single particle suspended in turbulent flow were discussed. Furthermore, the particle equation of motion in a Lagrangian frame of reference was considered and the various forces affecting particle motion, due to particle-fluid interactions were evaluated and discussed.

Analysis based on the equation of motion for a specific particle, yields predictions which are related to a specific particle with defined initial conditions. Results so obtained, such as particle velocity and trajectory are basically restricted to the motion of a single wandering particle. Although valuable from a fundamental point of view, such results are of little interest in engineering applications. Instead, particulate properties associated with an ensemble or collection of particles, such as the particulate concentration density or the velocity at a specified point in the flow field, are of relatively greater practical importance.

Analysis of the flow based on the governing equations formulated in Eulerian coordinates is generally capable of providing such information for a particle-laden flow. Such an approach does also allow, at least in principle, for the particle-particle collision effects. These can be formally incorporated in the momentum-balance equations by the inclusion of a particulate viscosity accounting for the momentum exchange between particle caused by inter-particle collision. In the analysis for single particle motion based on

Lagrangian equations, particle-particle collision effects can be included by incorporating a spatially and temporally function describing a distributed collision force. Consequently, in the majority of single particle investigations it is customary to neglect the collision effects between particles and to adopt the assumption of forces produced by fluid interactions. Although such an assumption may be justified for dilute particulate flows, it is unacceptable for concentrated flows.

On the basis of the preceeding argument, a development of the governing equations in Eulerian coordinates is desired, which will remain invariant with respect to changes in particulate concentration. As will be seen, however, expressions in Lagrangian coordinates will be required to derive a closure for the Eulerian transport equations.

In the following sections, conservation equations for the mass, mean momentum and mean kinetic energy of the fluid and particulate phases are developed. Transport equations for fluid turbulent kinetic energy and dissipation of kinetic energy are also derived. By incorporation of appropriate boundary conditions and the closure relations in the transport equations, numerical solutions for the equations presented are subsequently obtained.

3.1 Continuum Model for a Cloud of Particles

A derivation of the governing equations for a particulate phase in terms of Eulerian coordinates, requires a continuum model approach for the cloud of particles. The continuum assumption allows for a replacement of the fluid-particle heterogeneous mixture by the two interacting

phases governed by their respective conservation lows. Therefore, a fixed "point" in the flow field is here defined as an infinitesimal volume element consisting of many small solid particles coexisting with the fluid phase, and for which a statistical averaging of the various properties of the particulate phase is feasible and meaningful. The infinitesimal element thus defined should be small compared to the smallest dynamical scale in the flow fluid, Kraiko and Sternin [1965], yet large enough to contain a sufficient number of particles to make meaningful the local definitions of macroscopic properties, such as velocity and density, obtained through statistical averaging.

It has been shown that under conditions of negligible particle interactions, the RMS fluctuations in the density of a particulate volume element decrease with an increase in the element size, Lumley [1976]. However, as the element size becomes of the order of the macroscopic flow scales, it can experience spatial variations in mean density.

The condition for smallness of the particle characteristic length scale when compared to the smallest length scale in the flow requires that:

$$\ell_p \ll \eta \tag{3.1.1}$$

In Eq. (3.1.1), ℓ_p represents the average interparticle distance and η is the Kolmogorov length scale in turbulent flow. For a large number of uniformly distributed and equally spaced solid spherical particles with $\ell_p/d_p > 10$ a simple analysis yields;

$$\ell_p \simeq d_p \sqrt[3]{\frac{\pi}{6\alpha}} \tag{3.1.2}$$

where α is the particulate volume fraction.

Comparing Eqs. (3.1.2) with (3.1.1) yields:

$$\alpha \gg \left(\frac{d_p}{\eta}\right)^3 \frac{\pi}{6} \tag{3.1.3}$$

Thus, the continuum requirement renders a condition for the particulate volume fraction in the flow. Alternatively, from Eq. (3.1.3);

$$\frac{d_p}{\eta} \ll \left(\frac{6\alpha}{\pi}\right)^{1/3} \tag{3.1.4}$$

which is a condition for the ratio of particle size to Kolmogorov length scale for a given particulate volume fraction. The same analysis which led to the Eq. (3.1.1) yields:

$$\alpha_{max} = \frac{\pi}{6} \tag{3.1.5}$$

which indicates that the right side of Eq. (3.1.4) is always smaller than, or at most equal to, unity. Hence:

$$\frac{d_p}{\eta} \ll 1 \tag{3.1.6}$$

In the case of Brownian motion for the particles, the associated mean free path of the particles becomes the appropriate length scale. In analogy with molecular random motion and from kinetic theory of gases, Vincenti and Kruger [1965], one can define the particle mean free path as:

$$L_{p-p} \equiv \frac{d_p}{6\sqrt{2}\alpha} \tag{3.1.7}$$

In analogy with gas molecules, the random Brownian-type motion of particles is assumed to be generated by collisions of rigid spherical particles. The analogy is more justified for very fine, sub-micron particle sizes for which the collisions with carrier gas molecules can also be significant, Yeung [1978]. For larger particle sizes, the Brownian-type motion is more likely to happen in concentrated particle-fluid suspensions with relatively small mean free path and high collision frequency per particle. In a dilute mixture, viscous drag effects of the carrier fluid tend to deccelerate the particle after, and prior to, a collision.

It is reasonable to assume that in the cases of dilute suspensions, particles are more strongly affected by the fluid, although collision effects with other particles may still be considered. Therefore, it can be concluded that in contrast with collision-dominated particulate elements for which the local equilibrium is established by inter-collision of particles, in the viscous-dominated cases the equilibrium condition is reached by interactions with the carrier fluid in which the particles are contained.

The random movement of the particles with different velocities and in different directions in a particulate volumetric element leads to the definition of a distribution function $f_p(x_{p_i}, u_{p_i}, t)$ for the averaged local variables.

For uniformly sized particles and steady mean flows, the value;

$$f_p(x_i, v_{p_i})\ dx_1\ dx_2\ dx_3\ dv_{p_1}\ dv_{p_2}\ dv_{p_3} \qquad (3.1.8)$$

represents the number of particle with velocities between v_{p_i} and $v_{p_i} + dv_{p_i}$ at the position bounded by x_i and $x_i + d_{x_i}$. Local averaged variables can be obtained by integration over all particles within a volume element with f_p as the weighting fuction. The derivation of a probability distribution function f_p for "gas-like particles" requires solution to a Boltzmann type equation with particle characteristics incorporated. This requires a careful evaluation of the forces exerted on the particulate phase. In the investigation of Culick [1964] several simplifying assumptions have been made and an appropriate solution was obtained. In that analysis was included the collision between two class sizes of particles with non-zero relative velocity due to differences in their respectively induced motion by fluid viscous. In Culick's analysis, the inclusion of various simplifying assumptions, however, restricts the range of applicability of the result obtained. In the investigation by Marble [1963], the conservation equations for the particulate phase have been obtained using the Boltzmann equation without derivation of f_i function.

The situation of viscous-established particulate equilibrium with weak particle-particle collision effects is more likely to arise in dilute suspensions as opposed to concentrated flows. In dilute cases, the length scale characterizing fluid-particle interaction effects should be small compared to the characteristic length scale for

particle-particle collision. The fluid-particle length scale for turbulent suspensions is defined by Soo [1969] as;

$$L_{f-p} \equiv \tau_m \, \Delta\tilde{u} \tag{3.1.9}$$

where,

$$\Delta\tilde{u} = \overline{(u_f - u_p)^2}^{1/2} \tag{3.1.10}$$

with u_f and u_p as direction-averaged fluctuating velocities for the fluid and particulate phases, respectively.

Thus, for a viscous-dominated suspension:

$$L_{f-p} \ll L_{p-p} \, , \tag{3.1.11}$$

which from Eqs. (2-2-6) and (2-2-8) it would yield the condition:

$$\alpha \ll \frac{d_p}{6\sqrt{2}\, \tau_m \, \Delta\tilde{u}} \, , \tag{3.1.12}$$

for the volume fraction of the solid phase.

From the above condition it can be shown that for a fixed α, it is the more responsive particles which are affected primarily by viscous, as opposed to inter-particle collision, effects. For small τ_m, particle volume fractions can assume higher values with almost no significant particle-particle collision effects and local equilibrium is established by interactions with the fluid rather than direct inter-particle collisions.

Finally, it can be stated in support of the continuum approach that good agreement is found in the literature between experimental data and theoretical analyses incorporating the approach. For example, the studies by Stukel and Soo [1969], Nagarajan [1972] and Kramer and Depew [1972a] can be mentioned. The work of Kramer and Depew was specifically conducted to verify the particle phase continuum hypothesis in a turbulent pipe flow configuration. In their study, the authors investigated particle sizes of 62 and 200 μm, with volume fractions as low as 10^{-3}, and found good agreement between their theoretical and experimental results.

3.2 Conservation Equations for Two-Phase Turbulent Flows

The general form of the conservation equations for mass and momentum in two phase flow have been presented by Soo [1967], Drew [1966], and Hinze [1962]. The transport equation for fluid turbulent kinetic energy has been given by Hinze [1972], Danon et al. [1977] and Drew [1976a]. In this section the equations are developed to yield their time-averaged forms, using Reynold's decomposition procedure. In addition, time-averaged transport equations for the turbulent kinetic energy and the dissipation of turbulent kinetic energy, for the fluid phase, are also derived and presented.

The following assumptions are implied in the equations:

1 - Steady state, isothermal flow and imcompressible, Newtonian fluid

2 - Constant fluid and particle properties

3 - Continuum hypothesis for the dispersed phase composed of uniform size, spherical particles.

4 - The main dynamical interaction between fluid and particulate phase is due to Stoke's viscous drag

5 - Dilute particulate suspensions with $\alpha << 1$ everywhere in the flow field.

6 - For fluid phase the viscous diffusion is neglected compared to turbulent diffusion.

7 - For particulate phase the Brownian and Bernoullion diffusion are negligible compared to the turbulent diffusion induced by the fluid motion.

8 - Third-order terms containing particle concentration fluctuations are assumed negligible.

9 - Local isotropy for the fluid-particle turbulence.

3.2.1 Mass conservation equations

a) Fluid phase

The mass balance for a fluid element with volume fraction $(1-\alpha)$, yields, Hinze [1962]:

$$\frac{\partial \tilde{\rho}_f(1-\alpha)U_{f_i}}{\partial x_i} = 0 \qquad (3.2.1)$$

This is the continuity equation for a fluid phase in the presence of particulates with volume fraction α. However, from the assumptions 2 and 5, the equation simplifies to:

$$\frac{\partial U_{f_i}}{\partial x_i} = 0 \quad . \tag{3.2.2}^*$$

Using Reynold's decomposition for velocity:

$$U_{f_i} = \overline{U}_{f_i} + u_{f_i} \quad , \tag{3.2.3}$$

and substituting in Eq. (3.2.2) followed by time-averaging, yields:

$$\frac{\partial \overline{U}_{f_i}}{\partial x_i} = 0 \quad . \tag{3.2.4}$$

Equation (3.2.4) is an adequate approximation for fluid mass conservation in a dilute fluid-particle flows.

b) Particulate phase

The same consideration leading to Eq. (3.2.1), when applied to the particulate phase of a third-particle suspension, will yield the solid phase continuity equation, Hinze [1962]:

$$\frac{\partial}{\partial x_i} (\tilde{\rho}_p \, \alpha \, U_{p_i}) = 0 \quad . \tag{3.2.5}$$

---

*Note that, rigorously, Eq. (3.2.4) includes a term $\overline{\alpha' u_{f_i}}$ which need not be zero. However, since $|\alpha'| = O(\alpha)$ and $\alpha << 1$, it is presumed that the term represents a negligible contribution to the balance equation.

Using Reynold's decomposition procedure:

$$\alpha = \bar{\alpha} + \alpha' \tag{3.2.6}$$

$$U_{p_i} = \bar{U}_{p_i} + u_{p_i} \quad , \tag{3.2.7}$$

for the mass conservation of particle phase one obtains:

$$\frac{\partial}{\partial x_i} \left(\bar{\alpha}\, \bar{U}_{p_i} + \overline{\alpha' u_{p_i}} \right) = 0 \tag{3.2.8}$$

In Eq. (3.2.8), first term represents a contribution to the particle mass flux due to mean motion while the second term represents that due to turbulent diffusion of the particulate phase, and any other contributing term must be modeled in terms of appropriate flow field variables. In turbulent two-phase flow, it is customary, Hinze [1972], to assume a gradient-type diffusion form for the correlation term in Eq. (3.2.8) in analogy with the turbulent diffusion of heat in single phase flows. Thus:

$$\overline{\alpha' u_{p_i}} = - \nu_{t_p}^{(\alpha)} \frac{\partial \bar{\alpha}}{\partial x_i} \tag{3.2.9}$$

where $\nu_{t_p}^{(\alpha)}$ represents turbulent diffusivity for particulate mass concentration. The gradient-type turbulent diffusion expressed by Eq. (3.2.9) denotes a local field effect, with no memory of the past history of the particles. It is, therefore, inapplicable to cases with significant "over-shooting" effect of the particles. As will be

discussed later for such cases, due to inertia, or under the influence of external forces, such as gravity, the particles do not necessarily remain in the vicinity of their initial neighboring fluid element and can "over-shoot" to a different fluid element. Since this process is associated with particle "memory" effects, it can not be accounted for by a gradient-type diffusion mechanism.

For cases of non-significant "over-shooting" effects, Eq. (3.2.9) will be used to close the governing mass concentration equation. As will be seen later in the sub-section for the momentum balance, a similar constitutive relation for turbulent transport of particle momentum will be assumed.

It has been argued that in dilute flows, the momentum transport process for the particulate phase is due to turbulent diffusion of particles as through the containing fluid. This is an extension of Reynold's analogy applied to the mass and momentum transport of the particulate phase as shown by Soo [1969] to yield;

$$\mu_{t_p} = A\, \tilde{\rho}_p\, \nu_{t_p}^{(\alpha)} \quad , \tag{3.2.10}$$

with A as a constant of order unity. From Eq. (3.2.10), therefore, a direct linear proportionality between particle mass and momentum diffusivity exists. Thus, by obtaining the relation between $\nu_{t_p}^{(\alpha)}$ and ν_{t_f}, fluid eddy diffusivity, a relation for the particle momentum diffusivity will also be obtained.

Substitution of Eq. (3.2.9) into Eq. (3.2.8) yields:

$$\frac{\partial}{\partial x_i}\left(\overline{\alpha}\,\overline{U}_{p_i}\right) - \frac{\partial}{\partial x_i}\left(\nu_{t_p}^{(\alpha)}\,\frac{\partial\overline{\alpha}}{\partial x_i}\right) = 0 \qquad (3.2.11)$$

for particulate mass transport.

3.2.2 Momentum balance equations

Fluid phase

In a derivation of the fluid momentum-balance equation in a fluid-particle mixture, the dynamical effects due to presence of the particles should be considered. In gases, for example, it has been shown that the presence of particles effects the momentum exchange process between gas molecules, and hence the gas viscosity. Thus Einstein [1906] obtains:

$$\mu \simeq \mu_0\,(1 + 2.5\alpha) \qquad (3.2.12)$$

where μ and μ_0 denote fluid laminar viscosities with and without particles. Such a change of fluid molecular viscosity is not significant here, due to the diluteness assumption as well as the assumption of negligible molecular transport compared to turbulence diffusion.

The momentum balance equation for the fluid phase is therefore a balance among various forces of inertial, pressure and viscous origin, and includes the flow-resistance forces induced by the particles on the fluid element.

The instantaneous fluid momentum transport equation is given by Soo [1967]:

$$\frac{\partial}{\partial x_j}\left[\tilde{\rho}_f(1-\alpha)U_{f_i}U_{f_j}\right] = -\tilde{\rho}_p\,\alpha\,\frac{U_{f_i}-U_{p_i}}{\tau_m} - (1-\alpha)\,\frac{\partial}{\partial x_j}\left(P\delta_{ij}\right) + \frac{\partial}{\partial x_j}\left(\mu\,\frac{\partial U_{f_i}}{\partial x_j}\right) \tag{3.2.13}$$

I II III IV

with the following interpretation for various terms;

I - inertia term

II - particle-induced drag force

III - pressure force

IV - viscous force

The assumption 5 above, that is:

$$\alpha \ll 1 \tag{3.2.14}$$

can be incorporated in Eq. (3.2.13), resulting in the following equation for the instantaneous momentum:

$$\tilde{\rho}_f\,\frac{\partial}{\partial x_j}\left(U_{f_i}U_{f_j}\right) = -\tilde{\rho}_p\,\alpha\,\frac{U_{f_i}-U_{p_i}}{\tau_m} - \frac{\partial}{\partial x_j}\left(P\delta_{ij}\right) + \frac{\partial}{\partial x_j}\left(\mu\,\frac{\partial U_{f_i}}{\partial x_j}\right) \tag{3.2.15}$$

Thus, depending on $(U_{f_i} - U_{p_i})$ being positive or negative, the effect of the particulate phase is to decelerate or to accelerate the fluid.

Application of Reynolds decomposition procedure on Eq. (3.2.15) and averaging results in the following equation for the fluid mean momentum:

$$\rho_f \frac{\partial}{\partial x_j}\left(\overline{U}_{f_i}\,\overline{U}_{f_j}\right) = -\frac{\rho_p}{\tau_m}\left[\overline{\alpha}\left(\overline{U}_{f_i} - \overline{U}_{p_i}\right) + \overline{\alpha'\left(u_{f_i} - u_{p_i}\right)}\right] - \frac{\partial}{\partial x_j}\left(\overline{p}\,\delta_{ij}\right)$$

$$II_a \qquad\qquad II_b$$

$$+ \rho_f \frac{\partial}{\partial x_j}\left(\nu_{eff}\frac{\partial \overline{U}_{f_i}}{\partial x_j}\right) \qquad (3.2.16)$$

In this equation the Boussinesq assumption has been used for expressing the Reynolds stresses. Thus,

$$-\overline{u_{f_i} u_{f_j}} = \nu_{t_f}\left(\frac{\partial \overline{U}_{f_i}}{\partial x_j} + \frac{\partial \overline{U}_{f_j}}{\partial x_i}\right) - \frac{2}{3}\,\delta_{ij}k$$

where $k = 1/2\ (\overline{u_{f_i} u_{f_i}})$ is the fluid turbulent kinetic energy. Also, from the previous assumptions of negligible viscous diffusion, in Eq. (3.2.16);

$$\nu_{eff} = \nu + \nu_{t_f} \approx \nu_{t_f}$$

The fluid-particle interaction in Eq. (3.2.16) is comprised of two terms. The first term (II_a) represents the mean viscous drag induced by the particles, and the second term (II_b) is the drag contribution induced by the turbulent diffusion of the particles.

The fluid-particle interaction in Eq. (3.2.16) is comprised of two terms. The first term (II_a) represents the mean viscous drag induced by the particles, and the second term (II_b) is the drag contribution induced by the turbulent diffusion of the particles.

It has been postulated by Hinze [1972] and Davidson and McComb [1975] that:

$$\overline{u_{f_i}\alpha'} = - \nu_{t_f}^{(\alpha)} \frac{\partial \bar{\alpha}}{\partial x_i} \tag{3.2.17}$$

with $\nu_{t_f}^{(\alpha)}$ denoting the turbulent diffusivity for the transport of the scalar α. The ratio:

$$Sc_{t_f}^{(\alpha)} = \frac{\nu_{t_f}}{\nu_{t_f}^{(\alpha)}}$$

thus represents the eddy Schmidt number for the transport of particles by velocity fluctuations.

The governing equation for the fluid fluctuating velocity, u_{f_i}, is obtained by subtraction of the instantaneous momentum balance Eq. (3.2.13) from the time-averaged Eq. (3.2.16); the result is:

$$\tilde{\rho}_f \frac{\partial}{\partial x_j} \left(\bar{U}_{f_i} u_{f_j} + u_{f_i} \bar{U}_{f_j} + u_{f_i} u_{f_j} \right)$$

$$= - \frac{\tilde{\rho}_p}{\tau_m} \left[\bar{\alpha}(u_{f_i} - u_{p_i}) + \alpha'(\bar{U}_{f_i} - \bar{U}_{p_i}) + \alpha'(u_{f_i} - u_{p_i}) - \overline{\alpha'(u_{f_i} - u_{p_i})} \right]$$

$$- \frac{\partial p}{\partial x_i} + \frac{\partial}{\partial x_j} \left(\mu \frac{\partial u_{f_i}}{\partial x_j} \right) \tag{3.2.18}$$

Equation (3.2.18) will be used later to obtain the transport equation for the fluid turbulent kinetic energy (k) and its rate of dissipation (ε). Equation (3.2.18) could also be used to derive a transport equation for $\overline{\alpha' u_{f_i}}$ and so obleviate the gradient diffusion assumption. However, this approach leads to higher order and increasingly more complex correlations which, in turn, require closure. Due mainly to the difficulty of modeling higher order terms involving fluctuating pressure, concentration and viscous effects, this approach is not pursued here.

An investigation on the limiting behavior of the correlations $\overline{\alpha' u_{f_i}}$ and $\overline{\alpha' u_{p_i}}$ yields:

$$\overline{\alpha' u_{f_i}} = \overline{\alpha' u_{p_i}} \qquad (3.2.19)$$

when $\tau_m/T = 0$

and

$$\overline{\alpha' u_{f_i}} = \overline{\alpha' u_{p_i}} = 0 \qquad (3.2.20)$$

when $\tau_m/T \to 0$

with T denoting a characteristic local time scale of the turbulent fluid eddies.

The condition shown by Eq. (3.2.19) is obtained since in the limit of small τ_m/T values the particles behave very much like fluid. However, in the limit of large τ_m/T, Eq. (3.2.20), the fluid and particulate motion become non-correlated resulting in $\overline{\alpha' u_{f_i}} = 0$.

Also, since $\overline{\alpha' u_{p_i}}$ is proportional to particulate mass eddy diffusivity, Eq. (3.2.9), its value diminishes as τ_m/T becomes large and ν_{t_p} goes to zero.

Based on Eq. (3.2.19) and (3.2.20) it can be assumed that:

$$\overline{\alpha' u_{f_i}} = \overline{\alpha' u_{p_i}} \tag{3.2.21}$$

for all τ_m/T values. The Eq. (3.2.21) is also in accordance with Hinze [1972] regarding the possible proportionality of the correlation terms. Substitution of Eq. (3.2.21) in Eq. (3.2.16) results in:

$$\tilde{\rho}_f \frac{\partial}{\partial x_j}(\overline{U}_{f_i}\overline{U}_{f_j}) = -\frac{\tilde{\rho}_p \alpha}{\tau_m}(\overline{U}_{f_i} - \overline{U}_{p_i}) - \frac{\partial}{\partial x_j}(P\delta_{ij}) + \tilde{\rho}_f \frac{\partial}{\partial x_j}\left[\nu_{t_f}\left(\frac{\partial \overline{U}_{f_i}}{\partial x_j} + \frac{\partial \overline{U}_{f_j}}{\partial x_i}\right)\right] \tag{3.2.22}$$

which is the modelled momentum equation for the fluid phase.

Particulate phase

The momentum balance for the particulate phase is derived noting that the only major driving force retained is that due to the fluid viscous drag. As noted by Soo [1976], contributions of the particulate phase to pressure-gradient force are negligible in dilute systems and, therefore, are not included in formulation. A balance between instantaneous inertial and viscous drag forces results in the following equation; Soo [1967]:

$$\frac{\partial}{\partial x_j}(\alpha U_{p_i} U_{p_j}) = \frac{1}{\tau_m}[\alpha(U_{f_i} - U_{p_i})] \tag{3.2.23}$$

In the presence of the external force fields like gravity or electrostatic forces, these should be included in the balance.

Time-averating the Reynolds-decomposed form of Eq. (3.2.23) yields:

$$\frac{\partial}{\partial x_j}\left(\bar{\alpha}\,\bar{U}_{p_i}\bar{U}_{p_j}\right) = \underbrace{\frac{1}{\tau_m}\left[\bar{\alpha}(\bar{U}_{f_i}-\bar{U}_{p_i})\right]}_{\text{I}} + \underbrace{\frac{1}{\tau_m}\left[\overline{\alpha'(u_{f_i}-u_{p_i})}\right]}_{\text{II}}$$

$$\underbrace{-\frac{\partial}{\partial x_j}\left(\bar{\alpha}\,\overline{u_{p_i}u_{p_j}}\right)}_{\text{III}} \underbrace{-\frac{\partial}{\partial x_j}\left(\bar{U}_{p_j}\overline{\alpha' u_{p_i}}\right)}_{\text{IV}} \underbrace{+\bar{U}_{p_i}\overline{\alpha' u_{p_j}}}_{\text{V}} \qquad (3.2.24)$$

in which the triple correlation term is neglected according to assumption 8. The first term on the left side of Eq. (3.2.24) is the convective contribution to the changes in particle momentum in the i^{th} direction. The terms (I) and (II) on the right side of Eq. (3.2.24) are the various contributions to momentum by the Stoke's viscous drag which had also appeared in the corresponding fluid momentum balance with opposite sign.

The term (III) on the right represents a contribution to the mean momentum balance due to the correlation of particulate velocity fluctuations and is similar to the Reynolds stress term in the fluid momentum balance. Implicit in Eq. (3.2.23) was the neglect of Brownian-type diffusion. However, the turbulent inertial effects give rise to the Reynolds-stress type term which, here, will be expressed in terms of particulate phase eddy viscosity.

The Boussinesq assumption will be extended to the particulate phase by assuming:

$$- \overline{u_{p_i} u_{p_j}} = \nu_{t_p} \left(\frac{\partial \overline{U}_{p_i}}{\partial x_j} + \frac{\partial \overline{U}_{p_j}}{\partial x_i} \right) - \frac{2}{3} \delta_{ij} \left(k_p + \nu_{t_p} \frac{\partial \overline{U}_{p_\ell}}{\partial x_\ell} \right) \quad (3.2.25)$$

with $k_p = 1/2\ u_{p_i} u_{p_j}$ as the particulate phase turbulent kinetic energy which can be obtained, for instance, from Eq. (4.2.6). The divergence term in Eq. (3.2.25) is necessary to ensure constistency when the summation of diagonal terms is considered. A similar term, however, does not appear in the fluid phase Reynolds stress relation given earler since it becomes approximately zero for dilute suspensions. The assumption of zero divergence for the particulate phase velocity as made by Hinze [1972] is not justified as evidenced by the particulate mass balance equation.

The term (IV) in Eq. (3.2.24) represents transport of the fluctuating momentum $\rho_p\ \alpha' u_{p_i}$ by the mean motion and the next term (V) is viewed as the transport of particulate mass by the turbulent motion contributing to the mean momentum. After substitution of the relations Eqs. (3.2.9), (3.2.21) and (3.2.25) in Eq. (3.2.24) one obtains:

$$\frac{\partial}{\partial x_j} \left(\overline{\alpha}\ \overline{U}_{p_i} \overline{U}_{p_j} \right) = \frac{1}{\tau_m} \overline{\alpha} (\overline{U}_{f_i} - \overline{U}_{p_i})$$

$$- \frac{\partial}{\partial x_j} \left[- \overline{\alpha} \nu_{t_p} \left(\frac{\partial \overline{U}_{p_i}}{\partial x_j} + \frac{\partial \overline{U}_{p_j}}{\partial x_i} \right) + \frac{2}{3} \overline{\alpha} \delta_{ij} \left(k_p + \nu_{t_p} \frac{\partial \overline{U}_{p_\ell}}{\partial x_\ell} \right) \right]$$

$$- \frac{\partial}{\partial x_j} \left[\nu_{t_p} \left(\overline{U}_{p_j} \frac{\partial \overline{\alpha}}{\partial x_i} + U_{p_i} \frac{\partial \overline{\alpha}}{\partial x_j} \right) \right] \quad (3.2.26)$$

The governing equation for the particulate fluctuating velocity U_{p_i} can be obtained accordingly. This equation will be used later for the derivation of the particle turbulent kinetic energy which, though not to be solved, is beneficial in further interpretation and analysis of various interaction terms in the k transport equation. The transport equation for u_{f_i} is obtained from substraction of Eq. (3.2.24) from Eq. (3.2.23) with the result:

$$\frac{\partial}{\partial x_j}\left[(\bar{\alpha}+\alpha')(u_{p_i}\bar{U}_{p_j}+\bar{U}_{p_i}u_{p_j}+u_{p_i}u_{p_j})+\alpha'\overline{U_{p_i}U_{p_j}}-\overline{\alpha u_{p_i}u_{p_j}}-\bar{U}_{p_j}\overline{\alpha' u_{p_i}}-\bar{U}_{p_i}\overline{\alpha' u_{p_j}}\right]$$

$$=\frac{1}{\tau_m}\left[\alpha'(\bar{U}_{f_i}-\bar{U}_{p_i})+(\bar{\alpha}+\alpha')(u_{f_i}-u_{p_i})-\overline{\alpha'(u_{f_i}-u_{p_i})}\right] \qquad (3.2.27)$$

3.2.3 Transport equations for the mean kinetic energy of the phases

These equations are obtained by multiplying the appopriate momentum equation in the i direction by the mean velocity in the same direction and invoking the repeated index summation convention. The results for the fluid and particle phases are given below:

Fluid phase

$$\tilde{\rho}_f\frac{\partial}{\partial x_j}\left[\bar{U}_{f_j}\left(\frac{1}{2}\bar{U}_{f_i}\bar{U}_{f_i}\right)\right]=-\frac{\tilde{\rho}_p}{\tau_m}\left[\bar{\alpha}\left(\bar{U}_{f_i}\bar{U}_{f_i}-\bar{U}_{f_i}\bar{U}_{p_i}\right)+\bar{U}_{f_i}\overline{\alpha'(u_{f_i}-u_{p_i})}\right]$$

$$\overline{I}_f \qquad\qquad \overline{II}_f$$

$$-\bar{U}_{f_i}\frac{\partial}{\partial x_j}(p\delta_{ij})+\rho_f\bar{U}_{f_i}\frac{\partial}{\partial x_j}\left[\mu_{t_f}\left(\frac{\partial\bar{U}_{f_i}}{\partial x_j}+\frac{\partial\bar{U}_{f_j}}{\partial x_i}\right)\right]$$

(3.2.28)

Particulate phase

$$\tilde{\rho}_p \frac{\partial}{\partial x_j}\left[\bar{\alpha}\,\bar{U}_{p_j}\left(\frac{1}{2}\bar{U}_{p_i}\bar{U}_{p_i}\right)\right] - \frac{\tilde{\rho}_p}{2}\bar{\alpha}\frac{\partial}{\partial x_j}\left(\bar{U}^2_{p_i}\bar{U}_{p_j}\right) - \frac{\tilde{\rho}_p}{2}\bar{U}_{p_j}\,\partial\left(\bar{\alpha}\,\bar{U}^2_{p_i}\right)$$

$$= \frac{\rho_p}{\tau_m}\Bigg[\underbrace{\bar{\alpha}\left(\bar{U}_{f_i}\bar{U}_{p_i} - \bar{U}_{p_i}\bar{U}_{p_i}\right)}_{\overline{I}_p} + \underbrace{\bar{U}_{p_i}\left(\overline{\alpha' u_{f_i}} - \overline{\alpha' u_{p_i}}\right)}_{\overline{II}_p}\Bigg]$$

$$- \bar{U}_{p_i}\frac{\partial}{\partial x_j}\left(\overline{\alpha'\,\overline{u_{p_i}u_{p_j}}}\right) - \bar{U}_{p_i}\frac{\partial}{\partial x_j}\left(\bar{U}_{p_j}\overline{\alpha' u_{p_i}} + \bar{U}_{p_i}\overline{\alpha' u_{p_j}}\right) \tag{3.2.29}$$

The transport equations for the mean kinetic energy of the phases are not solved since the distribution and the transport of mean kinetic energies are of little interest here. However, as will be shown later, these equations will be used to assist with the interpretation of the interaction terms in the equations for turbulent kinetic energies of the fluid and particulate phases, respectively.

3.2.4 Transport equation for the fluid turbulent kinetic energy (k)

The transport equation for the turbulent kinetic energy of the fluid phase is obtained by multiplying both sides of the governing equation for the fluctuating velocity by the fluctuating velocity and time-averaging the result. The transport equation for the fluid turbulent kinetic energy is:

$$\tilde{\rho}_f \overline{U}_{f_j} \frac{\partial}{\partial x_j}\left(\frac{1}{2}\overline{u_{f_i} u_{f_i}}\right) = -\tilde{\rho}_f \frac{\partial}{\partial x_j}\left[u_{f_j}\left(\frac{1}{2} u_{f_i} u_{f_i}\right)\right]$$

$$- \tilde{\rho}_f \overline{u_{f_i} u_{f_j}} \frac{\partial \overline{U}_{f_i}}{\partial x_j} + \frac{\partial}{\partial x_j}\left(2\mu \overline{s_{f_{ij}} u_{f_i}}\right) - 2\mu \overline{s_{f_{ij}} s_{f_{ij}}}$$

$$+ \frac{\tilde{\rho}_p}{\tau_m}\left[-\overline{\alpha}\left(\overline{u_{f_i} u_{f_i}} - \overline{u_{f_i} u_{p_i}}\right) - \overline{\alpha' u_{f_i}}\left(\overline{U}_{f_i} - \overline{U}_{p_i}\right) - \overline{\alpha' u_{f_i}\left(u_{f_i} - u_{p_i}\right)}\right]$$

$$I_f \qquad II_f \qquad III_f$$

(3.2.30)

with:

$$s_{f_{ij}} = \frac{1}{2}\left(\frac{\partial u_{f_i}}{\partial x_j} + \frac{\partial u_{f_j}}{\partial x_i}\right)$$

as the fluctuating rate of strain for the fluid phase.

The interpretation of all but the particle interaction terms of Eq. (3.2.30) is given in the appendix II describing the two-equation (k-ε) model of turbulence. The presence of a particulate phase and its dynamic interaction with the turbulent eddies creates additional mechanisms for energy exchange between the two phases. Thus, Eq. (3.2.30) contains fluid-particle interaction terms which alter the distribution of the fluid turbulent kinetic energy. These are discussed below.

3.2.5 Transport equation for the particle turbulent kinetic energy (k_p)

The development of an equation for the turbulent kinetic energy of the particulate phase, $k_p = 1/2(\overline{u_{p_i} u_{p_i}})$ is of value mainly for a thorough interpretation of the phase interaction terms. The derivation follows the same procedure which resulted in Eq. (3.2.30), and the result is:

$$\tilde{\rho}_p \frac{\partial}{\partial x_j}\left[\overline{U}_{p_j}\overline{(\bar{\alpha}+\alpha')\left(\frac{1}{2}u_{p_i}u_{p_i}\right)}\right] = -\tilde{\rho}_p\overline{u_{p_i}\frac{\partial}{\partial x_j}\overline{U}_{p_i}u_{p_j}(\bar{\alpha}+\alpha')}$$

$$-\tilde{\rho}_p\frac{\partial}{\partial x_j}\left[\overline{(\bar{\alpha}+\alpha')u_{p_j}\left(\frac{1}{2}u_{p_i}u_{p_i}\right)}\right] - \tilde{\rho}_p\overline{u_{p_i}\frac{\partial}{\partial x_j}(\alpha'\overline{U}_{p_i}\overline{U}_{p_j})}$$

$$+\frac{\tilde{\rho}_p}{\tau_m}\left[-\bar{\alpha}(-\overline{u_{f_i}u_{p_i}}+\overline{u^2_{p_i}}) + \overline{\alpha' u_{p_i}}(\overline{U}_{f_i}-\overline{U}_{p_i}) + \overline{\alpha'(u_{p_i}u_{f_i}-u^2_{p_i})}\right]$$

$$\qquad I_p \qquad\qquad II_p \qquad\qquad III_p \tag{3.2.31}$$

The first three terms on the right side arise due to inertial effects and are caused by the interactions between the particle turbulent and mean motions. These terms are complicated due to the fluctuations in particle concentration, and also by the non-zero divergence of the particle phase velocity which generates terms in excess of those obtained in single-phase flows.

The last term in Eq. (3.2.31) arise due to fluid-particle interactions. These terms are used in the following to interpret various mechanisms for transfer of energy from the fluid to the particulate phase and vice versa. It should be noted that no attempt is being made here to solve Eq. (3.2.31) and the particulate turbulent kinetic energy will, instead, be obtained from an algebraic expression which will be derived in Chapter 4.

Transport of fluid turbulent kinetic energy and the particle interaction effects

In this section, various fluid-particle interaction terms in the kinetic energy transport equations for the mean and turbulent motion of the phases are compared and interpreted. The terms labelled as I_f and I_p in the Eqs. (3.2.30) and (3.2.31) are re-written as:

$$I_f = \frac{\tilde{\rho}_p \bar{\alpha}}{\tau_m} \left[\overline{u_{f_i} (u_{f_i} - u_{p_i})} \right]$$

and

$$I_p = \frac{\tilde{\rho}_p \bar{\alpha}}{\tau_m} \left[\overline{u_{p_i} (u_{f_i} - u_{p_i})} \right]$$

Following Eq. (4.1.16) for the modeled form of $\overline{u_{f_i} u_{p_i}}$, this correlation is bounded as:

$$0 \leq \overline{u_{f_i} u_{p_i}} \leq 2k$$

where lower and upper bound limits are for small and large values of τ_m/T_L respectively.

Accordingly,

$$-2\frac{\tilde{\rho}_p\bar{\alpha}k}{\tau_m} \leq I_f \leq 0$$

The negative value of I_f generally implies a loss of turbulent kinetic energy for the fluid phase. The analogous term I_p in k_p equation can be re-written as;

$$I_p = \frac{\tilde{\rho}_p\bar{\alpha}}{\tau_m}\left[\overline{u_{p_i}(u_{f_i}-u_{p_i})} + \overline{u_{f_i}(u_{f_i}-u_{p_i})} - \overline{u_{f_i}(u_{f_i}-u_{p_i})}\right] \quad (3.2.32)$$

or;

$$I_p = \underset{(+)}{-I_f} - \underset{(-)}{\varepsilon_D} \quad (3.2.33)$$

with

$$\varepsilon_D \equiv \frac{\tilde{\rho}_p\bar{\alpha}}{\tau_m}\overline{(u_{f_i}-u_{p_i})^2}$$

The result implied by Eq. (3.2.33) is significant. It shows a generation rate or "source" for k_p exactly equal to the loss represented by I_f in transport equation for k. However, during the process of energy transfer from fluid to particulate phase a net dissipation of turbulent kinetic energy will occur, as shown by the second term on the right side of Eq. (3.2.23). This term is always negative in value, irrespective of the sign and magnitudes of u_{f_i} and u_{p_i}. The additional dissipation mechanism caused solely by the presence of the particles will be negligible only if perfectly

responsive particles are suspended in the fluid and no slip velocity arise between the phases. This dissipation term is usually referred to as the "drag dissipation", Drew [1976a], and has a similar counterpart in the mean motion. This can be shown by a comparison between the terms $\overline{I}_f$ and $\overline{I}_p$ in Eqs. (3.2.28) and (3.2.29). Therefore, for the mean motion the dissipation due to viscous drag is equal to:

$$\frac{\tilde{\rho}_p \bar{\alpha}}{\tau_m} (\bar{U}_{f_i} - \bar{U}_{p_i})^2 \tag{3.2.34}$$

which is analogous to the drag dissipation term in the turbulent motion as indicated by Eq. (3.2.33). The evolution of drag dissipation is not restricted to the I_f and I_p terms. Since by comparing the terms III_f and III_p one can write:

$$III_p = -\frac{\tilde{\rho}_p}{\tau_m} \overline{\alpha'(u_{f_i} - u_{p_i})^2} - III_f$$

which suggests an additional drag dissipation, ε_{D_1}, given by:

$$\varepsilon_{D_1} = \frac{\tilde{\rho}_p}{\tau_m} \overline{\alpha'(u_{f_i} - u_{p_i})^2}$$

and is caused by the fluctuating mass of the particulate phase when it correlates with the fluctuating slip velocity.

The drag dissipation associated with the terms I_f and I_p is based on the mean particle mass as shown by Eq. (3.2.33). The term III_p is, however, neglected in the calculation according to the assumption 8 above. Therefore, due to presence of the particles an

additional mechanism to "sink" the fluid turbulent kinetic energy is established which is represented by term I_f in Eq. (3.2.30). A fraction of this extracted energy will be transferred to the particulate phase (term I_p in Eq. (3.2.31)) while the rest will be dissipated (term ε_D in Eq. (3.2.32)) due to a non-zero slip velocity between the phases in the flow. Therefore, for a two-phase third-particle flow in general:

$$\text{total dissipation} = \varepsilon + \varepsilon_D$$

in which ε is the dissipation caused by fluid viscous effects and ε_D is drag dissipation caused by fluid-particle interactions. The expression for ε_D is given by Eq. (3.2.33) and the transport equation for ε will be derived in the next section. The ε-transport equation, however, is further modified by the fluid-particle interaction effects which will be discussed.

For interpretation of the term II_f in k-transport equation, the counterpart term (II_p) in the k_p-transport equation should also be examined. In single phase flows, the transfer of energy from the mean motion to the turbulence is due to interactions between the Reynolds stress and the mean shear, that is;

$$\text{Production (for } \bar{\alpha}=0) = -\overline{u_{f_i} u_{f_j}} \frac{\partial \bar{U}_{f_i}}{\partial x_j}$$

The associated transfer process is the well-known "cascading process", Tennekes and Lumley [1972], responsible for an energy exchange over a range of scales between the mean and the turbulent motion. However, the presence of the particles and the subsequent dynamic interactions

between the phases gives rise to an additional transfer mechanism by means of which fluid kinetic energy could further be exchanged between the mean motion and the turbulence.

It has already been shown that the interaction terms $\overline{I}_f$ and $\overline{I}_p$ in the Eqs. (3.2.28) and (3.2.29), respectively, are mainly responsible for the energy exchange between the mean motions. This exchange is also associated with a mean energy dissipation proportional to the square of mean velocity difference between the phases as shown by Eq. (3.2.34). The second interaction terms, $\overline{II}_f$ and $\overline{II}_p$, can be re-written as:

$$\overline{II}_f = - \frac{\tilde{\rho}_p}{\tau_m} \left[\overline{U}_{f_i} (\overline{\alpha' u}_{f_i} - \overline{\alpha' u}_{p_i}) \right]$$

and

$$\overline{II}_p = \frac{\tilde{\rho}_p}{\tau_m} \left[\overline{U}_{p_i} (\overline{\alpha' u}_{f_i} - \overline{\alpha' u}_{p_i}) \right]$$

The coupling effects between the phases result in an energy exchange for the mean motions. The net excess energy resulting from such an exchange is obtained from:

$$\overline{II}_p = - \overline{II}_f - \varepsilon_E \qquad (3.2.35)$$

with;

$$\varepsilon_E = - \frac{\tilde{\rho}_p}{\tau_m} \left[(\overline{U}_{p_i} - \overline{U}_{f_i}) \; (\overline{\alpha' u}_{f_i} - \overline{\alpha' u}_{p_i}) \right]$$

Examination of the corresponding interaction terms, II_f and II_p, in the transport equations for k and k_p, Eqs. (3.2.30) and (3.2.31), shows that the next excess energy represented by Eq. (3.2.35) is transferred to the turbulence to be distributed between the interacting phases. This can be shown from Eqs. (3.2.30) and (3.2.31):

$$II_f + II_p = \frac{\tilde{\rho}_p}{\tau_m} \left[(\bar{U}_{p_i} - \bar{U}_{f_i}) \, (\overline{\alpha' u_{f_i}} - \overline{\alpha' u_{p_i}}) \right]$$

which is exactly equal, and opposite in sign, to the net excess mean kinetic energy exchanged between the mean motion of the phases. The preceding argument suggests that in two-phase turbulent flows, dynamical interaction effects between the phases can develop an additional mechanism for the dissipation of kinetic energy. Furthermore, an additional process can be established by which kinetic energy will be exchanged between the mean and the turbulent motions.

3.2.6 The transport equation for dissipation of fluid turbulent kinetic energy (ε)

The procedure for obtaining the transport equation for the dissipation rate of fluid turbulent kinetic energy, ε, is to:

1 - take the derivative of both sides of the governing equation for u_{f_i}, Eq. (3.2.18), with respect to x_ℓ,

2 - multiply both sides of the equation by $\nu \, \partial u_{f_i} / \partial x_\ell$,

3 - time-average the resulting equation.

The result for a dilute suspension is:

$$\tilde{\rho}_f \overline{U}_{f_j} \frac{\partial \varepsilon}{\partial x_j} = -\frac{\tilde{\rho}_p \overline{\alpha}}{\tau_m}\left[\nu \overline{\frac{\partial u_{f_i}}{\partial x_\ell}\left(\frac{\partial u_{f_i}}{\partial x_\ell} - \frac{\partial u_{p_i}}{\partial x_\ell}\right)}\right]$$

I_ε II_ε

$$-\tilde{\rho}_f \frac{\partial}{\partial x_j}\left[\overline{u_{f_j}\varepsilon} + \frac{\nu}{\tilde{\rho}_f}\overline{\frac{\partial p}{\partial x_\ell}\frac{\partial u_{f_j}}{\partial x_\ell}} - \nu\frac{\partial \varepsilon}{\partial x_j}\right]$$

III_ε

$$-2\nu\tilde{\rho}_f \overline{u_{f_j}\frac{\partial u_{f_i}}{\partial x_\ell}} \cdot \frac{\partial^2 U_{f_i}}{\partial x_\ell \partial x_j} - 2\nu\tilde{\rho}_f \overline{\frac{\partial u_{f_i}}{\partial x_j}\frac{\partial u_{f_i}}{\partial x_\ell}\frac{\partial u_{f_j}}{\partial x_\ell}}$$

IV_ε V_ε

$$-2\nu\tilde{\rho}_f \frac{\partial U_{f_j}}{\partial x_j}\left(\overline{\frac{\partial u_{f_i}}{\partial x_j}\frac{\partial u_{f_i}}{\partial x_\ell}} + \overline{\frac{\partial u_{f_\ell}}{\partial x_i}\frac{\partial u_{f_j}}{\partial x_i}}\right) - 2\nu^2\tilde{\rho}_f \overline{\frac{\partial^2 u_{f_i}}{\partial x_j \partial x_\ell}\frac{\partial^2 u_{f_i}}{\partial x_j \partial x_\ell}}$$

VI_ε VII_ε

(3.2.36)

In the derivation of the transport equation for ε above the terms $\overline{\partial\alpha'/\partial x_\ell\ \partial u_{f_i}/\partial x_\ell}$ and $\overline{\alpha'\partial u_{f_i}/\partial x_\ell}$ are neglected due to the assumption of local isotropy which is assumed to be associated with the small scale structure of turbulence. The terms in Eq. (3.2.36) are:

I_ε - convection by mean motion

II_ε - fluid-particle interaction terms

III_ε - diffusion due to turbulence, pressure fluctuations and viscous effects

IV_ε - secondary production by mean flow

V_ε - production by self-stretching of turbulence

VI_ε - production by mean flow

VII_ε - dissipation by viscosity

The pressure of the particulate phase and subsequent interaction between the phases ar responsible for the fluid-particle term (II_ε) which disappears as the particle volume fraction, $\bar{\alpha}$, goes to zero. The term II_ε in Eq. (3.2.36) is the correlation between the fluid fluctuating rate of strain, represented by;

$$s_{f_{ij}} = \frac{\partial u_{f_i}}{\partial x_j}$$

and the rate of strain associated with the fluctuating slip velocity:

$$s_{f\text{-}p_{ij}} = \frac{\partial}{\partial x_j} \left(u_{f_i} - u_{p_i} \right)$$

The term can be re-cast as:

$$II_\varepsilon = - \frac{\tilde{\rho}_p \bar{\alpha}}{\tau_m} \left[\varepsilon - \nu \overline{\frac{\partial u_{f_i}}{\partial x_\ell} \frac{\partial u_{p_i}}{\partial x_\ell}} \right] \qquad (3.2.37)$$

Therefore, closure for the particle-fluid interaction terms in the ε equation is only required for the correlation term shown in Eq. (3.2.37). This correlation is modeled further on in the text. For this second-order correlation term it can be shown that:

$$\nu \overline{\frac{\partial u_{f_i}}{\partial x_\ell} \frac{\partial u_{p_i}}{\partial x_\ell}} \to \varepsilon \qquad (3.2.38)$$

$$\text{as } \frac{\tau_m}{T} \to 0$$

and

$$\nu \overline{\frac{\partial u_{f_i}}{\partial x_\ell} \frac{\partial u_{p_i}}{\partial u x_\ell}} \to 0 \qquad (3.2.39)$$

$$\text{as } \frac{\tau_m}{T} \to \infty$$

These expressions correspond to the limits of perfectly responsive and non-responsive particles, respectively.

As will be shown in Chapter 4, the limiting behavior of the correlation term given above will be used as the criteria for testing the validity of an expression derived for the correlation term. Therefore, using the limits in Eq. (3.2.37), one obtains:

$$II_\varepsilon \to 0 \qquad (3.2.40)$$

$$\text{as } \frac{\tau_m}{T} \to 0$$

and,

$$II_{\varepsilon} \rightarrow - \frac{\tilde{\rho}_p \bar{\alpha} \varepsilon}{\tau_m} \qquad (3.2.41)$$

$$\text{as} \quad \frac{\tau_m}{T} \rightarrow \infty$$

Therefore, according to the result in Eq. (3.2.41), the transport equation for ε can show a reduction in ε caused by dynamic interactions between high-frequency, small scale turbulent eddies with the solid particle phase.

In the data of Zisselmar and Molerus [1979] for solid-liquid pipe flow a decrease in fluid turbulent kinetic proportional to α for most regions of the flow was observed. With the fluid Taylor microscale, λ, remaining constant with the particle loading, reduction in k translates into a reduction in ε since,

$$\varepsilon = 15\nu \frac{\tilde{u}^2}{\lambda^2} = 10\nu \frac{k}{\lambda^2} \qquad (3.2.42)$$

with $u^2 = 2/3\ k$.

The increase in ν with the particle volume concentration is not high enough to overcome the decrease in k and, therefore, in ε. From experimental data the value of τ_m/T_L can be calculated to be approximately equal to 0.2 following the expression, Hinze [1975]:

$$T_L = C_T \frac{k}{\varepsilon}$$

for T_L with $C_T = 0.41$.

For this value of τ_m/T_L and by taking $T = T_L$ (which will be shown in Chapter 4), the experimentally observed reduction in ε can be predicted theoretically using Eq. (3.2.36). The reduction is demonstrated theoretically in the II_ε term which shows a linear variation with $\bar{\alpha}$. The linear variation is also observed in the experiment of Zisselmar and Molerus [1979] based on which Fig. 7.12 is plotted. The figure shows the variation of turbulent kinetic energy with $\bar{\alpha}$ at various distances from the pipe well. Therefore, according to Eq. (3.2.42) this corresponds to similar linear variation for the turbulent dissipation rate.

The presence of particles gives rise to yet another mechanism by which an additional mechanism for dissipation of turbulent kinetic energy evolves. As shown earlier in a discussion involving a relative comparison of the k-transport equations, the "drag dissipation" based on particle mean concentration was defined as:

$$\varepsilon_D = \frac{\tilde{\rho}_p}{\tau_m} \bar{\alpha} \overline{(u_{f_i} - u_{p_i})^2}$$

By adopting the expressions for $\overline{u_{p_i}^2}$ and $\overline{u_{f_i} u_{p_i}}$ which will be derived in Chapter 4, Eq. (3.2.43) becomes:

$$\varepsilon_D = 2 \tilde{\rho}_p \bar{\alpha} \frac{k}{\tau_m + T_L} \qquad (3.2.44)$$

In the following, a comparison between the viscous dissipation, ε, and drag dissipation, ε_D, which constitute the total dissipation, is made. The comparison is conducted for small and large τ_m/T_L values.

In the limit of large τ_m/T_L, one can compare the net effect of the particle on the dissipation of k by comparing the decrease in viscous dissipation, as indicated by Eq. (3.2.41), to the increase due to drag dissipation as shown by Eq. (3.2.44). For large values of τ_m/T_L, ε_D is expanded as:

$$\varepsilon_D = 2 \tilde{\rho}_p \bar{\alpha} \frac{k}{\tau_m} \left[1 - \frac{T_L}{\tau_m} + 0\left(\frac{T_L}{\tau_m}\right)^2\right] \tag{3.2.45}$$

This equation is an expression for the drag component of the total dissipation. The term II_ε in Eq. (3.2.41) represents a "sink" for ε and will account for reduction in this quantity.

In the limit of small τ_m/T_L values, the rate of change in ε due to particle effects is zero, as shown by Eq. (3.2.40) while the increase in total dissipation is:

$$\varepsilon_D = 2 \tilde{\rho}_p \bar{\alpha} \frac{k}{T_L} \left[1 - \frac{\tau_m}{T_L} + 0\left(\frac{\tau_m}{T_L}\right)^2\right] \tag{3.2.46}$$

Therefore, the analysis indicates a net increase in total dissipation of turbulent kinetic energy with the viscous dissipation component, ε, of total dissipation not affected by fluid-particle interaction effects.

After substitution for T_L from Eq. (4.1.22) in Eq. (3.2.44), one obtains:

$$\varepsilon_D = 2 \tilde{\rho}_p \bar{\alpha} \frac{k\varepsilon}{C_T k + \tau_m \varepsilon} \tag{3.2.47}$$

with $C_T = 0(0.1)$.

The ratio of drag dissipation to the viscous dissipation becomes:

$$\frac{\varepsilon_D}{\varepsilon} = \frac{2}{C_T} \cdot \frac{\tilde{\rho}_p \bar{\alpha}}{\tilde{\rho}_f} \cdot \frac{T_L}{T_L + \tau_m} \tag{3.2.48}$$

In two phase liquid-solid flows with $\tilde{\rho}_p/\tilde{\rho}_f = O(1)$, a particulate volume fraction of $\bar{\alpha} << O(10^{-2})$ will give small $\varepsilon_D/\varepsilon$ values. Therefore, for these conditions the drag dissipation becomes small compared to the viscous dissipation.

For gas-solid flows, however, with:

$$\frac{\tilde{\rho}_p}{\tilde{\rho}_f} = O(10^3)$$

a small dissipation ratio is given far:

$$\bar{\alpha} << 10^{-4}$$

A consideration of this result shows that the range of $\bar{\alpha}$ is more restricted in gases than it is in liquids. However, as noted in Chapter 2, very small $\bar{\alpha}$ values might not be acceptable due to restriction imposed by the assumption of a continuum approximation.

To conclude this section, a comparison between the results obtained above and the established investigations in the field can be made. Owen [1969] considered the case of a dilute mixture of fine particles with a small response time compared to the characteristic times of energy-containing eddies and derived for the total dissipation of turbulent kinetic energy;

$$\varepsilon_{total} \propto \left(1 + \overline{\alpha}\ \frac{\tilde{\rho}_p}{\tilde{\rho}_f}\right)\varepsilon \qquad (3.2.49)$$

Equation (3.2.49) is a special case of the equations derived in this section. A general equation for the total dissipation can be obtained by summation of the drag dissipation, Eq. (3.2.44), and the viscous dissipation, ε. Thus, one obtains:

$$\varepsilon_{total} = \varepsilon + \varepsilon_D = \frac{\dfrac{2\tilde{\rho}_p\overline{\alpha}}{C_T\tilde{\rho}_f} + \left(1 + \dfrac{\tau_m}{T_L}\right)}{1 + \dfrac{\tau_m}{T_L}}\ \varepsilon \qquad (3.2.50)$$

In the limit of $\tau_m/T_L \ll 1$, corresponding to the case considered by Owen [1969], Eq. (3.2.50) can be expanded to give;

$$\varepsilon_{total} = \left[1 + \frac{2}{C_T}\ \frac{\tilde{\rho}_p\overline{\alpha}}{\tilde{\rho}_f} + 0\left(\frac{\tau_m}{T_L}\right)\right]\varepsilon \qquad (3.2.51)$$

Equation (3.2.51) has the same form as that derived by Owen [1969], Eq. (3.2.49), except for the proportionality constant $2/C_T$ which is unity in the Owen's analysis.

3.3 Boundary conditions for the fluid phase

In the following section boundary conditions for the fluid phase in two-phase fluid-particulate flows are presented. These conditions consist of a set of boundary expressions to be incorporated in the fully elliptic transport equations for the solution of the fluid

velocities, turbulent kinetic energy and dissipation of turbulent kinetic energy. In Appendix (II) the boundary conditions for the single phase flow using two-equation ($k-\varepsilon$) model of turbulence are described and Table (1) contains a summary of the results. In the case of turbulent fluid-particle flows the expressions for single-phase flows should, however, be modified to account for the particle interaction effects. This is done in the following section.

Momentum balance

The transport equation for the fluid mean momentum is given by the Eq. (3.2.16) with particle-fluid interaction effects incorporated. The treatment, however, at the solid walls is rather independent of the rigorously derived fluid mean momentum equation, since the region between the node closest to the wall itself is patched by the standard logarithmic distribution for streamwise velocity in accordance with experimental observations. Such a treatment is a good approximation as long as the wall node is positioned in the inertial sublayer region where turbulent transport of the mean fluid streamwise velocity, should also be incorporated. The investigation of Peskin and Dwyer [1965] shows no significant effect when inter-particle distances of particles with small inertial effects are large compared to the length scale of energy-containing eddies since the effect of particles is then merely to cause viscous disturbances far apart from one another, with no possibility of an overlap. The results of Peskin and Dwyer investigation, furthermore, shows that for large interparticle distances, an increase in the particle inertia is associated with inertial

disturbances and a decrease in the laminar sublayer thickness which is equivalent to a downward shift of the velocity profile. For the non-inertial particles, the same analysis shows that for relatively small inter-particle distances the increase in fluid viscosity in the vicinity of the solid wall causes an increase in the viscous-sublayer thickness and a subsequent reduction in skin friction, which is associated with an upward shift in the log-well relation for fluid velocity.

In the investigations of Virk et al [1967] and Wells et al [1968] a logarithmic velocity profile similar to that in single-phase flow was observed. However, thickening of the laminar sublayer causes an upward displacement of the velocity profile equivalent to the existence of a virtual slip at the wall, with consequent drag reduction at the wall. In such cases the same scaling relations for the velocity in the viscous and inertial sub-layers exists as argued by Lumley [1973]. The preceeding observations justify the assumption of the existence of a log-wall relationsip for fluid streamwise velocity in the inertial sublayer of two-phase flow. This assumption is even more justified when dilute fluid-particle systems are considered. Consequently, the expression for the fluid wall shear stress from Table (1) which is derived on the basis of a logarithmic velocity profile will be used.

k-transport equation near the solid wall

The wall treatment in single phase flows is often based on the assumption of a local equilibrium condition in the vicinity of the wall. For this condition, the production of turbulent kinetic energy, extracted from the mean motion through vortex-stretching of fluid

filaments, becomes equivalent to the local viscous dissipation. The incorporation into k equation of the local equilibrium effect then yields an expression for turbulent shear stress in terms of a linear variation of turbulent kinetic energy in the inertia sublayer as given by:

$$-\frac{\overline{u_{f_1} u_{f_2}}}{k} = C_\mu^{1/2} \tag{3.3.1}$$

with C_μ as the constant in Prandtl-Kolmogorov relation and the coordinates x_1 and x_2 represent directions parallel and normal to the wall. In Fig. 1 of Appendix (II) lateral variation of the ratio (turbulent shear stress/turbulent kinetic energy) is shown for straight channel, mildly curved channel and strongly curved channel flow.

The constancy of this ratio in regions close to walls is observed as a partial verification of Eq. (3.3.1) in single phase flows. In two-phase fluid-particle flows the k-transport equation, Eq. (3.2.30), may be similarly reduced at the wall to the following form:

$$-\frac{\overline{u_{f_1} u_{f_2}}}{k} = C_\mu^{1/2} \left\{ 1 + \frac{\tilde{\rho}_p}{\tilde{\rho}_f \tau_m \varepsilon} \left[\overline{\alpha(\overline{u_{f_i} u_{f_i}} - \overline{u_{f_i} u_{p_i}})} + \overline{\alpha' u_{f_i}} (\overline{U}_{f_i} - \overline{U}_{p_i}) \right] \right\}^{1/2} \tag{3.3.2}$$

In which are included the Boussinesq relation for the turbulent shear stress and the Prandtl-Kolomogorov relation for eddy viscosity. Comparison between Eqs. (3.3.1) and (3.3.2) indicates the possibility

of modifying the single phase wall expressions by inclusion of fluidparticle interaction effects. It can be seen that for zero particle concentrations, Eq. (3.3.2) becomes equivalent to its single phase version, Eq. (3.3.1). The expression in brackets in Eq. (3.3.2) accounts for the particulate effects on the ratio $\overline{(-u_{f_1}u_{f_2}/k)}$ in vicinity of the wall. It is a complicated function of α, τ_m, k and ε. The main complexity is due to unknown and yet unexplored wall effects. It should be noted that in the closure for the term $\overline{u_{f_i}u_{p_i}}$, as will be shown in Chapter 4, the complex wall effects are not included. Therefore, the incorporation of the far from-the-wall $\overline{u_{f_i}u_{p_i}}$ modeled Eq. (3.3.2) for near-the-wall regions is not justified which could lead to erroneous results. The same reasoning is also applied for the term $\overline{\alpha' u_{f_i}}$.

At this point, it seems necessary to further the analysis on the basis of available experimental data. The data presented by Zisselmar and Molerus [1979] for turbulent pipe flow of 53 μm particles is one of few detailed measurements for which non-interfering Laser-Doppler velocimeter has been utilized. Figure (3.1) shows the lateral variation of the ratio $\overline{u_{f_1}u_{f_2}}/k$ at various particulate concentrations in the vicinity of the wall which has been obtained from the data of Zisselmar and Molerus. It can be observed that similar to the single phase flows, a constant $(\overline{u_{f_1}/u_{f_2}}/k)$ ratio in vicinity of the wall does exist which shows some variations with respect to the particle volume concentration $(\bar{\alpha})$.

Interestingly, the value of the ratio for $\bar{\alpha} = 0$, i.e., clear fluid, is close to that of Laufer's data shown in Fig. 1 of Appendix II. The variation of the ratio $(\overline{u_{f_1} u_{f_2}}/k)_{\bar{\alpha}}/(\overline{u_{f_1} u_{f_2}}/k)_{\bar{\alpha}=0}$ vs. $\bar{\alpha}$ for the wall region of Zisselmar and Molerus [1979] data is shown in Fig. (3.2). This ratio represents the particle-interaction term in big brackets in Eq. (3.3.2). From Fig. (3.2) it can be seen that initial introduction of the solid particles in the fluid slightly increases the ordinate while with further increase in $\bar{\alpha}$, it decreases below that for the fluid with $\bar{\alpha} = 0$. Quantitatively, the relative maximum increase is about 12% at $\bar{\alpha} \approx .0171$ and the relative maximum decrease is about 25% at $\bar{\alpha} \approx .056$ which is the highest α tested.

From Fig. (3.2), the insignificant effects of dilute concentrations, $\bar{\alpha} < .005$ for instance, can also be observed and furthermore in the regions where $\bar{\alpha} \lesssim .035$ the maximum deviation from unity is about 12%. Therefore, considering experimental errors, which can be observed by the degree of non-symmetry of the various profiles in Fig. (10) of Zisselmar and Molerus [1979], one can assume no variation around unity for the region of $\bar{\alpha} \lesssim .035$. From Eq. (3.3.2) this assumption is equivalent to saying:

$$\left\{1 + \frac{\tilde{\rho}_p}{\tilde{\rho}_f \tau_m \varepsilon} \left[\overline{\alpha(u_{f_i} u_{f_i} - u_{f_i} u_{p_i})} + \overline{\alpha u_{f_i}}(\bar{U}_{f_i} - \bar{U}_{p_i})\right]\right\}^{1/2} \approx 1$$

which is justified for the wall regions of the flows with the values τ_m/T_L corresponding to that of the experiment. Calculations in previous sections showed that for the flow of Zisselmar and Molerus:

$$\frac{\tau_m}{T_L} \simeq 0.2$$

which is a moderate value of the order of unity. Equation (3.3.2) can be analyzed at high and low τ_m/T_L values.

For $\tau_m/T_L \ll 1$ values, one would have:

$$\overline{u_{f_i} u_{p_i}} \simeq \overline{u_{f_i} u_{f_i}}$$

and also:

$$\overline{U}_{p_i} \simeq \overline{U}_{f_i}$$

which would make the interaction terms in Eq. (3.3.2) vanish. On the other hand, for large values of the time scale ratio, $\tau_m/T_L \gg 1$, no correlation between the fluid and particle fluctuations is expected to exist, that is:

$$\overline{u_{f_i} u_{p_i}} \simeq 0$$

and

$$\overline{\alpha' u_{f_i}} \simeq 0$$

Therefore, substitution of above expressions in Eq. (3.3.2) yields:

$$\frac{-\overline{u_{f_1} u_{f_2}}}{k} \simeq C_\mu^{1/2} \left(1 + \frac{2\tilde{\rho}_p \bar{\alpha}}{\tilde{\rho}_f} \cdot \frac{k}{\tau_m \epsilon}\right)$$

Using Eq. (4.1.22) this may be re-written as:

$$\frac{-\overline{u_{f_1} u_{f_2}}}{k} \simeq C_\mu^{1/2} \left(1 + \frac{2}{C_T} \cdot \frac{\tilde{\rho}_p \bar{\alpha}}{\tilde{\rho}_f} \cdot \frac{T_L}{\tau_m}\right) \qquad (3.3.3)$$

Therefore, in the cases of large τ_m/T_L values, the fluid-particle interaction terms in Eq. (3.3.3) can be neglected if;

$$\frac{\tau_m}{T_L} \gg 4.8 \frac{\tilde{\rho}_p}{\tilde{\rho}_f} \bar{\alpha} \qquad (3.3.4)$$

for $C_T = .41$.

The condition expressed by Eq. (3.3.4) should be evaluated at various density ratios. In the case of liquid-solid flows, $\tilde{\rho}_p/\tilde{\rho}_f = O(1)$, the diluteness of the particulate phase guarantees the condition (3.3.4) to hold. For the gas-solid flows, $\tilde{\rho}_p/\tilde{\rho}_f = O(10^3)$ the condition (3.3.4) requires that:

$$\bar{\alpha} \ll .769 \times 10^{-4} \frac{\tau_m}{T_L} \qquad (3.3.5)$$

for large values of the ratio τ_m/T_L.

From this argument it is concluded that for all τ_m/T_L values of interest here, the interaction terms in Eq. (3.3.2) can be neglected. This conclusion is applicable to the wall regions of dilute fluid-particle flows. Following the analysis for large τ_m/T_L values, the condition (3.3.5) for the particle mean volume concentration has been developed and for moderate τ_m/T_L values, the analysis has been based on the experimental data of Zeisselmar and Molerus [1979]. The use of experimental data is justified since equations of motion and consequently the correlation terms do not contain complex wall effects and their substitution in equations written for wall regions is, therefore, not justified.

Based on the experimental results no modifications for particle effects on the form of the boundary expressions seems to be necessary. However, it should be noted that such a conclusion is based on a single set of experiment and therefore more detailed and consistent experimental data at different ranges of τ_m/T_L and $\bar{\alpha}$ values are required for an extension of this conclusion.

Particle-interaction effects on ε-Prandtl number (σ_ε)

In the single phase flows, by approximation of ε-transport equation in the near-wall regions an expression for σ_ε is obtained which is shown in the Appendix (II). Accordingly, from Eq. (3.2.36) one obtains the following result in the near-wall region:

$$0 = \frac{\partial}{\partial x_2}\left(\frac{\nu_{f_t}}{\sigma_\varepsilon}\frac{\partial \varepsilon}{\partial x_2}\right) + C_1\frac{\varepsilon}{k}G - C_2\frac{\varepsilon^2}{k} - \frac{II_\varepsilon}{\tilde{\rho}_f} \qquad (3.3.6)$$

where:

$$II_\varepsilon = \frac{2\tilde{\rho}_p \bar{\alpha}}{\tau_m} \left[\nu \overline{\frac{\partial u_{f_i}}{\partial x_\ell} \left(\frac{\partial u_{f_i}}{\partial x_\ell} - \frac{\partial u_{p_i}}{\partial x_\ell} \right)} \right]$$

represents the fluid-particle interaction effects.

With:

$$\varepsilon = C_\mu^{3/2} \frac{k^{3/2}}{\kappa x_2} \tag{3.3.7}$$

and assuming a nearly uniform k-distribution near the wall Eq. (3.3.6) reduces further to:

$$0 = -\frac{\partial}{\partial x_2} \left(\frac{C_\mu k^2}{\sigma_\varepsilon} \frac{1}{x_2} \right) + (C_1 - C_2) \left(\frac{C_\mu^{3/2} k^2}{\kappa^2 x_2^2} \right) - \frac{II_\varepsilon}{\bar{\rho}_f}$$

$$0 = \frac{C_\mu k^2}{\sigma_\varepsilon x_2^2} + (C_1 - C_2) \left(\frac{C_\mu^{3/2} k^2}{\kappa^2 x_2^2} \right) - \frac{II_\varepsilon}{\bar{\rho}_f}$$

and consequently:

$$\sigma_\varepsilon = \frac{\kappa^2}{(C_2 - C_1) C_\mu^{1/2}} \left[\frac{1}{1 + \underbrace{\frac{II_\varepsilon}{\rho_f} \frac{x_2^2}{k^2} \cdot \frac{\kappa^2}{(C_2 - C_1) C_\mu^{3/2}}}_{I_\sigma}} \right] \tag{3.3.8}$$

It can be seen that with no particles present, $\bar{\alpha} = 0$, the term II_ε vanishes and the value for single phase flow, Eq. 18 in Appendix II, results. The effect of particles is, as seen from Eq. (3.3.8), to reduce σ_ε below that for single-phase flows. The particle effect term in Eq. (3.3.8) is re-written as:

$$I_\sigma = \frac{\kappa^2}{(C_2-C_1)C_\mu^{3/2}} \cdot \frac{x_2^2}{k^2} \cdot \frac{2\tilde{\rho}_p\bar{\alpha}}{\tilde{\rho}_f\tau_m} \cdot \left[\nu \overline{\frac{\partial u_{f_i}}{\partial x_\ell}\left(\frac{\partial u_{f_i}}{\partial x_\ell} - \frac{\partial u_{p_i}}{\partial x_\ell}\right)} \right]$$

with the expression for II_ε substituted.

In the limit of very small τ_m/T values, the expression in brackets vanishes since the particle dynamics correspond to those of the surrounding fluid. However, in the limit of large values for τ_m/T, almost no correlation between the dynamics of the two phases exist. Therefore, in this limit;

$$I_\sigma = \frac{\kappa^2}{(C_2-C_1)C_\mu^{3/2}} \cdot \frac{\tilde{\rho}_p\bar{\alpha}}{\tilde{\rho}_f} \cdot \frac{x_2^2\varepsilon}{k^2\tau_m}$$

which is re-written as:

$$I_\sigma = \frac{1}{(C_2-C_1)C_\mu^{3/4}} \cdot \frac{\tilde{\rho}_p\bar{\alpha}}{\tilde{\rho}_f} \cdot \frac{\kappa\, x_2}{k^{1/2}\tau_m}$$

when the boundary value for ε, Eq. (3.3.7), is substituted for. The characteristic time scale for energy-containing eddies close to the wall is:

$$T = \sqrt{\frac{3}{2}}\,\frac{\kappa\, x_2}{k^{1/2}}$$

Therefore:

$$I_\sigma = 10.35 \frac{\tilde{\rho}_p \bar{\alpha}}{\tilde{\rho}_f} \cdot \frac{T}{\tau_m}$$

Thus, in the limit of large τ_m/T, it is possible to neglect the particle effects on σ_ε if:

$$\bar{\alpha} << 0.096 \frac{\tilde{\rho}_f}{\tilde{\rho}_p} \cdot \frac{\tau_m}{T} \qquad (3.3.9)$$

with the fluid time scale (T) defined on the basis of a linearly variable wall length scale and the local velocity scale.

3.4 Boundary conditions for the particulate phase

In most practical flows of interest where the flow domain is bounded by the solid walls, the complexity of the particle behavior at the walls has been an important factor hindering the development of numerical, and analytical, schemes for predicting two-phase solid-fluid flows. Such developments require a fundamental and thorough knowledge about the nature of solid particle-solid wall interactions in terms of the flow, particle, wall variables and characteristics. Recent developments in experimental methods and, specifically, the introduction of non-intrusive optical measurement techniques such as the laser-Doppler aremometer have increased the potential for acquiring such fundamental knowledge in wall regions of two-phase flows.

Derivation of the exact boundary conditions for the particulate phase requires an evaluation of the probability distribution function from a Boltzman-type equation for the particulate phase, as well as

knowledge about the laws governing particle rebound from the wall upon impact, as indicated by Yeung [1978]. However, due to the complexities involved and the lack of basic information, such a derivation has not been conducted yet. It should be noted that for fluid flow over solid walls, a zero slip boundary condition is not the exact condition but is only approximately true. In reality, the exchange of tangential momentum associated with the gas molecules rebounding from the wall gives rise to a velocity component parallel to and in the vicinity of the wall. This slip velocity is approximately equal to, White [1974]:

$$U_{f_w} \approx 0.75\, MC_f\, U_{f_\infty}$$

where M, C_f and U_{f_∞} represent the Mach number, friction coefficient and the free-stream velocity, respectively. Therefore, the slip velocity becomes very small for subsonic flows and for all practical purposes the zero slip velocity presents a satisfactory approximation for the fluid boundary condition on the solid boundary.

For the particulate flow, it has been observed that in the vicinity of solid walls, the particles do experience a non-trivial slip velocity parallel to the wall. This is evidenced by the experiments of many investigators among which are: Lee and Einav [1972] for flow on the flat wall, Stukel and Soo [1969] channel flow and Soo and Trezek [1966] for pipe flow. A brief survey on turbulent pipe flows and the associated well slip has been presented by Wakstein [1970]. Based on the assumption of potential flow, Soo and Tien [1955] have analyzed the motion of a single particle near a solid wall. In that investigation, the motion of the particle near the wall was assumed to be equivalent

to that of the particle and its virtual image with respect to the wall. Results are then obtained by incorporation of the Stokes viscous drag and the Bernoulli mutual force in the equations of motion. The results are valid for the cases when the ratio $d_p/2y_o$ becomes very small, with y_o being the typical distance from the wall. Further discussion of the Bernoulli forces which are caused by the relative motion of two spherical particles will be provided further on in the text.

Rarefied gas analogy for dilute suspensions

It is generally known for the flow of a rarefied gas over solid surfaces that a finite slip occurs at the wall as noted by Lugt and Schot [1974]. In these flows the mean free path of the gas molecules is of the order of, or larger than, some characteristic length associated with the solid wall, which can be identified as a pore diameter, or the height of a local roughness on the solid wall. Thus, although in the near wall regions continuum can not rigorously be assumed, it is generally agreed that the governing equation, such as the Navier-Stokes equations for Newtonian fluids, can still be applied with the slip boundary condition for tangential velocity at the wall imposed, as argued by Sherman [1969].

In dilute fluid-solid particle suspensions with the particle cloud governed by continuum equations, an analogous situation at the walls exists, where particle-particle collision becomes negligible compared to the collisions with the wall as argued by Soo [1962]. The analogy is not complete due to the obvious differences between the physical and

dynamical characteristics of macroscopic solid particles and microscopic gas molecules. However, in the absence of more rigorous expressions, such an analogy can be utilized to define an approximate boundary condition for the particulate phase. The agreement between predictions and measurements of Soo and Tung [1972] and Stukel and Soo [1969] justifies the application of rarefied-gas type boundary condition for the dilute particulate phase.

The slip velocity and the wall shear stress for the particulate phase are, respectively, defined by Stukel and Soo [1969] and Soo [1962] as:

$$\left(U_{p_w}\right)_j = L_{pF}\left(\Delta_{p_w}\right)_j + U_{p_o}\left(1 - \frac{L_s}{\tau_m U_{p_o}}\right)\delta_{js} \qquad (3.4.1)$$

and,

$$\left(\tau_{p_w}\right)_j = \frac{1}{2\sqrt{\pi}}\,\rho_{p_w}\left(\overline{U}_{p_w}\right)_j\left(\overline{u^2}_{p_w}\right)^{1/2} \qquad (3.4.2)$$

In Eq. (3.4.1) L_{pF} is the fluid-particle interaction length defined by Eq. (3.1.9), and (Δp_w) is the deformation rate for the particulate phase at the wall with x_j and x_s representing coordinates along the parallel and the stream-wise directions with respect to the wall. The second term in Eq. (3.4.1) is due to initial particle inertia effects which cause slip at the walls in the entrance regions of straight channels, Stukel and Soo [1969], or flat walls, Soo [1968]. It should be incorporated in the regions with distances from the leading edge L_s which satisfy the condition;

$$0 \leq L_s \leq U_{p_o} \tau_m \qquad (3.4.3)$$

where U_{f_o} represents the fluid entrance velocity to the pipe or channel.

The quantity $U_{p_o}\tau_m$ in Eq. (3.4.3) represents characteristic equilibrium length scale for the particulate phase. The appearance of the particle turbulent intensity for the wall region, U_{p_w}, in Eq. (3.4.2) implies that the momentum exchange with the wall is carried out by turbulent diffusion of solid particles through the viscous sublayer. This is consistent with the assumption of a relatively large particulate mean free path to maintain the analogy with a rarefied gas; since a large mean free path is associated with a longer retention of memory effects coming from regions outside the viscous sublayer in momentum exchange with the wall.

Equations (3.4.1), (3.4.2), and the condition of zero normal velocity constitute a set of boundary conditions which can be incorporated in the particle momentum equations in the cases where depositions or accumulation of the particles by the mean motion is not considered. It should be noted that the cases of non-vanishing normal mean particle velocity at the wall are associated with unsteady wall deposition which will not be considered in this work.

CHAPTER 4

SECOND-ORDER CLOSURE FOR FLUID-PARTICLE CORRELATION TERMS

In the previous chapters the transport equations for the fluid and particulate phases were presented. Furthermore, the boundary conditions were introduced and the related expressions were discussed. The second-order correlation terms in the continuity and momentum equations for the particulate phase were expressed through the analogy with single phase flow constitutive relations. The closure for various fluid correlation terms are discussed in Appendix II which describes the k-ε model of turbulence. In this chapter various fluid-particle correlation terms appearing in the fluid transport equations for k and ε (presented earlier) will be discussed, and alternate modeled expressions will be derived, thus making the problem of predicting two-phase fluid-particulate flow tractable.

The appearance of fluid-particle correlation terms in the governing equations is due to dynamical coupling effects of the phases. Therefore, it is required that in the limit of perfectly responsive particles (essentially zero response time), particles dynamics are in perfect accord with neighboring fluid element motion and all fluid-particle velocity correlations are equivalent to corresponding fluid-fluid correlation terms. On the other hand, for particles with large response time scales the fluid-particle correlation diminishes and the turbulent motion of the phases become essentially independent. The two limiting behaviors of the fluid-particle correlation terms as discussed

above constitute necessary, but not sufficient, criteria for examining the validity of the modeled expressions derived here.

4.1 The Correlation $\overline{u_{f_i} u_{p_i}}$ (k Equation)

The following analysis is based on the equation of motion for a single spherical particle with the Stokes drag as the only driving force. The equation of motion is obtained from Eq. (2.1.1) by neglecting all terms except for viscous drag. A modeled form of this equation will be valid for flows where the neglected terms have a minimal effect. Thus, Eq. (2.1.1) yields:

$$\frac{dU_{p_i}}{dt} = \frac{U_{f_i} - U_{p_i}}{\tau_m} \tag{4.1.1}$$

from which, using Reynolds decomposition (for example, $U_{f_i} = \overline{U}_{f_i} + u_{f_i}$) an equation of motion for the fluctuating velocity component, u_{p_i}, is obtained:

$$\frac{du_{p_i}}{dt} = \frac{u_{f_i} - u_{p_i}}{\tau_m} \tag{4.1.2}$$

For the flows of interest here it may be assumed that the flow field is stationary with respect to time and, therefore, the ensemble-averaged quantities become equivalent to their corresponding time-averaged quantities, with the ensemble averaging process taken over many independent particles which is possible for dilute conditions.

The solution to Eq. (4.1.2) is; Drew [1976]:

$$u_{p_i}(t) = \frac{e^{-t_o/\tau_m}}{\tau_m} \int_{t_o}^{t} e^{t'/\tau_m} u_{f_i}(t')dt' + u_{p_i}(t_o)\, e^{-t/\tau_m} \tag{4.1.3}$$

with t_o as the initial time for the onset of particle motion. In Eq. (4.1.3), the integration is along the trajectory of the particle. Using the transformation $\xi = t-t'$, Eq. (4.1.3) can be re-written as:

$$u_{p_i}(t) = \frac{1}{\tau_m} \int_{0}^{t-t_o} e^{-\xi/\tau_m} u_{f_i}(t-\xi)d\xi + u_{p_i}(t_o)\, e^{-(t-t_o)/\tau_m} \tag{4.1.4}$$

After multiplying both sides of Eq. (4.1.4) by $u_{f_i}(t)$ and ensemble averaging over a large number of independent particles, the following result is obtained:

$$\overline{u_{f_i} u_{p_i}} = \frac{1}{\tau_m} \int_{0}^{\Delta t} e^{-\xi/\tau_m} \overline{[u_{f_i}(t-\xi)u_{f_i}(t)]}d\xi + \overline{u_{p_i}(t_o)u_{f_i}(t)}\, e^{-\Delta t/\tau_m} \tag{4.1.5}$$

where:

$$\Delta t = t - t_o$$

represents the travelling time period for the particles. In the derivation of Eq. (4.1.5), $u_{f_i}(t)$ has been carried inside the integral since it is independent of ξ. In order to avoid the initial

transient effects in the integration of Eq. (4.1.5), Δt must be a time scale larger than that characterizing local velocity fluctuations. This condition is given by:

$$\Delta t \gg \tau_m \tag{4.1.6}$$

and leads to a negligible contribution from the second term on the right side of Eq. (4.1.5). Thus, to a good approximation:

$$\overline{u_{f_i} u_{p_i}} = \frac{1}{\tau_m} \int_0^{\Delta t} e^{-\xi/\tau_m} \left[\overline{u_{f_i}(t-\xi) u_{f_i}(t)}\right] d\xi \tag{4.1.7}$$

Thus, for obtaining an analytical expression for $\overline{u_{f_i} u_{p_i}}$, the form of $\overline{u_{f_i}(t-\xi) u_{f_i}(t)}$ must be specified. This term expresses the correlation between fluid velocity fluctuations of fluid elements which at time t pass through the particle location of interest (Point A in Fig. 4.1), and at time $t-\xi$ (earlier) were surrounding the same particle at some other location in space. In general, since the particles do not remain in the vicinity of their initial fluid elements and "over-shoot" to different fluid elements, the correlation becomes a complicated expression. The problem can be simplified if Tchen [1947] assumption is incorporated that the particle remains in the vicinity of the same fluid element.

In this case:

$$\overline{u_{f_1}(t-\xi) u_{f_1}(t)} = \overline{u_{f_1}^2} R_{f_L}(\xi) \tag{4.1.8}$$

with R_{f_L} representing the Lagrangian correlation coefficient for fluid phase. In Eq. (4.1.8) it is assumed that:

$$\overline{u_{f_1}^2} = \overline{u_{f_1}^2(t-\xi)} = \overline{u_{f_1}^2}$$

for stationary turbulence. Furthermore, by the assumption of local isotropy:

$$\overline{u_{f_1}^2} = \overline{u_{f_2}^2} = \overline{u_{f_3}^2} = \overline{u_f^2} = \frac{2}{3}k \qquad (4.1.10)$$

The Langrangian microscale (τ_L) and the integral time scales (T_L) are respectively defined as:

$$\frac{1}{\tau_L^2} = -\frac{1}{2}\left(\frac{d^2R_{f_L}}{d\xi^2}\right)_{\xi=0} \qquad (4.1.11)$$

and

$$T_L = \int_0^\infty R_{f_L}(\xi)\, d\xi \qquad (4.1.12)$$

At high Reynolds numbers τ_L becomes very small compared to T_L. For such conditions it has been argued, Hinze [1975] and Tennekes and Lumley [1972], that it is a good approximation to take:

$$R_{f_L}(\xi) = e^{-\xi/T_L} \quad \text{with} \quad \xi \geq 0 \qquad (4.1.13)$$

The exponential form for $R_{f_L}(\xi)$ has been shown by Kalinske and Pien [1944] to be in good agreement with experimental data obtained by the same authors. Furthermore, the adoption of an exponential form is not unprecedented since it has been incorporated by G. I. Taylor in the development of his theory of "diffusion by continuous movements", Taylor [1921].

Substituting Eq. (4.1.13) in Eq. (4.1.7) yields:

$$\overline{u_{f_i} u_{p_i}} = \overline{3u_f^2} \cdot \frac{T_L}{\tau_m + T_L} \cdot \left[1 - e^{-\Delta t \left(\frac{1}{\tau_m} + \frac{1}{T_L} \right)} \right] \qquad (4.1.14)$$

In line with the arguments presented earlier it is required that:

$$\Delta t \gg T_L$$

for which, it is found:

$$\overline{u_{f_i} u_{p_i}} = \overline{3u_f^2} \, \frac{T_L}{\tau_m + T_L} \qquad (4.1.15)$$

This equation is an expression for the fluid-particle velocity correlation at a fixed point in space, and is a function of the flow field variables at that point. Substituting Eq. (4.1.10) into (4.1.15) yields:

$$\overline{u_{f_i} u_{p_i}} = 2k \, \frac{T_L}{\tau_m + T_L} \qquad (4.1.16)$$

As discussed earlier it is necessary to investigate the limiting behaviors of the correlation given by Eq. (4.1.15). Deviations of this relation from expected limiting values will establish its limitations and applicability.

a) <u>The limit of perfect response</u>

In this limit the response time scale of the particulate phase, τ_m, becomes small compared to the turbulent fluid local time scale, T_L. This situation is representative of very small particles suspended in highly viscous flows. Equation (4.1.15) can be written as:

$$\overline{u_{f_i} u_{f_i}} = \frac{3\overline{u_f^2}}{1 + \frac{\tau_m}{T_L}} \tag{4.1.17}$$

which, in turn, can be expanded for small τ_m/T_L values to give:

$$\overline{u_{f_i} u_{p_i}} = 3\overline{u_f^2}\left[1 - \frac{\tau_m}{T_L} + \left(\frac{\tau_m}{T_L}\right)^2 - \ldots\right] \tag{4.1.18}$$

for $\tau_m/T_L \ll 1$.

Equation (4.1.18) indicates that, due to their small response time, particles adjust dynamically to fluid fluctuations and, therefore, will display the dynamic characteristics of surrounding fluid element.

b) The limit of no-response

In this case, the particle time scale becomes much larger than the local time scale of the fluid. This corresponds to cases of large inertial particles suspended in inviscid fluids. Therefore, a relatively weak correlation between the phases is to be expected. Equation (4.1.15) can be re-written as:

$$\overline{u_{f_i} u_{p_i}} = 3\overline{u_f^2}\,\frac{T_L/\tau_m}{T_L/\tau_m + 1} \tag{4.1.19}$$

which can be expanded for small T_L/τ_m values as:

$$\overline{u_{f_i} u_{p_i}} = 3\overline{u_f^2}\left(\frac{T_L}{\tau_m}\right)\left[1 - \frac{T_L}{\tau_m} + \left(\frac{T_L}{\tau_m}\right)^2 - \ldots\right] \tag{4.1.20}$$

Equation (4.1.20) shows that a weak correlation between fluid and particle velocity fluctuations arises for $T_L/\tau_m \ll 1$, as was expected. Thus, it is seen that the correlation given by Eq. (4.1.15) does indeed yield the correct limiting behavior of relative motion between the two phases.

At high Reynolds numbers, it has been shown that for short diffusion times of marked fluid elements, Hinze [1976]:

$$R_{f_L}(t) = 1 - C \frac{\epsilon t}{\overline{2u_f^2}} \tag{4.1.21}$$

In which C is a constant of order unity. The expression for $R_{f_L}(t)$ in Eq. (4.1.13) is then expanded as:

$$R_{f_L}(t) = 1 - \frac{t}{T_L} + 0\left(\frac{t}{T}\right)^2 \tag{4.1.22}$$

and a comparison between Eqs. (4.1.21) and (4.1.22) results in:

$$T_L = \frac{1}{C} \frac{\overline{2u_f^2}}{\epsilon} \tag{4.1.23}$$

The constant C must be evaluated from experimental data. Although direct measurements of the constant are not available at the present time, it can be determined from a knowledge of the relative ratio of the isotropic Lagrangian and Eulerian integral length scales, given by:

$$\beta_1 = \frac{\Lambda_L}{\Lambda_f} \tag{4.1.24}$$

Substitution of functional forms for Λ_L and Λ_f taken yields, Hinze [1975]:

$$\beta_1 = \frac{1.36}{\alpha \cdot C} \tag{4.1.25}$$

where $\alpha \approx 0.4$ is the Heisenberg constant and the numerical value of the constant β_1 depends on the type of flow. Most experimental results show a decrease in β_1 with an increase in the Reynolds number. In Table 4.1 various values of β_1 are shown.

Corrsin [1963] has proposed $\beta_1 \approx 2/3$. A value of $\beta_1 \approx 1.02$ corresponding to the investigation of Shlien and Corrsin [1974] provides a reasonably moderate estimate for this parameter. Incorporation of this value in Eq. (4.1.25) yields the corresponding estimate for $C = 3.33$. Substituting $C = 3.33$ into Eq. (4.1.23) yields:

$$T_L = C_T \, k/\varepsilon \tag{4.1.26}$$

with $C_T = 0.41$. Finally, substitution of Eq. (4.1.26) for T_L into Eq. (4.1.16) yields an explicit function of $\overline{u_{f_i} u_{p_i}}$ in terms of flow field variables calculable by the numerical algorithm.

It should be noted that in relation to the above derivations, Danon et al. [1977] proposed an exponential form for $\overline{u_{f_i} u_{p_i}}$. Their postulation was based on observations of the limiting values of $\overline{u_{f_i} u_{p_i}}$. Since the proposed form of their correlation is not rigorous (in fact it is a form constructed to satisfy the limiting conditions), its validity at intermediate values of τ_m/T_L is questionable.

Table 4.1

Investigator	Flow Condition	Reynolds Number	β_1
Uberoi and Corrsin [1953]	flow behind the grid	$Re_\lambda = 10$	$\simeq 2$
		$Re_\lambda = 100$	$\simeq 0.8$
Mickelsen [1955]	pipe flow	$Re_D \simeq 5 \times 10^5$	$\simeq 1.6$
Hay and Pasquil [1959]	atmospheric diffusion		$\simeq 0.15 - 0.6$
Shlien and Corrsin [1974]	flow behind the grid	$Re_{\lambda g} = 71.6$	$\simeq 1.02$
Snyder and Lumley [1971]	flow behind the grid	$Re_{grid} = 10^4$	$\simeq 0.4$

4.2 Particle Turbulent Kinetic Energy (k_p)

Whereas the transport equation for k_p has already been derived, the complexity of various second- and third-order correlation terms prevent its direct solution. From Eq. (4.1.4) for the particle fluctuating velocity, an algebraic expression for particle turbulent kinetic energy, $k_p = 1/2\ \overline{u_{p_i}^2}$, may be obtaied in terms of local variables.

Multiplying Eq. (4.1.4) by itself and ensemble averaging the results yields:

$$\overline{u_{p_i}^2} = \frac{1}{\tau_m^2} \int_0^t \int_0^\xi e^{-(\xi+\xi')/\tau_m} \overline{u_{f_i}(t-\xi) u_{f_i}(t-\xi')}\, d\xi\, d\xi' \quad (4.2.1)$$

The variables ξ and ξ' are independent and the term containing the initial condition is neglected following the same arguments which lead to Eq. (4.1.7).

Similarly, the high Reynolds number assumption leading to Eq. (4.1.3) gives for the present case:

$$\overline{u_{f_i}(t-\xi) u_{f_i}(t-\xi')} = \overline{u_f^2}\, e^{-(\xi-\xi'/\tau_m)} \quad (4.2.2)$$

Defining;

$$\xi - \xi' = \tau$$

Equation (4.2.1) becomes:

$$\overline{u_{p_i}^2(t)} = \frac{\overline{2u_{f_i}^2}}{\tau_m} \int_0^t d\xi \int_0^\xi e^{-\frac{2\xi}{\tau_m} + \left(\frac{1}{\tau_m} - \frac{1}{T_L}\right)\tau} d\tau \qquad (4.2.3)$$

Integration of this equation gives:

$$\overline{u_{p_i}^2(t)} = \overline{u_{f_i}^2(t)} \frac{T_L}{\tau_m(\tau_m - T_L)} \left[\tau_m\left(1-e^{-2t/\tau_m}\right) - \frac{2\tau_m T_L}{\tau_m + T_L}\left(1-e^{-t(1/\tau_m+1/T_L)}\right)\right] \qquad (4.2.4)$$

For large t values the stationary solution obtained is:

$$\overline{u_{p_i}^2} = \overline{u_{f_i}^2} \frac{T_L}{\tau_m + T_L} \qquad (4.2.5)$$

or equivalently:

$$k_p = k \frac{T_L}{\tau_m + T_L} \qquad (4.2.5a)$$

Equation (4.2.5) shows the same functional relationship as Eq. (4.1.15) for $\overline{u_{f_i} u_{p_i}}$. Hence, the results for the limiting behaviors of $\overline{u_{f_i} u_{p_i}}$ are also valid here; that is, for small τ_m/T_L values large $\overline{u_{p_i}^2}$ values are obtained and vice versa. Therefore, adoption of Eq. (4.2.5) implies that the fluid turbulence is the only source of energy for particulate turbulence and the turbulence energy exchange process between the phases is through viscous interaction.

4.3 Fluid-Particle Velocity Correlation Coefficient R_{f-p}

The fluid-particle velocity correlation coefficient at a fixed point is defined as:

$$R_{f-p} \equiv \frac{\overline{u_{f_1} u_{p_1}}}{\tilde{u}_{f_1} \cdot \tilde{u}_{p_1}} \tag{4.3.1}$$

which, by substitution from Eq. (4.1.15) and (4.2.5) yields:

$$R_{f-p} = \left(\frac{1}{1+\tau}\right)^{1/2}$$

in Eq. (4.3.2) is analogous to the non-dimensional distance ratio which appears in two-point spatial Eulerian correlations, or the non-dimensional time ratio appearing in temporal Lagrangian correlations.

4.4 Fluid-Particle Interaction Length Scale (L_{f-p})

The fluid-particle interaction length scale defined by Eq. (3.1.9) can be re-written, assuming local isotropy, as:

$$L_{f-p} = \tau_m \left[\overline{(u_f - u_p)^2}\right]^{1/2} \tag{4.4.1}$$

with:

$$\overline{u_f^2} = \frac{2}{3} k$$

$$\overline{u_p^2} = \frac{2}{3} k_p$$

Equation (4.4.1) may be re-written as:

$$L_{f-p} = \tau_m \left(\overline{u_f^2} + \overline{u_p^2} - 2\overline{u_f u_p}\right)^{1/2} \qquad (4.4.2)$$

and substitution from Eqs. (4.1.16) and (4.2.5) results in:

$$L_{f-p} = \left(\frac{2}{3} k\right)^{1/2} \frac{\tau_m^{3/2}}{(\tau_m + T_L)^{1/2}} \qquad (4.4.3)$$

which expresses the interaction length scale L_{f-p} in terms of various known field variables.

4.5 The Correlation $\overline{\partial u_{f_i}/\partial x_j \;\; \partial u_{p_i}/\partial x_j}$ (ε equation)

In order to close the transport equation for dissipation of kinetic energy, ε, the correlation term

$$\overline{\frac{\partial u_{f_i}}{\partial x_j} \frac{\partial u_{p_i}}{\partial x_j}}$$

must be modeled in terms of known field variables. In this section, an expression for the term is derived which will be examined in its dynamical limits. In the process of the derivation the results of the preceeding sections will be extensively used.

It is assumed here that the variables u_{f_i}, u_{p_i} and u_{f_i} u_{p_i} are continuous and differentiable with finite values in space. Using Taylor series expansion, it can be shown that:

$$u_{f_i}{}_{(b)} - u_{f_i}{}_{(a)} = \left(\frac{\partial u_{f_i}}{\partial x_\ell}\right)_{(a)} \Delta x_\ell + O(\Delta x_\ell)^2 \qquad (4.5.1)$$

and

$$u_{p_i}{}_{(b)} - u_{p_i}{}_{(a)} = \left(\frac{\partial u_{p_i}}{\partial x_\ell}\right)_{(a)} \Delta x_\ell + O(\Delta x_\ell)^2 \qquad (4.5.2)$$

For purposes of the analysis attention is restricted here to the case where $i = 1$, and $\ell = 2$ only corresponding to Figure 4.3. This figure shows two points (a) and (b) separated in space by a distance Δx_2 which is assumed to be small compared to the local length scale of the flow. Combining Eqs. (4.5.1), (4.5.2) and time-averaging, the result yields:

$$\left(\overline{\frac{\partial u_{f_1}}{\partial x_2}\,\frac{\partial u_{p_1}}{\partial x_2}}\right)_{(a)} =$$

$$\text{limit}\ \frac{1}{(\Delta x_2)^2}\left[\overline{u_{p_1}{}_{(b)}\,u_{f_1}{}_{(b)}} + \overline{u_{p_1}{}_{(a)}\,u_{f_1}{}_{(a)}} - \overline{u_{p_1}{}_{(a)}\,u_{f_1}{}_{(b)}} - \overline{u_{p_1}{}_{(b)}\,u_{f_1}{}_{(a)}}\right]$$

$$\text{as}\ \Delta x_2 \to 0 \qquad (4.5.3)$$

in which x_1 and x_2 refer to the stream-wise and lateral coordinate directions. Extra terms of the order of Δx_2, and higher powers, will also appear on the right hand side of Eq. (4.5.3) but disappear as the indicated limit is approached.

From Eq. (4.1.6) at point (a):

$$\overline{u_{f_1(a)} u_{p_1(a)}} = \frac{2}{3} k \frac{T_{L_{(a)}}}{T_{L_{(a)}} + \tau_m} \tag{4.5.4}$$

while at point (b) using the Taylor series expansion;

$$\overline{u_{f_1(b)} u_{p_1(b)}} = \frac{T_{L_{(a)}}}{T_{L_{(a)}} + \tau_m} \frac{2}{3} k_{(a)} + \frac{T_{L_{(a)}}}{T_{L_{(a)}} + \tau_m} \left(\frac{\partial k}{\partial x_2}\right)_{(a)} \Delta x_2 + \frac{2}{3} k_{(a)} \frac{\tau_m}{\left(T_{L_{(a)}} + \tau_m\right)^2} \left(\frac{\partial T_L}{\partial x_2}\right)_{(a)} \Delta x_2 + O(\Delta x_2)^2 \tag{4.5.5}$$

noting that τ_m is constant in space.

The correlation $\overline{u_{f_1(a)} u_{p_1(b)}}$ in Eq. (4.5.3) is one arising between the fluctuating fluid velocity at point (a) and that of the particle at point (b). A form for the correlation may be obtained as follows.

Rewriting Eq. (4.1.4) at point (b) gives:

$$u_{p_1(b)}(t) = \frac{1}{\tau_m} \int_0^{t-t_o} e^{-\xi/\tau_m} u_{f_1(b)}(t-\xi) d\xi + u_{p_1(b)}(t_o) e^{-(t-t_o)/\tau_m} \tag{4.5.6}$$

Multiplying both sides $u_{f_1}(t)$ and ensemble averaging, the result gives:

$$\overline{u_{p_1}(t)u_{f_1}(t)}_{(b)\ (a)} = \frac{1}{\tau_m}\int_0^{t-t_o} e^{-\xi/\tau_m}\,\overline{u_{f_1}(t-\xi)u_{f_1}(t)}_{(b)\ (a)}\,d\xi \tag{4.5.7}$$

in which it has been assumed that:

$$t - t_o \gg \tau_m$$

The evaluation of $\overline{u_{p_1}\ u_{f_1}}_{(b)\ (a)}$ from Eq. (4.5.7) requires knowledge of the correlation $\overline{u_{f_1}(t)u_{f_1}(t-\xi)}_{(a)\ (b)}$ which is the covariance between the Lagrangian velocity of a marked fluid particle at time $(t-\xi)$ with its trajectory passing through point (b) at time (t) [Fig. (4.3)]. The averaging process for $\overline{u_{f_1}(t)u_{f_1}(t-\xi)}_{(a)\ (b)}$ is an ensemble averaging which by substitution into Eq. (4.5.7) result in an ensemble averaged correla tion of fluid and particle velocities corresponding to the points (a) and (b) respectively. However, with the assumption of stationary flow the ensemble- and time-averaged values of $\overline{u_{f_1}(t)u_{p_1}(t)}_{(a)\ (b)}$ become identical.

As it has been pointed out, the evaluation of $\overline{u_{f_1}(t)u_{p_1}(t)}_{(a)\ (b)}$ requires a knowledge of the functional form of the velocity correlation $\overline{u_{f_1}(t)u_{f_1}(t-\xi)}_{(a)\ (b)}$. Substitution in Eq. (4.5.7) of this function and further integration will yield an expression for $\overline{u_{f_1}(t)u_{p_1}(t-\xi)}_{(a)\ (b)}$.

The correlation $\overline{u_{f_1}(t)u_{f_1}(t-\xi)}$ is a "mixed" Eulerian-Langrangian correlation which is not readily evaluated. This prevents a development of the velocity correlation $\overline{u_{p_1}(t)u_{f_1}(t)}$ from Eq. (4.5.7). Hence, at this stage, it is necessary to seek alternatives for obtaining the correlation.

The Eulerian correlation coefficient for velocities at two points (a) and (b) is defined as:

$$R_{E_{112}} = \frac{\overline{u_{f_1}{}_{(a)} \; u_{f_1}{}_{(b)}}}{\tilde{u}_{f_1}{}_{(a)} \cdot \tilde{u}_{f_1}{}_{(b)}} \tag{4.5.8}$$

This can be approximated by its parabolic form, Hinze [1975] as:

$$R_{E_{112}} = 1 - \left(\frac{\Delta x_2}{\lambda_g}\right)^2 \tag{4.5.9}$$

for $\Delta x_2 \ll \lambda_g$

where λ_g is the Taylor lateral microscale defined as:

$$\frac{1}{\lambda_g^2} = -\frac{1}{2}\left[\frac{d^2 R_{E_{112}}}{d(\Delta x_2)^2}\right]_{\Delta x_2 = 0} \tag{4.5.10}$$

For the velocity correlation $\overline{u_{f_1}{}_{(a)} \; u_{p_1}{}_{(b)}}$ which is the correlation between the velocity of different material phases at different points in space, a correlation coefficient can be defined as:

$$R_{f_{1(a)}-p_{1(b)}} \equiv \frac{\overline{u_{f_{1(a)}} u_{p_{1(b)}}}}{\tilde{u}_{f_{1(a)}} \cdot \tilde{u}_{p_{1(b)}}} \tag{4.5.11}$$

In the previous section, it was shown that, at a single point fixed in space, the correlation coefficient between fluid and particle velocities is a function of τ_m/T_L which is analogous to the non-dimensional variable $\Delta x_2/\lambda_g$ in the Eulerian correlation coefficient, (Eq. (4.5.9), or to ξ/T_L in the Langrangian correlation coefficient, Eq. (4.1.13). Therefore, it is assumed that the correlation coefficient defined in Eq. (4.5.11) is a function of both independent variables τ_m/T_L and $\Delta x_2/\lambda_g$. Thus:

$$R_{f_{1(a)}-p_{1(b)}} = R\left(\frac{\tau_m}{T_{L(b)}}, \frac{\Delta x_2}{\lambda_g}\right) \tag{4.5.12}$$

For the determination of the function R in Eq. (4.5.12) it is necessary to derive its governing equation. This can be formed by appropriate algebraic manipulations of the equations governing fluid and particle fluctuating velocities. The result, however, is quite complex, and requires further closure for various higher order interaction terms arising between the material phases being at two different positions in space.

The approximate form for the Eulerian correlation coefficient as shown in Eq. (4.5.9) implies; that:

$$\Delta x_2 \ll \lambda_g$$

Therefore, for both the points (a) and (b), λ_g represents the local length scale.

Fluid-particle interactions at point (b) corresponding to the correlation in Eq. (4.5.12) imply a dependency on the local velocity time scale at point (b). Since direct particle-fluid interactions at point (b) affect the fluid turbulence at that point. These in turn will affect fluid fluctuations at point (a) due to the fluid-fluid correlation which exists between the two points. The argument, therefore, suggests a correlation between fluctuations of fluid velocity at (a) and fluctuations of particle velocity at (b). Therefore, the fluid time scale T_L in the correlation $\overline{u_{p_{1_{(b)}}} u_{f_{1_{(a)}}}}$, and the coefficient $R_{f_{1_{(a)}}-p_{1_{(b)}}}$ in Eq. (4.5.11), in Eq. (4.5.11), should be evaluated at the point where the particle perturbation are introduced into the correlation. Thus, the fluid time scale $T_{L_{(b)}}$ is chosen as the appropriate scale in the correlation coefficient defined by Eq. (4.5.11) and Eq. (4.3.12) and the parameter $\tau_m/T_{L_{(b)}}$ for the time scale ratio must appear in Eq. (4.5.12).

The correlation coefficient of Eq. (4.5.12) can be separated into two independent functions as:

$$R_{f_{1_{(a)}}-p_{1_{(b)}}}\left(\frac{\tau_m}{T_{L_{(b)}}}, \frac{\Delta x_2}{\lambda_g}\right) = \mathcal{T}\left(\frac{\tau_m}{T_{L_{(b)}}}\right) \cdot \chi\left(\frac{\Delta x_2}{\lambda_g}\right) \qquad (4.5.13)$$

In order to determine the functional forms of $\mathcal{T}$ and χ it is necessary to inspect the limiting values for the correlation coefficient of Eq. (4.5.11). These are:

$$\text{i)} \quad R_{f_{1_{(a)}}-p_{1_{(b)}}}\left(\frac{\tau_m}{T_{L_{(b)}}}, \frac{\Delta x_2}{\lambda_g}\right) \longrightarrow R_{E_{f_{1_{(a)}}-f_{1_{(b)}}}}\left(\frac{\Delta x_2}{\lambda_g}\right) \tag{4.5.14}$$

as;

$$\frac{\tau_m}{T_{L_{(b)}}} \longrightarrow 0$$

$$\text{ii)} \quad R_{f_{1_{(a)}}-p_{1_{(b)}}}\left(\frac{\tau_m}{T_{L_{(b)}}}, \frac{\Delta x_2}{\lambda_g}\right) \longrightarrow R_{f_{1_{(a)}}-p_{1_{(a)}}}\left(\frac{\tau_m}{T_{L_{(a)}}}\right) \tag{4.5.15}$$

as;

$$\frac{\Delta x_2}{\lambda_g} \longrightarrow 0$$

with the points (a) and (b) coinciding.

The correlation coefficient in Eq. (4.5.13) must satisfy the above boundary conditions. Comparing Eqs. (4.5.14) and (4.5.15) with (4.5.13) gives:

$$\chi\left(\frac{\Delta x_2}{\lambda_g}\right) = \frac{1}{\mathcal{T}(0)}\left[1 - \frac{(\Delta x_2)^2}{\lambda_g^2}\right] \tag{4.5.16}$$

and;

$$\mathcal{T}\left(\frac{\tau_m}{T_{L_{(b)}}}\right) = \frac{1}{\chi(0)} \left[\frac{1}{1+\tau_m/T_{L_{(b)}}}\right]^{1/2} \qquad (4.5.17)$$

In which the Eulerian and fluid-particle correlation coefficients from Eq. (4.5.9) and (4.3.2) are incorporated, respectively. The factors $\mathcal{T}(0)$ and $\chi(0)$ are non-zero constants and satisfy the conditions:

$$\mathcal{T}(0) \cdot \chi(0) = 1 \qquad (4.5.18)$$

Substitution of Eq. (4.5.6) and (4.5.17) in Eq. (4.5.13) yields:

$$R_{f_{1_{(a)}}-p_{1_{(b)}}} = \left[\frac{T_{L_{(b)}}}{T_{L_{(b)}}+\tau_m}\right]^{1/2} \cdot \left[1 - \frac{\Delta x_2^2}{\lambda_g^2}\right] \qquad (4.5.19)$$

and similarly:

$$R_{f_{1_{(b)}}-p_{1_{(a)}}} = \left(\frac{T_{L_{(a)}}}{T_{L_{(a)}}+\tau_m}\right)^{1/2} \cdot \left[1 - \frac{(\Delta x_2)^2}{\lambda_g^2}\right] \qquad (4.5.20)$$

It should be noted that the particular form of a parabolic Eulerian correlation coefficient, as introduced in Eq. (4.5.9), imposes no restrictions on the derivation procedure which could have been based on a more general $R_E(\Delta x_2)$ function. However, it is the parabolic form of this correlation which is of interest to this study as shown further on on this section.

The argument leading to Eq. (4.5.19) is based on the assumption that the variables which determine the correlation coefficient, $\Delta x_2/\lambda_g$ and τ_m/T_L, are independent of each other. Equation (4.5.19) shows that the correlation coefficient $R_{f_{1(a)}-p_{1(b)}}$ consists of the product of two functions each of which is smaller than, or at most equal to, unity. Therefore, the effect of either variable, spacial or interactional, is to reduce further the magnitude of the correlation. Figure 4.4 illustrates the correlation coefficient as given by Eq. (4.5.19).

Using Eq. (4.2.5) in combination with Eqs. (4.5.19) and (4.5.20) corresponding velocity correlations can be obtained and are given by:

$$\overline{u_{f_{1(a)}} u_{p_{1(b)}}} = \frac{2}{3}\left(k_{(a)} \cdot k_{(b)}\right)^{1/2} \cdot \frac{T_{L_{(b)}}}{T_{L_{(b)}} + \tau_m} \cdot \left[1 - \frac{(\Delta x_2)^2}{\lambda_g^2}\right] \quad (4.5.21)$$

and

$$\overline{u_{f_{1(b)}} u_{p_{1(a)}}} = \frac{2}{3}\left(k_{(a)} \cdot k_{(b)}\right)^{1/2} \cdot \frac{T_{L_{(a)}}}{T_{(a)} + \tau_m} \cdot \left[1 - \frac{(\Delta x_2)^2}{\lambda_g^2}\right] \quad (4.5.22)$$

At this point, with all the velocity correlation terms in Eq. (4.5.3) defined, the velocity gradient correlation term $\overline{\partial u_{f_1}/\partial x_2 \; \partial u_{p_1}/\partial x_2}$ can be obtained. Subsequently, summing over all indices the correlation term $\overline{\partial u_{f_i}/\partial x_j \; \partial u_{p_i}/\partial x_j}$ in ε-equation is obtained. The results which are required for the derivation are re-written as:

$$\overline{u_{f_{1_{(a)}}} u_{p_{1_{(a)}}}} = \frac{2}{3} k_{(a)} \cdot \frac{T_{L_{(a)}}}{T_{L_{(a)}} + \tau_m} \tag{4.5.23}$$

$$\overline{u_{f_{1_{(b)}}} u_{p_{1_{(b)}}}} = \frac{2}{3} k_{(b)} \cdot \frac{T_{L_{(b)}}}{T_{L_{(b)}} + \tau_m} \tag{4.5.24}$$

$$\overline{u_{f_{1_{(a)}}} u_{p_{1_{(b)}}}} = \frac{2}{3} [k_{(a)} \cdot k_{(b)}]^{1/2} \cdot \left[1 - \frac{(\Delta x_2)^2}{\lambda_g^2}\right] \cdot \frac{T_{L_{(a)}}}{T_{L_{(a)}} + \tau_m} \tag{4.5.25}$$

$$\overline{u_{f_{1_{(b)}}} u_{p_{1_{(a)}}}} = \frac{2}{3} [k_{(a)} \cdot k_{(b)}]^{1/2} \cdot \left[1 - \frac{(\Delta x_2)^2}{\lambda_g^2}\right] \cdot \frac{T_{L_{(a)}}}{T_{L_{(a)}} + \tau_m} \tag{4.5.26}$$

Using a Taylor series expansion, the variables at point (b) can be expressed in terms of corresponding variables at point (a). In this way:

$$T_{L_{(b)}} = T_{L_{(a)}} + \left(\frac{\partial T_L}{\partial x_2}\right)_{(a)} \Delta x_2 + \left(\frac{\partial^2 T_L}{\partial x_2^2}\right)_{(a)} \frac{\Delta x_2^2}{2} + \ldots \tag{4.5.27}$$

and

$$k_{(b)} = k_{(a)} + \left(\frac{\partial k}{\partial x_2}\right)_{(a)} \Delta x_2 + \left(\frac{\partial^2 k}{\partial x_2^2}\right)_{(a)} \frac{\Delta x_2^2}{2} + \ldots \tag{4.5.28}$$

hence:

$$k_{(b)}^{1/2} = k_{(a)}^{1/2}\left[1 + \frac{1}{2k_{(a)}}\left(\frac{\partial k}{\partial x_2}\right)_{(a)}\Delta x_2 + \left[\frac{1}{4k_{(a)}}\left(\frac{\partial^2 k}{\partial x_2^2}\right)_{(a)} - \frac{1}{8k_{(a)}^2}\left(\frac{\partial k}{\partial x_2}\right)_{(a)}^2\right]\Delta x^2 + \ldots\right] \tag{4.5.29}$$

Equation (4.5.29) is obtained by using a binomial series expansion with the assumption that:

$$\left|\frac{1}{k_{(a)}}\left(\frac{\partial k}{\partial x_2}\right)_{(a)}\Delta x_2 + \frac{1}{k_{(a)}}\left(\frac{\partial^2 k}{\partial x_2^2}\right)_{(a)}\frac{\Delta x_2^2}{2} + \ldots\right| \leq 1 \tag{4.5.30}$$

which is the case for small $\Delta x_2/\ell$. The quantity ℓ represents the fluid local integral length scale. It characterizes the distance over which significant variations in mean values are expected. Thus, we may expect:

$$\frac{\partial k}{\partial x_2} = 0\left(\frac{k}{\ell}\right) \tag{4.5.31}$$

It has been assumed in the analysis that $\Delta x_2 << \lambda_g$ and an expression for λ_g/ℓ given by Tennekes and Lumley [1972] is:

$$\frac{\lambda_g}{\ell} \simeq \frac{A}{Re^{1/2}} \tag{4.5.32}$$

It is seen that at high Reynolds number the condition for inequality (4.5.30) is established.

Likewise:

$$\frac{T_{L_{(b)}}}{\tau_m+T_{L_{(b)}}} = \frac{T_{L_{(a)}}}{\tau_m+T_{L_{(a)}}} \cdot \left[1 + \frac{\tau_m}{T_{L_{(a)}}(\tau_m+T_{L_{(a)}})} \left(\frac{\partial T_L}{\partial x_2}\right)_{(a)} \Delta x_2 \right.$$

$$\left. + \frac{\tau_m}{2T_{L_{(a)}}(\tau_m+T_{L_{(a)}})} \left(\frac{\partial^2 T_L}{\partial x_2^2}\right)_{(a)} \Delta x_2^2 - \frac{\tau_m}{T_{L_{(a)}}(\tau_m+T_{L_{(a)}})^2} \left(\frac{\partial T_L^2}{\partial x_2}\right)_{(a)} \Delta x_2^2 + O(x_2)^3 \right]$$

(4.5.33)

which requires that:

$$\left| \frac{1}{T_{L_{(a)}}} \left(\frac{\partial T_L}{\partial x_2}\right)_{(a)} \Delta x_2 + \frac{1}{2T_{L_{(a)}}} \left(\frac{\partial^2 T_L}{\partial x_2^2}\right)_{(a)} \Delta x_2^2 + \ldots \right| \leq 1$$

which is similarly established along the lines of the preceeding arguments.

Substitution of Eqs. (4.5.27)-(4.5.33) in Eqs. (4.5.23)-(4.5.26) and final substitution in Eq. (4.5.3) results in an expression for increasing powers of Δx_2 which should be taken to its limit. After some algebraic manipulation, terms of the order $(\Delta x_2)^0$ and $(\Delta x_2)^1$ are eliminated and the remaining terms are of order $(\Delta x_2)^2$ and higher powers. Therefore, taking the limit $\Delta x_2 \to 0$, the following result is obtained:

$$\left(\overline{\frac{\partial u_{f_1}}{\partial x_2}\frac{\partial u_{p_1}}{\partial x_2}}\right)_{(a)} = \frac{1}{3}\frac{\tau_m}{[\tau_m+T_{L_{(a)}}]}\left(\frac{\partial k}{\partial x_2}\right)_{(a)}\left(\frac{\partial T_L}{\partial x_2}\right)_{(a)}$$

$$+\frac{1}{6k_{(a)}}\frac{T_{L_{(a)}}}{\tau_m+T_{L_{(a)}}}\left(\frac{\partial k}{\partial x_2}\right)^2_{(a)}+\frac{4}{3}\frac{k_{(a)}T_{L_{(a)}}}{\tau_m+T_{L(a)}}\times\frac{1}{\lambda_g^2} \qquad (4.5.34)$$

By using the assumption of local isotropy and summing over all coordinate indices, the following result is obtained:

$$\left(\overline{\frac{\partial u_{f_i}}{\partial x_\ell}\frac{\partial u_{p_i}}{\partial x_\ell}}\right)_{(a)} = \frac{\tau_m}{[\tau_m+T_{L_{(a)}}]^2}\left(\frac{\partial k}{\partial x_\ell}\right)_{(a)}\left(\frac{\partial T_L}{\partial x_\ell}\right)_{(a)}$$

$$+\frac{1}{2k_{(a)}}\frac{T_{L_{(a)}}}{\tau_m+T_{L_{(a)}}}\left(\frac{\partial k}{\partial x_\ell}\right)^2_{(a)}+\frac{10k_{(a)}T_{L_{(a)}}}{\tau_m+T_{L_{(a)}}}\cdot\frac{1}{\lambda_g^2} \qquad (4.5.35)$$

In the last term of Eq. (4.5.35) the relation for streamwise Taylor microscale (λ_f) given by Hinze [1975];

$$\lambda_f = \sqrt{2}\,\lambda_g \qquad (4.5.36)$$

is used.

In line with the earlier arguments for high Reynolds numbers;

$$\lambda_f \ , \ \lambda_g \ll \ell$$

This allows the second term on the right-hand side of the Eq. (4.5.35) to be neglected. That this is the case can be shown by evaluating the order of magnitude of the second and the third terms on the right side of Eq. (4.5.35), that is:

$$\frac{1}{2k} \ \frac{T_L}{\tau_m+T_L} \left(\frac{\partial k}{\partial x_\ell}\right)^2 \ = \ 0\left(\frac{k}{\ell^2}\right) \cdot \frac{T_L}{\tau_m+T}$$

and:

$$10k \ \frac{T_L}{\tau_m+T_L} \cdot \frac{1}{\lambda_g^2} \ = \ 0 \ \frac{k}{\lambda_g^2} \cdot \frac{T_L}{\tau_m+T_L}$$

Hence the ratio of the second to the third term in Eq. (4.3.35) becomes of the order of $(\lambda_g/\ell)^2$ which is very small at high Reynolds numbers.

Equation (4.5.35) simplifies to:

$$\overline{\frac{\partial u_{f_i}}{\partial x_\ell} \frac{\partial u_{p_i}}{\partial x_\ell}} \ = \ \frac{\tau_m}{(\tau_m+T_L)^2} \ \frac{\partial k}{\partial x_\ell} \ \frac{\partial T_L}{\partial x_\ell} \ + \ 10k \ \frac{T_L}{\tau_m+T_L} \cdot \frac{1}{\lambda_g^2} \qquad (4.5.37)$$

which is used for the closure of the transport equation for fluid dissipation of turbulent kinetic energy in Eq. (4.5.37) the transverse Taylor microscale is given by:

$$\lambda_g = (10\nu \frac{k}{\varepsilon})^{1/2} \tag{4.5.38}$$

see Hinze [1975].

In order to be certain of the validity of Eq. (4.5.37) it is essential to investigate its limiting behavior. The limiting expressions for this correlation should become identical to the specific relations corresponding to the properties of the correlation term, when the limits are approached. The two cases are investigated below.

The no-response limit ($\tau_m \gg T_L$)

In this limit, the particle does not respond to the neighboring fluid velocity fluctuations and this is expected to result in a weak correlation. From Eq. (4.5.37) it can be seen that:

$$\overline{\frac{\partial u_{f_i}}{\partial x_\ell} \frac{\partial u_{p_i}}{\partial x_\ell}} \to 0 \tag{4.5.39}$$

$$\text{as} \quad \frac{\tau_m}{T_L} \to \infty$$

which is the expected behavior for this limiting condition.

The perfect-response limit ($\tau_m \ll T_L$)

This limit corresponds to an almost perfectly responsive particles in the fluid, with no distinction between the dynamics of the particulate phase and the neighboring fluid elements. Hence from Eq. (4.5.37) it is seen that:

$$\overline{\frac{\partial u_{f_i}}{\partial x_\ell}\frac{\partial u_{p_i}}{\partial x_\ell}} \rightarrow 10\frac{k}{\lambda_g^2} \qquad (4.5.40)$$

$$\text{as} \quad \frac{\tau_m}{T_L} \rightarrow 0$$

However, at high Reynolds numbers the corresponding limit of the gradient correlation is:

$$\overline{\frac{\partial u_{f_i}}{\partial x_\ell}\frac{\partial u_{p_i}}{\partial x_\ell}} + \overline{\frac{\partial u_{f_i}}{\partial x_\ell}\frac{\partial u_{f_i}}{\partial x_\ell}} = \frac{\varepsilon}{\nu} \qquad (4.5.41)$$

$$\text{as} \quad \frac{\tau_m}{T_L} \rightarrow 0$$

Corresponding the above two limiting expressions:

$$\frac{\varepsilon}{\nu} = \frac{10k}{\lambda_g^2} \qquad (4.5.42)$$

or, in keeping with the assumption of local isotropy:

$$\frac{\varepsilon}{\nu} = 15\,\frac{\overline{u_f^2}}{\lambda_g^2} \qquad (4.5.43)$$

Equation (4.5.43) is exactly the definition of ε as shown in Hinze [1975]. It is seen that Eq. (4.5.37) does indeed display appropriate limiting behavior. The modeled equation will thus be used for numerical calculation of ε-transport equation.

CHAPTER 5

DIFFUSION PROCESSES IN TWO PHASE FLOWS

The complexity of two-phase fluid-particulate flow dynamics is associated with the variously different modes of diffusion governing the relative motion of the dispersed phase in the carrier fluid. In addition to convection, particulate phase diffusion processes can also be important in determining the transport of mean particulate quantities such as momentum and mass concentration. Therefore, it is essential to account for such transport processes when the particulate mean conservation equations are considered.

In general, the processes governing particulate diffusion arise from interactions of the particles with the fluid, and/or interactions of particles with neighboring particles and nearby walls. The diffusion processes associated with the fluid forces are generally functions of both the fluid and particulate phase characteristics. For example for the case of diffusion by turbulent fluid drag on the particles, the investigation of Soo [1956] and Peskin [1962] are noteworthy. For very small submicron-sized particles, collisions with the carrier gas molecules can be significant and may establish a different mode for particle diffusion. In the cases of significant particle-particle collisions a Brownian-type diffusion caused by mutual particle interactions will arise. It has been argued by Hinze [1975] that the viscous drag and Brownian-type diffusion are practically independent. Consequently, their respective contributions to the particulate phase mean momentum

A form for Eq. (4.5.37) more suitable for numerical computation can be obtained by substituting Eq. (4.5.38) for λ_g in Eq. (4.5.37), to obtain:

$$\overline{\frac{\partial u_{f_i}}{\partial x_\ell} \frac{\partial u_{p_i}}{\partial x_\ell}} = \frac{\tau_m}{(\tau_m+T_L)^2} \frac{\partial k}{\partial x_\ell} \frac{\partial T_L}{\partial x_\ell} + \frac{T_L}{\tau_m+T_L} \cdot \frac{\varepsilon}{\nu} \qquad (4.5.44)$$

With all the variables on the right hand side of Eq. (4.5.44) defined, it can be used for closure of the ε-transport equation.

momentum is additive which simplifies the analysis, particularly when one contribution becomes negligible with respect to the other. The situation is analogous to the high Reynolds number single phase flows in which laminar viscosity becomes negligible compared to its turbulent eddy diffusion counterpart. Finally, indirect particle-particle interactions are represented by the so-called Bernoulli forces and are associated with a corresponding diffusion process as shown by Peskin [1959].

In this chapter the above diffusion processes for the particulate phase will be analyzed with the view of incorporating the significant components in the particulate momentum balance equations.

5.1 Diffusion by turbulent drag

One of the significant characteristics of turbulent flow is their capability for dispersing quantities such as momentum, heat, mass and related quantities. For an accurate prediction of the mean values of such quantities, it is essential to have a sufficiently adequate knowledge of the relevant turbulent diffusion processes. The dispersion of solid particles into the atmosphere in the form of pollutants from smokestacks, and the diffusion of particles toward the walls of a channel with subsequent deposition are among many practical cases of particle turbulent diffusion induced by fluid motions. Various experimental investigations have been conducted in regard to fluid turbulence-induced particle diffusion, some of these are briefly discussed in this section. The experiment of Rouse [1939] deals with the turbulent transport of sand particles in water which are kept in suspension by the

vertical oscillations of a metallic lattice. In this case gravity effects tended to settle down the particles while turbulent diffusive effects opposed particle settling, with a tendency to uniformizing the particle concentration distribution. In order to analyze the flow, the assumptions of a gradient-type mass diffusion flux and of a constant particulate turbulent diffusivity were made and subsequently incorporated in the mass balance equations. The analysis revealed an exponential variation for the particulate phase mass concentration in the vertical direction which agreed well with experimental data from the same study. The investigation by Rouse then, not only illustrates the significance of turbulent diffusion effects on the concentration distribution, it also demonstrates the usefulness of the gradient-type hypothesis assumption for particulate phase diffusion mass flux. Under certain conditions, turbulent diffusion effects has a predominant influence on the wall deposition of solid particles in straight pipe flows as has been shown by Friedlander and Johnstone [1957]. In this investigation, solid particles with a size range of 0.8 μm to 2.63 μm were used in air. The results show a drastic increase in the wall deposition of solid particles when transition from laminar to turbulent regime occurs. The deposition rate subsequently increased with increase in the flow Reynolds number. The particle turbulent diffusivity was assumed to be identical to that of the fluid, resulting in a fairly accurate prediction of particle wall deposition. A collective review of particle eddy diffusivity has been made by Householder and Goldschmidt [1969].

Since the earliest investigations relating to two phase flows, the problem of solid particle diffusion by turbulent fluid action has presented itself as one of the most difficult and fundamental issues. The results of the majority of investigations have consistently shown the dependence of solid particle diffusion on the turbulent characteristics of the carrier fluid as well as a dependence on particle characteristics. A thorough knowledge of the fluid turbulence structure and its diffusive characteristics, particularly in relation to fluid-particle interactions is necessary.

The concept of eddy viscosity was introduced originally in the early work of Boussinesq [1877]. This concept has been broadly incorporated in various closures modeling turbulent flows. Later, in 1883, the well-known experiments of Reynolds showed the chaotic and irregular fluid patterns shown by the turbulence-induced dispersion of colored dye. In 1925 Prandtl introduced the concept of mixing length for fluid elements in a turbulent stream based on an analogy with the mean free path of gas molecules. Prior to Prandtl, Taylor [1921] introduced the theory of "diffusion by continuous movements" in homogeneous turbulence. The theory is based on the concept that fluid elements move in a continuous and correlated fashion; distinguishable from molecular or Brownian motion which is a purely random motion in space and time. The diffusion coefficient derived by Taylor is defined as:

$$\nu_{t_f} \equiv \frac{1}{2} \frac{d}{dt} \overline{x_f^2(t)} \qquad (5.1.1)$$

$$\text{as} \quad t \to \infty$$

in analogy with molecular diffusion. In this expression $x_f(t)$ is the mean square displacement of the fluid element. The Taylor theory of "diffusion by continuous movements" provides an expression for $x_f(t)$ as:

$$\overline{x_f^2(t)} = 2\,\overline{u_f^2} \int_0^t dt' \int_0^{t'} R_{L_f}(\tau)\, d\tau \qquad (5.1.2)$$

with $R_{L_f}(t)$ indicating the Lagrangian correlation coefficient.

It is seen that a knowledge of the Lagrangian correlation coefficient is necessary in order to obtain the turbulent diffusion coefficient defined by (5.1.1). The incorporation of expressions for $R_{L_f}(\tau)$ corresponding to small and large values of τ yields, respectively:

$$\overline{x_f^2(t)} = \overline{u_f^2}\, t^2 \qquad \text{for } t \ll \tau_{L_f} \qquad (5.1.3a)$$

and

$$\overline{x_f^2(t)} = 2\,\overline{u_f^2}\, T_{L_f}\, t \qquad \text{for } t \gg T_{L_f} \qquad (5.1.3b)$$

where T_{L_f} and τ_{L_f} are, respectively, the Lagrangian integral and micro-time scales of turbulence for the fluid. Hence, for long diffusion times, Hinze [1975]:

$$\nu_{t_f} = \overline{u_f^2} \int_0^\infty R_{L_f}(\xi)\, d\xi = \overline{u_f^2}\, T_{L_f} \qquad (5.1.4)$$

The application of Eq. (5.4.1) requires a knowledge of the Lagrangian time scale characteristics of the fluid.

The diffusion theory outlined above can be extended to the motion of a single particle suspended in a turbulent fluid. The problem reduces to an evaluation of $R_{L_p}(t)$ and of the mean square displacement, $\overline{x_p^2}$ for the particle motion. The mean square displacement for a single particle can be obtained from the general equation of motion, Eq. (2.1.1). However, as already noted, a rigorous solution of this equation is not straightforward, and all practial investigations to date are essentially based on simplified forms of the particle equation of motion. The classical investigation of Tchen [1947] is one of the early works in this regard for the motion of a single particle in an unsteady flow field and was discussed in Chapter 2. One of the major assumptions embodied in Tchen's investigation is that a particle remains in the vicinity of the same fluid element it initially encountered. This implies identical turbulent diffusivities for the fluid and solid particle. In the computations of two phase turbulent flows such an assumption will lead to significant simplifications in relation to particulate momentum balance closure. The assumption is correct only for perfectly responsive particles with respect to turbulent fluid fluctuations. For this case, the particle length and time scales satisfy the following conditions:

$$d_p < \eta$$

$$\tau_m < \tau$$

which η and τ representing Kolmogorov length and the scales, respectively. The conditions above impose restrictions on the two phase flow to be considered.

There are numerous examples of experimental data which do not support Tchen's assumption. Among these are the studies by Goldschmidt et al. [1972], Yuu et al. [1978] and Soo and Peskin [1958]. The investigations point out to the so-called "over-shooting" effect, due to which inertial particles will not remain in the vicinity of the original fluid element, and thus resulting in a different diffusion coefficients for the fluid and particle phases. For large, non-inertial particles the deformation of neighboring fluid elements should be accounted for since, due to the stretching, shortening and in general the complete distortion of the neighboring fluid element, the particle will hardly remain in its vicinity even if inertial "overshooting" effects are negligible. In such cases, the particle response time should be compared to the time scale characteristic of fluid element deformation.

The basis for the derivation of a particle-to-fluid diffusivity ratio in Tchen's investigation is Taylor's diffusion theory and the utilization of Eq. (5.1.2) specifically for particle mean displacement. Using integration by parts, this equation can be re-written as:

$$\overline{x_p^2}(t) = 2\,\overline{u_p^2} \int_0^t (t-\tau)\, R_{L_p}(\tau)\, d\tau$$

which has been derived by Kampe de Fériet and shown by Hinze [1975]. The results of Tchen's study for the case of statistically stationary particulate motion show that for short and long diffusion times the ratios of particle to fluid eddy diffusivity are, Tchen [1947]:

$$\frac{\nu_{t_p}}{\nu_{t_f}} = \frac{\overline{u_p^2}}{u_f^2} \qquad \text{(for short times)} \qquad (5.1.6)$$

and

$$\frac{\nu_{t_p}}{\nu_{t_f}} = 1 \qquad \text{(for long times)} \qquad (5.1.7)$$

Equation (5.1.6) show that for short diffusion times the diffusivity ratio becomes proportional to the ratio of mean square velocities in any direction for the case of isotropic turbulence. However, for long diffusion times the ratio becomes unity, Eq. (5.1.7).

The derivation of a more general diffusivity ratio requires a knowledge of the Lagrangian energy-spectrum functions for the fluid and particle phases, $E_{L_f}(n)$ and $E_{L_p}(n)$, respectively. Although a relation for the ratio of the two spectrum functions is available from Tchen's analysis, it can not be used to obtain the individual diffusion coefficients. However, by assuming an exponential form for the Lagrangian correlation coefficient, an approximate expression for $E_{L_f}(n)$ can be obtained, Hinze [1975]. The incorporation of this expression in the equations of motion results in time-dependent relations for the

eddy diffusivities and the turbulence intensities of each phase. Hinze's analysis, however, shows that for long diffusion times the diffusivity ratio becomes unity and is consistent with Tchen's result. In another investigation, Friedlander [1957] used the particle equation of motion to obtain:

$$\overline{x_p^2}(t) = 2\,\overline{u_f^2}t \int_0^\infty R_f(\Theta)\, d\Theta \qquad (5.1.8)$$

in which $R_f(\theta)$ is the fluid correlation coefficient encountered by the particle along its path and has a functional form which depends on the relative motion of the suspended particle phase. Two limiting cases can be considered:

a) for small non-inertial particles perfectly following the fluid element, $R_f(\theta)$ becomes equivalent to the fluid Lagrangian correlation coefficient, $R_{Lf}(\theta)$, already defined. In this case the diffusion coefficients become identical.

b) In the case of large heavy particles which do not remain in the vicinity of the same fluid element the particles experience a series of turbulent eddies which, for relatively high particle terminal velocity values, are essentially frozen with respect to the particle motion. In this situation, $R_f(\theta)$ becomes identical with the fluid Eulerian correlation coefficient.

Finally, in the case of large inertial particles with high τ_m values the diffusivity ratio for small diffusion times becomes, Friedlander [1957]:

$$\frac{\nu_{t_p}}{\nu_{t_f}} \propto \frac{t^2}{\tau_m^2} \tag{5.1.9}$$

The ratio given by Eq. (5.1.9) is quite small compared to unity and indicates the slow response of inertial particles to fluid motion.

Gravity effects

The studies on the Lagrangian behavior of solid particles with non-negligible terminal velocities constitute a significant part of the investigations on many-particle diffusion, of practical interest in relation to atmospheric diffusion of solid pollutants and dust particles in the atmosphere. The existence of a non-negligible terminal velocity for a solid particle will cause the particle to depart from the vicinity of its initial neighboring fluid element and eventually to fall-out under gravity effect. The particle will experience a series of different eddies during its gravity-induced descent through the fluid. This effect, which is usually referred to as "crossing-trajectories," results in a more rapid decrease in the particle Lagrangian correlation coefficient and has a significant influence on the heavy particle diffusion coefficient. The argument presented earlier, given by Friedlander [1957], regarding the limiting conditions for small and large terminal velocities can be generalized to give, Csanady [1963]:

$$R_f = R_f(\tau_1, \xi_1) \tag{5.1.11}$$

This relation can be substituted in Eq. (5.1.8) with τ_1 the traveling time in the direction of gravity, $\xi_1 = \tau_1 u_t$ the corresponding distance travelled by the particle, Yudine [1959], and u_t representing the particle terminal velocity. The correlation coefficient in Eq. (5.1.11) becomes identical to the Lagrangian coefficient when u_t is small, while for large u_t values it becomes equivalent to the spatial Eulerian correlation coefficient. Therefore, in general, the correlation coefficient in Eq. (5.1.11) is a combination of the two limiting correlation coefficients. Furthermore, analysis based on the use of such "mixed" correlation coefficients shows a reduction in ν_{t_p} with a increase in particle terminal velocity, u_t, as indicated by Yudine [1959]. For an evaluation of the "mixed" correlation coefficient with fall-out effects included, Csanady [1963] has suggested that:

$$R_f(\tau_1,\xi_1) = \exp\left[-\frac{\tau_1}{L_E}\left(u_t^2 + \frac{L_E^2}{T_L^2}\right)^{1/2}\right] \qquad (5.1.12)$$

where L_E and T_L are the Eulerian integral length and the Lagrangian integral time scales, respectively, which are to be evaluated in the direction of the particle terminal velocity. This proposed form for $R_f(\tau_1,\xi_1)$ above is based on the investigation of Mickelsen [1955] regarding exponential forms for both the Lagrangian and the Eulerian correlation coefficients.

The incorporation of Eq. (5.1.12) in (5.1.10) results in the following expression for the diffusivity ratio:

$$\frac{\nu_{t_p}}{\nu_{t_f}} = \left(1 + \frac{T_L^2}{L_E^2}\, u_t^2\right)^{-1/2} \qquad (5.1.13)$$

Consistent with previous investigations, this expression shows a reduction in ν_{t_p} with an increase in terminal velocity. It should be noted from Eq. (5.1.13) that, for zero terminal velocity, identical diffusion coefficients for the fluid and particle phases will be obtained. This is because in the analysis leading to Eq. (5.1.13), the particle inertial effects have not been included. In a related investigation, Meek and Jones [1973] have derived a modified particle energy spectrum function with the particle terminal velocity incorporated. The particle Lagrangian correlation coefficient obtained by them is:

$$R_{L_p}(\tau_1) = \frac{1}{1-\theta}\left[e^{-\tau_1/T'} - \theta\, e^{-\tau_1/(\theta T')}\right] \qquad (5.1.14)$$

with:

$$\theta = \frac{\tau_m}{T_L}$$

and:

$$T_L' = T_L\left[1 + (u_\tau/u_p)^2\right]^{1/2}$$

The inclusion of Eq. (5.1.14) in the expression for mean square displacement from Taylor's diffusion theory (Eq. (4.1.12)), results in the following expression for the eddy diffusivity ratio:

$$\frac{\nu_{t_p}}{\nu_{t_f}} = \left[1 + \left(\frac{u_t}{\tilde{u}_f}\right)^2 (1 + \theta)\right]^{-1/2} \qquad (5.1.15)$$

This expression shows that the diffusivity ratio is smaller than, or at most equal to, unity. The presence of u_t in Eq. (5.1.15) indicates how the "crossing-trajectories" effect tends to reduce the particle eddy diffusivity relative to that of the fluid. For zero terminal velocity the diffusivity ratio in Eq. (5.1.15) becomes equal to unity, consistent with the result given by Eq. (5.1.13). In relation to gravity effects it may be concluded that an important non-dimensional variable is $u_t/\tilde{u}_f$, in addition to the non-gravity τ_m/T_L already introduced. The presence of gravity effects tends to diminish particle eddy diffusivity as well as the particle Lagrangian correlation coefficient. Physically, this means that due to particle fall-out under the influence of gravity, various regions of the flow will be encountered by the particle which are not correlated with its motion and, therefore, will reduce the particle correlation coefficient as particle terminal velocity increases. Among the experimental investigations supporting this notion is the work by Snyder and Lumley [1971]; in which diffusion coefficients for solid particles with terminal velocities ranging from 1.67 cm/sec to 44.2 cm/sec in grid generated turbulence have been measured.

Particle inertia effects

In problems of solid particle dispersion induced by turbulent fluid drag, particle inertia has a significant influence on the particle phase diffusion process. It is because inertia effects that: small, non-inertial, particles tend to follow turbulent fluctuations almost completely; while inertial particles lag behind high frequency fluctuations of turbulent fluid motion. In the case of the latter, particles tend not to remain in the vicinity of the same fluid element. This results in a different eddy diffusivity for the particulate phase compared to that of the fluid phase. The investigations of Soo [1956] and Liu [1956], based on a Fourier series representation of fluid turbulence in confirmation with the particle equation of motion yielded solutions showing different eddy diffusivities for the fluid and particle phases when particle inertia was significant. Particle inertia is also responsible for the penetration of solid particles from the turbulent core of the flow into the viscous sub-layer in turbulent pipe flow resulting in particulate wall deposition shown by Friedlander and Johnstone [1957].

The major assumption in most investigations related to particle turbulent diffusion is that originally introduced by Tchen [1947], namely that the particle remains in the neighborhood of its initial fluid element. This idealized assumption poses limitations on the applicability of the results derived to more real flow conditions in which "over-shooting" effects can be significant. "Over-shooting"

refers to the condition in which inertial particles are removed from the neighborhood of their initial accompanying fluid elements resulting in a diminished particulate phase diffusion coefficient. This has been shown by Peskin [1959] and Soo and Peskin [1958] through introduction of the statistically defined the most probable fluid element encountered by the particle at a certain time in flow domain. It should be noted that the escape of the particle from one flow region to another is associated with a weakening of the particle-fluid velocity correlation function.

Through statistical treatments, Peskin [1962] has derived a particle-fluid eddy diffusivity ratio which shows a dependence not only on the time scale ratio τ_m/T_L, but also on the Lagrangian and Eulerian microscales of the fluid. The derivation is based on the particle equation of motion (2.1.1) with the Stokes viscous drag term as the only driving force present in the momentum balance. At a time t after the start of the motion, the fluid element surrounding a particle is different from that which the particle originally encountered. The derivation is then reduced to determining the most probable fluid velocity encountered by the particle at time t given the velocity of the initially-encountered fluid element at time t_o. The most probable fluid velocity is obtained by assuming a joint Gaussian probability distribution function for the particle-encountered fluid velocities. In addition, statistically stationary isotropic turbulence random variables are assumed. The results show that on average the fluid velocity encountered by a particle becomes equal to the velocity

of the fluid initially encountered at time t_o multiplied by the two-point Eulerian coefficient based on the fluid velocities encountered at time t. The most probable fluid velocity surrounding a particle at time t obtained in this way is then substituted in Eq. (2.2.9) with a parabolic expression for the correlation coefficient as given in Eq. (4.5.9), an expression for the particle mean square displacement is obtained and is ensemble-averaged over all the possible fluid velocity encountered. Throughout the derivation process, the fluid Lagrangian correlation coefficient has been approximated by the exponential function given by Eq. (4.1.13). The result for the diffusion coefficient ratio is, Peskin [1962]:

$$\frac{\nu_{t_p}}{\nu_{t_f}} = 1 - \frac{T_L^2 \overline{u_f^2}}{\lambda_E^2} \frac{3K^2}{K+2} + O\left(\frac{1}{\lambda_E^4}\right) \qquad (5.1.16)$$

with:

$$K = \frac{2\tau_m}{T_L}$$

Equation (5.1.16) is significant since it accounts for "over-shooting" as well as local response effects. In the derivation process leading to Eq. (5.1.16) it is assumed by Peskin that the particle, although allowed to over-shoot the original fluid element, stays in regions close to it so that the second term on the right hand side of Eq. (5.1.16) remains small compared to unity. The parameter K is characteristic of the particle response to the fluid fluctuations. For inertial particles with high K values, deviation from initially

neighboring fluid elements results in a reduction of the particle eddy diffusion coefficient as predicted by earlier investigations.

Particle size effects

Several investigations on turbulent diffusion of solid particles, have shown that the ratio of particle size to the local length scale of turbulence is a significant parameter. Among these investigations are those by: Tchen [1947], Peskin [1962], Yuu et al. [1978] and Abramovich et al. [1974]. In general, it has been shown that with an increasing particle size the diffusion coefficient ratio, ν_{t_p}/ν_{t_f}, decreases. This is usually referred to as the "filtering" effect by which the particles "filter-out" the influence of eddies with length scales smaller than the particle diameter, thus resulting in a reduction of the turbulence-induced particulate diffusivity. The above investigations show the following limiting conditions:

$$\frac{\nu_{t_p}}{\nu_{t_f}} \to 1 \quad \text{as} \quad \frac{d_p}{\lambda_E} \to 0 \tag{5.1.17}$$

and;

$$\frac{\nu_{t_p}}{\nu_{t_f}} \to 0 \quad \text{as} \quad \frac{d_p}{\lambda_E} \to \infty \tag{5.1.18}$$

with λ_E as the fluid Eulerian microscale.

Using the assumption of stationary, homogeneous and isotropic turbulence, Hinze [1971] has approximated the turbulence energy spectrum function from which the ratio ν_{t_p}/ν_{t_f}, as a function of d_p/L_e, is derived; L_e representing the length scale of the

energy-containing eddies. In this derivation the "filtering" effect of small eddies by large particles, discussed above, was included. Analytical results so obtained for the diffusivity ratio, for intermediate values of particle diameter, dp, are consistent with the experimental data of Goldschmidt et al. [1971]. For the intermediate particle size range contained by:

$$\lambda_E \lesssim d_p \lesssim 0.5\, L_e \tag{5.1.19}$$

the data shows a diffusivity ratio larger than unity, Hinze [1971]. For a physical interpretations of this remarkable result, Hinze [1971] has re-written the diffusion coefficient ratio as:

$$\frac{\nu_{t_p}}{\nu_{t_f}} = \frac{\Lambda_{L_p}}{\Lambda_{L_f}} \cdot \frac{u_p}{u_f} \tag{5.1.20}$$

with Λ_{L_p} and Λ_{L_f} denoting the particle and the fluid particle Langragian integral length scales. Hinze then argues that for the ranges where:

$$d_p < 0.5\, L_e \tag{5.1.21}$$

the length scale ratio in Eq. (5.1.20) will increase with increasing particle size, since large inertial particles will correlate over longer distances as compared to small non-inertial particles. Although the velocity scale ratio in Eq. (5.1.20) will decrease with increasing particle size, it can not compensate for the increase in the length scale ratio, thus resulting in an overall increase in the diffusivity ratio. For ranges corresponding to the particle sizes larger than L_e the same argument suggests implies diffusivity ratios values smaller than unity.

In closing section 5.1 it may be remarked that in addition to the various effects reviews above relating to particle turbulent diffusivity, the wall effects has been investigated by Gudmundsson and Bott [1977]. Based on the results of various experimental studies, these authors have proposed that in wall regions of the flow, particulate turbulent viscosity can be modeled by:

$$\nu_{t_p} = \nu_{t_f} + \tau_m\left(\overline{u_f^2}\right)$$

This proposal is based purely on physical arguments without rigorous mathematical proof. Other noteworthy investigations relating to particulate turbulent diffusion of less importance to the present study are those by: Lilly [1973] and Eskinazi and Goldschmidt [1966]. In addition, Peskin and Kau [1979] have developed a numerical scheme for the direct simulation of particle dispersion in turbulent channel flow. Their deterministic method is based on solution to Eq. (2.1.1) with the Stokes drag term as the only driving force incorporated in the particle momentum balance.

5.2 Brownian Diffusion for Solid Particles

Brownian diffusion of solid particles suspended in a viscous fluid is caused by random collisions among solid particles, or, in the case of sub-micron particles, by collision of fluid molecules with the particles.

A relation for the particle mean square Brownian displacement and a corresponding diffusion coefficient has been obtained by Peskin [1959] which is based on Eq. (2.2.10) describing the particle position. In the Brownian motion of solid particles, the diffusion process evolves by collisions which are random in nature and which have no correlation with the particle position and velocity. The use of Eq. (2.2.10) for predicting particle Brownian motion requires a knowledge of the function A(t) representing the random particle acceleration induced by neighboring particle and/or molecular impacts. Peskin [1959] assumes that the A(t) statistics are similar to those characteristic of a perfect gas. Thus, a Maxwellian probability density is used in combination with an assumed form of the auto-correlation function of A(t) given by:

$$\overline{A(t)\ A(t+\xi)} = \sigma^2\ \delta(\xi) \tag{5.2.1}$$

with $\delta(\xi)$ the Dirac function.

For long diffusion times it is assumed that the particle is in thermal equilibrium with the neighboring fluid in which case Peskin obtains:

$$\sigma^2 = \frac{2k_B T'}{m\tau_m} \tag{5.2.2}$$

with $m = \tilde{\rho}_p\ \pi(d_p)^3/6$, k_B and T' as the mass of solid particle, Boltzman constant and flow temperature, respectively.

The function A(t) defined by Eq. (5.2.1) when substituted in Eq. (2.2.10) yields an expression for the mean square particle displacement, corresponding to long diffusion times, given by:

$$\overline{x_p^2(t)} = \frac{2k_B T'}{3\pi\mu d_p} t \qquad (5.2.3)$$

Using this result in the definition for diffusion coefficient given by Eq. (5.1.1) yields the following expression for solid particle Brownian diffusivity:

$$\nu_{B_p} = \frac{k_B T'}{3\pi\mu d_p} \qquad (5.2.4)$$

Equation (5.2.4) is identical to the Einstein relation for Brownian diffusion of solid particles in a viscous fluid, Einstein [1906]. An order of magnitude analysis will show that for most practical cases, Brownian diffusion is negligible compared to turbulence-induced diffusion.

5.3 Diffusion of Solid Particles by Bernoulli Forces

The relative motion of a discrete spherical particle with respect to another particle in inviscid potential flow results in mutual forces between the particles caused by the pressure gradients which arise due to their relative motion. Such forces are usually referred to as Bernoulli forces. The derivation of the velocity potential function for this case has been described by Milne-Thompson [1968]. The procedure is to assume that the overall potential function is a linear combination of the individual particle velocity potential functions.

Subsequently, by means of an iterative analytical procedure, an overall potential function is derived such that its spatial derivatives yield the values of the individual particle velocities from which it is formed.

In the case of the motion of a cloud of particles suspended in a fluid, randomly arising Bernoulli forces between pairs of particles in the cloud will account for diffusion of the particulate phase. While Brownian diffusion is due to direct particle-particle or particle-molecule interactions, Bernoulli diffusion is due to the mutually induced, but indirect, particle-particle interactions.

Bernoulli diffusion has been investigated by Peskin [1959] and the corresponding diffusion coefficient has been derived. The derivation is based on Eq. (2.2.10) in which probability distribution function was incorporated. The analytical results obtained by Peskin for particle mean square displacement and solid phase diffusion coefficient show that a field of randomly located (relatively) stationary particles has a significant effect on the instantaneous motion of any one particle. The effect which referred to as "dynamic friction" can have a retarding influence on the motion of a single particle with a consequent reduction in its diffusivity. The results of Peskin derivations also show a direct proportionality of particle diffusion coefficient to solid particle-fluid volume ratio. Furthermore, the Bernoulli diffusivity becomes significant only for large inertial particles and is negligible for small, non-inertial particles. Due to the dependence of Bernoulli diffusivity on particulate volume fraction, the effect is negligible in practically all dilute fluid-particle flows of interest.

CHAPTER 6

SINGLE-PHASE FLOW MODELING, EROSION MODEL AND NUMERICAL METHOD

This chapter consists of three different sections. In section 6.1, the modifications to two-equation (k-ε) model of turbulence for computation of single-phase flows in developing curved channels is discussed. In section 6.2 the mathematical model for the computation of erosion is described and, finally, the general numerical method for the computation of two-phase and single-phase flow is discussed in section 6.3.

6.1 Computation of Single-Phase Curved Channel Flows

In this section the general mathematical formulation for the computation of single-phase developing curved channel flows is briefly discussed. The detailed derivation and the related considerations are presented in appendix II.

Correct prediction of single-phase turbulent curved channel flows by two-equation (k-ε) model of turbulence, requires a direct incorporation of the curvature effects not only in the governing equations but also into the structure of the turbulence model through modifications of turbulence constants and also the boundary conditions. This is achieved through re-arrangement of Reynolds stress transport equations and their further reduction to algebraic terms with the wall-induced dampening effects included in their corresponding pressure-strain correlation terms. This leads to a general expression for C_μ in Prandtl-Kolmogorov relation:

$$\nu_{t_f} = C_\mu \frac{k^2}{\varepsilon}$$

based on the assumption that $\overline{u_{f_i} u_{f_j}}/k$ is constant as shown in appendix II. The general expression for C_μ thus obtained, successfully reduced to the less general expressions present in the literature. The incorporation of such general C_μ function in numerical scheme does produce the increase and decrease in turbulent length scale at the outer and inner walls, respectively.

The effect of wall-induced pressure fluctuations in the pressure-strain terms is considered by introduction of a wall function, $f(\ell/y)$. The f function depends on the length scale ℓ of the energy containing eddies and is diminished with the increasing distance y from the wall which induces the largest contributions to the wall-convection terms, that is, the concave wall in a curved channel. It is proposed here to take:

$$f = \frac{k^{3/2}}{C_w \varepsilon} \left[\frac{1}{y} + \frac{(y/\Delta)^m}{\Delta - y} \right]$$

the constants C_w is chosen such that $f \to 1$ and $y \to 0$ and the constant m is determined exactly from experimental measurements for strongly curved, $R_c/\Delta < 20$, and weakly curved, $R_c/\Delta > 20$ flows. For $m = 0$ the above expression reduces to the straight channel situation.

The expressions for boundary conditions in the standard two-equation (k-ε) model when applied to curved channel flows requires special modifications which could accomodate changes in turbulent length scales in the vicinity of the outer and inner walls. This last modification shows a better prediction of the wall shear stress for both concave and convex walls. The combination of modifications as outlined above when incorporated in the numerical scheme show an overall improvement in the prediction of fluid velocity, turbulent kinetic energy and wall shear stress for developing curved channel flow. The results are shown in Appendix II.

6.2 Erosion Wear Model and Related Considerations

Erosion of walls in curved channel flows is controlled by the dynamics of the flow. Therefore, for an analysis of wall erosion under various flow conditions, the prediction of the fluid mechanical variables of the flow is necessary. The computation of erosive wear ultimately requires the selection of a proper mathematical model for surface erosion. The mechanism of erosion of solid walls by solid particulates depends on various factors among which are: particle impact velocity, direction, and mass, as well as particle shape, size, hardness and the physical nature of the wall material.

Finnie [1972] has introduced a mathematical model for erosion wear of ductile materials which shows good agreement with experimental data at small angles of impingement. In that model, the cutting action of the solid particles is assumed to be similar to that of cutting tools

with the cutting depth depending on wall physical properties. Based on this model the rate of volumetric material removed from the wall surface per unit area is:

$$\dot{E} = c \frac{\dot{m}}{p_1} q_p^2 f(\beta_{imp}) \qquad (6.2.1)$$

In Eq. (6.2.1) a friction coefficient of order 2 between particles and the wall is implied and for the moment of inertia for a single particle is approximated by the value for a sphere:

$$I = \frac{mr^2}{3}$$

with m and r representing mass and the radius of a single particle.

In Eq. (6.2.1) above the variables are defined as:

$\dot{E}$ erosion rate in terms of volume per unit area and time

c fraction of the number of particles cutting in an idealized manner

p_1 taken as Vickers hardness of the wall material

$\dot{m}$ mass of the particles striking the surface per unit area and unit time

q_p the magnitude of the particulate phase impact velocity

$f(\beta_{imp})$ function of angle of attack, β_{imp} (see Fig. (6.1) which is defined as:

$$f(\beta_{imp}) = \sin(2\beta_{imp}) - 4 \sin^2\beta \qquad \beta_{imp} \leq 14°$$

$$f(\beta_{imp}) = \cos^2\beta_{imp}/4 \qquad \beta_{imp} > 14°$$

6.3 Numerical Method

The numerical method for the calculation of the single and two phase flows is discussed in this section. The mathematical models and the corresponding boundary conditions for the flows have been discussed in the previous chapters and in the appendices. The discussion here is restricted to steady, fully elliptic, two-dimensional, incompressible and isothermal flows although the method can be extended to more general flows.

The numerical scheme to be discussed is based on the work of many investigators among which are Gosman and Pun [1974], Spalding [1972], Patankar and Spalding [1972] and Harlow and Welch [1965]. A more detailed description of the numerical method is available in Patankar [1980], and its application to laminar and turbulent curved duct flows has been carried out by Humphrey [1978] and Humphrey, Whitelaw and Yee [1981].

6.3.1 Grid system

The grid system is such that scalar quantities such as pressure and turbulent kinetic energy are stored at the grid points while velocity components are calculated at points located midway between the grid nodes. In this so-called "staggered" grid system the velocity components are positioned such that the flow of a scalar quantity into its control volume can be easily calculated. This is illustrated in Fig. (6.2a) which shows the control volume for the scalar dependent variables. The U velocities are staggered in x direction and, accordingly, the V velocities in y direction. The control volume for U and V are shown in Figs. (6.2b) and (6.2c), respectively.

6.3.2 Derivation of finite-difference equations

The finite-difference equations are descriptions of the distribution of independent variables for discrete grid points. They are obtained by volume integration of the differential equations describing the transport of a mean quantity ϕ. The control volume over which the integration is performed, corresponds to the cell volume surrounding the grid point for either a scalar or vector quantity. The derivation of finite-difference equations are described is defined as the "control-volume" formulation which is a special case of the method of "weighted residuals" discussed by Patankar [1980].

The modeled partial differential transport equations for either fluid or the particulate phase can be written in the following generalized form:

$$\frac{\partial}{\partial x_j} \left(\overline{\rho}\, \overline{U}_j\right)_m \phi - \frac{\partial}{\partial x_j} \Gamma \frac{\partial \phi}{\partial x_j} = S_\phi \qquad (6.3.1)$$

with subscript m referring to either fluid or particulate phase. The first term on the left hand side of Eq. (6.3.1) is the convection of quantity ϕ and the second term is the diffusion of ϕ; Γ being the corresponding diffusion coefficient. $S\phi$ represents the source term for the independent variable ϕ. Integration of Eq. (6.3.1) yields:

$$\int_{A_c} \left[\frac{\partial}{\partial x_j} \left(\overline{\rho}\, \overline{U}_j\right)_m \phi - \frac{\partial}{\partial x_j} \Gamma \frac{\partial \phi}{\partial x_j}\right] dA_j = \int_{V_c} S_\phi \, dV \qquad (6.3.2)$$

where A_c and V_c represent the surface and the volume of the cell and A_j is the area normal to the coordinate x_j. The integral on left hand side of Eq. (6.3.2) is the net eflux of the quantity ϕ for the cell with volume V_c, Fig. (6.2), due to combined effects of convection and diffusion. The term on right hand side of Eq. (6.3.2) is the integral of source term S_ϕ over the cell volume. When the source term is a function of ϕ it is preferably expressed in a linear form. The linearization of the source term is done for the purpose of preserving the linearity of the corresponding finite-difference equation which can then be solved by the usual techniques for linear algebraic equations. Hence:

$$\int_{V_c} S_\phi \, dV = (S_u + S_p\phi) \, V_c \qquad (6.3.3)$$

The exact solution for Eq. (7.2.1) for a one-dimensional case with $S_\phi = 0$ corresponding to Fig. (6.2e) is, Spalding [1972]:

$$\frac{\phi-\phi_n}{\phi_{n+1}-\phi_n} = \frac{\exp\,(P_e x/\Delta x)-1}{\exp\,(P_e)-1} \qquad (6.3.4)$$

with:

$$P_e \equiv \frac{(\bar{\rho}\,U)_m \Delta x}{\Gamma}$$

as the Peclet number.

Application of the exact solution to, for instance, the east side of the cell in Fig. (6.2a) results in:

$$j_e = (\overline{\rho_e U_e})_m \; f_e \phi_p + (1-f_e)\phi_e \qquad (6.3.5)$$

with

$$f_e \equiv \frac{\exp[(P_e)_e}{\exp[(P_e)_e]-1}$$

as weighing factor for the convective flux and

$$(P_e)_e \equiv \frac{(\rho_e U_e)_m \, \Delta x_{Pe}}{\Gamma_e}$$

in the cell Peclet number calculated at its east boundary.

The flux in Eq. (6.3.5) is due to combined effects of convection and diffusion. Although it is the exact solution to the one-dimensional transport equation its incorporation in the numerical scheme is not appropriate since the exponential terms in f_e of Eq. (6.3.5) are expensive to evaluate. Also, it should be remembered that Eq. (6.3.4) has been obtained with the assumption that $S_\phi \equiv 0$ and is not applicable for cases when $S_\phi \neq 0$.

For the computation of convective-diffusive flux at the cell boundaries a numerical scheme called "Hybrid" scheme is incorporated. It is an approximation to the exact solution and was developed initially by Spalding [1972]. The "hybrid" scheme is a combination of

upwind-difference and central-difference schemes which becomes identical to above schemes when local Peclet number, P_e , becomes larger or smaller than 2, respectively. The "Hybrid" scheme is selected here since it does not have the instabilities associated with the "central-difference" scheme at high P_e numbers, and, in addition, it is more accurate than "upwind-difference" scheme at low P_e numbers.

The result of Eq. (6.3.2) thus becomes:

$$\dot{J}_e A_e - \dot{J}_w A_w + \dot{J}_n A_n - \dot{J}_s A_s = (S_u + S_p \phi) V_c \qquad (6.3.6)$$

where J's are the fluxes and A's represent the surfaces at the corresponding boundaries.

Using the "hybrid" scheme the flux at the east boundary, for instance, becomes:

$$j_e = (\rho_e \bar{U}_e)_m \begin{cases} \frac{1}{2}\left[(1+2P_e^{-1})\phi_p + (1-2P_e^{-1})\phi_e\right] & \text{for } |P_e| < 2 \\ \phi_p \quad \text{for } P_e \geq 2 \\ \phi_e \quad \text{for } P_e \leq -2 \end{cases} \qquad (6.3.7)$$

Substitution of Eq. (6.3.7) and similar expressions for other boundaries, in Eq. (6.3.6) results in the following linear algebraic equation:

$$(a_p - S_p)\phi_p = \sum_{i=1}^{4} a_i \phi_i + S_u \qquad (6.3.8)$$

which is the finite-difference equation corresponding to transport equation (6.3.7) with a linearized source term. The coefficients in Eq. (6.3.8) are:

$$a_e = \text{Max}\left[-(\rho U)_e \ , \ \left(\frac{\Gamma}{\Delta x}\right)_e - \frac{(\rho U)_e}{2} \ , \ 0\right]$$

$$a_w = \text{Max}\left[(\rho U)_w \ , \ \left(\frac{\Gamma}{\Delta x}\right)_w + \frac{(\rho U)_w}{2} \ , \ 0\right]$$

$$a_n = \text{Max}\left[-(\rho U)_n \ , \ \left(\frac{\Gamma}{\Delta x}\right)_n - \frac{(\rho U)_n}{2} \ , \ 0\right]$$

$$a_s = \text{Max}\left[(\rho U)_s \ , \ \left(\frac{\Gamma}{\Delta x}\right)_s + \frac{(\rho U)_s}{2} \ , \ 0\right]$$

where the symbol Max [ ] refers to the largest of the arguments contained within the brackets.

The solution for the velocity field needs, however, special attention. This is due to the presence of the pressure gradient terms in the momentum balance equation which not readily available from the numerical scheme throughout the flow field but rather indirectly specified through continuty equations. In order to obtain the pressure gradient for the solution of finite-differenced momentum balance the numerical procedure known as SIMPLE (Semi-Implicit Method for Pressure-Linked Equation) in utilized, Patanker [1980]. The algorithm is based on solving equations for the momentum balance corresponding to a "guessed" pressure field, P*, as well as the equation governing pressure correction component, P'. The pressure is composed of P* and P':

$$P = P^* + P'$$

The governing equation for P' is obtained from the fluid continuity equation using a procedure of decomposing the velocities into "guessed", u*, and "corrected", u' components corresponding to "guessed" and "corrected" pressure field.

6.3.3 Solution of the Finite Difference Equations

The finite difference equations presented in their general form as Eq. (6.3.8) in the previous section constitute a set of linear algebraic equations which are solved a set of linear algebraic equations which are solved using the Gaussian elimination method. The algorithm used for this purpose is TDMA (Tri-Diagonal-Matrix Algorithm) which uses a recurrence process through the corresponding recurrence relations. For two-dimensional problems, the substitution along a grid line is processed assuming known values for the neighboring grid lines which are available from the previous iterations.

The procedure is then repeated for all the grid lines in direction of one coordinate. The numerical algorithm for this purpose is called LBL (Line-By-Line) algorithm.

The finite difference equation governing transport of the quantity ϕ is then:

$$(a_p - S_p)\phi_p = \sum a_n \phi_n + S_u$$

The numerical stability of the equation above is described by the Scarborough criterion which states the sufficient condition for the convergence to be that:

$$\left| a_p - S_p \right| \geq \left| \sum a_n \right|$$

Treatment of boundary conditions

At the inlet and outlet the boundary conditions are inserted by simply imposing the indicated values. Near a solid wall the treatment is different depending on the type of boundary condition. For scalar quantities the boundary condition is given either by the flux or by the magnitude of that quantity. In the first situation the normal link ϕ_p ϕ_w, Fig. (6.2d), is broken by setting

$$a_w = 0$$

and the flux is included as a "false" source in the difference equation. In the latter case for the boundary value indicated, the treatment is the same except that with the flux written using the boundary and the wall-node values, the coefficients in the source term will be different from the first case. For tangential velocity the link ϕ_p-ϕ_w is again broken and the effects of wall is incorporated through inclusion of wall shear stress in the source term.

The procedure to obtain the fluid velocity field and other dependent variables is:

1 - Guess the pressure field.

2 - Solve the finite-difference momentum equations corresponding to the "Guessed" pressure field.

3 - Using the velocities from previous step the equation for pressure correction term can be solved.

4 - The total pressure is then obtained by addition of the "guessed" and the "corrected" pressure field.

5 - Fluid momentum equations are solved using the adjusted pressure field obtained in step 4.

6 - After obtaining the adjusted velocities, other velocity-dependent variables can be solved from their finite-difference governing equations.

7 - The pressure obtained in step 4 is then used as a new guessed pressure and the procedure is repeated until convergency is obtained.

8 - The residual source, R_ϕ, is defined as:

$$R_\phi \equiv a_p\phi_p - \sum a_n\phi_n - S_\phi$$

The criteria for convergence here is:

$$\frac{\Sigma|R_\phi|}{R_{\phi,ref}} \leq 5 \times 10^{-3}$$

where $R_{\phi,ref}$ is a reference residual value.

9 - In order to slow-down the changes in the quantities ϕ during iterations; they are under-relaxed according to:

$$\phi = (1 - F_\phi)\, \phi_{old} + F_\phi\, \phi_{new}$$

where F_ϕ is the under relation factor. In this work, it is taken as 0.5 for velocities and scalar quantities except for pressure for which it is taken as 1.0.

The grid system for curved channel is shown schematically in Fig. (6.3). The calculations were performed on 18 × 50 and 20 × 40 grid for straight and curved channel flow, respectively, which were evenly spaced in streamwise and unevenly spaced in lateral directions. The storage required on a CDC 7600 computer for straight (curved) channel flow was 155(135) k_8 words and a typical converged run after 150(226) iterations was 130(196) CPU seconds.

Although the above has been a cursory overview of the numerical method it should be noticed that detailed derivations of the scheme, its testing and practical applications have already been given in the references quoted. Finally, in appendix (II) the application of the same scheme to single-phase curved channel flows is being shown.

CHAPTER 7

TWO-PHASE FLOW RESULTS AND DISCUSSION

In this chapter results are presented corresponding to the numerical computation of various two-phase flow experiments of dilute concentration documented in the literature. In addition, the calculation procedure has also been used to predict two-phase curved channel flow and erosion over a wide range of values for the parameters of interest not previously documented.

A review of the two-phase, fluid-particulate turbulent flow literature, shows that there are only a few consistent and reliable experimental investigations which can be used for testing and evaluating a two-phase turbulence model such as the one of this work. There are even fewer studies which provide detailed and directly measured turbulence characteristics in addition to the mean flow quantities. For example, in curved channel flows, the data available for experimental measurement is usually related to secondary effects. These arise as a consequence of the flow and are manifested by such observable quantities as location and amount of erosion wear, and rate of wall deposition of the particulate phase. In such cases, proven models of erosion, or deposition, can be utilized to predict these effects, with the flow-dependent input provided by the turbulence model. While valuable, such comparisons are of limited value for establishing the validity and use of a two-phase flow turbulence model. Therefore, whenever possible, comparisons will be made with direct measurements of mean flow and turbulence quantities.

7.1 Straight Channel/Pipe Flow Results

Table 7.1 presents a summary of the experimental conditions pertaining to the straight channel/pipe flows predicted in this section.

Prediction of mean streamwise fluid velocity and of mean particulate velocity are presented in Figures (7.1) and (7.2) for the pipe flow study by Kramer and Depew [1972b]. The velocity profiles are normalized by respective center line values and the flow conditions are indicated in the figures. In general, agreement between the measurements and the predictions of this work is good, although for higher $\bar{\alpha}_{in}$ it is less satisfactory for fluid velocity in the flow region near the pipe wall where discrepancies of the order of 13% are found. The fact that these discrepancies arise for the more concentrated particulate flow is in agreement with the turbulence model limitations. However, measurement errors in the velocity profiles, estimated from the information given by Kramer and Depew, suggest a root mean square variation of 4-6% in the measurements. Sources and quantification of possible systematic errors in the measurements were not documented by Kramer and Depew, nor are they estimable from their paper. In view of the above, the discrepancies observed between fluid velocity measurements and calculations is not judged to be serious.

Figures 7.3 - 7.6 show the results of fluid and particle velocity prediction for the two-phase straight channel flow experiment of Stukel and Soo [1969]. The flow characteristics are indicated in the figures. Figure 7.3 shows calculated mean particle velocities in excess of

Table 7.1

Investigators	Flow Geometry	Re_D	Two-Phase System	Particle size, d_p(μm)	$\frac{\tilde{\rho}_p}{\tilde{\rho}_f}$	Particle mean volumetric concentration at the inlet ($\bar{\alpha}_{in}$)
Zisselmar and Molerus [1979]	pipe	10^5	glass particles/ methyl benzoate	53	2.51	$\leq 5.6\times10^{-2}$
Kramer and Depew [1972b]	pipe	$5670-5\times10^4$	glass particles/ air	62,200	2.2×10^3	$\leq 4.2\times10^{-3}$
Stukel and Soo [1969]	channel	13000-69800	magnesia particles/ air	14	1.4×10^3	$\leq 6.9\times10^{-5}$

corresponding measurements by as much as 12% in the near wall region of the flow $0.05 \lesssim y/D \lesssim 0.2$. The over-prediction can be attributed in part to the presence of electrostatic effects in the experiment which are not included in the model formulation. In the experiment, the particulate phase consisted of 14 μm magnesia particles in a very dilute concentration, i.e., $\bar{\alpha}_{in} = O(10^{-5})$. By repeated contacts with the electrically grounded wall, the particles became electrically charged and moved toward the walls. This resulted in an increase in particle concentration in the wall region. Due to the electrostatic attraction, particles in the vicinity of the wall undergo a reduction in longitudinal momentum, and hence velocity. In addition, the electrostatic force increases particle concentration near the wall relative to the core region of the flow (see Stukel and Soo [1969]). Particle accumulation in the wall region tends to decelerate the fluid longitudinal velocity through particle viscous drag effects (see Eq. (3.2.13)). Thus, indirectly, the particles act on the fluid in such a way as to reduce the longitudinal momentum. Figure 7.4 shows the corresponding fluid velocity profiles for the same longitudinal locations as Figure 7.3. Although there are no experimental measurements for comparison, it is worth noting that due to smallness of the particles the fluid and particulate phase velocities are in close agreement at any streamwise location.

The centerline values of developing fluid and particle velocities are shown in Figures 7.5 and 7.6. The velocities are non-dimensionalized with respect to the corresponding inlet velocities,

and the longitudinal distance measured from the channel inlet is non-dimensionalized in terms of both inlet velocity and fluid kinematic viscosity. Similarly, to conform with the manner in which the data is provided by Stukel and Soo, for particulate centerline velocity, the distance from the channel leading edge is non-dimensionalized by an "equilibrium length", $\tau_m(\bar{U}_{f_x})_{in.}$ defined in Chapter 2. This practice has the advantage of including the particulate phase responsiveness characteristics without referring to a specific particle size or fluid property. The prediction in these two figures show linearly increasing values of both fluid and particle center-line velocities with streamwise position and in very good agreement with the experimental data. The longitudinal variation of particulate phase wall-slip velocity is given in Fig. 7.7. The good agreement between measurements and prediction is an indirect confirmation of the validity of the wall treatment model presented in Chapter 3. From Fig. 7.7 it can be seen that for small values of $x/(\bar{U}_{f_{in.}}\tau_m)$, the wall-slip velocity, $\bar{U}_{p_w}$, varies linearly with $x/(\bar{U}_{f_{in.}}\tau_m)$ indicating the dominance of the inertial component to $\bar{U}_{p_w}$ in the entrance region as anticipated. It is interesting to note that for particulate phase mean volume fraction, $\bar{\alpha}$, as low as 10^{-5}, corresponding to the Stukel and Soo experiment predicted here, the continuum model for the Eulerian system of equations presented is still yielding fairly accurate results.

Comparisons between predicted and measured lateral variation of longitudinal slip velocity, $U_{f_z}-U_{p_z}$, are shown in Figs. 7.8 and

7.9 for the experiment of Kramer and Depew [1972b]. Figure 7.8 corresponds to the case with $\bar{\alpha}_{in.} = 8.4 \times 10^{-4}$ while Fig. 7.9 to the case with $\bar{\alpha}_{in.} = 4.2 \times 10^{-3}$. In each case the slip velocity is predicted for two particle sizes in flows which, otherwise, have the same characteristics. As shown in the figures, the larger 200 μm diameter particles are less responsive to the fluid motion and produce a higher slip velocity than the 62 μm particles. In the experiment, estimated values of the partcle response times non-dimensionalized by the time scale of the mean fluid motion ($D/U_{f_{in.}}$) were 552 and 53, respectively. The tenfold increase in particle response time for the larger particles relative to the small corresponds to a relative increase of about 2.7 in slip velocity at the pipe centerline for both values of particulate volume fractions. While both figures show good predictions for the 62 μm particles, predictions for the 200 μm particles show a considerable disagreement with respect to the data. This poor agreement can be explained by reference to several factors. The major source of discrepancy is the assumption of Stokes viscous drag for particle motion. The Reynolds number based on particle diameter and mean longitudinal slip velocity for the 62 μm and 200 μm particles are, $Re_p \simeq 12$ and $Re_p \simeq 130$, respectively. These values correspond to the pipe centerline for $\bar{\alpha}_{in.} = 8.4 \times 10^{-4}$. The rather high Reynolds number of the larger particles indicates the invalidity of a Stokes drag law assumption for the large particle calculations. Furthermore, the assumption of a continuum model for the particulate phase may be violated by relatively large particles. As already

mentioned, in order for the continuum model to hold in turbulent flow, the particle size should be smaller than the Kolmogorov length scale η. Estimates of η for the 0.5 in. pipe diameter flow experiment of Kramer and Depew give $10 \leq \eta \leq 100$ μm. This suggests that neither particle size conforms to the continuum assumption ($d_p \ll \eta$). However, it is clear that the 200 μm particles are in more serious violation of the assumption than the 62 μm particles for which predictions are in fairly good agreement with the measurements. In addition to the above two arguments accounting for the discrepancies observed between measurements and calculations, it should be noticed that the expression used for particle turbulent diffusivity in the calculation model is that of Peskin [1962] and is rigorously valid only for particles small enough that inertial forces will not displace them significantly from the vicinity of their initially neighboring fluid elements. The slip velocity profiles in Figs. 7.8 and 7.9 show maxima occurring at the pipe centerline. The slip velocity becomes zero as the wall is approached and it eventually attains a negative value due to the fact that while the fluid must come to rest on the wall, the particle phase is allowed to slip by.

The effect of particle volumetric concentration, or loading, for the 0.5 in. diameter pipe flow of Kramer and Depew [1972b] is shown in Fig. 7.10 with particulate mean velocity difference as the abscissa. Higher particulate volume fractions are associated with larger dissipation of fluid mean kinetic energy and, hence, fluid mean velocity. In the core region, fluid velocity will be decreased as is evident by the

data of Kramer and Depew. However, since the same particle size is used in each loading, the slip velocity remains roughly the same (see Figs. 7.8 and 7.9 resulting in a decrease in particulate mean velocity with increase in particulate volume fraction. The increase in the wall region shown by prediction of this work can be explained due to incorporation of a particulate wall shear stress which is proportional to particulate volume fraction, Eq. (3.4.2), resulting in larger velocities for more dilute flows.

So far only mean velocity prediction and their comparsion with corresponding measurements have been considered. Figure 7.11 provides a comparison between measurements and calculation of particle volume fraction, α, for different particle loading ratios (particle mass flow/ air mass flow). The experimental data were reported by Kramer and Depew [1972b] for a 0.5 in. pipeflow, at Re = 24,500, of 62 μm glass particles in air. The measurements show a radial dependence in α for loading ratios larger than about 3, with $\bar{\alpha}$ larger at the pipe centerline than at the wall. This phenomenon has not been explained by Kramer and Depew and, in fact, there appears to be conflicting information in the literature (see the same authors for such a discussion) concerning the correct variation of α with distance from the wall. In general, particles can be moved transversely to the main flow by the influence of body forces, thus setting up transverse variations in $\bar{\alpha}$ dictated by the sense of the applied body force. Since in the experiment by Kramer and Depew it appears that body forces were about normal to the pipe wall, if their observations are correct, the variation of α

with radial position must be due to a concentration-dependent fluid-particule interaction. Corresponding predictions of α given in Fig. 7.11 do not display the radial dependence shown by the experimental data. In the absence of body forces the two-phase flow turbulence model predicts uniform distributions of $\bar{\alpha}$ for all particle load ratios due, mainly, to the homogeneity influence of turbulence diffusion. Since the weak radial variation of $\bar{\alpha}$ measured by Kramer and Depew has not been explained by those authors and, in any event, the discrepancy between measurements and predictions is less than 16% for the highest load ratio, it may be concluded that a uniform prediction of $\bar{\alpha}$ is physically reasonable and certainly accurate enough for the present work.

Zisselmar and Molerus [1979] have measured the influence of particle concentration, $\bar{\alpha}$, on fluid turbulent characteristics for the case of 53 μm glass particles in liquid pipe flow using Laser-Doppler technique. Figure 7.12 shows predicted profiles of the transverse variation of fluid turbulent kinetic energy as a function of α, non-dimensionalized by the pure fluid phase value. Both experiments and calculations show that increasing the particle concentration lowers the level of fluid turbulence which can be dampened by as much as 50% for $\alpha_{in.} = 5.6\%$. As discussed in Chapter 3, with reference to term I_f of equation (3.2.30), the reduction in turbulent kinetic energy can be attributed to the turbulent energy transfer from the fluid to the particulate phase. The two-phase turbulence model presented in this work is capable of predicting such a variation as evidenced in the

figure. Deviations from the experimental data at the higher particulate concentrations are due to the diluteness assumption limitation present in the two-phase flow model. The under-prediction of the data at higher concentrations is, however, larger at the core region of the flow relative to the wall region as shown in Fig. 7.12. This can be attributed to the significance of mean convection and turbulent diffusion terms in the core region relative to the wall region where production and viscous dissipation effects are more dominant (see Eq. (3.2.30)). It should be noted that the mean convection, turbulent diffusion and production terms in k-transport equation contain a factor $(1-\bar{\alpha})$ which is assumed to be unity when the diluteness assumption is incorporated.

Variation of turbulent shear stress, $-\tilde{\rho}_f \overline{u_{f_r} u_{f_z}}$, with particulate concentration corresponding to the data of Zisselman and Molerus [1979] is shown in Fig. 7.13. The data corresponds to the radial position of y/D = 0.05 where maximum values for shear stress is reported by the authors. The reduction in fluid shear stress with increasing concentrations in predicted with good agreement by this work. The reduction in $-\overline{u_{f_r} u_{f_z}}$ can be explained by writing that:

$$-\overline{u_{f_r} u_{f_z}} \simeq c_\mu \frac{k^2}{\varepsilon} \frac{\partial \bar{U}_{f_z}}{\partial y}$$

at the wall region and in which the Prandtl-Kolmogorov relation for fluid eddy viscosity is incorporated. The experimental data of Kramer

and Depew [1972b] already presented show no significant variation in fluid longitudinal velocity gradient at the wall region of turbulent pipe flows. Therefore, the reductions in $-\overline{u_{f_r} u_{f_z}}$ with $\bar{\alpha}$ is attributed to corresponding decreases in k values which was already discussed. Similar to Fig. 7.12 and Fig. 7.13 also shows prediction deviations from data at higher concentrations which are due to incorporation of diluteness assumption.

7.2 Curved Channel Flow and Erosion Results

a) Testing

In contrast to straight channel flow, the lack of experimental data for fluid mechanical variables for two phase curved channel flows precludes any direct comparison between the calculations and corresponding experimental results.

A survey of literature shows that the basic dynamics of two-phase flow in curved channels and pipe geometries remain yet to be investigated. Techniques such as Laser-Doppler velocimetry have the potential for future research in this respect. For a thorough understanding of many effects of practical interest such a fundamental investigation is necessary. Among these are the erosion at walls caused by the impingement of solid particles, and wall deposition of solid particles.

The prediction of the relative rate of erosion at the concave walls of two-phase curved duct flows are shown in Figs. 7.14 and 7.15 for the experimental cases investigated by Mason and Smith [1972]. In their study the authors measured the erosion rate as a function of bend

angles for Reynolds numbers of 96000 and 140000 respectively in bends of different curvature. It can be seen that the qualitative pattern of erosion wear at the outer (concave) wall is well predicted.

The pattern shows an initially abrupt increase in the erosion rate maximizing at about a duct angle of 20°-25°. This is followed by a monotonic decrease in erosion until the duct exit is approached. The angular position corresponding to maximum erosion rate is predicted with good accuracy with the percentage deviation of prediction from experiment being about 5% at Re = 96000 and 2% at Re = 140000. Very good qualitative agreement is found between measurements and predictions of erosion rate over the first 20°-25° of duct curvature. The same agreement is not, however, found for bend angles larger than the maximum erosion position. In the region immediately following this location, prediction of erosive wear are larger than the corresponding measurements. This over-prediction is partly due to the absence of three-dimensional secondary flows in the calculation scheme which arise in practice; see Humphrey, Whitelaw and Yee [1981]. The lateral motion induced by the secondary flow, tends to reduce the particle angle of impingement as well as its mean kinetic energy of impingement by re-directing and dragging the particles in the lateral direction. Such an increase in the particle effective path-length through the duct increases the chances for repeated collisions with the bend walls which, by reducing the particulate kinetic energy of impingement, also reduce the rate of erosion. In the inlet region of the curved duct, the secondary motion is relatively weak and the closer agreement between

measurements and predictions is to be expected. It should be noticed that for bend angles following the position of maximum erosion, the experimental data, particularly for Re = 96000, shows considerable scatter rendering a comparison, at best, qualitative. However, in this region of the flow secondary motions clearly favor the overall reduction of erosive wear at concave wall as shown by the trend in the experiments.

Besides the secondary flow effects just discussed, an over-prediction of relative erosion rate in regions following the point of maximume erosion can also be attributed to particle wall rebounding effects which are not included in the prediction model. Particles with low mean kinetic energy rebounding from the band wall can slow down, directly through collision or induced drag, the more energetic particles approaching the wall. Consequently, the rate of erosive wear is reduced.

It should be noted that in spite of the lack of an inclusion of secondary flow and particle rebounding effects, the present model has reliably predicted the points of maximum erosion rates as well as the fairly large ratio of erosion wear throughout the inlet band region.

b) Applications

The results presented in the previous subsection have demonstrated the adequacy of the calculation procedure for predicting turbulent two-phase flow in straight and curved channels. In the following subsection the calculation procedure is used to document various characteristics of turbulent two-phase curved channel flow for which

there does not exist experimental information. In particular, predictions are presented and discussed for fluid and particle phase velocities, kinetic energies, and dissipation of fluid phase kinetic energy. Erosive wear is also predicted over a range of relevant parameters including particle size, response time and concentration, and fluid velocity.

Fluid mechanical results

Velocity profiles for both the fluid and the particle phase are shown in Figs. 7.15 - 7.19, and correspond to the cases of ψ = .01 (highly responsive), 1 and 100 (non-responsive) particles, respectively. The parameter ψ is a non-dimensional particle response time which is defined as:

$$\psi \equiv \frac{\tau_m \Delta}{\overline{U}_{f_o}}$$

with Δ and U_{f_o} as the channel width and fluid mean streamwise velocity at the channel inlet, respectively. For the cases predicted, Re = 10^5 and Rc/Δ = 12. The particle to fluid density ratio was typical of that of coal in water ($\tilde{\rho}_p/\tilde{\rho}_f$ = 1.8).

From the velocity profile calculations shown in Figs. 7.16 - 7.18 it is seen that the slip velocity, $\left|\overline{U}_{f_\theta} - \overline{U}_{p_\theta}\right|$, becomes more significant as ψ increases with the largest slip velocity corresponding to ψ = 100. For ψ = .01 there is virtually no difference between the velocity of the two phases. For this case, the ratio of slip velocity at the wall, where the highest velocity difference is expected, to the local

friction velocity, U_τ, is about 0.05; small enough to conclude that particulate wall slip velocities are negligible when $\psi < 0.01$. For $\psi = 1$, the local wall slip velocity is still small except in the wall regions where it is not negligible. As the parameter ψ increases the particulate phase becomes less responsive to the fluid motion and lags behind as shown in Fig. 7.18. The slip velocity increases as the flow proceeds through the channel. For large ψ values the particulate velocity profiles show slower particle motion in the vicinity of the outer wall as compared to the inner wall. The decrease is attributed to the presence of the Coriolis term in the particulate phase longitudinal momentum equation (the term $\bar{U}_{p_r}\bar{U}_{p_\theta}/r$ in Eq. (I.19)). For high ψ values the Coriolis force has a dominant effect compared to that of the viscous drag. The Coriolis force becomes particularly more significant at the outer wall where it becomes large in its value. For small ψ values the particulate motion is influenced much more directly by fluid-induced viscous drag. A comparison between the results in Fig. 7.18 for $\bar{\alpha}_{in.} = 0.1$ and Fig. 7.19 for $\bar{\alpha}_{in.} = 0.001$ shows that the magnitude of the slip velocity is independent of concentration for $\bar{\alpha}_{in.} \lesssim 0.1$.

Transverse variation of fluid turbulent kinetic energy and dissipation are plotted in Figs. 7.20 - 7.22 for various values of the parameters ψ and $\bar{\alpha}_{in.}$. The plots show that both k and ε decrease with increasing particle concentration. The decrease in fluid turbulent

kinetic energy is a manifestation of the dampening influence of the particulate phase on the flow. The energy lost by the fluid is transferred to the particulate phase, in the form of a particulate kinetic energy of turbulence through particle-fluid interaction, and/or dissipated, i.e., the so-called "drag dissipation". For both large, $\psi = 100$, and small, $\psi = 0.01$, values of the particle response parameter the reduction in ε is small. At intermediate values of ψ ($\simeq 1$) contributions to the balance of ε arising from the particle-fluid interaction term (see Eq. (3.2.36)) are maximized leading to more pronounced reductions in ε as a function of $\bar{\alpha}_{in.}$. It is a corresponding interaction which accounts for the reduction of k. Plots of the fluid turbulent kinetic energy for two values of the particle response time parameter are shown in Fig. 7.20 for $\alpha_{in.} = 0.01$. The profiles, show that small particles, with small response times, are more effective in extracting turbulent kinetic energy from the fluid to raise their own level of turbulent kinetic energy. The mechanism for this interaction was previously discussed in section 2 of Chapter 3.

Profiles for the transverse variation of dissipation of fluid kinetic energy of turbulence, shown in Fig. 7.21, display a notable dependence on the concentration ($\bar{\alpha}_{in.}$) at $\psi = 1$, which is not evident at the higher and lower values of the particle responsive parameter (i.e., $\psi = 100$ and $\psi = 0.01$). The sensitivity to α at intermediate values of ψ can be explained by reference to Eq. (3.2.30). In this equation for large values of τ_m ($\psi = 100$, for example) the fluid particle interaction term II_ε in the ε equation does not contribute

significantly to the balance of ε; hence variations in the magnitude of the term which are due to changes in α_{in} go unnoticed. Similarly, when τ_m is small (ψ = 0.01) particles respond so quickly to fluid fluctuations that differences between fluid and particle velocity gradients are small. This, again, leads to a reduced contribution of term II_ε to the balance of ε. However, at intermediate values of the particle response time parameter (ψ = 1) for which particle and velocity fluctuations are not entirely in phase, the predicted level of dissipation is significantly dependent on the concentration ($\bar{\alpha}$) of the particulate phase.

With respect to the above, it is important to note that while the fluid dissipation ε decreases with increasing concentration α, the total dissipation ε_t (the sum of ε and the additional "drag dissipation", ε_D; see Eq. 3.2.33) may actually increase.

Transverse profiles of particulate phase turbulent kinetic energy (k_p) are given in Figs. 7.23 and 7.24 for various values of ψ and α_{in}. The profiles in Fig. 7.23 show that particles with relatively large response times, ψ = 100, have lower values of k_p due to their inertia, while particles with smaller ψ (1 - 0.1), because they are able to respond to fluid fluctuations more readily, show larger values of turbulent kinetic energy. Values of k_p were predicted from Eq. (4.2.5a), $k_p = k\ T_L/(T_L + \tau_m)$. For small values of the particle response time τ_m, k_p approaches the fluid kinetic energy distribution result, as shown by the profile for ψ = 0.01. However, for larger values of τ_m, corresponding to ψ = 1 and 100 respectively,

the behavior of k_p is that of k, modulated by the ratio T_L/τ_m. This ratio of time scales is proportional to k/ε and is responsible for the peaks in the k_p distributions near the walls.

The dependence of k_p on $\bar{\alpha}_{in}$. is displayed in Fig. 7.24. The peaks in the distribution arise for the reasons explained above. In addition, the profiles show that as the particulate phase concentration is increased, dampening effects diminish the levels of fluid kinetic energy of turbulence k, thus reducing (see formula for k_p above) the source of kinetic energy for the particulate phase.

Erosion wear results

Figures 7.25 through 7.29 provide the bulk of the calculated results obtained in this study relating to erosive wear at the concave wall of a two-dimensional curved channel flow. As in the previous sections, the channel curvature ratio was $R_c/\Delta = 12$. Values of the Reynolds number and particle response time parameter investigated were:

$$Re = 10^4,\ 5 \times 10^4,\ 10^5,\ 5 \times 10^5,\ 10^6$$

$$\psi = 0.01,\ 0.1,\ 1.0,\ 10.0,\ 100.0$$

The choice of the values covers almost the complete range of situations of practical interest.

Erosion predictions were made using the model of Finnie as described in Chapter 6, and the results are given in the form of dimensionless rates of erosion wear as a function of the curved channel angle (streamwise location). In the plots, the quantity $\dot{E}$ is the volume eroded of wall material per unit area per unit time, p_1 is the

Vickers hardness of the material, m_p is the mass flux of the particulate phase at the channel inlet and $(\overline{U}_{p\theta_{in.}})$ is the particulate phase mean velocity at the same location.

Figures 7.25 - 7.29 show that, for a fixed Reynolds number, the rate of erosion ($\dot{E}$) increases with an increase in the particle response time parameter (ψ). Physically, this is realistic since large inertial particles, large ψ, can be expected to deport more significantly from an alignment with the fluid streamlines at the outer wall, than the smaller more responsive particles.

Calculations for $\psi = 4.9 \times 10^{-5}$ (not shown here) corresponding to 5 μm solid particles at a Re = 10^4 with $\tilde{\rho}_p/\tilde{\rho}_f = 1.8$ show no particulate phase impingement on the concave channel wall and almost identical velocity profiles for both phases. However, for $\psi = 0.01$, corresponding to 72 μm particles with the same density ratio and at the same Reynolds number, particles impinge on the concave wall only after a channel angle of $\theta \simeq 38°$, causing erosion of the channel wall as of the location. Between $\theta = 38°$ and the channel inlet, for this case the particulate phase inertial forces are balanced by fluid viscous drag which controls the movement of the particles and prevents any collision with the wall. Nevertheless, as the flow proceeds downstream, the centrifugal force due to flow curvature induces a radial component of motion on the particles which eventually results in their particulate impingement on the concave wall. For this case it follows that:

centrifugal force > radial viscous drag force

and from Fig. (6.1):

$$\frac{\overline{U}_p^2}{r} > \frac{\overline{v}_p}{\tau_m} \tag{7.2.1}$$

in which the radial fluid velocity component is neglected with respect to the particulate phase velocity. Therefore, the angle of impingement ($\beta_{imp.}$) is, approximately:

$$\tan \beta_{imp.} < \frac{\overline{U}_p}{\overline{U}_{f_o}} \cdot \frac{\tau_m}{T} \cdot \frac{\Delta}{r} \tag{7.2.2}$$

For small values of τ_m/T, $U_p \approx U_{f_o}$ and thus from Eq. (7.2.2) one obtains:

$$\beta_{imp.} \leq \tan^{-1} (\tau_m/T \cdot \Delta/r) \tag{7.2.3}$$

This expression gives an upper limit for the angle of impingement when centrifugal forces are significant. For $R_c/\Delta = 12$ and $\tau_m/T = 4.7 \times 10^{-5}$, corresponding to 5 μm solid particles with $\tilde{\rho}_p/\tilde{\rho}_f = 1.8$, the maximum impingement angles is; $\beta_{max} \approx 2.2 \times 10^{-4}$ which is too small to cause significant erosion.

Table 7.2 provides a comparison between values of the maximum particle impingement angle calculated from Eq. (7.2.3) and also from the numerical turbulence model of this work for a curved channel with $R_c/\Delta = 12$. Given the relatively good agreement for the order of magnitudes shown between corresponding results for a given ψ, it may be inferred that for $0.01 < \psi < 1.0$ the centrifugal and viscous drag forces are in approximate balance and Eq. (7.2.3) provides a convenient

Table 7.2

ψ	β_{max} (from Eq. (7.2.3))	β_{max}, (from turbulence model of this work)		
		$Re = 10^4$	$Re = 10^5$	$Re = 10^6$
.01	4.8×10^{-2}	2×10^{-2}	1.4×10^{-2}	1.5×10^{-2}
0.1	0.48	0.20	0.29	0.28
1.0	4.8	5.2	3.3	3.0

estimate for the particle phase impingement angle at the concave wall. For larger values of ψ, the approximation $U_p \approx U_{f_0}$ can not be made due to the importance of particle inertial effects and Eq. (7.2.3) for predicting β_{max} does not apply.

With increasing values of ψ, particles become less responsive to the fluid motion at a fixed Reynolds number and the point of initial erosion moves further upstream in the channel. This is shown in Fig. (7.2.5) for Re = 10^4 in which the increase in ψ from .01 to 0.1 causes the initial erosion point to be moved from 38° to 22° while at Re = 10^6 the same increase moves that point from 40° to 12° which is an indication of the particles' increased inertial effects in the higher Reynolds numbers. The situations for ψ = .1 and ψ = 1 values correspond to 226 μm and 715 μm particles with $\tilde{\rho}_p/\tilde{\rho}_f$ = 1.8 at Re = 10^4.

The increase in ψ will increase the erosion rates accordingly. However, the increase is not linear as is shown in Figs. 7.2.5 to 7.2.9. At Re = 10^4 the increase in ψ from .01 to 100, four order of magnitudes, will cause an erosion rate by as much as six orders of magnitudes higher.

Based on above arguments it is concluded that for a constant Reynolds number different erosion patterns could be observed depending on ψ values. For small values of ψ the non-dimensional erosion rate increases as one proceeds downstream and the maximum erosion rate occurs at the exit. However, for large ψ values, i.e., for $\psi > 10$, the erosion patterns becomes completely different. It reaches a maximum initially and then descends down until it reaches an almost constant

value as the channel exit is approached. It is interesting to note that for such large ψ values the shape of the profile remains the same irrespective of ψ values or the Reynolds number and the profiles corresponding to the larger ψ values are shifted slightly upwards. This means that in this region of high ψ starting approximately from $\psi = 10$ (corresponding to, for instace, 226$^{\mu}$ particle with $\tilde{\rho}_p/\tilde{\rho}_f = 1.8$ at $Re = 10^6$) to higher ψ-values (corresponding to higher particle sizes at any Reynolds number $\geq 10^4$) the absolute value for erosion rate at a fixed point on the curved channel outer wall becomes proportional to:

$$\dot{E} \propto \bar{\alpha}_{in}\left(\bar{U}_{p_{in}}\right)^3 \tag{7.2.4}$$

irrespective of Reynolds number and ψ. Although, strictly speaking it is a weak function of the latter variable as shown in Figs. 7.25 - 7.29. It is interesting to note that the same dependency as above, of the erosion rate on the mean characteristic velocity in the range of high ψ value was also obtained by Laitone [1979b]. In that investigation the erosion caused by the laminar, two-phase, fluid-particulate flow for a flat wall was analyzed in which the mean time scale T was defined by the free stream velocity and a characteristic length scale. The same conclusion was also reached by Yeung [1977] who investigated the erosion in curved pipes using a Lagrangian formulation in laminar flow. In the latter study the erosion results were subdivided into respectively high and low velocity categories, equivalent to high and low values of ψ here. The dependency of $\dot{E}$ on $\bar{\alpha}_{in}$ is linear as shown by Eq. (7.2.4). This has also been concluded by Yeung [1977].

The non-dimensionalized erosion rate profiles, for $\psi > 1.0$, are characterized by a maximum at $\theta \simeq 20°$ after which the profiles descends slightly to approach asymptotic values. The existence of the maximum point of erosion for large ψ values, corresponding to rather large and non-responsive particles, is due to erosion effects by initial momentum of the entering particles. In this situation, unlike the case for small ψ values, i.e., small and responsive particles, the fluid viscous drag is not capable of aligning the particles rapidly enough with the fluid streamlines at the concave wall which subsequently results in impaction with the wall and erosion of the wall material. The decline in profile following the maximum is due to reductions in the particulate mean kinetic energy as one moves downstream.

In the experiment of Mason and Smith [1972] at Re = 140000, Fig. 7.15, the corresponding ψ value is about 5.24 and therefore shows the high erosion pattern. The non-dimensional erosion rate becomes, approximately, constant as the channel exit is approached. This is due to counteracting effects of longitudinal reduction in the mean kinetic energy which is being balanced by the centrifugal force acting in such a way as to push the particles outwards and therefore enhance the the impingement on the wall. In Fig. 7.30 the longitudinal variation of mean kinetic energy of impact at various ψ values at Re = 10^5 is shown. It can be seen that as ψ increases the reduction in kinetic energy becomes more significant as the exit is approached. The streamwise variation of angle of impingement is shown in Fig. 7.31.

The velocity vector plots corresponding to various ψ values at $Re = 10^5$ are shown in Figs. 7.32 - 7.34. It can be seen that with decreasing ψ, the particulate velocity at the outer wall becomes more aligned with the fluid velocity. From Figs. 7.25 to 7.29 it is observed that for large ψ values the magnitude of non-dimensional erosion wear remains almost constant with respect to changes in Reynolds number. However, for small ψ values its magnitude will increase with the Reynolds number and the increase is more enhanced for lower ψ value. For example, for an increase of Reynolds number from 10^4 to 10^6 the non-dimensional erosion rate at the channel exit for $\psi = .1$ is almost doubled while for $\psi = .01$ it is as much as ten times higher.

From the practical point of view and for the design of pipeline components and apparatus it is the maximum erosion rate of the wall material which plays a decisive role in the design process. Figure 7.35 shows the variation of normalized maximum erosion rate versus Reynolds number for various ψ values which correspond to different particle size, fluid properties and channel widths.

CHAPTER 8

CONCLUSIONS AND RECOMMENDATIONS

The main conclusions of this study are summarized below.

1 - The purpose of this work has been twofold:

a) To formulate, and predict two-phase turbulent flows based on modeled transport equations for the fluid and particulate phases as well as the equations governing fluid turbulent kinetic energy and dissipation of turbulent kinetic energy.

b) Related to the above, to develop a model of turbulence for dilute two-phase fluid-particulate flows. The turbulence model is based on the two-equation (k-ε) model of turbulence considered here in its fully-elliptic form to allow for possible flow recirculation.

2 - The analysis of solid particulate effects on the fluid turbulence in dilute two-phase flow shows the following results:

a) Viscous interactions between the fluid and suspended solid particles causes a reduction in the fluid turbulent kinetic energy and also in the small scale dissipation rate of viscous fluid turbulent kinetic energy.

b) The presence of solid particulates in turbulent two-phase flows, and attendant dynamical interactions between the two phases, provide a second mechanism for the dissipation of turbulent, and mean, kinetic energy. The dissipation rate associated with this process is referred to as "drag dissipation".

c) Furthermore, an additional mechanism is evolved by which kinetic energy is exchanged between the mean and the turbulent motion of both phases.

3 - The fluid-particle velocity and velocity-gradient correlation terms which appear in the transport equations for fluid turbulent kinetic energy and dissipation rate of fluid turbulent kinetic energy, respectively, are modeled using the particulate Lagrangian equation of motion with Stokes' drag as the only driving force considered. Modeled terms obtained in this manner display expected limiting forms in the formulation.

4 - Predictions based on the turbulence model presented in this work, of various characteristics of straight channel turbulence two-phase flow, are generally in good agreement with the available experimental data. Deviations from the experimental data occur for the cases in which: particulate concentration exceeds 5% by volume; particle Reynolds number becomes much larger than unity; field forces arise, such as electrostatic, which have not been included in the model formulation.

5 - The variation of various fluid turbulence quantities such as turbulent kinetic energy and turbulent shear stress with particulate concentration are correctly predicted by the model. Significant deviations from experimental data occur at high particulate concentrations, for which the turbulence model is not valid.

6 - For curved channel flows, the pattern of erosion rate and the streamwise location of the point of maximum erosion on the outer channel wall are well predicted using the models for turbulence

and erosion presented in this work. Deviations from experimental data are due mainly to the non-inclusion of cross-stream (secondary) flows in the prediction scheme, as well as the absence of particle wall rebounding effects in the erosion model.

The following recommendations are offered for continuing research along the lines of the present approach. For the prediction of a wider class of turbulent two-phase flows, further generalization of the model presented in this work is in order. This can be achieved by reconsidering and minimizing the simplifying assumptions made during the course of the analysis in order to extend the range of validity of the dependent variables in the formulation. Among these, an extension of solid particulate concentrations to higher values is probably the most desirable. This is because in most solid-liquid flows of industrial interest, like slurry flows or pneumatic conveying of solid particulates, the particulate volume concentration can reach values as high as 50%. The model and the numerical technique presented in this work can be used as a basis for further developments in this regard. The inclusion of field forces such as electrostatic, gravity, etc., will also extend the range of applicability of the model. The adoption of a more general expression for the particulate phase eddy diffusivity in terms of known field variables should also be considered. Finally, based on the arguments given in Chapter 7, for improved predictions of the erosion pattern at the outer wall of curved ducts, cross-stream (secondary) flows and particulate wall rebounding effects should be included in the model formulation.

Although there have been and continue to be numerous research activities in the field of fluid-particulate turbulent flows, high quality fundamental investigations still remain an absolute necessity. In particular, there is a serious need for quantitative experimental work yielding accurate results of value for guiding and testing numerical models for these flows. While the practical need to predict the characteristics of turbulent two-phase flows has been the main incentive for this work, the author believes that more improved model formulations can only be achieved at a pace comparable to that of the discovery of basic facts through experimentation. Strategically planned, carefully executed, fundamental experimental work will continue to play a dominant role in future theoretical and modeling advancements relating formulations to turbulent two-phase flows.

REFERENCES

Abramovich, G.N. (1971)
"Effect of solid-particle or droplet admixture on the structure of a turbulent gas jet," International Journal of Heat and Mass Transfer, 14, pp. 1039-1045.

Abramovich, G.N. and Girshovich, T.A. (1974)
"Diffusion of heavy-particles in turbulent gas streams," Sov. Phys. Dokl., 18, no. 9, pp. 587-589.

Abuaf, N. and Gutfinger, C. (1974)
"Trajectories of charged solid particles in an air jet under the influence of an electrostatic field," International Journal of Multiphase Flow, 1, pp. 513-523.

Basset, A.B. (1888)
"A Treatise On Hydrodynamics," Deighton-Bell and Co., Cambridge, England.

Baw, P.S. and Peskin, R.L. (1971)
"Some aspects of gas-solid suspension turbulence," Trans. ASME, J. Basic Eng., 93D, pp. 631-635.

Boothroyd, R.G. (1971)
"Flowing Gas-Solids Suspensions," Chapman and Hall Ltd., London, England.

Boussinesq, J. (1903)
"Theorie analytique de la chaleur," Gauthier-Villars, Paris.

Boyce, M.P. and Blick, E.F. (1970)
"Fluid flow phenomena in dusty air," ASME paper 69-WA/FE-24.

Brun, R.J. and Mergler, H.W. (1973)
"Impingement of water droplets on a cylinder in an incompressible flow field and evaluation of rotating multicylinder method for measurement of droplet-size distribution, volume-median droplet size, and liquid-water content in clouds." NACA TN 2904.

Bryant, D. and Humphrey, J.A.C. (1976)
Conservation equations for laminar and turbulent flows in general three-dimensional curvilinear coordinates, Rep. No. CHT/76/6, Imperial College of Science and Technology, London.

Chao, B.T. (1964)
"Turbulent transport behavior of small particles in dilute suspensions," Osterreichisches Ingenieur-Archiv, 18, no. 1/2, pp. 7-21.

Corrsin, S. (1963)
"Estimates of the relations between Eulerian and Lagrangian scales in large Reynolds number turbulence," J. Atm. Sci., 20, p. 115.

Corrsin, S. and Lumley, J.L. (1956)
"The equation of motion for a particle in turbulent fluid," Applied Scientific Research, sec. A, 6, pp. 114-116.

Crowe, C.T. and Pratt, D.T. (1972)
"Two-dimensional gas-particle flows," Proc. Heat Trans. and Fluid Mech., Inst. 23rd Meeting, June 14-16, Stanford University Press, Calif.

Cox, R.G. and Mason, S.G. (1971)
"Suspended particles in fluid flow through tubes," Ann. Rev. Fluid Mech., 3, pp. 291-316.

Csandy, G.T. (1963)
"Turbulent diffusion of heavy particles in the atmosphere," J. Atm. Sci., 20, pp. 201-208.

Culick, F.E.C. (1964)
"Boltzmann equation applied to a problem of two-phase flow," The Physics of Fluids, 7, no. 12, pp. 1898-1904.

Danon, H., Wolfshtein, M., Hetsroni, G. (1977)
"Numerical calculations of two-phase turbulent round jet," International Journal of Multiphase Flow, 3, pp. 223-234.

Davidson, G.A. and McComb, W.D. (1975)
"Turbulent diffusion in an aerosol jet," J. Aerosol Sci., 6, pp. 227-247.

Drew, D.A. (1975)
"Turbulent sediment over a flat bottom using momentum balance," J. Appl. Trans. ASME, 97E, pp. 38-44.

Drew, D.A. (1976a)
"Production and dissipation of energy in the turbulent flow of a particle-fluid mixture, with some results on drag reduction," J. Appl. Mech. Trans. ASME, no. 4, pp. 543-547.

Drew, D.A. (1976b)
"Two phase flows: constitutive equations for lift and Brownian motion and some basic flows," Archive for Rational Mechanics and Analysis, 62, no. 2, pp. 149-163.

Einstein, A. (1906)
"Eine neu Bestimmung der Molekuldimensionen," Ann. Physik., 19, pp. 289-306.

Finnie, I. (1972)
"Some observations on the erosion of ductile metals," Wear, 19, pp. 81-90.

Friedlander, S.K. (1957)
"Behavior of suspended particles in a turbulent fluid," A.I.Ch.E. Journal, vol. 3, no. 3, pp. 381-385.

Friedlander, S.K. and Johnstone, H.F. (1957)
"Deposition of suspended particles from turbulent gas streams," Industrial and Engineering Chemistry, 49, no. 7, pp. 1151-1156.

Genchev, Zh.D. and Karpuzov, D.S. (1980)
"Effects of the motion of dust particles on turbulence transport equations," J. Fluid Mech., 101, part 4, pp. 833-842.

Glauert, M. (1940)
"A method of constructing the paths of raindrops of different diameters moving in the neighborhood of (1) a circular cylinder, (2) an aerofoil, placed in a uniform stream of air; and a determination of the rate of deposit of the drops on the surface and the percentage of drops caught." R&M, British A.R.C. no. 2025.

Goldschmidt, V. and Eskinazi, S. (1966)
"Two-phase turbulent flow in a plane jet," J. App. Mech., Trans. ASME, 33E, pp. 735-747.

Goldschmidt, V.W., Householder, M.K., Ahmadi, G. and Chuang, S.C. (1972)
"Turbulent diffusion of small particles suspended in turbulent jet," Prog. Heat Mass Transf., 6, pp. 487-508.

Gosman, A.D. and Pun, W.M. (1974)
"Calculation of Recirculating Flows," (lecture notes), Dept. of Mech. Eng., Imperial College, London, Rep. No. HTS/74/2.

Gudmundsson, J.S. and Bott, T.R. (1977)
"Particle diffusivity in turbulent pipe flow," J. Aerosol Sci., 8, pp. 317-319.

Harlow, F.H. and Nakayama, P.I. (1967)
"Turbulence transport equations," Phys. of Fluids, 10, no. 11, pp. 2323-2332.

Harlow, F.H. and Welch, J.E. (1965)
"Numerical calculation of time-dependent viscous incompressible flow of fluid with free surface," Phys. of Fluids, 8, no. 12, pp. 2182-2189.

Hay, J.S. and Pasquil, F. (1959)
"Diffusion from a continuous source in relation to the spectrum and scale of turbulence," Advances in Geophysics, 6, p. 345.

Hedman, P.O. and Smoot, L.D. (1975)
"Particle-gas dispersion effects in confined coaxial jets," A.I.Ch.E., 21, no. 2, pp. 372-379.

Hino, M. (1963)
"Turbulent flow with suspended particles," Proc. ASCE Journal, J. Hydr. Div., HY4, pp. 161-187.

Hinze, J.O. (1962)
"Momentum and mechanical energy balance equations for a flowing homogeneous suspension with slip between the two phases," Appl. Sci. Res., 11, section A, pp. 33-46.

Hinze, J.O. (1972)
"Turbulent fluid and particle interactions," Prog. in Heat and Mass transfer, 6, Pergamon Press, New York, pp. 433-452.

Hinze, J.O. (1975)
"Turbulence," McGraw-Hill Inc., New York.

Hjemfelt, Jr., A.T. and Mockros, L.F. (1966)
"Motion of discrete particles in a turbulent flow," Appl. Sci. Res., 16, pp. 149-161.

Householder, M.K. and Goldschmidt, V.W. (1969)
"Turbulent diffusion and Schmidt number of particles," J. Eng. Mech. Div., EM6, ASCE.

Hughes, R.R. and Gilliland, E.R. (1952)
"The mechanics of drops," Chem. Eng. Prog., 48, no. 10, pp. 497-504.

Humphrey, J.A.C. (1978)
"Numerical calculation of developing laminar flow in pipe of arbitrary curvature radius," Can. J. Chem. Eng., 56, p. 151.

Humphrey, J.A.C., Whitelaw, J.H. and Yee, G. (1981)
"Turbulent flow in a square duct with strong curvature," J. Fluid Mech., 103, pp. 443-463.

Kada, H. and Hanratty, T.J. (1960)
"Effects of solids in turbulence in a fluid," A.I.Ch.E. Jour., 6, no. 4, pp. 624-630.

Kalinske, A.A. and Pien, C.L. (1944)
"Eddy diffusion," Ind. Eng. Chem., 36, no. 3, pp. 220-223.

Kraiko, A.N. and Sternin, L.E. (1965)
"Theory of flows of a two-velocity continuous medium containing solid or liquid droplets," Appl. Math. and Mech. (PMM), 29, no. 3, pp. 482-496.

Kramer, T.J. and Depew, C.A. (1972a)
"Analysis of mean flow characteristics of gas-solids suspensions," J. Basic Eng. Trans. ASME, 94D, pp. 731-738.

Kramer, T.J. and Depew, C.A. (1972b)
"Experimentally determined mean flow characteristics of gas-solid suspensions," ASME, paper no. 72-FE-29.

Laitone, J.A. (1979a)
"Separation Effects in Gas-Particle Flows at High Reynolds Numbers," Ph.D. thesis, University of California, Berkeley.

Laitone, J.A. (1979b)
"Erosion prediction near a stagnation point resulting from aerodynamically entrained solid particles," J. Aircraft, 16, no. 11, pp. .

Langmuir, I. and Blodgett, K.B. (1946)
"A mathematical investigation of water droplet trajectories," Tech. Rep. No. 5418, Air Material Command, AAF.

Lee, S.L. and Einav, S. (1972)
"Migration in a laminar suspensions boundary layer measured by the use of a two-dimensional Laser-Doppler anemometer," Prog. in Heat and Mass Trans., 6, pp. 385-403.

Levich, V.G. and Kuchanov, S.I. (1967)
"Motion of particles suspended in turbulent flow," Soviet Physics-Doklady, 12, no. 6, pp. 546-551.

Lilly, G.P. (1973)
"Effect of particle size on particle eddy diffusivity," Ind. Eng. Chem. Fund., 12, no. 3, pp. 268-275.

Liu, V.C. (1956)
"Turbulent dispersion of dynamic particles," J. of Meteorology, 13, pp. 399-405.

Liu, B.Y.H. and Ilori, T.A. (1974)
"Aerosol deposition in turbulent pipe flow," Envir. Sci. Technol., 8, pp. 351-356.

Lugt, H.J. and Schot, J.W. (1974)
"A review of slip flow in continuum physics," Proceedings of the Second Symposium on Fluid-Solid Surface Interactions, Bethesda, Md., pp. 101-136.

Lumley, J.L. (1957)
"Some Problems Connected with the Motion of Small Particles in Turbulent fluid," Ph.D. thesis, Johns Hopkins University, Baltimore, Maryland.

Lumley, J.L. (1973)
"Drag reduction in turbulent flow by polymer additives," J. Polymer Sci., Macromolecular Reviews, 7, pp. 263-290.

Lumley, J.L. (1976)
"Two phase and non-Newtonian flows," Topics in Applied Physics-Turbulence, 12, Springer-Verlag, pp. 289-324.

Marble, F.E. (1963)
"Dynamics of a gas containing small solid particles," Combustion and Propulsion, Fifth AGARD Colloquim-High Temperature Phenomena, Pergamon Press, New York, pp. 175-215.

Marble, F.E. (1964)
"Mechanism of particle collision in one-dimensional dynamics of gas-particle mixture," Phys. Fluids, 7, pp. 1270-1282.

Mason, J.S. and Smith, B.V. (1972)
"The erosion of bands by pneumatically conveyed suspensions of abrasive particles," Powder Technology, 6, pp. 323-335.

McCarthy, H.E. and Olson, J.H. (1968)
"Turbulent flow of gas-solids suspensions," Ind. and Eng. Chem. Fund., 5, no. 3, pp. 417-477.

Meek, C.C. and Jones, B.G. (1973)
"Studies on the behavior of heavy particles in a turbulent fluid flow," J. Atm. Sci., 30, pp. 239-244.

Melville, W.K. and Bray, K.N.C. (1977)
"The two-phase turbulent jet," Int. J. Heat Mass Transfer, 22, pp. 279-287.

Mickelsen, W.R. (1955)
"An experimental comparison of the Lagrangian and Eulerian correlation coefficients in homogeneous isotropic turbulence," NACA TN 3570.

Milne-Thomson, L.M. (1968)
Theoretical Hydrodynamics, The Macmillan Press Ltd.

Murray, J.D. (1965)
"On the mathematics of fluidization," J. Fluid Mech., 21, Part 3, pp. 465-493.

Nagarajan, M. and Murgatroyd, W. (1971)
"A simple model of turbulent glass-solids flow in a pipe," Aerosol Sci., 2, pp. 15-22.

Nagarajan, M. (1972)
"On the turbulent pipe flow of gas-solids suspensions," Aerosol Sci., 3, pp. 157-165.

Odar, F. (1966)
"Verification of proposed equation for calculation of forces on a sphere accelerating in a viscous fluid," J. Fluid Mech., 25, no. 3, pp. 591-592.

Oseen, C.W. (1927)
Neuere Methoden und Ergebnisse in der Hydrodynamik, part 16, Akademische Verlagsgesellschaft, Leipzig.

Owen, P.R. (1969)
"Pneumatic transport," J. Fluid Mech., 39, part 2, pp. 407-432.

Patankar, S.V. (1980)
"Numerical Heat Transfer and Fluid Flow," Hemisphere Publishing Co., Washington.

Patankar, S.V. and Spalding, D.B. (1972)
"A calculation procedure for heat, mass and momentum transfer in three-dimensional parabolic flows," Int. J. Heat and Mass Transfer, 15, pp. 1787-1806.

Peskin, R.L. (1959)
"Some Effects of Particle-Particle and Particle-Fluid Interactions in Two-Phase Flow Systems," Ph.D. thesis, Princeton University, Princeton, New Jersey.

Peskin, R.L. (1962)
"The diffusivity of small suspended particles in turbulent fluids," Presented at the National Meeting A.I.Ch.E., Baltimore, Maryland.

Peskin, R.L. (1975)
"Some fundamental research problems in gas-solids flows," Am. Inst. of Chem. Eng. Symposium Series, 71, no. 147, pp. 42-59.

Peskin, R.L. and Dwyer, H.A. (1965)
"Study of mechanis of turbulent gas-solid shear flows," ASME, paper no. 65-WA/FE-24.

Peskin, R.L. and Kau, C.J. (1979)
"Numerical simulation of particulate motion in turbulent gas-solid channel flow," J. Fluids Engineering, vol. 101, pp. 319-325.

Popper, J., Abauf, N. and Hetsroni, G. (1974)
"Velocity measurements in a two-phase turbulent jet," Int. J., Multi-phase Flow, 1, pp. 715-726.

Reddy, K.V.S. and Pei, D.C.T. (1969)
"Particle dynamics in solid-gas flow in a vertical pipe," Ind. Eng. Chem. Fund., 8, no. 3, pp. 490-497.

Rodi, W. (1970)
"Basic Equations for Turbulent Flow in Cartesian and Cylindrical Coordinates," Department of Mechanical Engineering, Imperial College of Science and Technology, London, Report No. BL/TN/A/36.

Rouse, H. (1939)
"Experiments on the mechanics of sediment suspension," Proc. Fifth Int. Cong. Appl. Mech., John Wiley and Sons, New York, pp. 550-554.

Rubinow, S.I. and Keller, J.B. (1961)
"The transverse force on a spinning sphere moving in a viscous fluid," J. Fluid Mech., 11, pp. 447-459.

Saffman, P.G. (1965)
"The lift on a small sphere in a slow shear flow," J. Fluid Mech., 22, Part 2, pp. 385-400.

Schlichting, H. (1968)
"Boundary Layer Theory," Mc-Graw Hill Book Co.

Segre, G. and Silberberg, A. (1962)
"Behavior of macroscopic rigid spheres in poiseuille flow," J. Fluid Mech., 14, pp. 115-157.

Sherman, F.S. (1969)
"The transition from continuum to molecular flow," Annual Review of Fluid Mechanics, 1, pp. 317-340.

Shlien, D.J. and Corrsin, S. (1974)
"A measurement of Lagrangian velocity autocorrelation in approximately isotropic turbulence," J. Fluid Mech., 62, p. 255.

Singleton, R.E. (1965)
"The compressible gas-solid particle flow over a semi-infinite flat plate," J. App. Math. Phys. (ZAMP), 16, pp. 421-449.

Smith, P.J., Fletcher, T.H. and Smoot, L.D. (1980)
"Two-dimensional model for pulverized coal combustion and gasification," Meeting of the Combustion Institute, Western States Section, University of California at Irvine, pp. 21-22.

Snyder, W.H. and Lumley, J.L. (1971)
"Some measurements of particle velocity autocorrelation functions in a turbulent flow," J. Fluid Mech., 48, part 1, pp. 41-71.

Soo, S.L. (1956)
"Statistical properties of momentum transfer in two-phase flow," Chem. Eng. Sci., 5, no. 2, pp. 57-67.

Soo, S.L. (1962a)
"Fully developed turbulent pipe flow of a gas-solid suspension," Ind. and Eng. Chem. Fundamentals, 1, no. 1, pp. 33-37.

Soo, S.L. (1962b)
"Boundary layer motion of a gas-solids suspension," Proceedings of Symposiun on "Interactions Between Fluids and Particles, Institute of Chemical Engineers, London, pp. 50-63.

Soo, S.L. (1967)
"Fluid Dynamics of Multiphase Systems," Blaisdell Publishing Co., Waltham, Massachusetts.

Soo, S.L. (1968)
"Non-equilibrium fluid dynamics-Laminar flow over a flat plate," ZAMP, 19, pp. 545-563.

Soo, S.L. (1969)
"Pipe flow of suspensions," Appl. Sci. Res., 21, pp. 68-84.

Soo, S.L. (1971)
"Pipe flow of suspensions in turbulent fluid. Electrostatic and gravity effects," Appl. Sci. Res., 24, pp. 83-97.

Soo, S.L. (1975)
"Equation of motion of a solid particle suspended in a fluid," The Physics of Fluids, Research Notes, 18, no. 2, pp. 263-264.

Soo, S.L. (1976)
"Net effect of pressure gradient on a sphere," Physics of Fluids, Research Notes, 19, no. 5, p. 757.

Soo, S.L., Ihrig, Jr., H.K. and El Kough, A.F. (1960)
"Experimental determination of statistical properties of two-phase turbulent motion," J. Basic Eng., Trans. ASME, 82D, no. 3, pp. 609-621.

Soo, S.L. and Peskin, L. (1958)
"Statistical distribution of solid phase in two-phase turbulent motion," Project SQUID Technical Report PR-80-R.

Soo, S.L., Regalbuto, J.A. (1960)
"Concentration distribution in two-phase pipe flow," Can. J. of Chem. Eng., 38, no. 5, pp. 160-166.

Soo, S.L., Tien, C.L. (1960)
"Effect of the wall on two-phase turbulent motion," Journal of Applied Mechanics, Trans. ASME, 27E, no. 1, pp. 5-15.

Soo, S.L. and Trezek, G.J. (1966)
"Turbulent pipe flow of magnesia particles in air," Ind. and Eng. Chem. Fundamentals, 5, no. 3, pp. 388-392.

Soo, S.L. and Tung, S.K. (1972)
"Deposition and entrainment in pipe flow of a suspension," Powder Technology, 6, pp. 283-295.

Spalding, D.B. (1972)
"A novel finite difference formulation for differential expressions involving both first and second derivatives," Int. J. Num. Methods in Eng., 4, pp. 551-559.

Stukel, J.J. and Soo, S.L. (1969)
"Turbulent flow of a suspension into a channel," Powder Technology, 2, pp. 278-289.

Stukel, J.J. (1970-71)
"Integral method as applied to a turbulent boundary layer of a gas-solid suspension," Powder Technology, 4, pp. 163-165.

Taylor, G.I. (1921)
"Diffusion by continuous movements," Proc. London Math. Soc., 20, pp. 196.

Tchen, C.M. (1947)
"Mean Value and Correlation Problems Connected with the Motion of Small Particles in a Turbulent Fluid," Ph.D. thesis, Delft, Martinus Nijhoff, The Hague.

Tennekes, H. and Lumley, J.L. (1972)
"A First Course in Turbulence, MIT Press," Cambridge, Massachusetts.

Torobin, L.B. and Gauvin, W.H. (1959)
"Fundamental aspects of solids-gas flow," Can. J. Chem. Eng., 37, p. 129, 167, 224.

Torobin, L.B. and Gauvin, W.H. (1960)
"Fundamental aspects of solids-gas flow," Can. J. Chem. Eng., 38, p. 142, 189.

Torobin, L.B. and Gauvin, W.H. (1961)
"Fundamental aspects of solids-gas flow," Can. J. Chem. Eng., 39, p. 113.

Vincenti, W.G. and Kruger, Jr., C.H. (1965)
"Introduction to Physical Gas Dynamics," John Wiley and Sons, Inc., New York.

Virk, P.S., Merrill, E.W., Mickley, H.S., Smith, K.A. and Mollo-Christensen, E.L. (1967)
"The Toms phenomena: turbulent pipe flow of a dilute polymer solutions," J. Fluid Mechanics, 30, Part 2, pp. 305-328.

Wakstein, C. (1970)
"A simple picture of turbulent two-phase pipe flow," Aerosol Science, 1, pp. 69-74.

Wallis, G.B. (1969)
"One-Dimensional Two-Phase Flow," McGraw-Hill, New York.

Wells, Jr. C.S., Harkness, J. and Meyer, W.A. (1968)
"Turbulence measurements in pipe flow of a drag-reducing non-Newtonian fluid," AIAA J. 6, no. 2, pp. 250-257.

White, F.M. (1974)
"Viscous Fluid Flow," McGraw-Hill Book Co., New York.

Yeung, W.S. (1977)
"Erosion in a Curved Pipe," Lawrence Berkeley Laboratory, Berkeley, California, Report No. LBL-7354.

Yeung, W.S. (1978)
"Fundamentals of the Particulate Phase in a Gas-Solid Mixture," Lawrence Berkeley Laboratory, Berkeley, California, Report No. LBL-8440.

Yudine, M.I. (1959)
"Physical considerations on heavy-particle diffusion," Atmospheric Diffusion and Air Pollution, Advances in Geophysics, 6, New York, Academic Press, pp. 185-191.

Yuu, S., Yasukouchi, N., Hirosawa, Y. and Jotaki, T. (1978)
"Particle turbulent diffusion in a dust laden jet," A.I.Ch.E. Journal, 24, no. 3, pp. 409-519.

Zisselmar, R. and Molerus, O. (1979)
"Investigations of solid-liquid pipe flow with regard to turbulence modification," Chem. Eng. J., 18, pp. 233-239.

FIGURE CAPTIONS

Fig. 3.1 Lateral variation of $(-\overline{u_{f_r} u_{f_z}}/k)$ in two-phase pipe flow.

Fig. 3.2 Variation of $-\overline{u_{f_r} u_{f_z}}/k$ with particulate concentration.

Fig. 4.1 The positions of a solid particle at two different times when contained in a viscous fluid.

Fig. 4.2 The plot of fluid-particle correlation coefficient.

Fig. 4.3 Definition of points (a) and (b) in space separated by Δx_2 in lateral direction.

Fig. 4.4 The plot of fluid-particle correlation coefficient being at two different points in space.

Fig. 6.1 Definition of velocity and angle of impingement for erosion caused by a solid particle.

Fig. 6.2 Control-volume for scalar and vector quantities.

Fig. 7.1 Transverse variation of normalized fluid mean velocity for different particulate volume concentration in two-phase straight pipe flow.

Fig. 7.2 Transverse variation of normalized particulate mean velocity for different particulate volume concentration in two-phase straight pipe flow.

Fig. 7.3 Transverse variation of particulate mean velocity in developing two-phase straight channel flow.

Fig. 7.4 Transverse variation of fluid mean velocity for two-phase developing straight channel flow.

Fig. 7.5 Streamwise variation of fluid normalized mean velocity in developing two-phase straight channel flow.

Fig. 7.6 Streamwise variation of normalized particulate mean velocity in developing two-phase straight channel flow.

Fig. 7.7 Streamwise variation of particulate phase wall-slip velocity in developing two-phase straight channel flow.

Fig. 7.8 Transverse variation of normalized mean slip velocity for different particle sizes in two-phase straight pipe flow.

Fig. 7.9 Transverse variation of normalized mean slip velocity for different particle sizes in two-phase straight pipe flow.

Fig. 7.10 The effect of particle concentration on the transverse variation of mean particulate velocity for two-phase straight pipe flow.

Fig. 7.11 Transverse variation of particulate mean volume fraction at different particulate loadings for two-phase straight pipe flow.

Fig. 7.12 The effect of particulate mean volume concentration on fluid turbulent kinetic energy at different radial positions in two-phase fully-developed straight pipe flow.

Fig. 7.13 Variation of fluid normalized turbulent shear stress with particulate mean volume concentrations in the fully developed region of two-phase straight pipe flow.

Fig. 7.14 Two-dimensional predictin of relative erosion rate at the concave wall of a two-phase curved duct three-dimensional flow.

Fig. 7.15 Two-dimensional prediction of the relative erosion rate at the concave wall of a two-phase curved duct three-dimensional flow.

Fig. 7.16 Transverse variations of fluid and particulate mean longitudinal velocity at different streamwise locations in two-phase curved channel flows.

Fig. 7.17 Transverse variations of fluid and particulate mean longitudinal velocity at different streamwise positions in two-phase curved channel flows.

Fig. 7.18 Transverse variations of fluid and particulate mean longitudinal velocity at different streamwise positions in two-phase curved channel flows.

Fig. 7.19 Transverse variations of fluid and particulate mean longitudinal velocity at different streamwise positions in two-phase curved channel flows.

Fig. 7.20 Transverse variation of normalized fluid turbulent kinetic energy for different particle response parameters in fully developed region of two-phase curved channel flow.

Fig. 7.21 Transverse variation of normalized fluid turbulent kinetic energy for different particulate concentrations in fully-developed region of curved channel flows.

Fig. 7.22 Transverse variation of normalized dissipation rate of fluid turbulent kinetic energy in fully developed region of two-phase curved channel flows.

Fig. 7.23 Transverse variation of particulate turbulent kinetic energy for different particulate response parameters in fully developed region of two-phase curved channel flow.

Fig. 7.24 Transverse variation of particulate turbulent kinetic energy for different particulate concentrations in fully developed region of two-phase curved channel flow.

Fig. 7.25 Streamwise variation of normalized erosion rate at the outer wall of two-phase curved channel flow for different particle response parameters.

Fig. 7.26 Streamwise variation of normalized erosion rate at the outer wall of two-phase curved channel flow for different particle response parameters.

Fig. 7.27 Streamwise variation of normalized erosion rate at the outer wall of two-phase curved channel flow for different particle response parameters.

Fig. 7.28 Streamwise variation of normalized erosion rate at the outer wall of two-phase curved channel flow for different particle response parameters.

Fig. 7.29 Streamwise variation of normalized erosion rate at the outer wall of two-phase curved channel flow for different particle response parameters.

Fig. 7.30 Streamwise variation of normalized particulate phase impingement mean kinetic energy at the outer wall of two-phase curved channel flows.

Fig. 7.31 Streamwise variation of particulate phase impingement angle at the outer wall of two-phase curved channel flow for different particle response parameters.

Fig. 7.32 Velocity vector plot for fluid and particulate phase velocities in developing two-phase curved channel flow.

Fig. 7.33 Velocity vector plot for fluid and particulate phase velocities in developing two-phase curved channel flow.

Fig. 7.34 Velocity vector plot for fluid and particulate phase velocities in developing two-phase curved channel flow.

Fig. 7.35 Variation of normalized maximum erosion rate with Reynolds number for various particle response parameters.

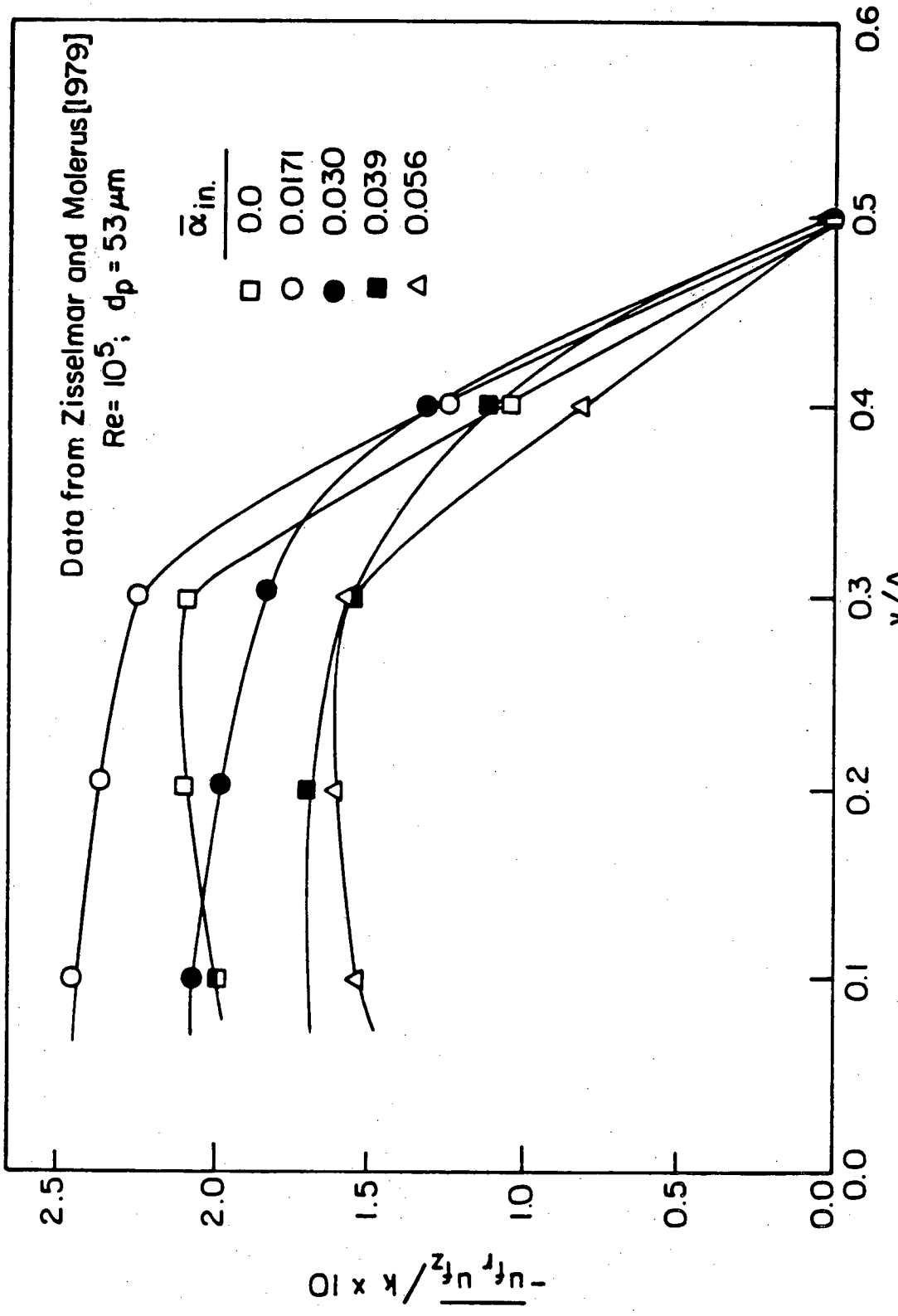

XBL 824-2202

Fig. 3.1

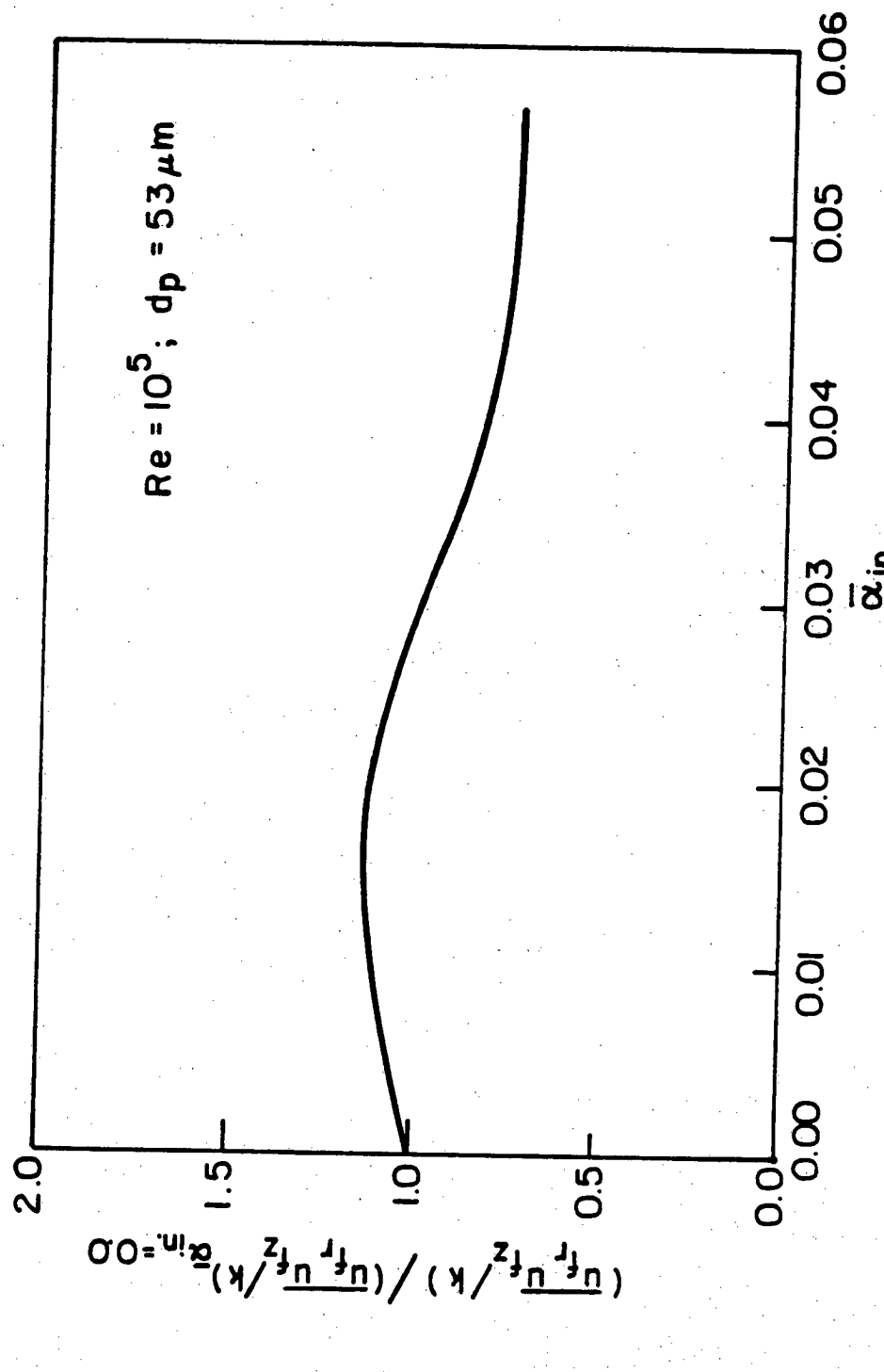

XBL 824-2203

Fig. 3.2

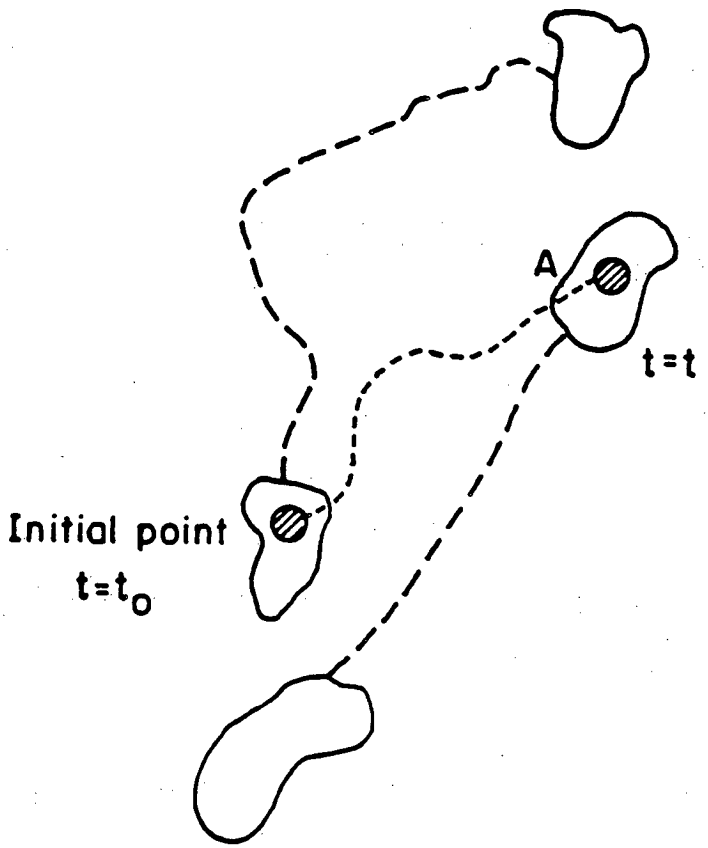

XBL 824-2204

Fig. 4.1

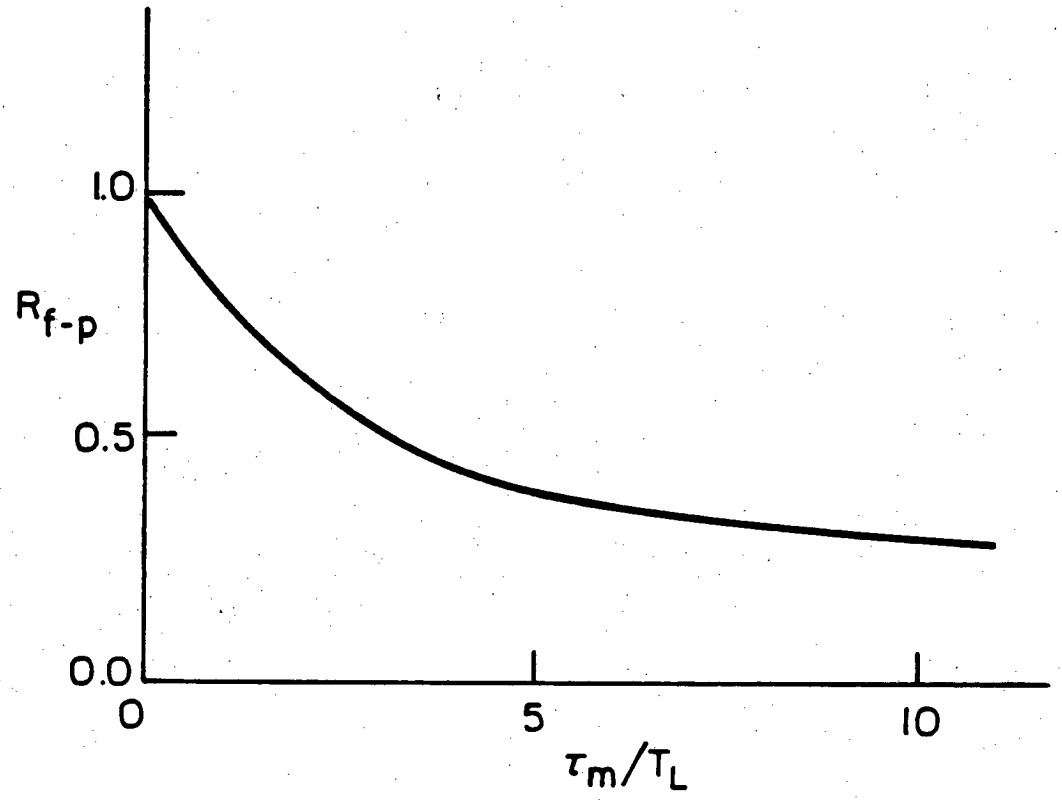

XBL 824-2205

Fig. 4.2

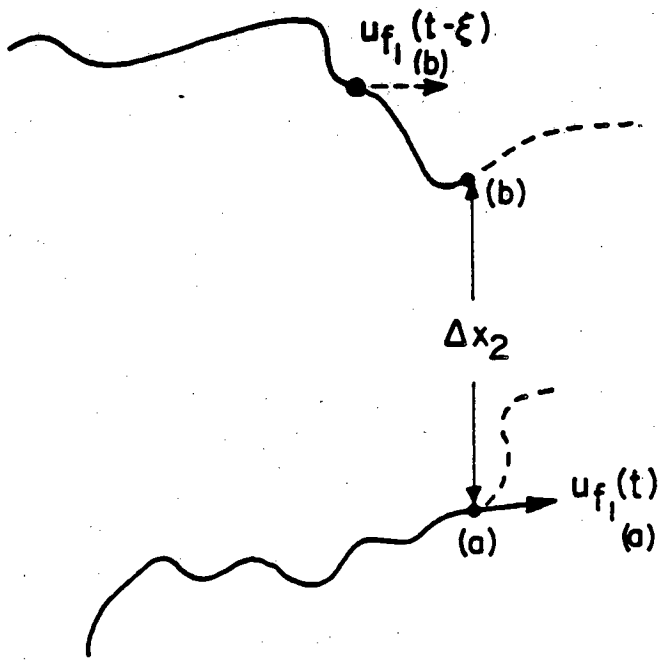

XBL 824-2206

Fig. 4.3

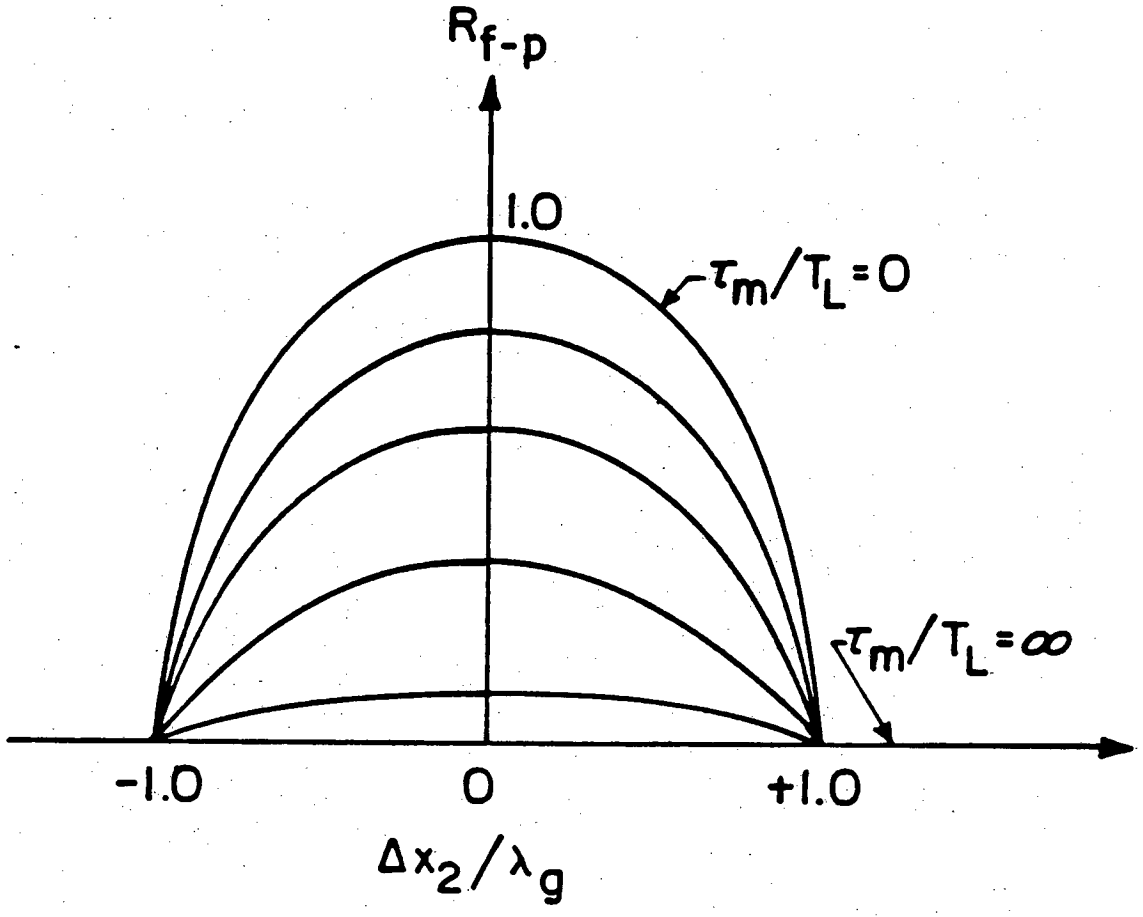

XBL 824-2207

Fig. 4.4

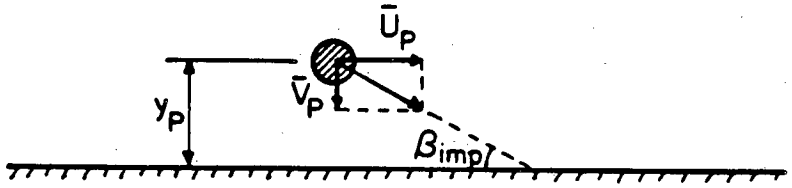

(a)

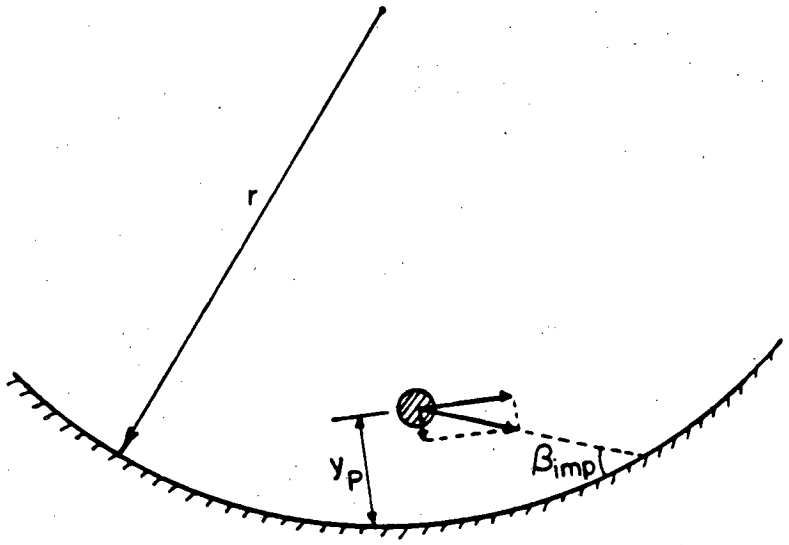

(b)

XBL 824-2208

Fig. 6.1

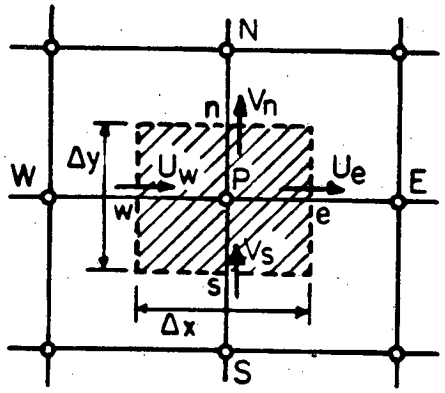

(a) 'scalar' cell

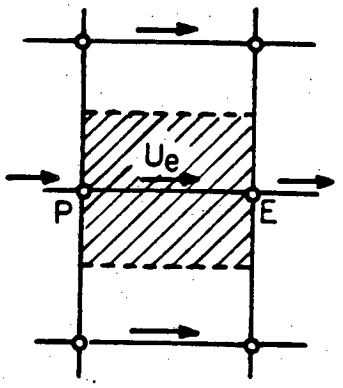

(b) 'U' -cell

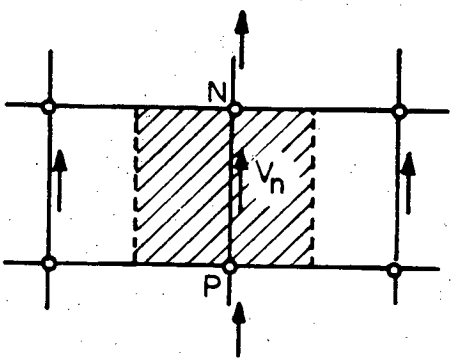

(c) 'V' cell

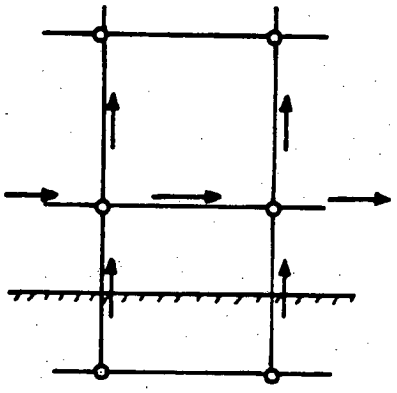

(d) grid arrangement at the wall region

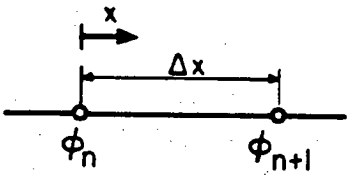

(e)

XBL 824-2209

Fig. 6.2

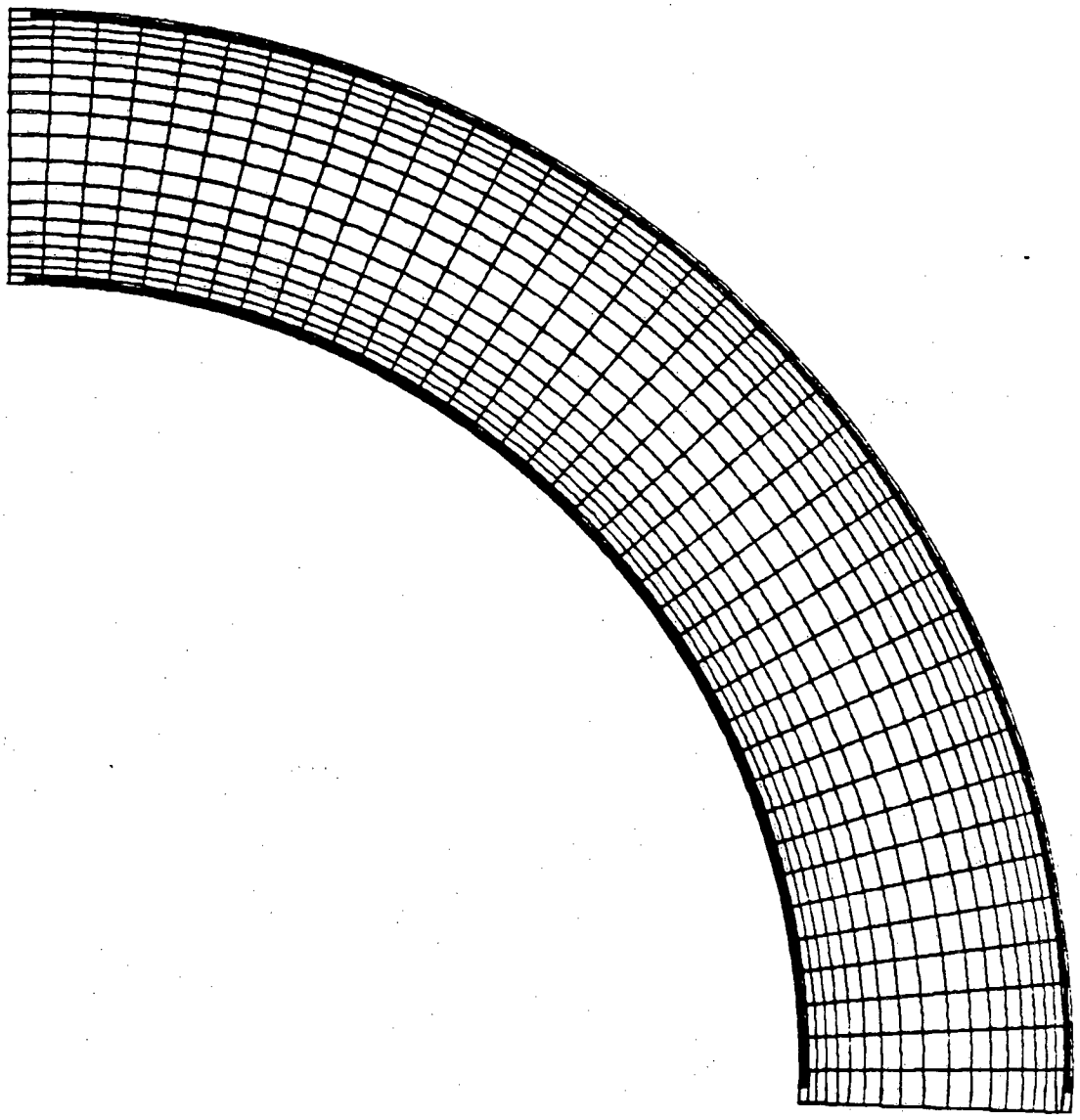

XBL 824-2144

Fig. 6.3

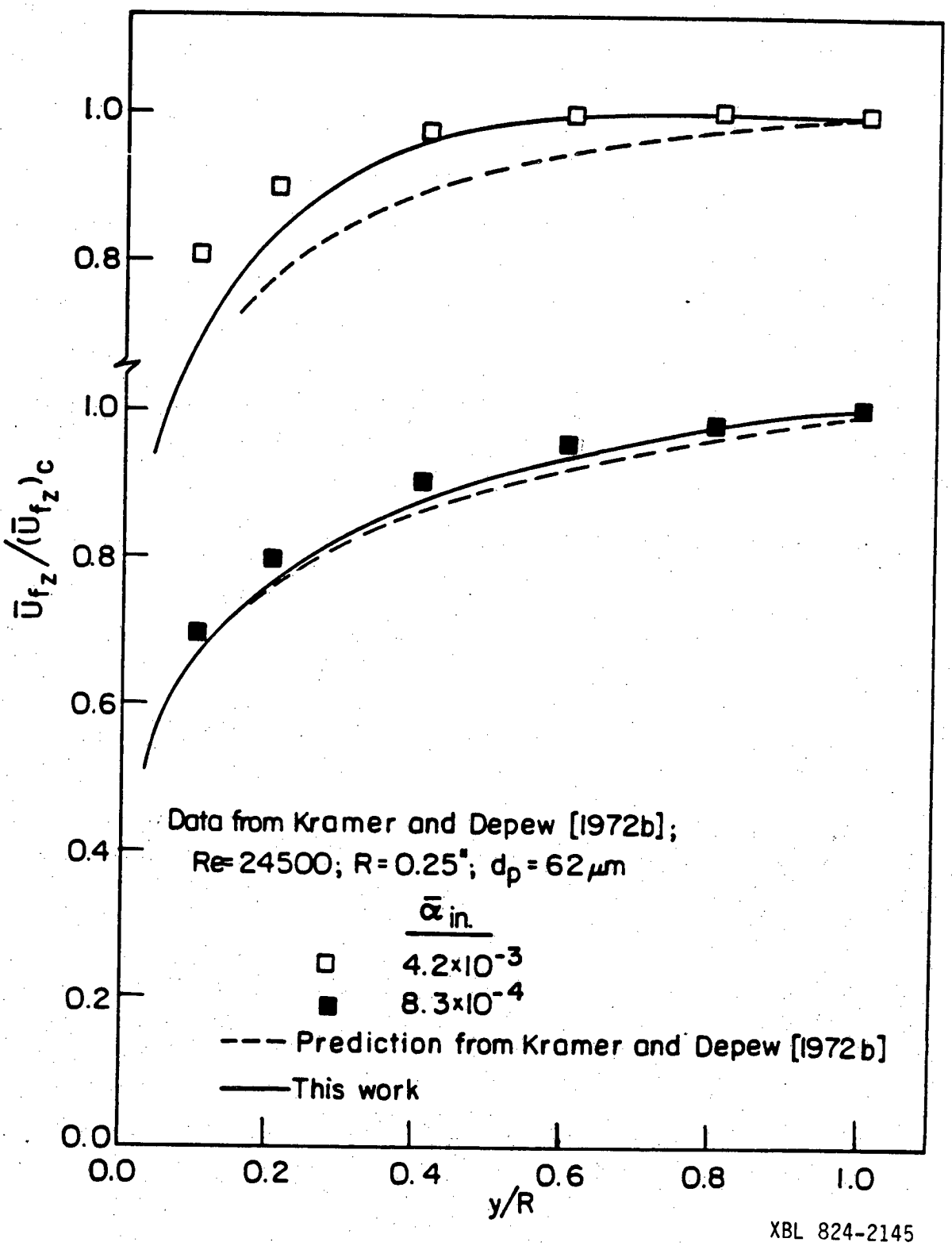
1.0
0.8
1.0
0.8
0.6
0.4
0.2
0.0
0.0
0.2
0.4
0.6
0.8
1.0
$\bar{U}_{f_z}/(\bar{U}_{f_z})_c$
y/R
Data from Kramer and Depew [1972b];
Re=24500; R=0.25"; d_p=62 μm
$\bar{\alpha}_{in.}$
4.2×10^{-3}
8.3×10^{-4}
Prediction from Kramer and Depew [1972b]
This work
XBL 824-2145

Fig. 7.1

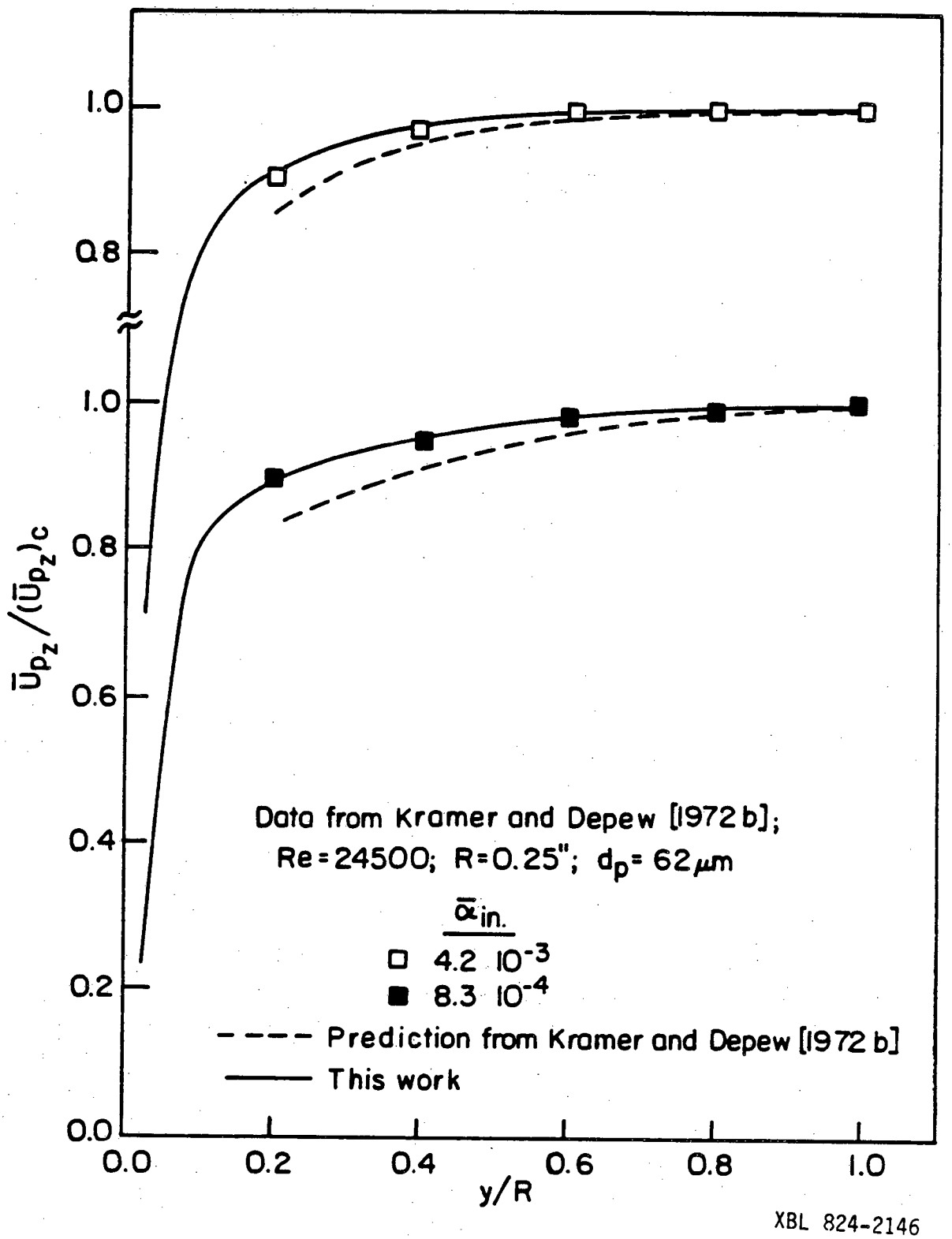
1.0
0.8
1.0
0.8
0.6
0.4
0.2
0.0
0.0
0.2
0.4
0.6
0.8
1.0
$\bar{U}_{p_z}/(\bar{U}_{p_z})_c$
y/R
Data from Kramer and Depew [1972 b];
Re = 24500; R = 0.25"; d_p = 62 μm
$\bar{\alpha}_{in.}$
4.2 10^{-3}
8.3 10^{-4}
Prediction from Kramer and Depew [1972 b]
This work
XBL 824-2146

Fig. 7.2

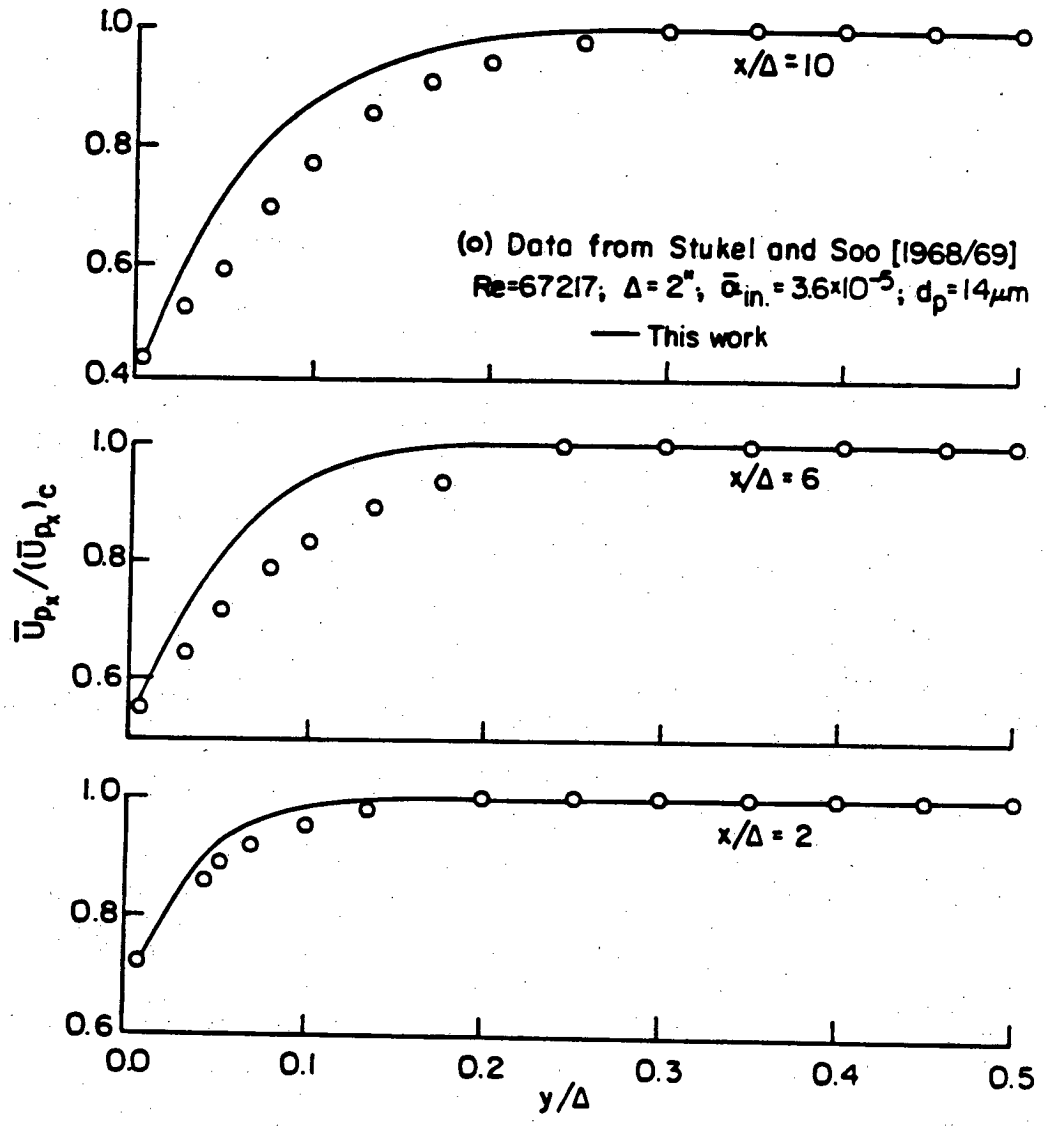

XBL 824-2147

Fig. 7.3

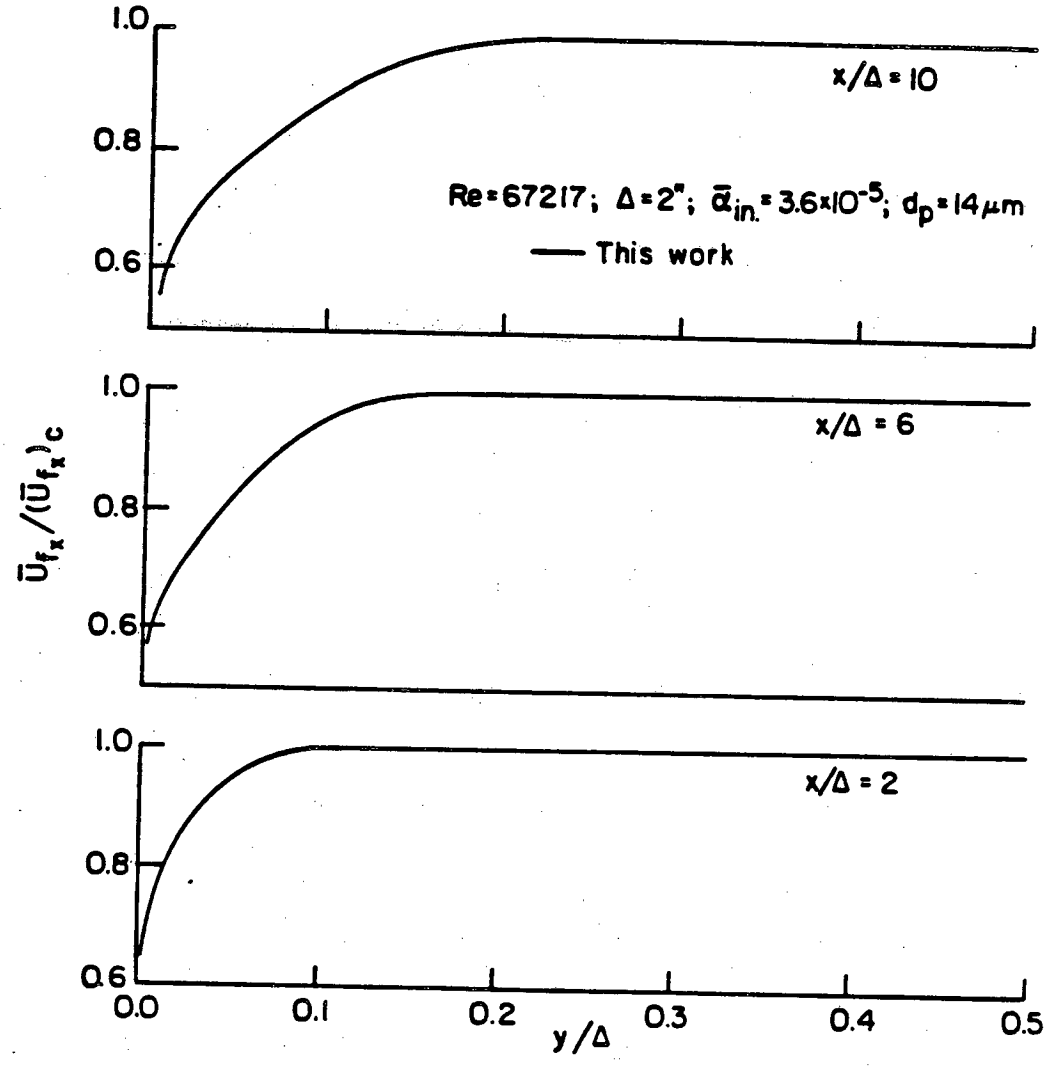

XBL 824-2148

Fig. 7.4

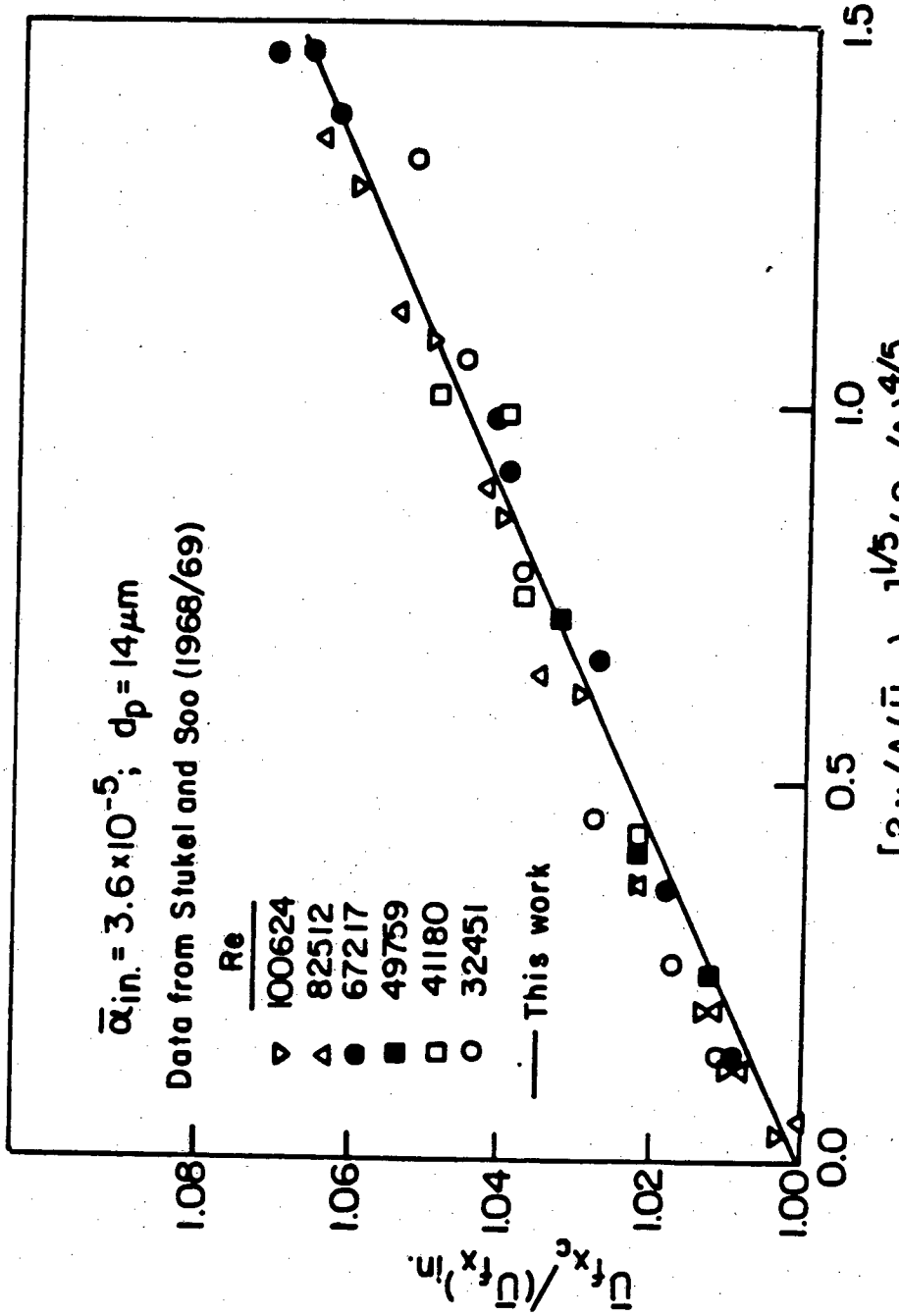

XBL 824-2149

Fig. 7.5

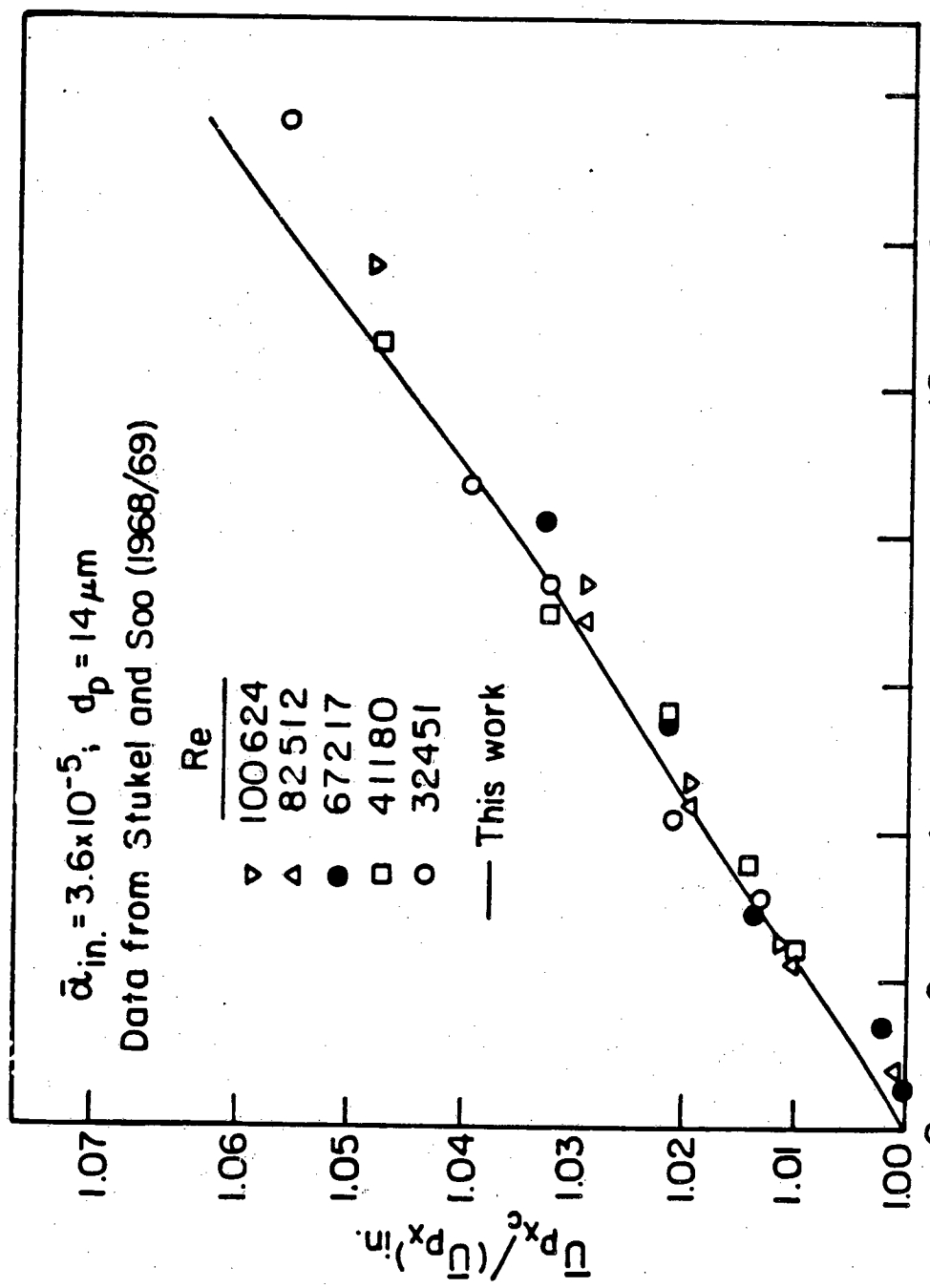

XBL 824-2150

Fig. 7.6

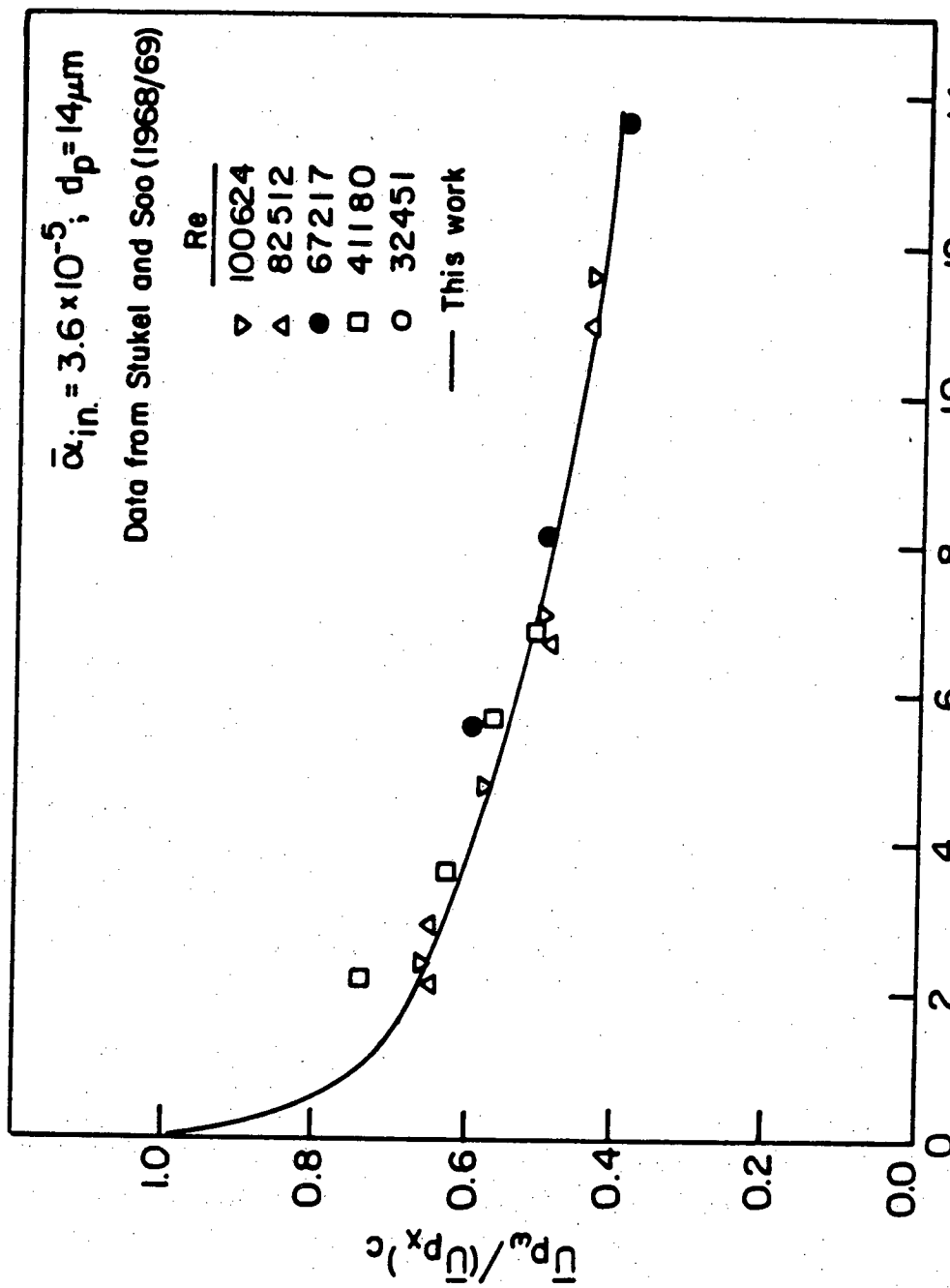

XBL 824-2151

Fig. 7.7

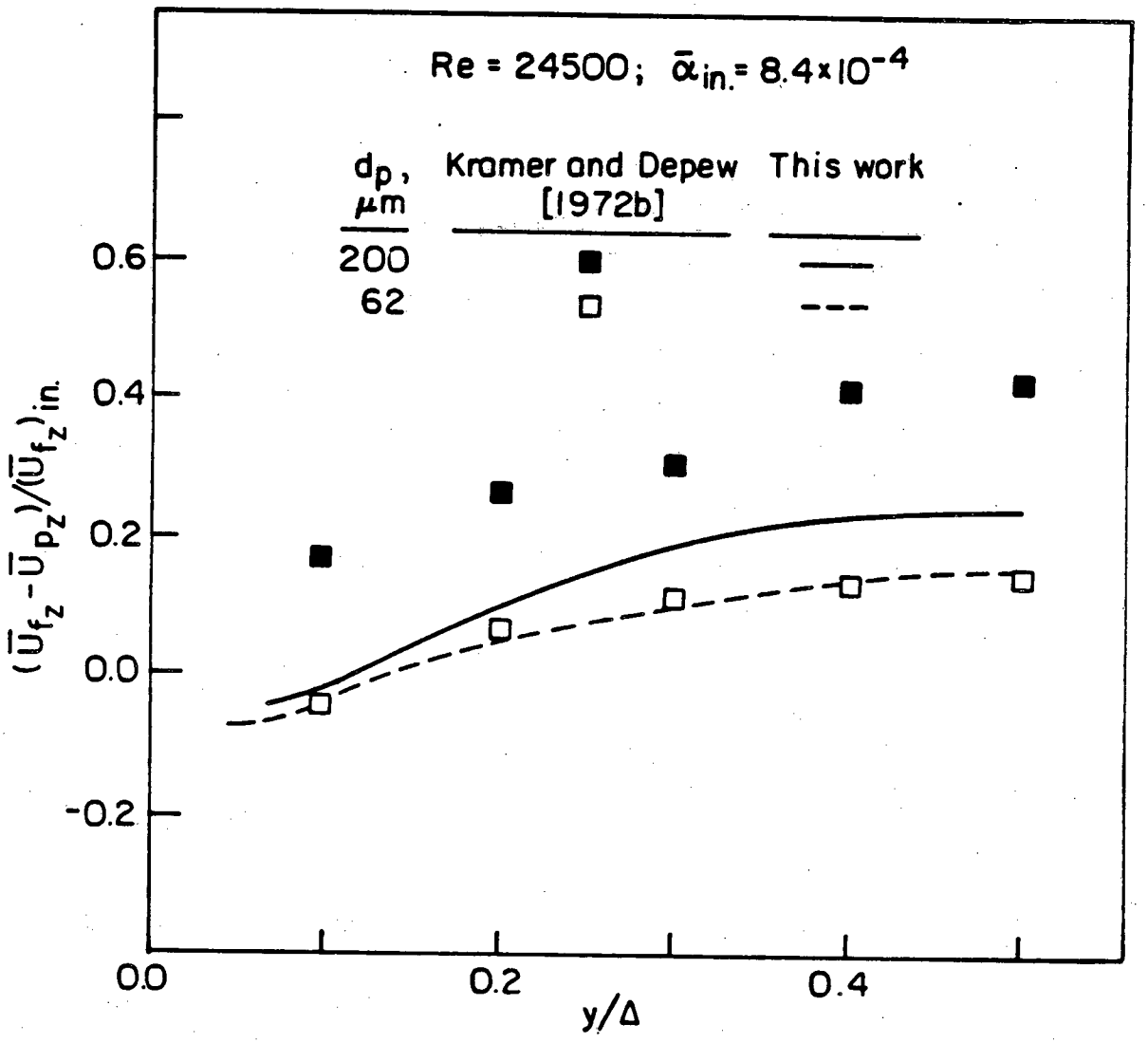

XBL 824-2152

Fig. 7.8

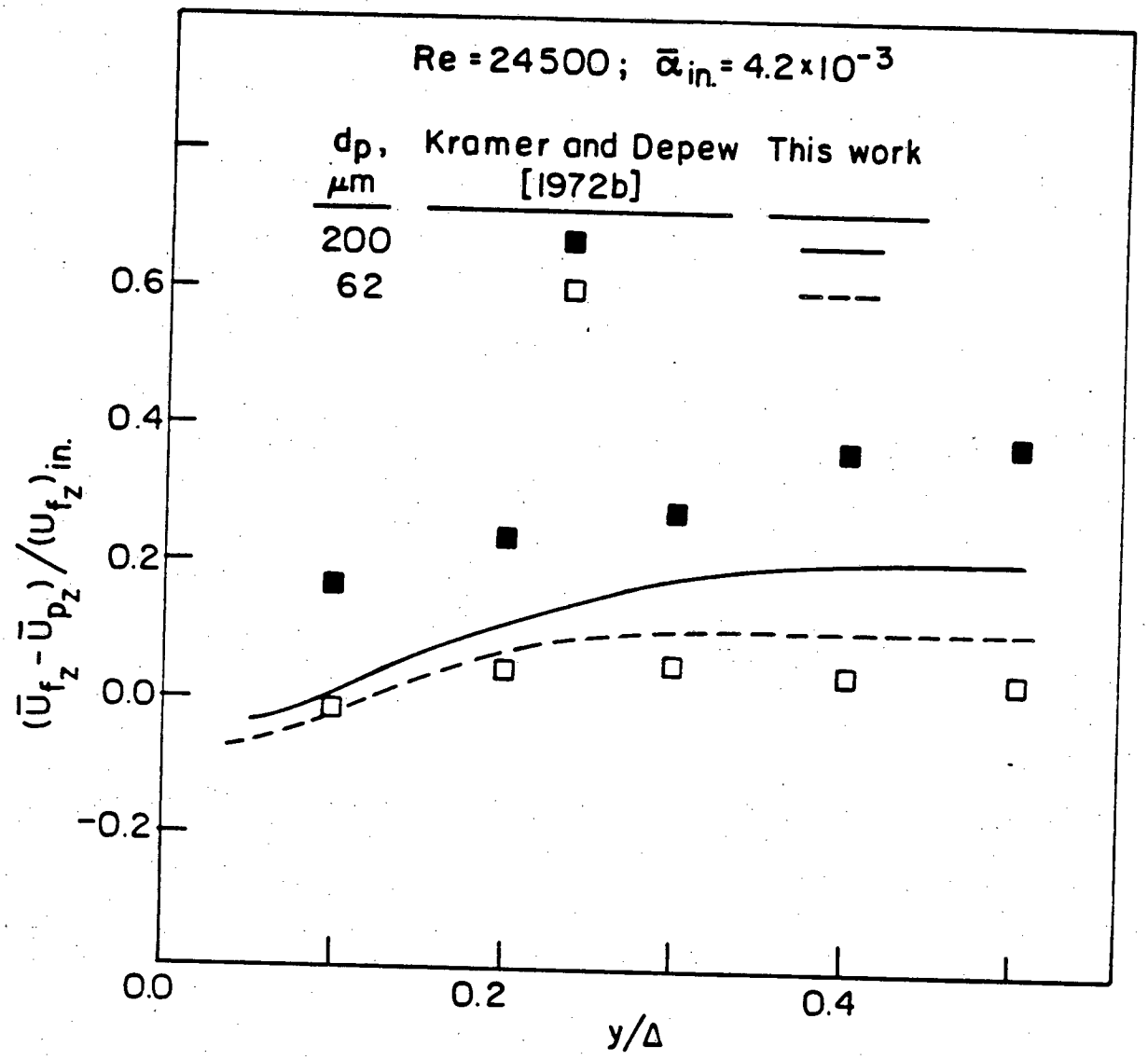
Re = 24500; $\bar{\alpha}_{in.} = 4.2 \times 10^{-3}$
d_p, μm
Kramer and Depew [1972b]
This work
200
62
0.6
0.4
0.2
0.0
-0.2
$(\bar{U}_{f_z} - \bar{U}_{p_z})/(U_{f_z})_{in.}$
0.0
0.2
0.4
y/Δ
XBL 824-2153

Fig. 7.9

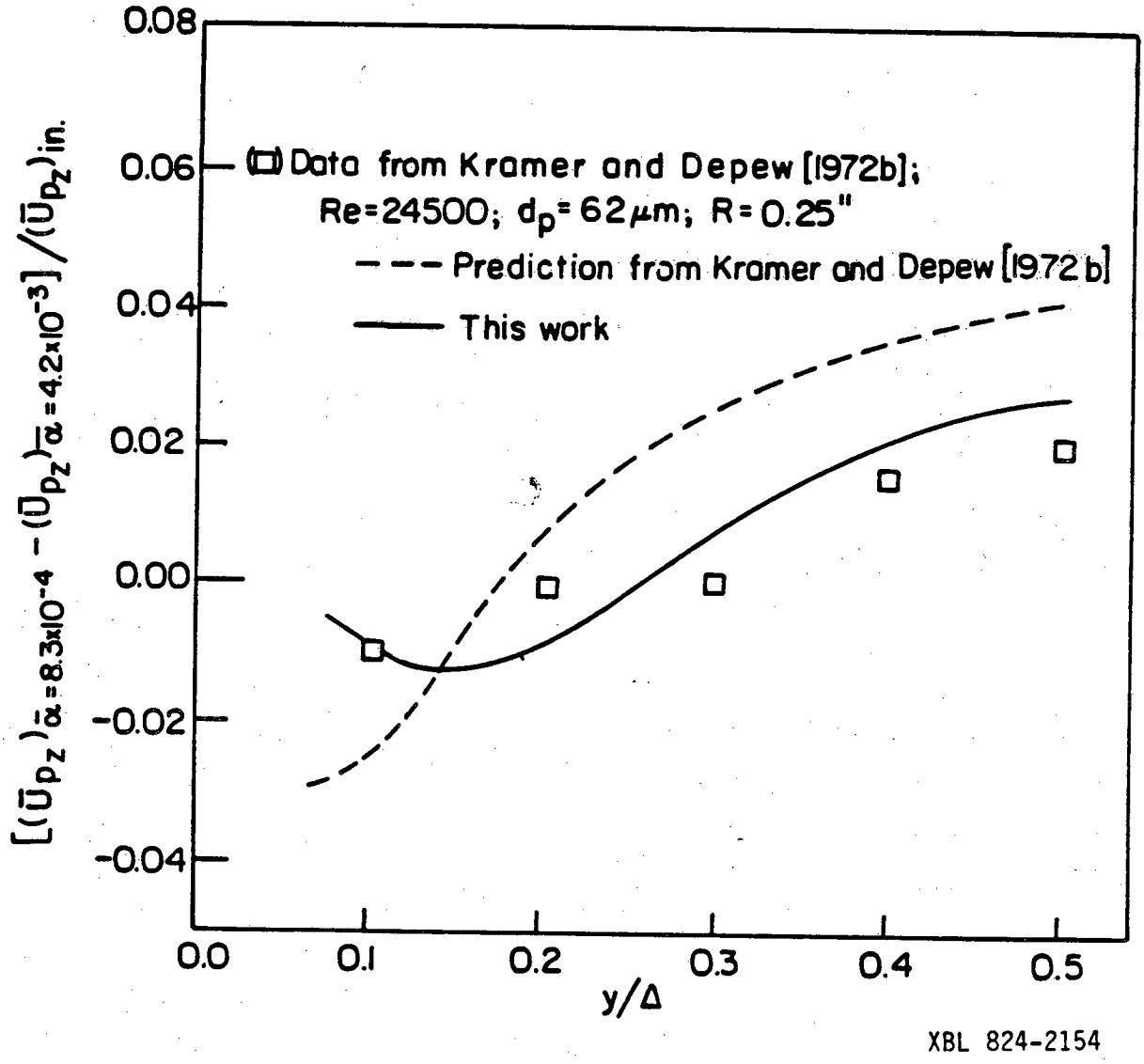
0.08
0.06
0.04
0.02
0.00
-0.02
-0.04
0.0
0.1
0.2
0.3
0.4
0.5
y/Δ
Data from Kramer and Depew [1972b];
Re=24500; d_p= 62 μm; R= 0.25"
Prediction from Kramer and Depew [1972b]
This work
$[(\bar{U}_{pz})_{\bar{\alpha}=8.3\times10^{-4}} - (\bar{U}_{pz})_{\bar{\alpha}=4.2\times10^{-3}}] / (\bar{U}_{pz})_{in.}$
XBL 824-2154

Fig. 7.10

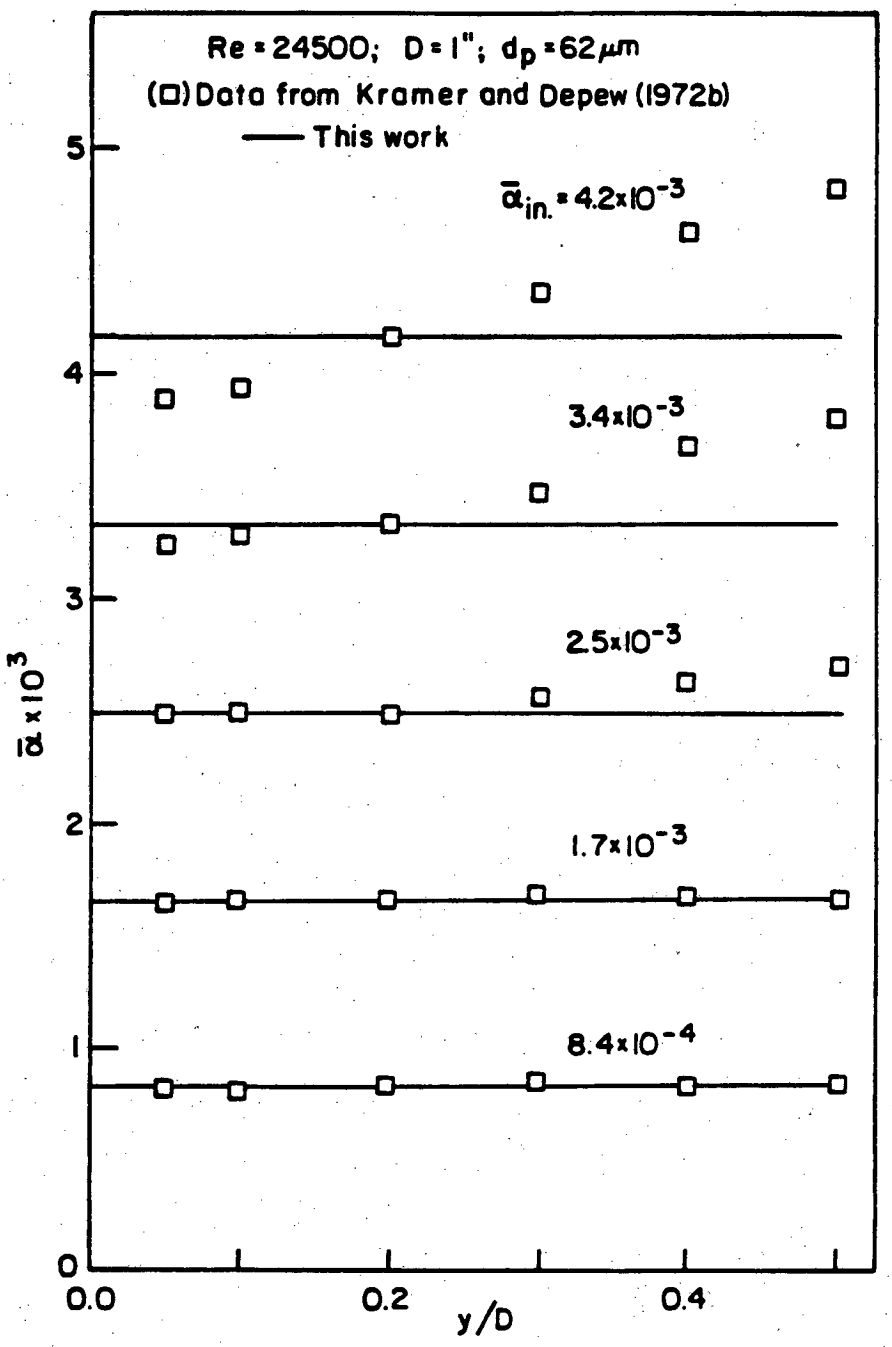

XBL 824-2155

Fig. 7.11

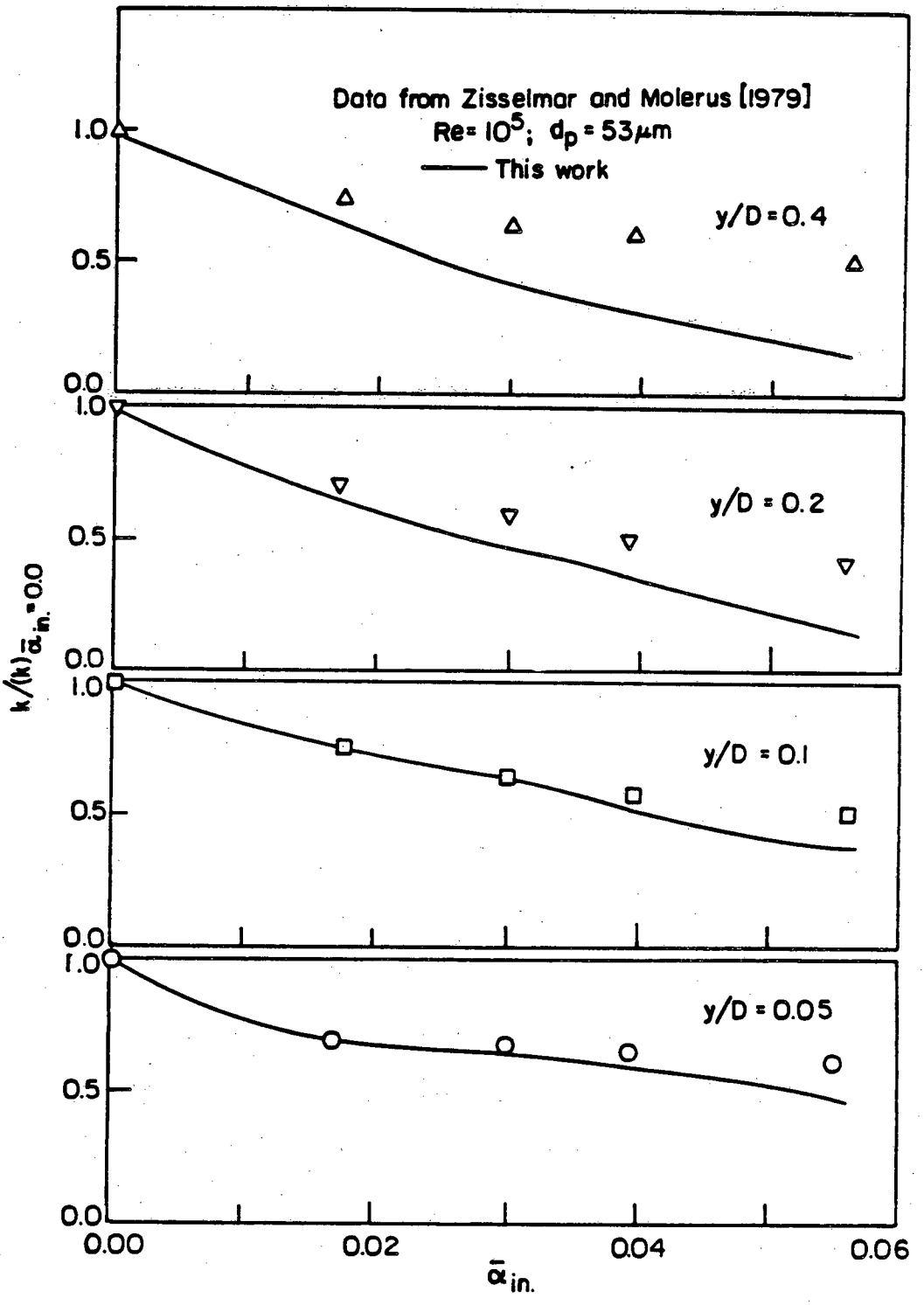
Data from Zisselmar and Molerus [1979]
Re= 10^5; d_p = 53μm
This work
y/D = 0.4
y/D = 0.2
y/D = 0.1
y/D = 0.05
k/(k)_ᾱin.=0.0
ᾱin.
1.0
0.5
0.0
0.00
0.02
0.04
0.06
XBL 824-2156

Fig. 7.12

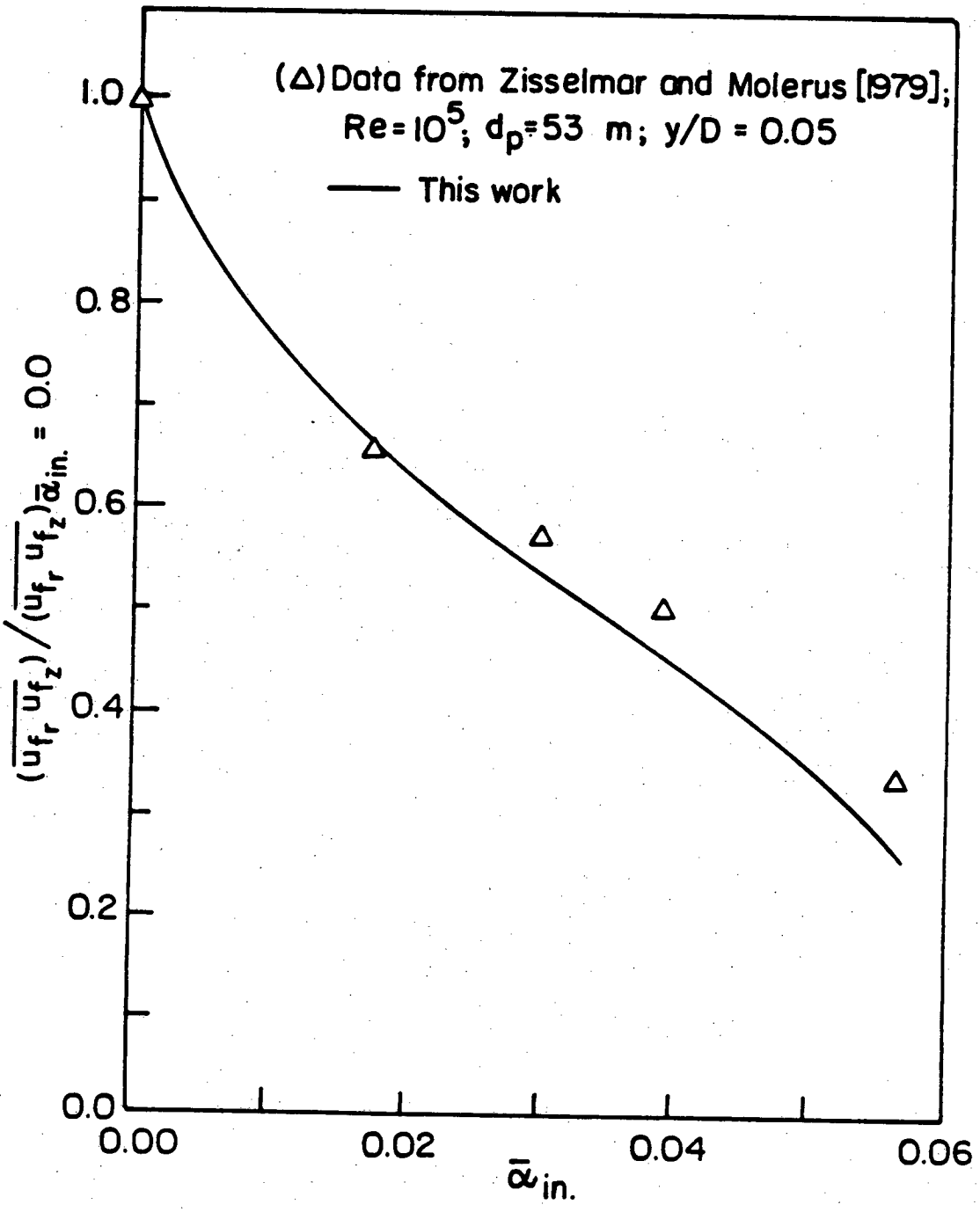

XBL 824-2157

Fig. 7.13

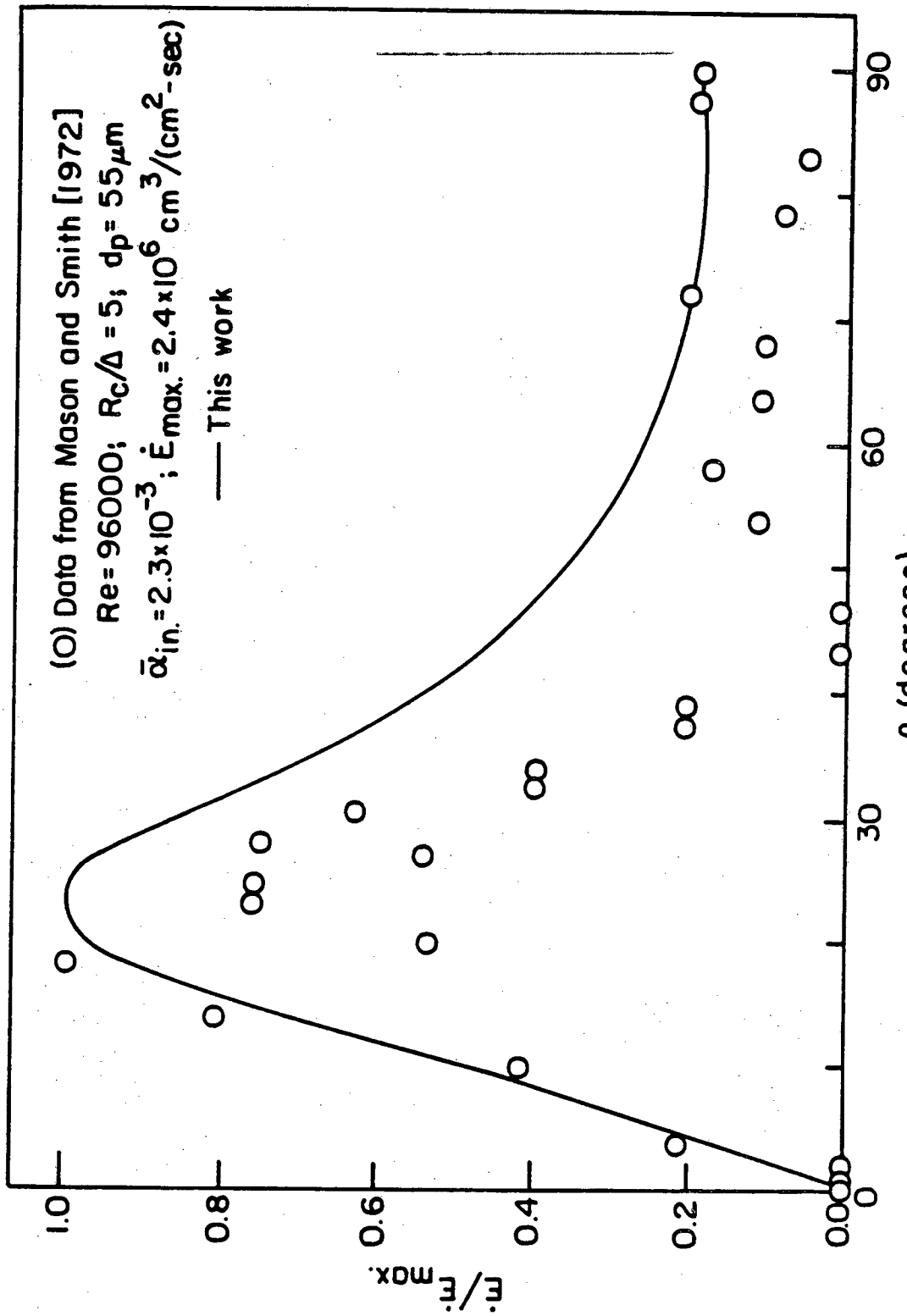

XBL 824-2158

Fig. 7.14

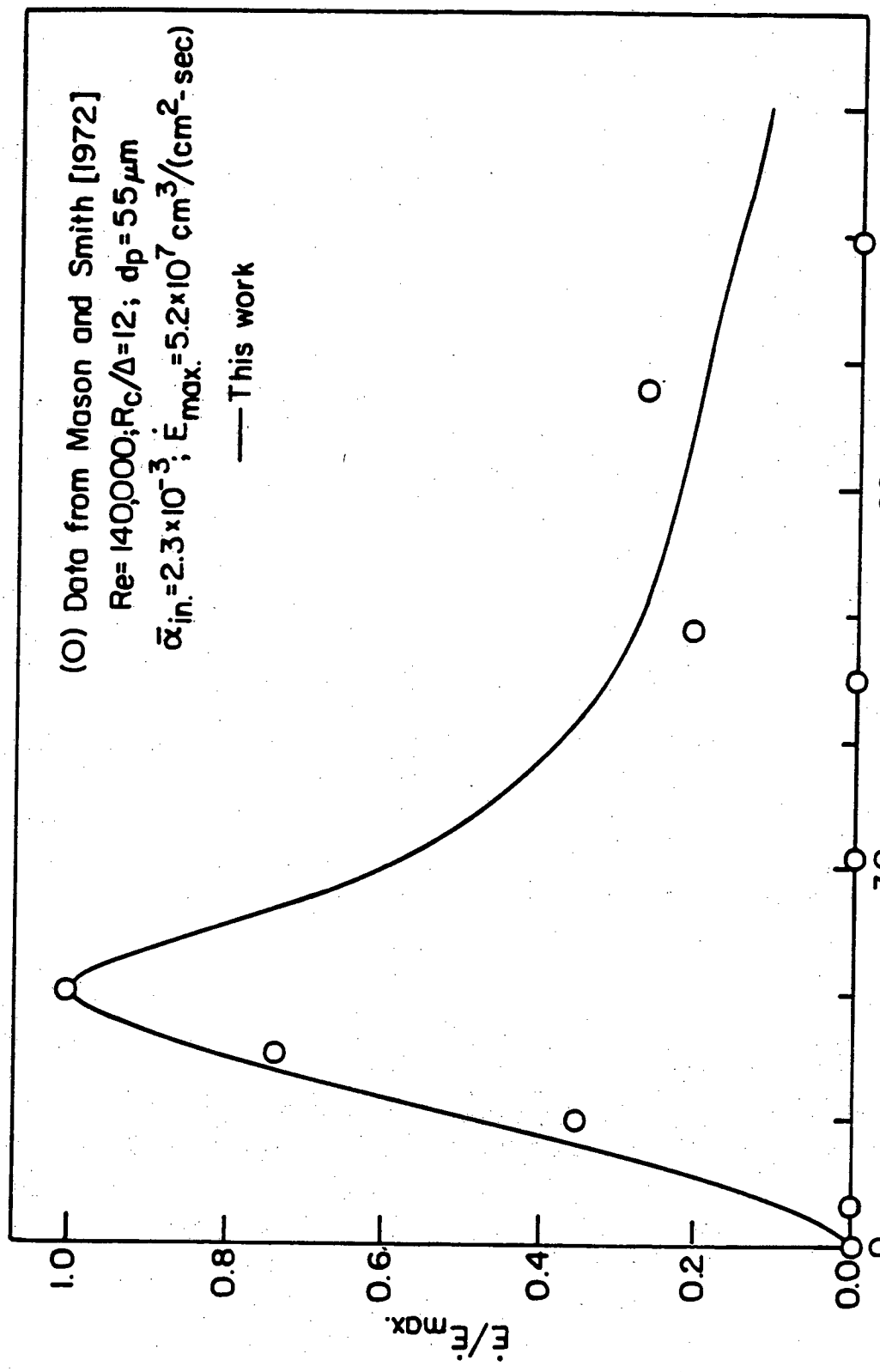

XBL 824-2159

Fig. 7.15

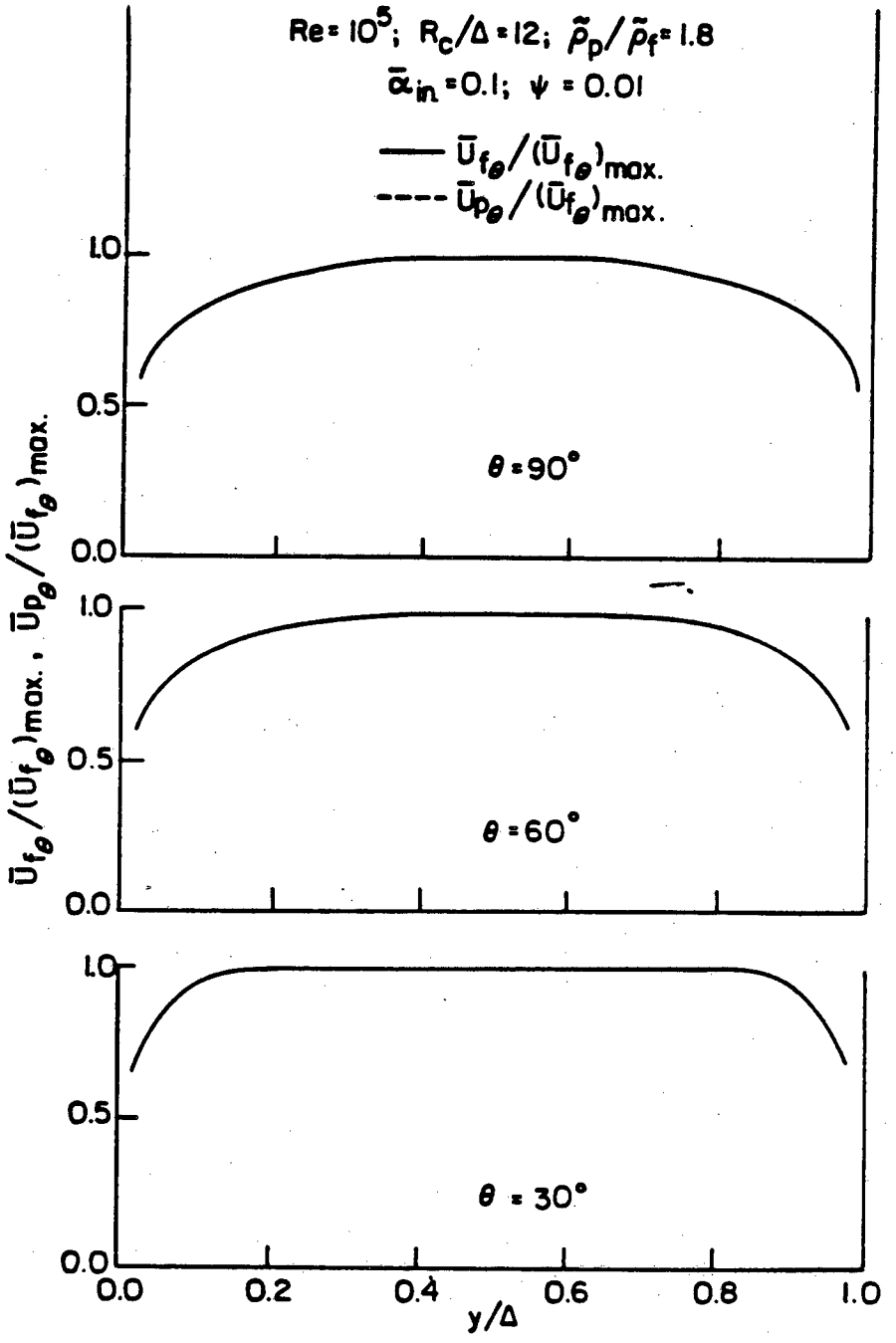

XBL 824-2160

Fig. 7.16

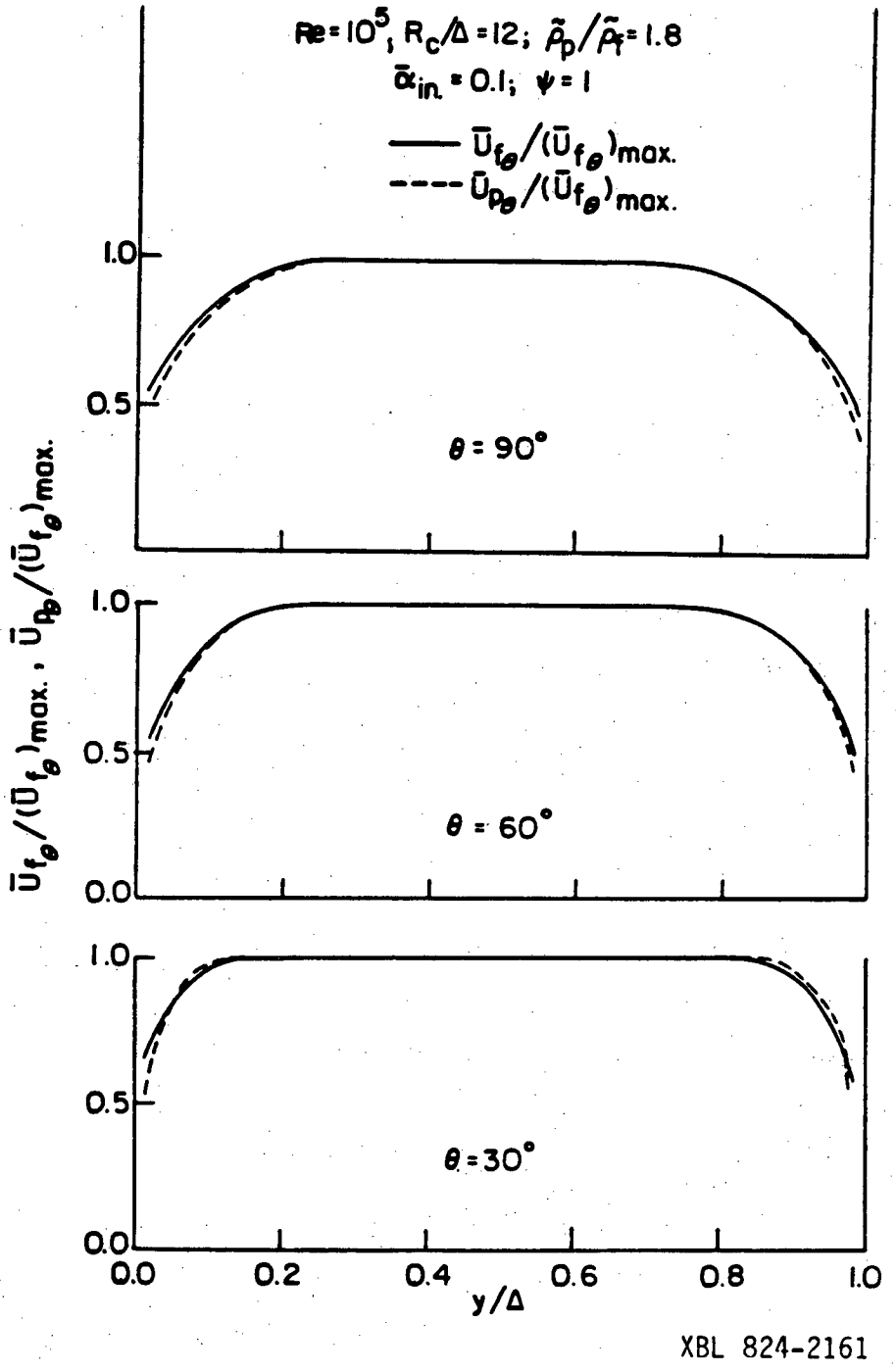
Re = 10^5; R_c/Δ = 12; ρ̃_p/ρ̃_f = 1.8
ᾱ_in. = 0.1; ψ = 1
Ū_fθ/(Ū_fθ)max.
Ū_pθ/(Ū_fθ)max.
θ = 90°
θ = 60°
θ = 30°
Ū_fθ/(Ū_fθ)max. , Ū_pθ/(Ū_fθ)max.
y/Δ
0.0
0.2
0.4
0.6
0.8
1.0
0.5
XBL 824-2161

Fig. 7.17

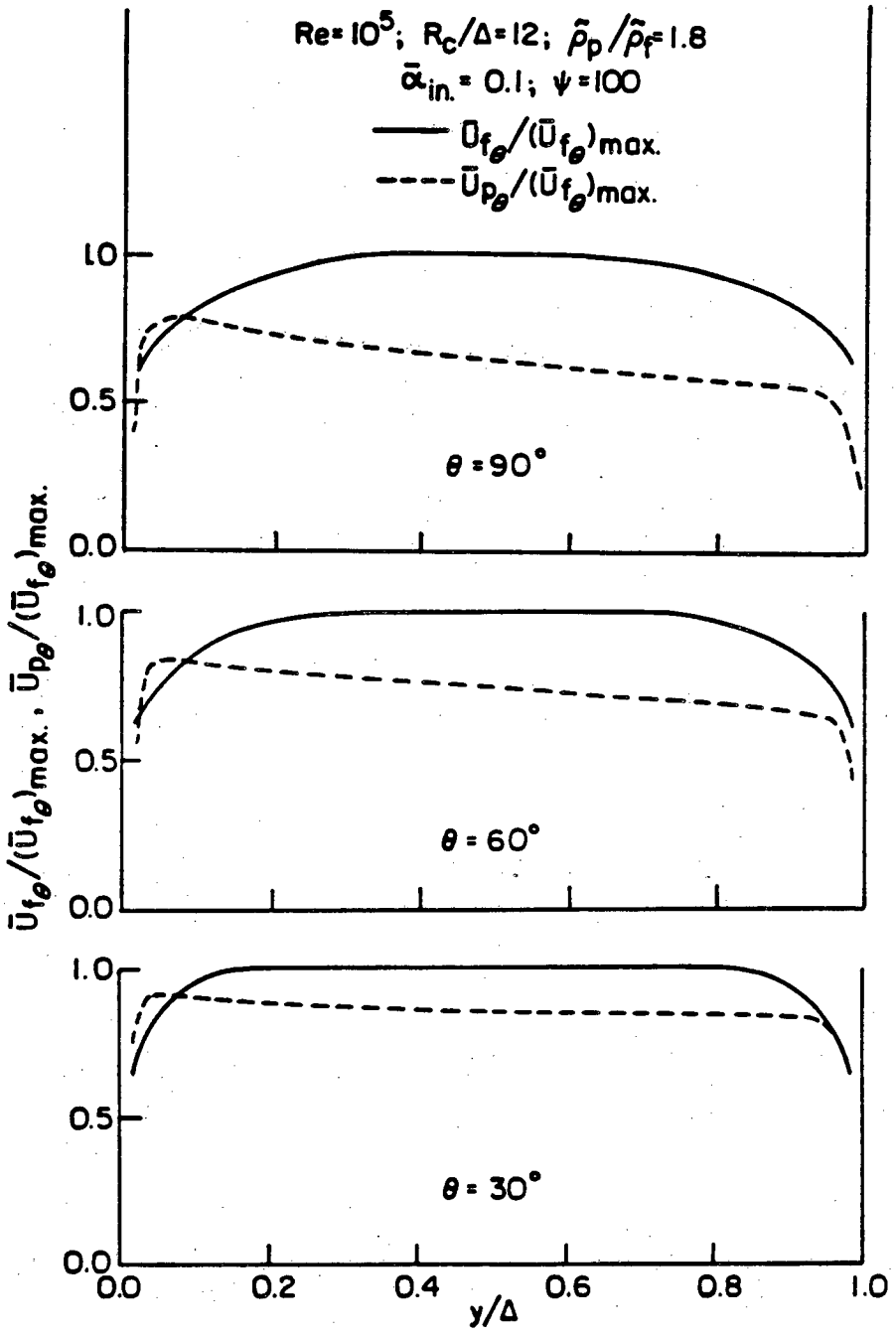

XBL 824-2162

Fig. 7.18

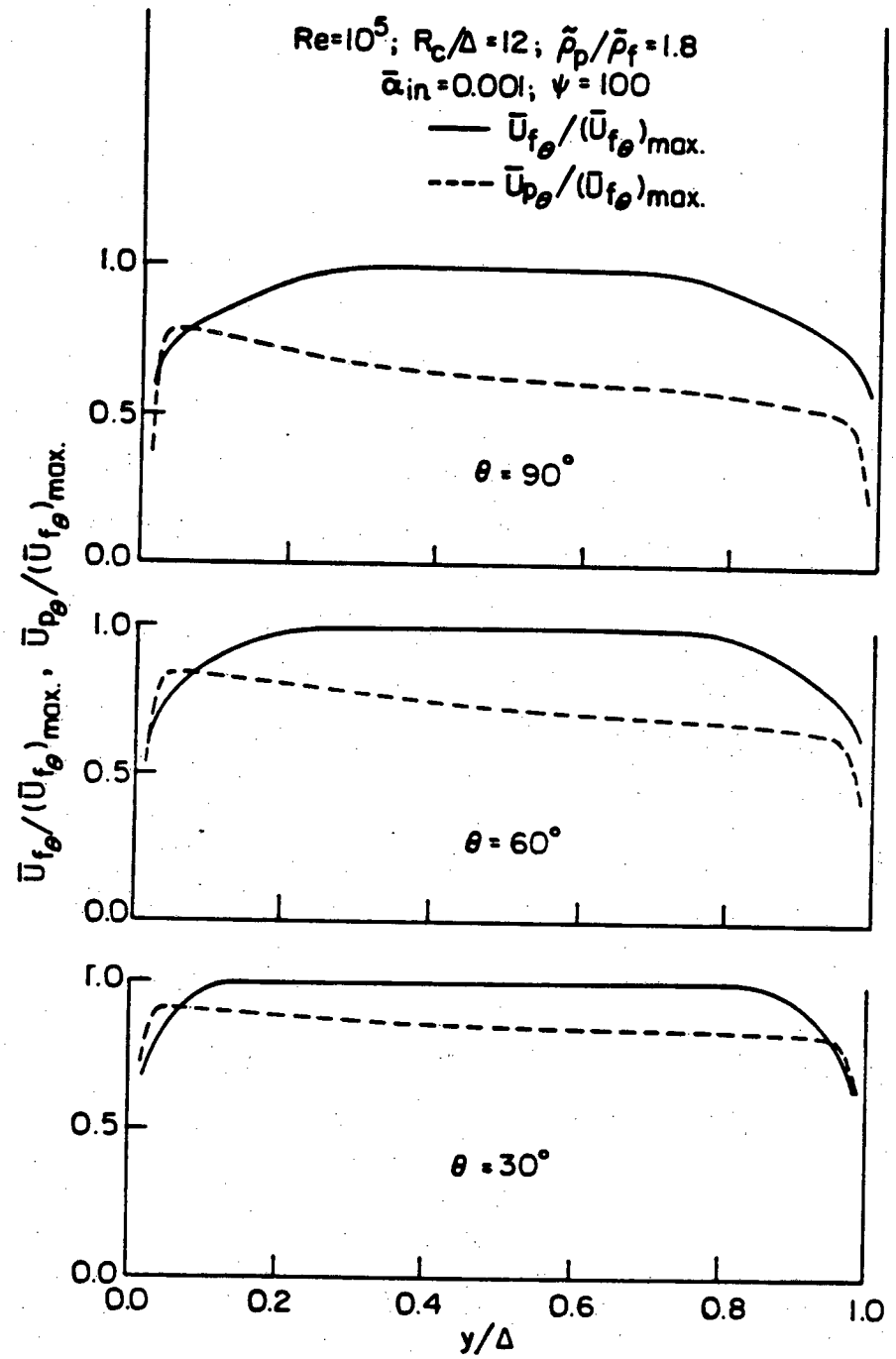

XBL 824-2163

Fig. 7.19

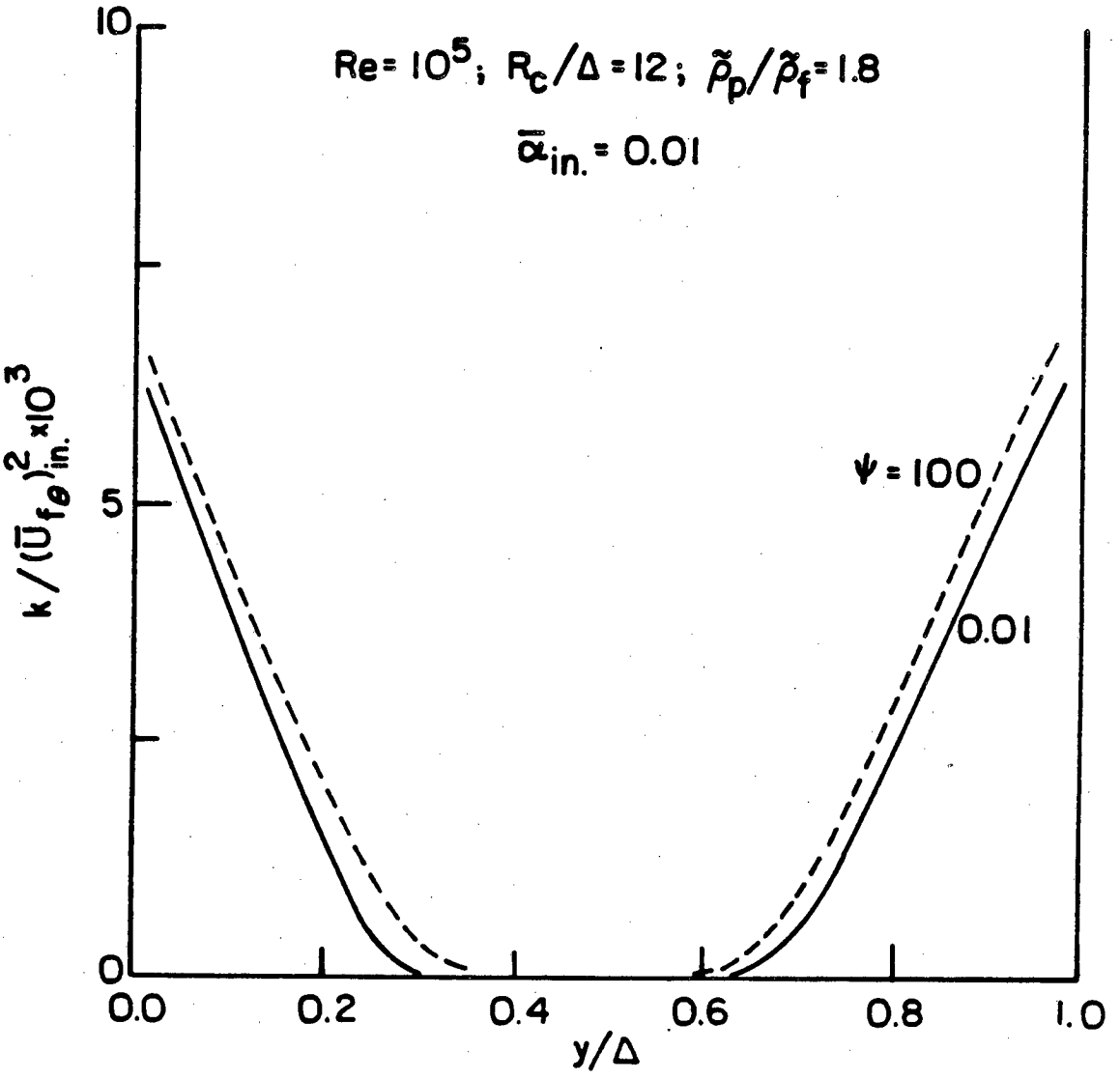

XBL 824-2165

Fig. 7.20

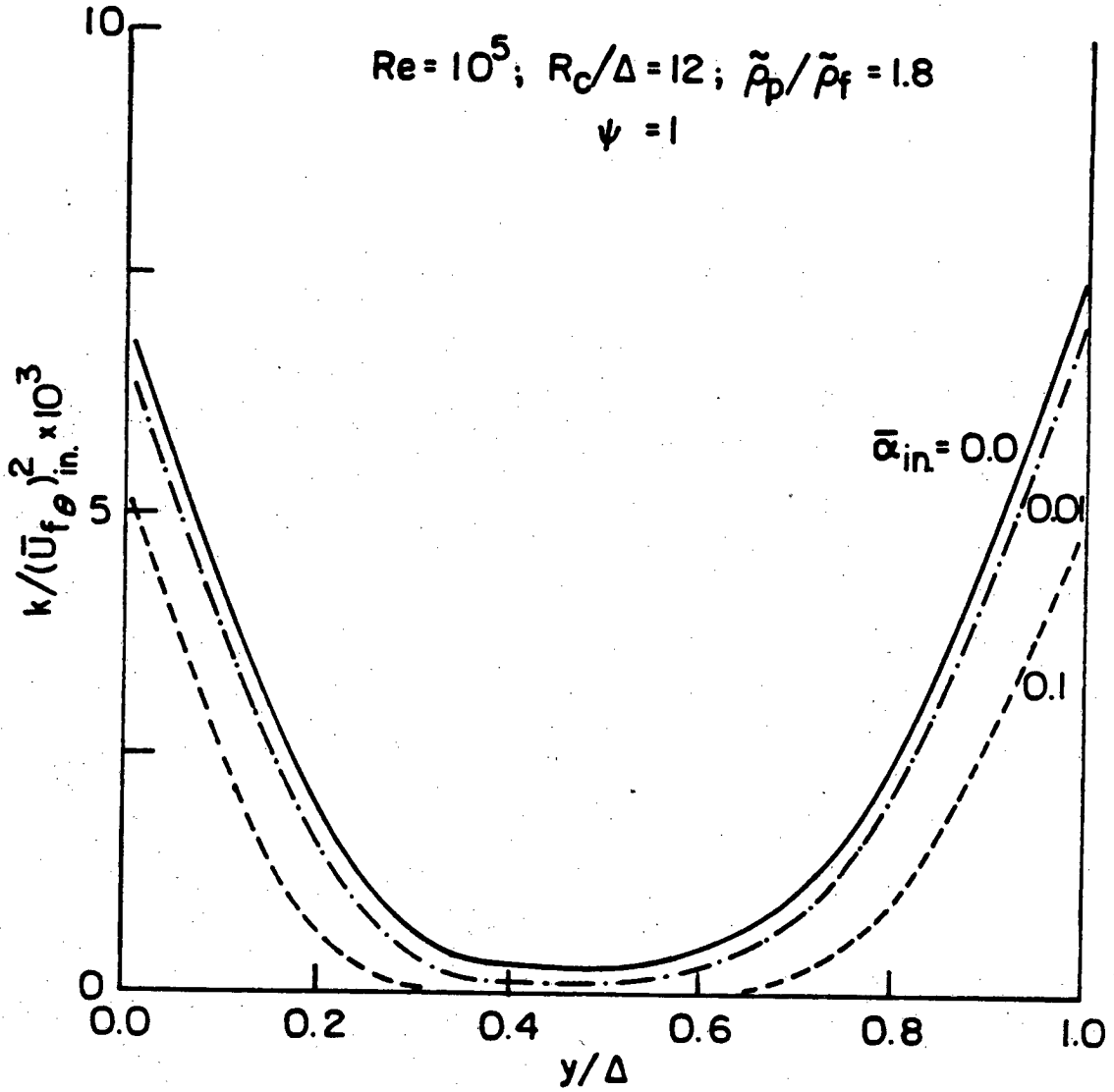

XBL 824-2166

Fig. 7.21

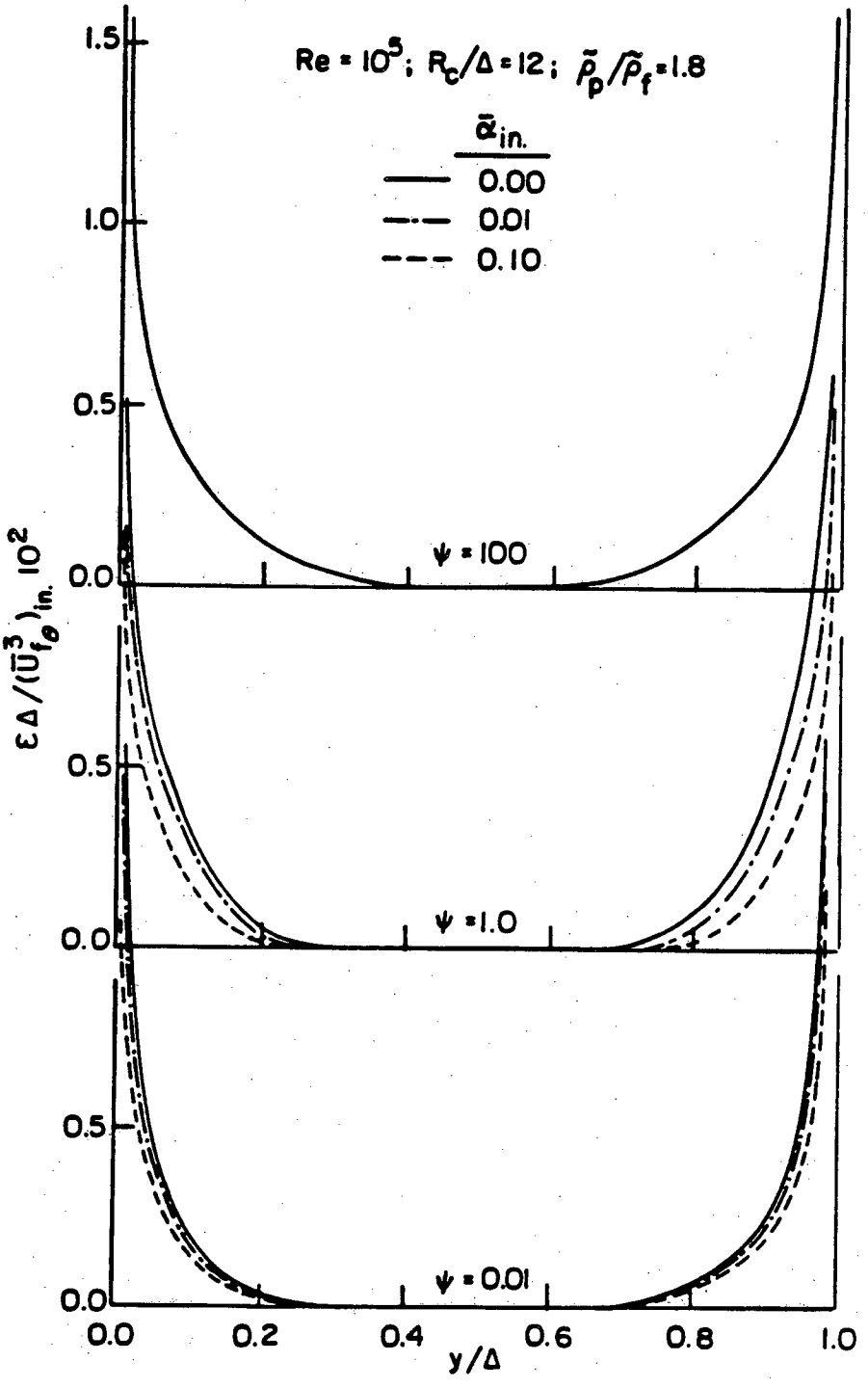

XBL 824-2164

Fig. 7.22

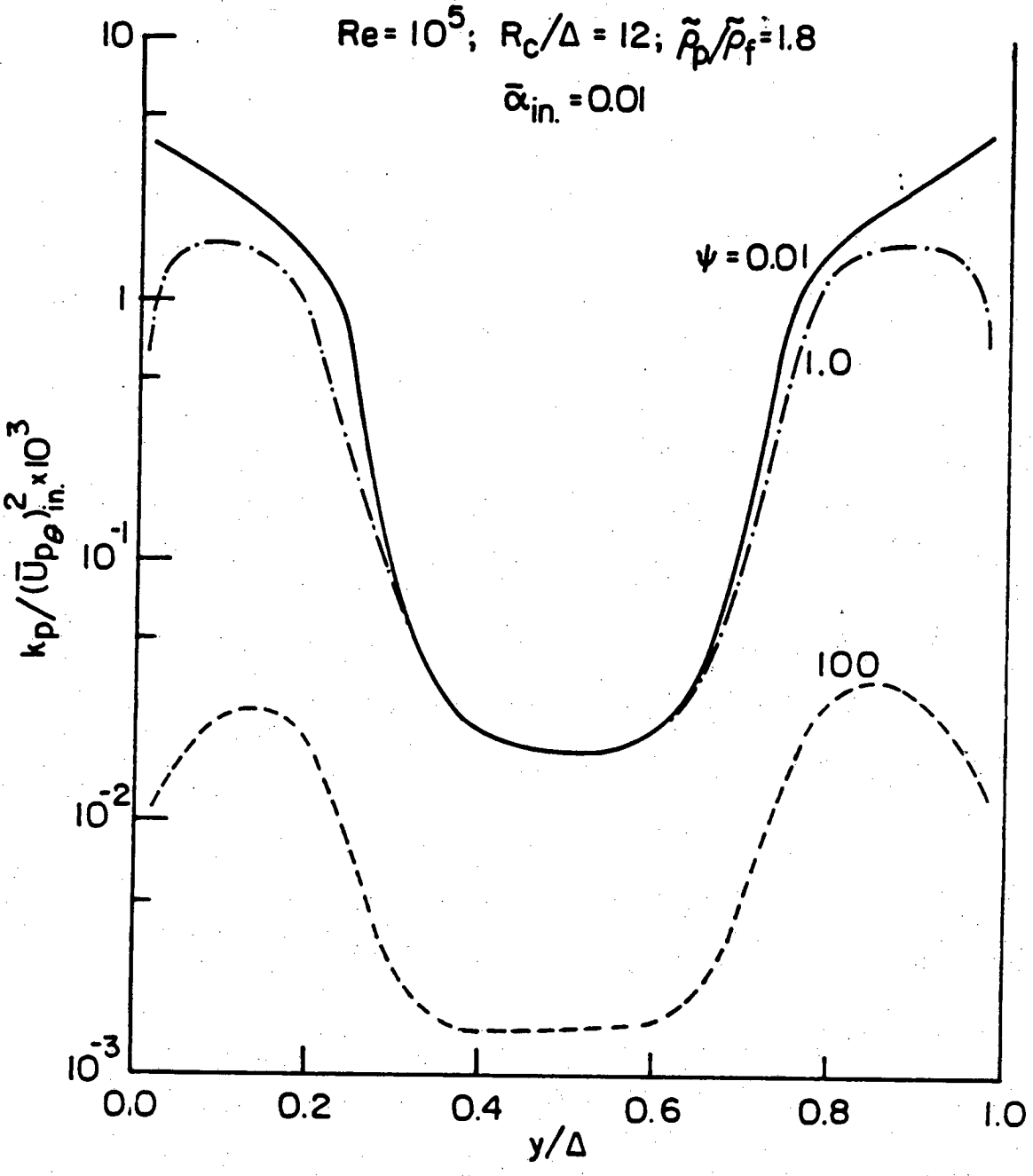

XBL 824-2167

Fig. 7.23

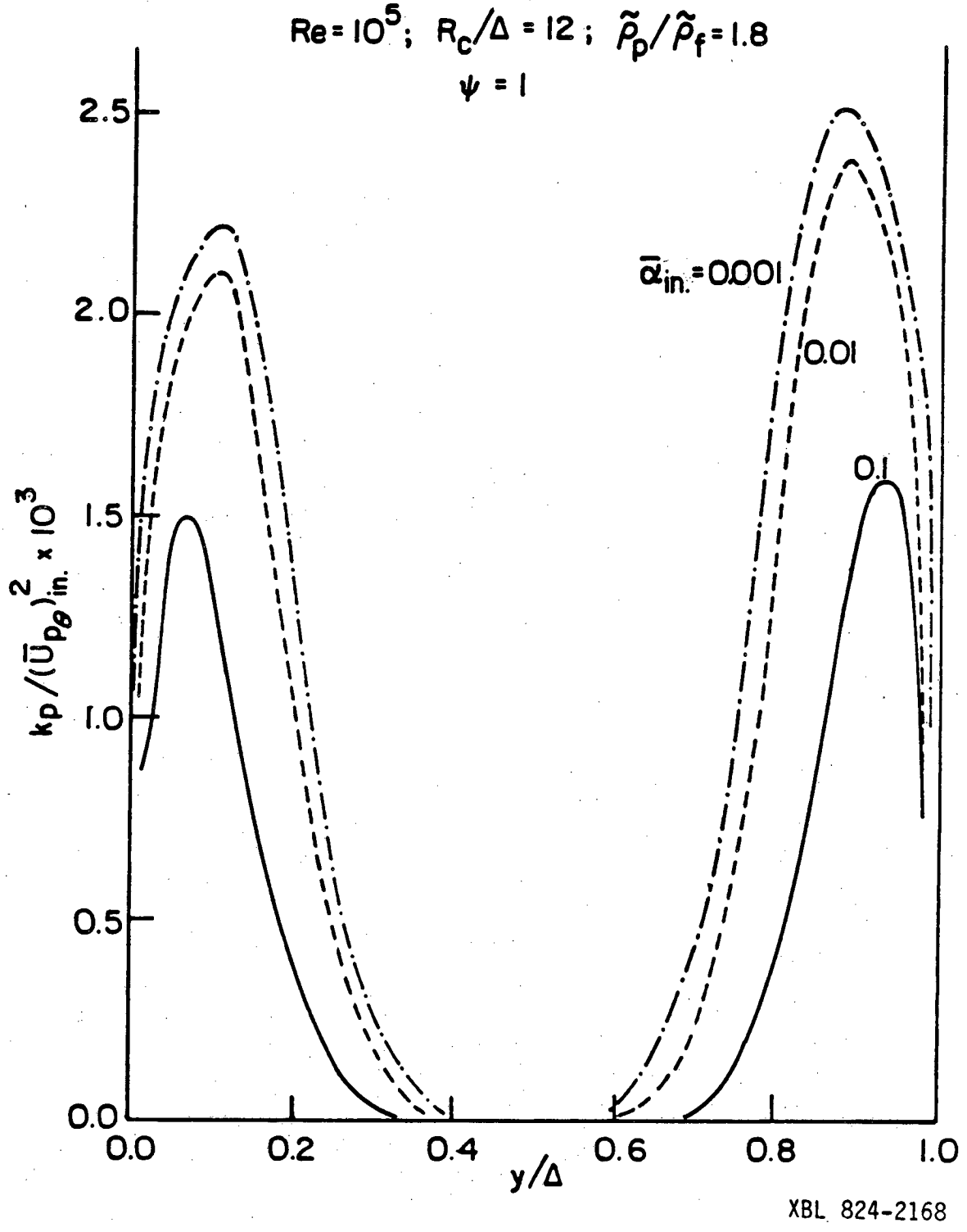
Re = 10^5; R_c/Δ = 12; ρ̃_p/ρ̃_f = 1.8
ψ = 1
ᾱ_in. = 0.001
0.01
0.1
k_p/(Ū_pθ)²_in. × 10³
y/Δ
0.0
0.5
1.0
1.5
2.0
2.5
0.0
0.2
0.4
0.6
0.8
1.0
XBL 824-2168

Fig. 7.24

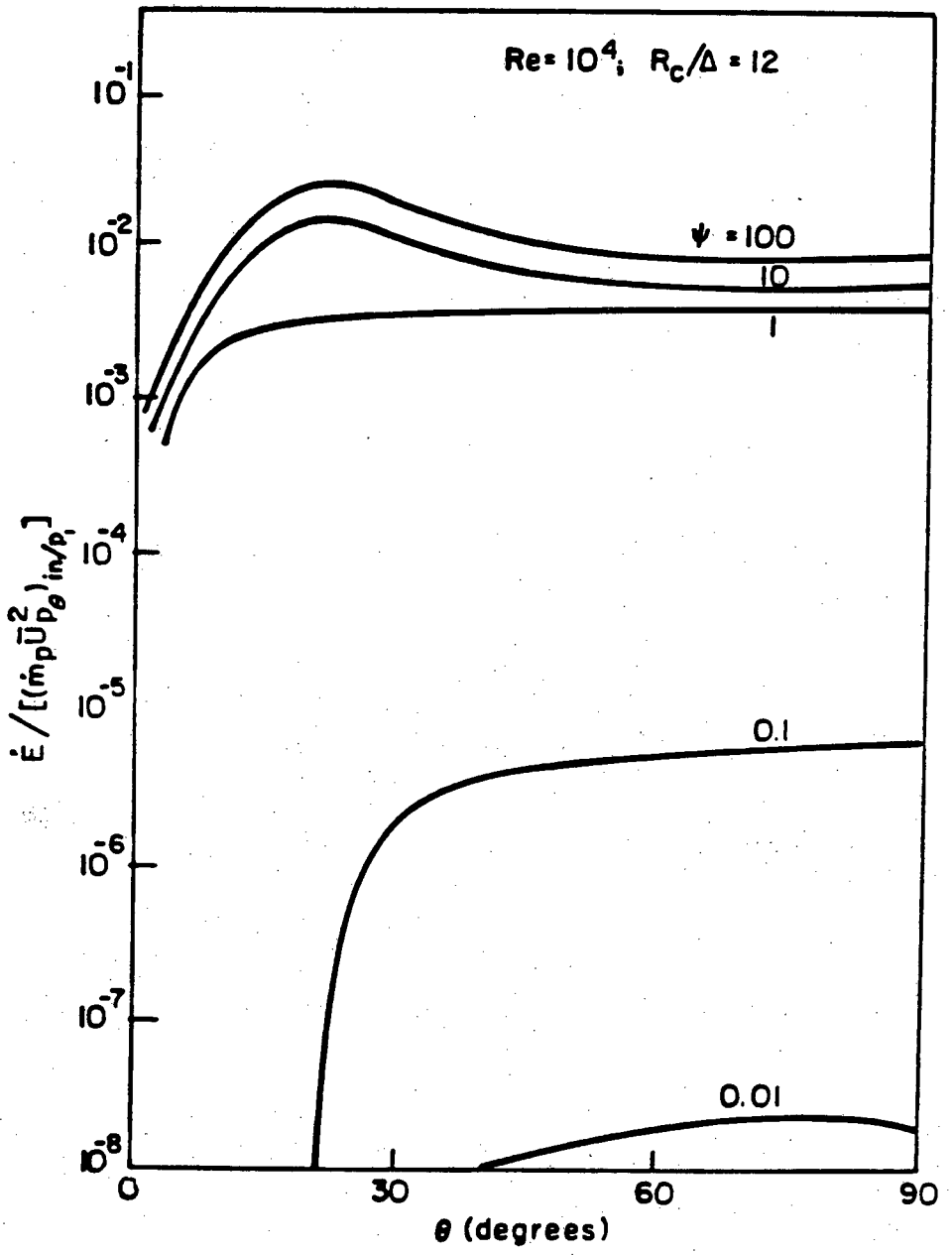

XBL 824-2169

Fig. 7.25

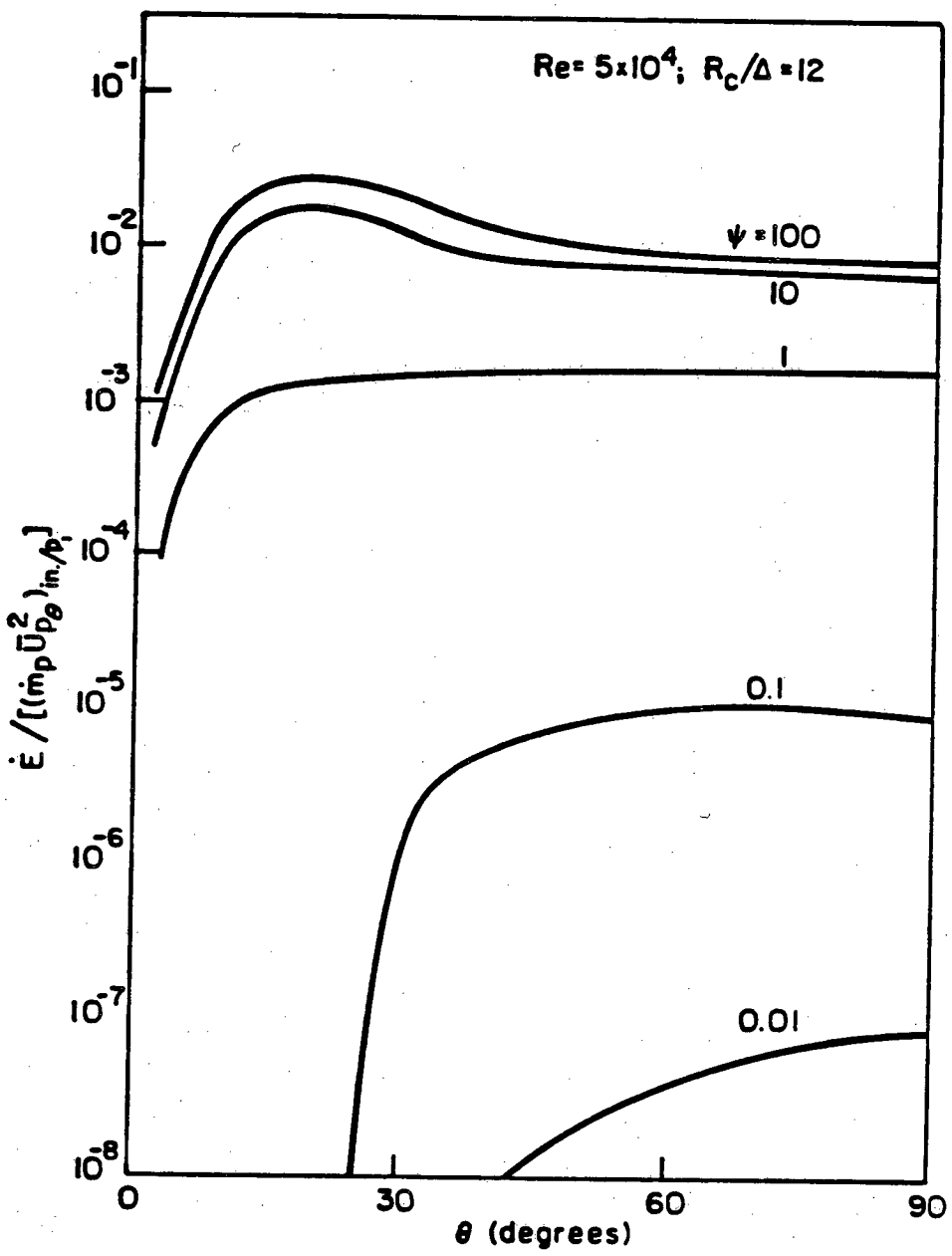

XBL 824-2170

Fig. 7.26

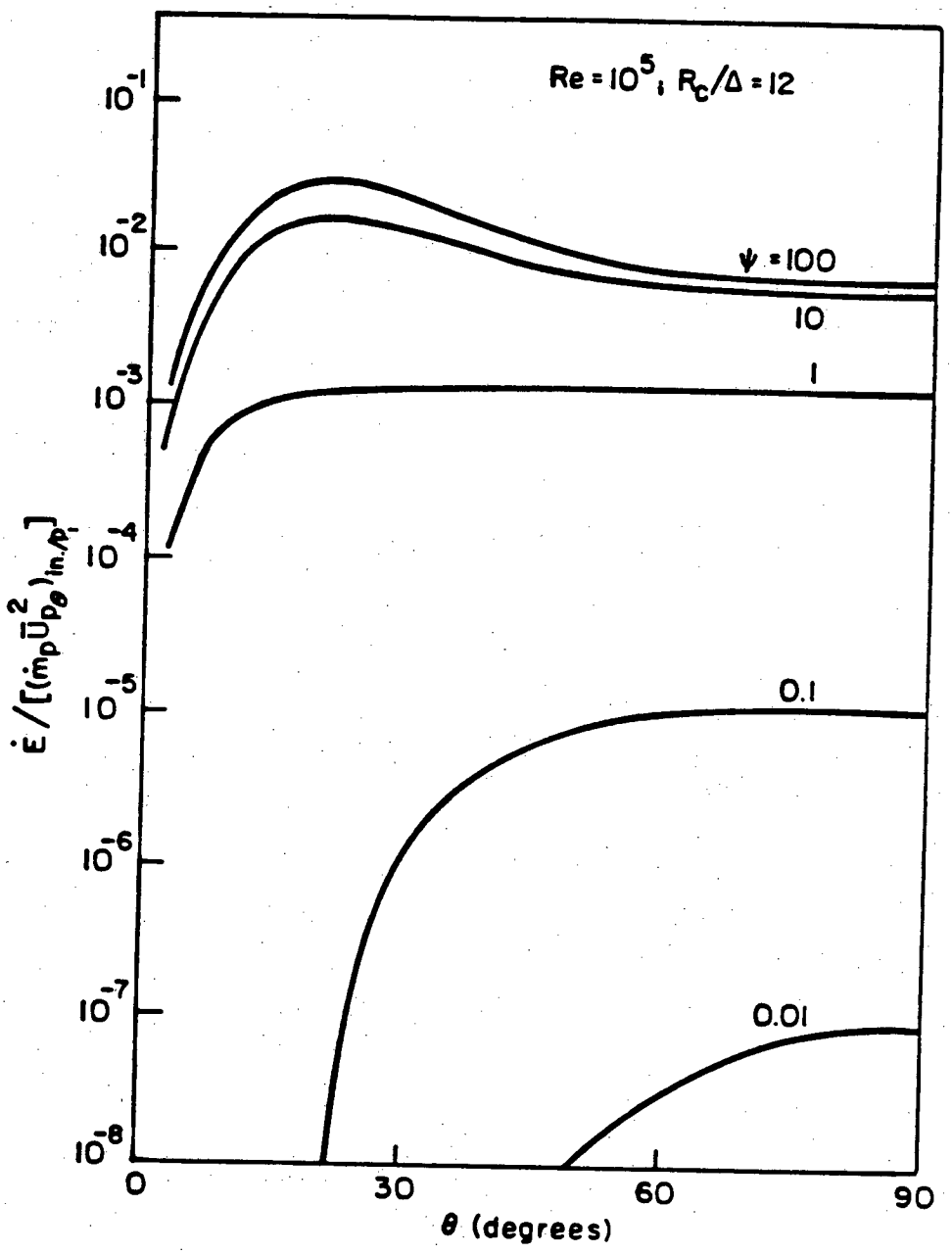

XBL 824-2171

Fig. 7.27

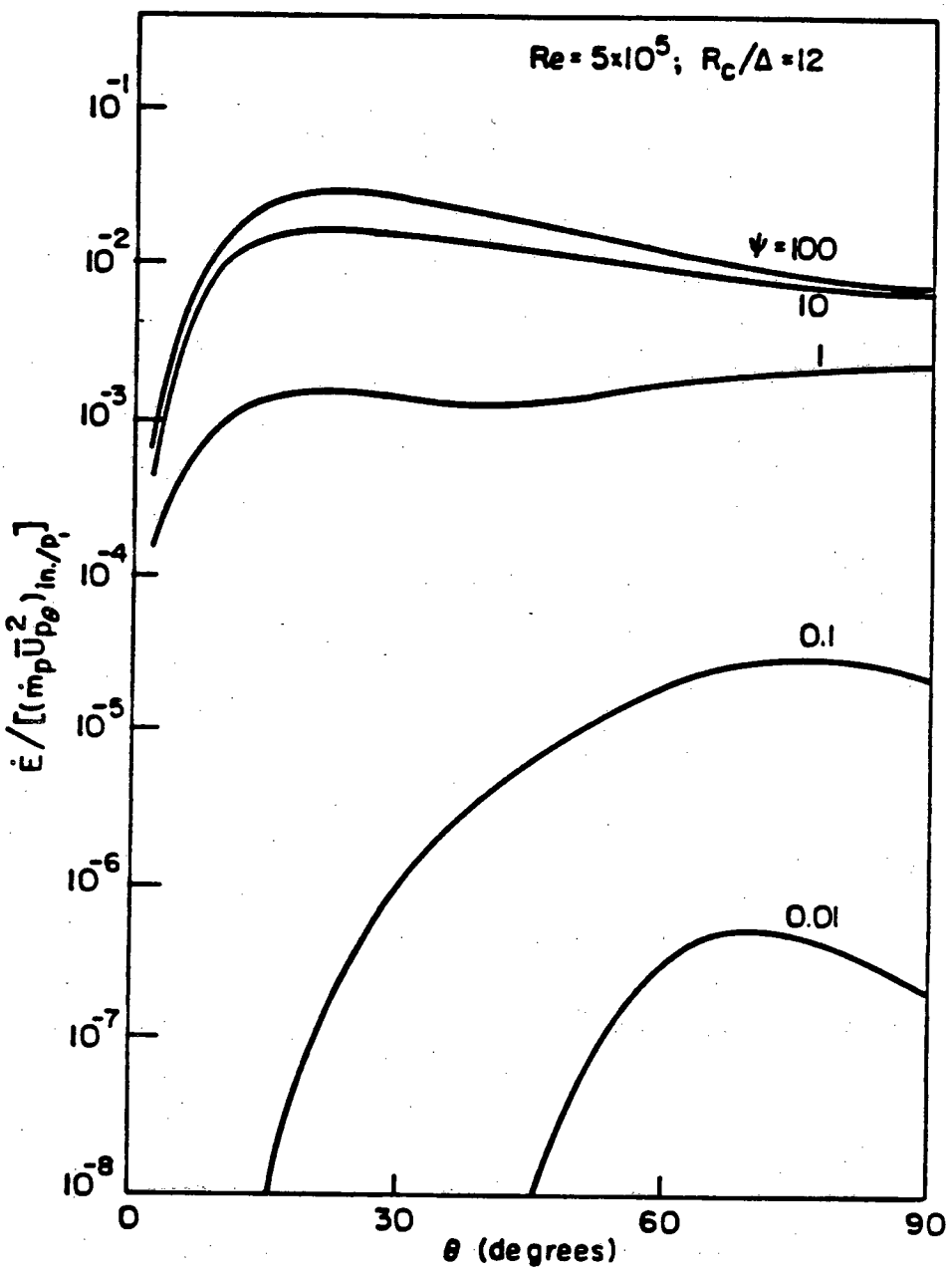
Re = 5×10^5; R_c/Δ = 12
ψ = 100
10
1
0.1
0.01
10^-1
10^-2
10^-3
10^-4
10^-5
10^-6
10^-7
10^-8
Ė/[(ṁ_p Ū^2_pθ)_in./p_i]
0
30
60
90
θ (degrees)
XBL 824-2172

Fig. 7.28

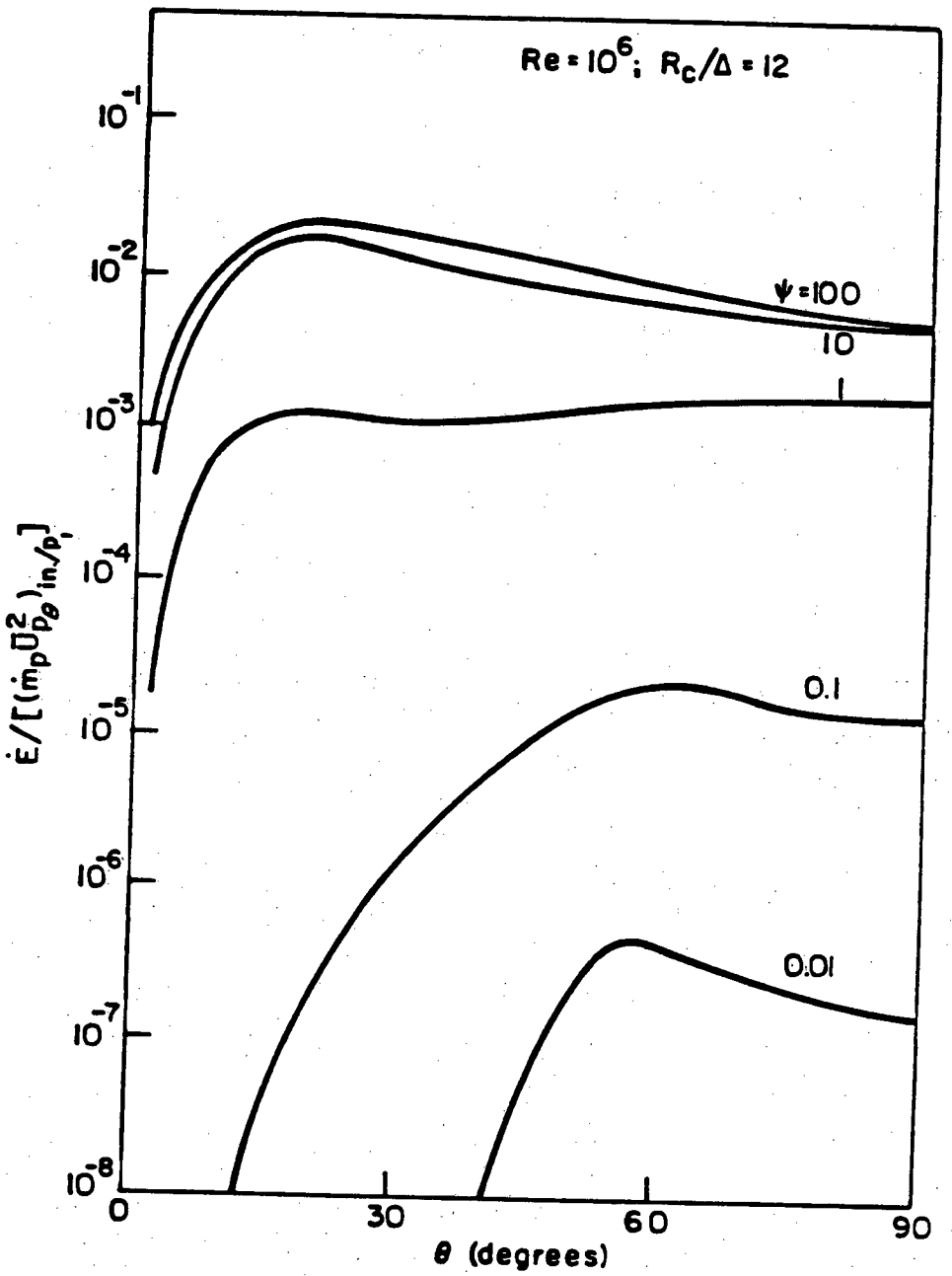

XBL 824-2173

Fig. 7.29

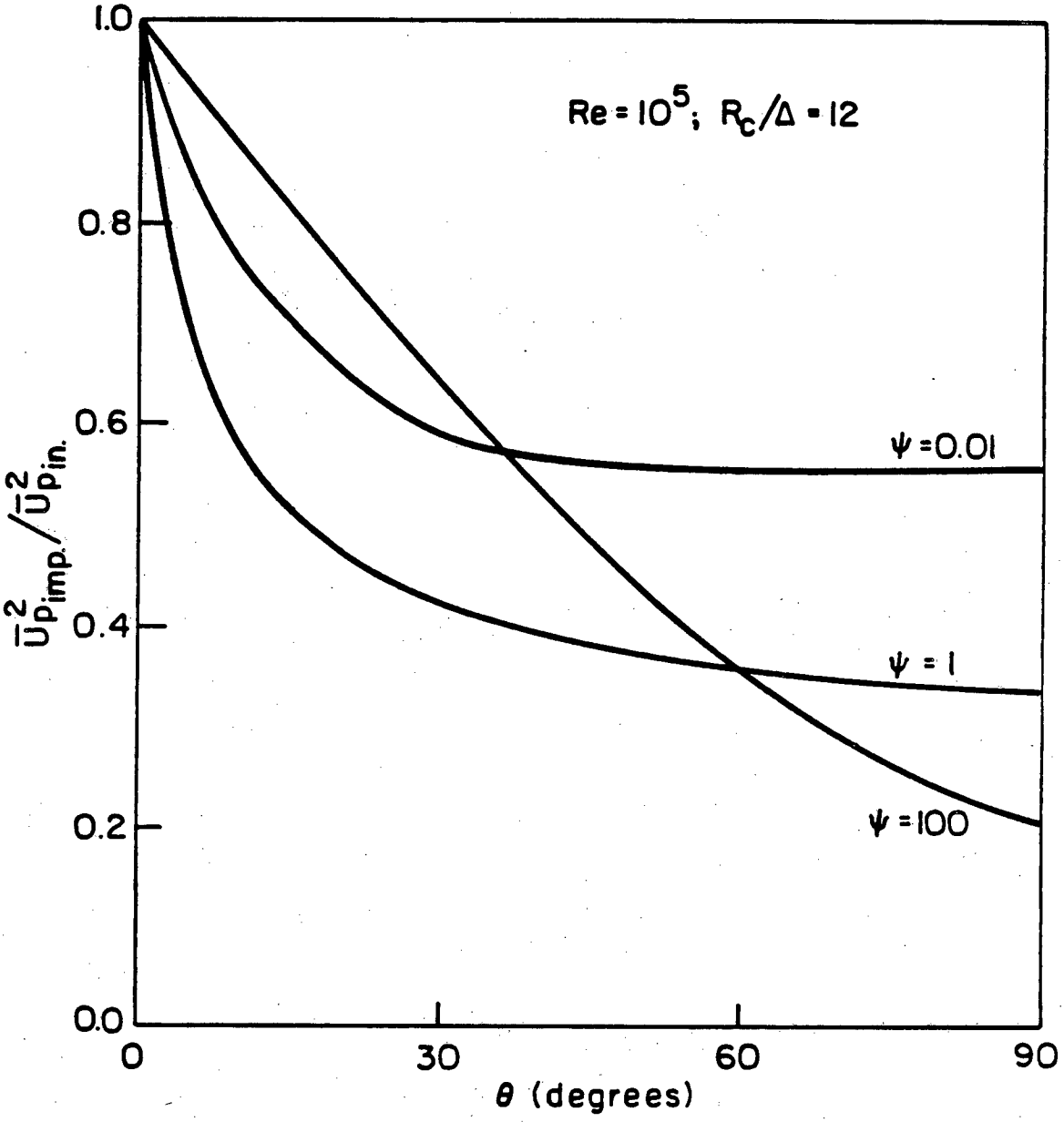
1.0
0.8
0.6
0.4
0.2
0.0
0
30
60
90
θ (degrees)
$\bar{U}^2_{p_{imp.}} / \bar{U}^2_{p_{in.}}$
Re = 10^5; R_c/Δ = 12
ψ = 0.01
ψ = 1
ψ = 100
XBL 824-2174

Fig. 7.30

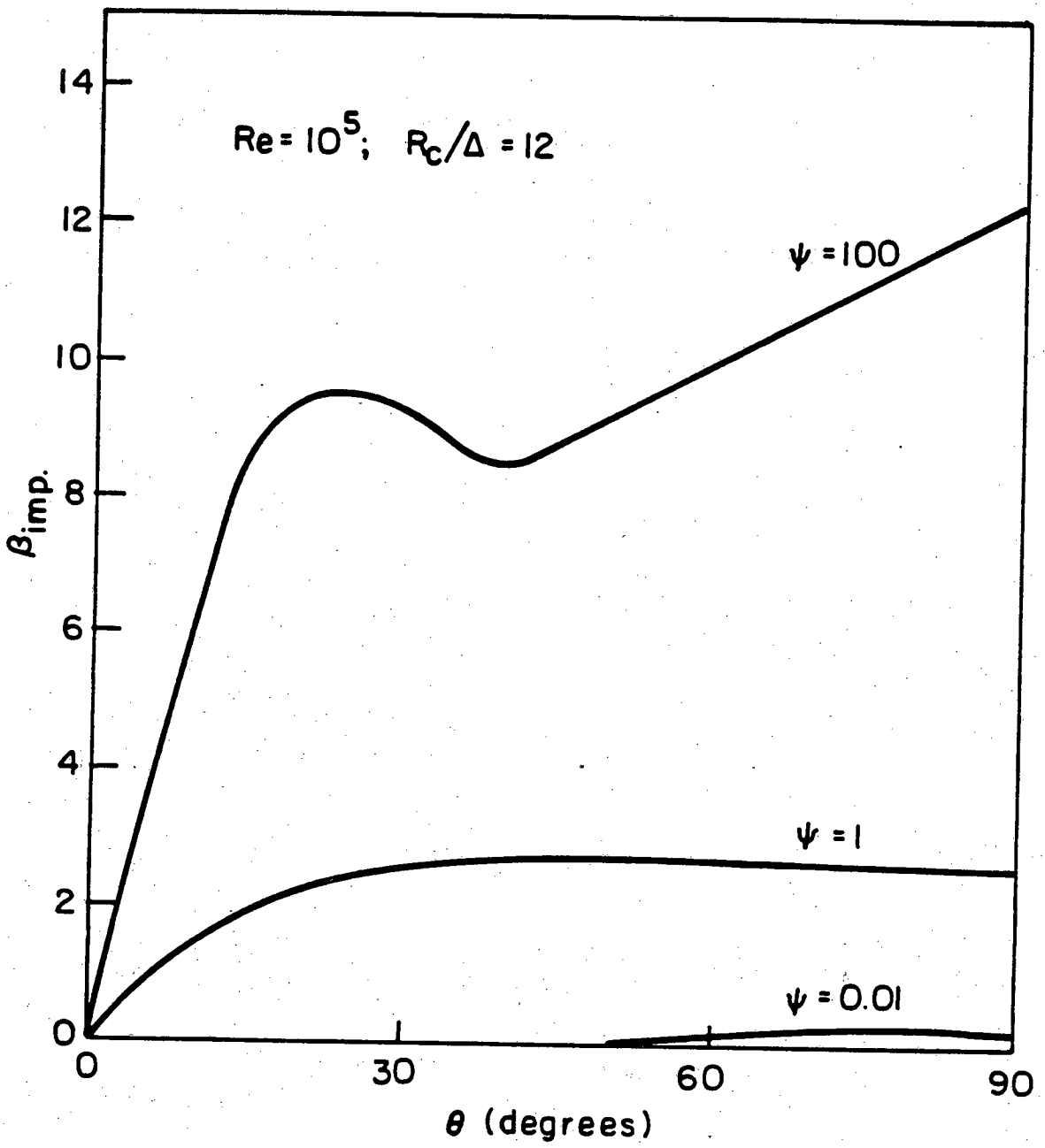

XBL 824-2175

Fig. 7.31

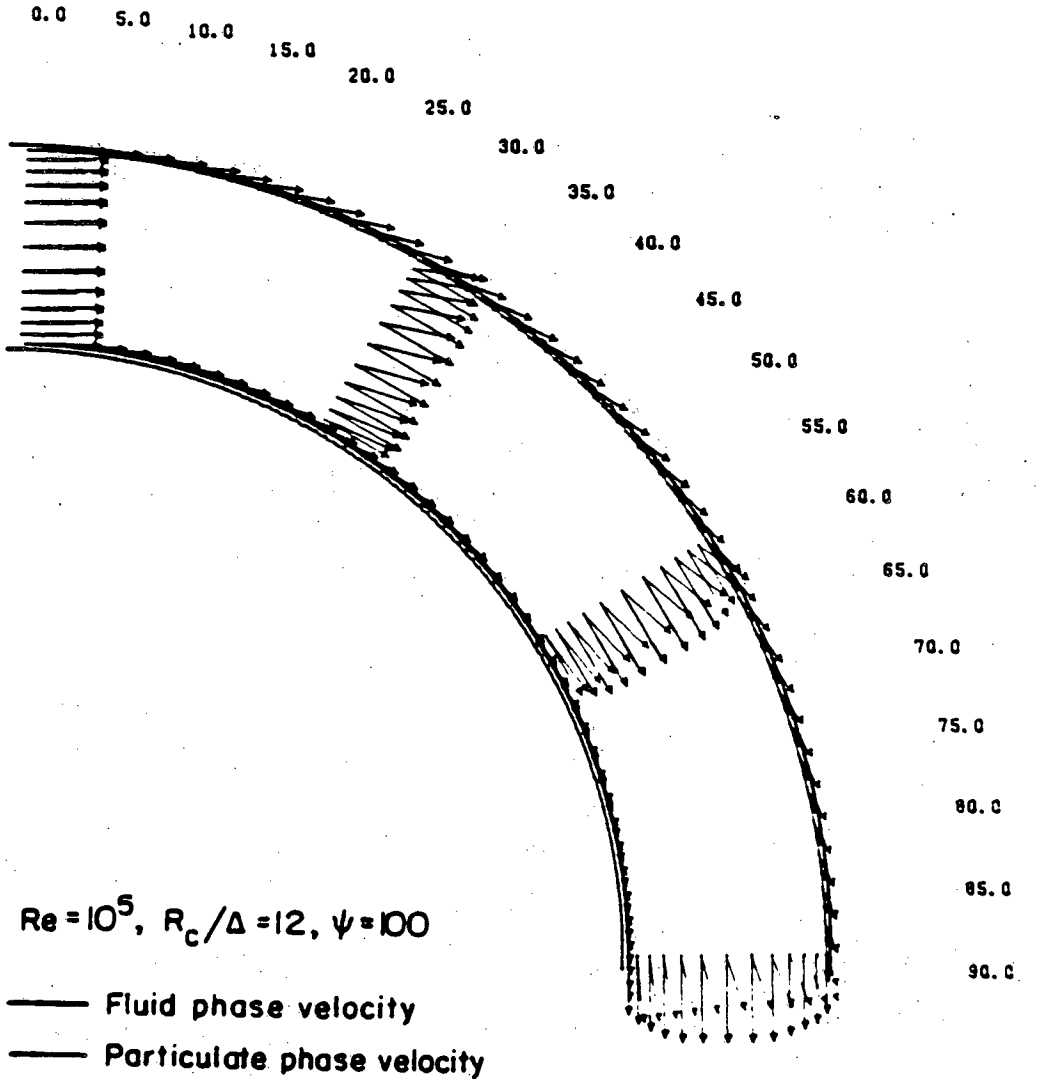
0.0
5.0
10.0
15.0
20.0
25.0
30.0
35.0
40.0
45.0
50.0
55.0
60.0
65.0
70.0
75.0
80.0
85.0
90.0
Re = 10^5, R_c/Δ = 12, ψ = 100
Fluid phase velocity
Particulate phase velocity
CBB 825-4133

Fig. 7.32

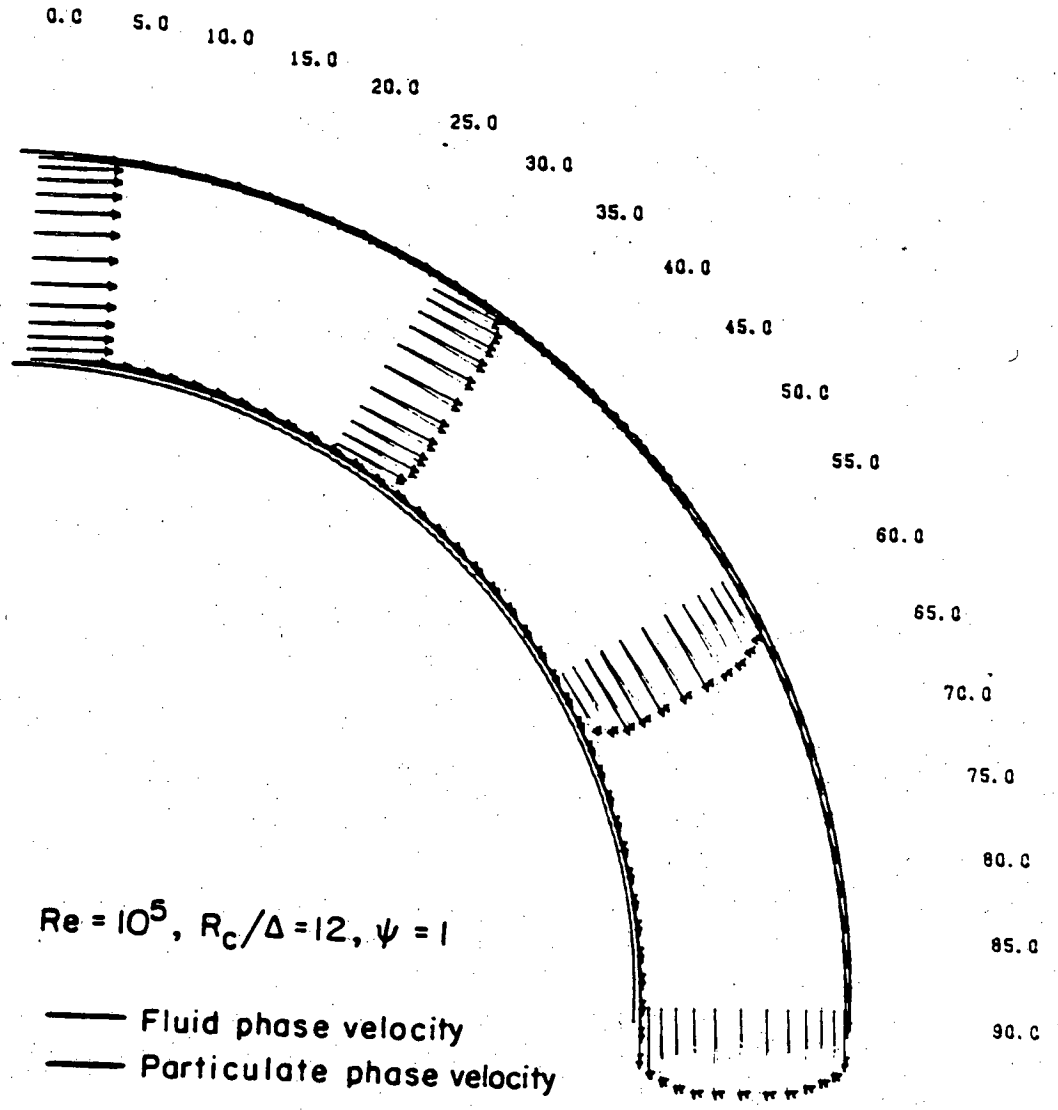
0.0
5.0
10.0
15.0
20.0
25.0
30.0
35.0
40.0
45.0
50.0
55.0
60.0
65.0
70.0
75.0
80.0
85.0
90.0
Re = 10^5, R_c/Δ = 12, ψ = 1
Fluid phase velocity
Particulate phase velocity
CBB 825-4131

Fig. 7.33

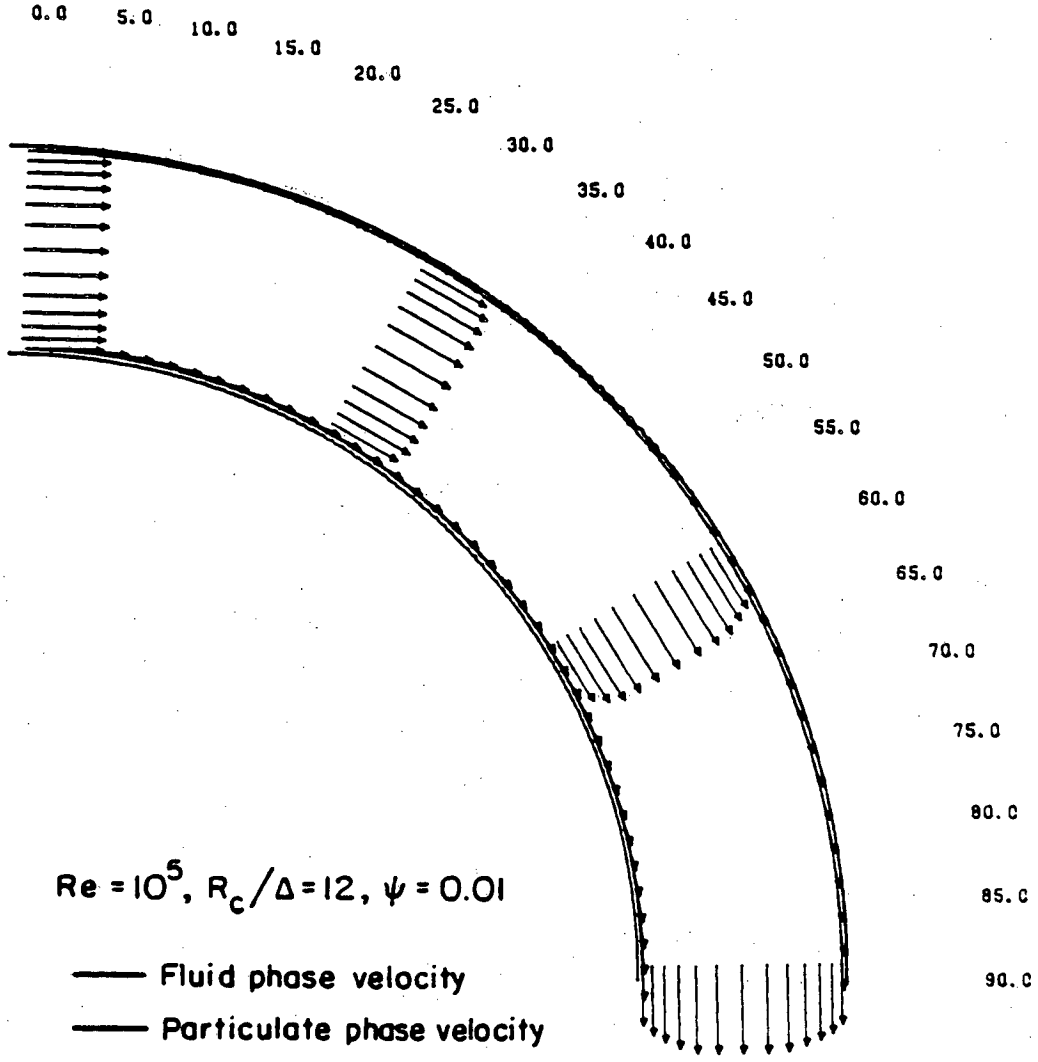
0.0
5.0
10.0
15.0
20.0
25.0
30.0
35.0
40.0
45.0
50.0
55.0
60.0
65.0
70.0
75.0
80.0
85.0
90.0
Re = 10^5, R_c/Δ = 12, ψ = 0.01
Fluid phase velocity
Particulate phase velocity
CBB 825-4129

Fig. 7.34

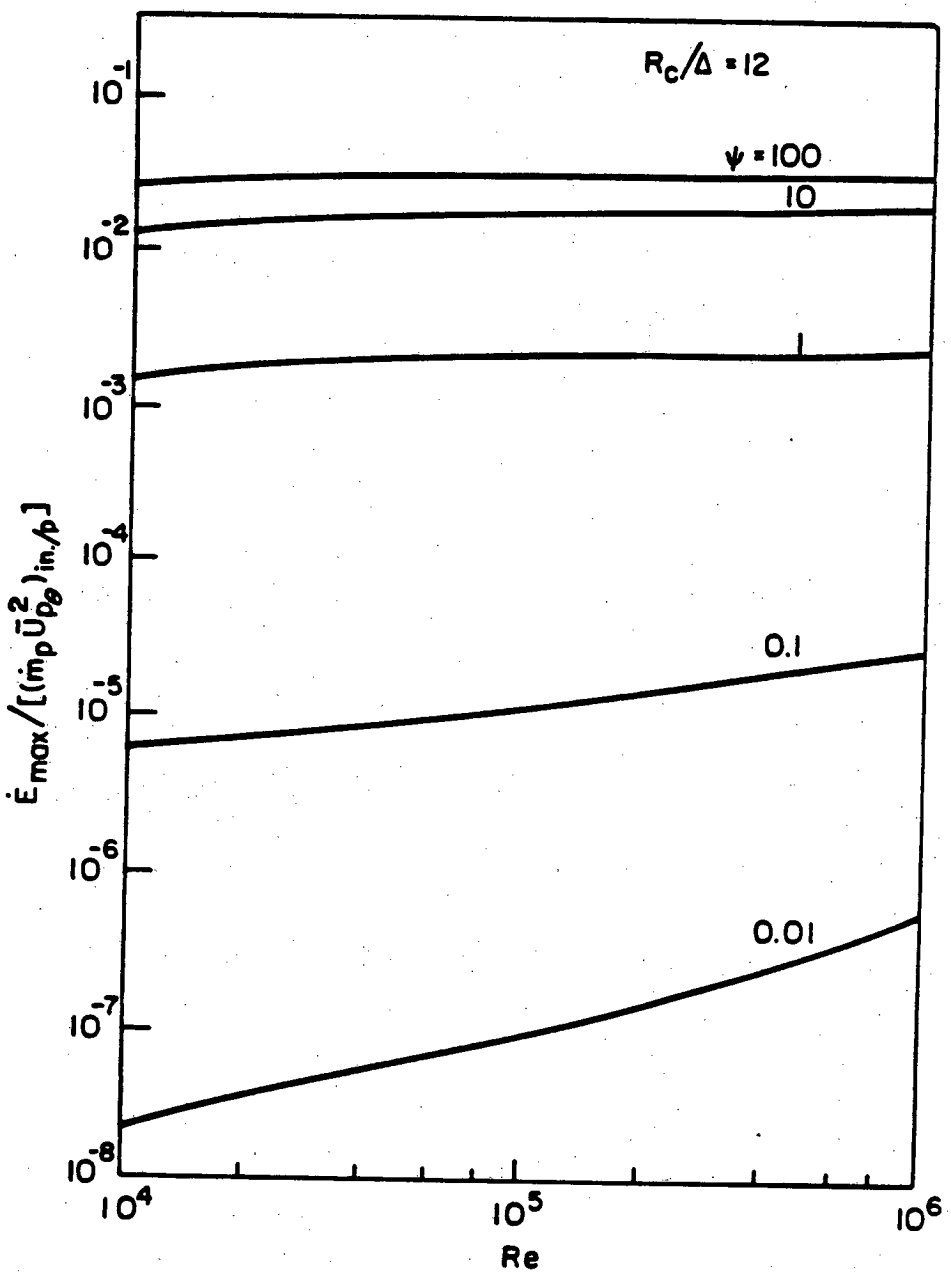

XBL 824-2179

Fig. 7.35

APPENDIX I

CONSERVATION EQUATIONS FOR TURBULENT TWO-PHASE FLOWS

In this appendix the general transport equations are presented for turbulent two-phase flows in cartesian and cylindrical coordinates. In the case of zero particulate volume fraction, the equations reduce to the single-phase conservation equations given by Bryant and Humphrey [1976] and Rodi [1979].

I.1 Cartesian Coordinates (x,y,z)

I.1.1 fluid phase

mass balance:

$$\frac{\partial \overline{U}_{f_x}}{\partial x} + \frac{\partial \overline{U}_{f_y}}{\partial y} + \frac{\partial \overline{U}_{f_z}}{\partial z} = 0 \qquad (I.1)$$

momentum balance:

x:
$$\tilde{\rho}_f \frac{D\overline{U}_{f_x}}{Dt} = -\frac{\tilde{\rho}_p \overline{\alpha}}{\tau_m}(\overline{U}_{f_x} - \overline{U}_{p_x}) - \frac{\partial \overline{P}}{\partial x}$$

$$+ \mu \nabla^2 \overline{U}_{f_x} - \tilde{\rho}_f \frac{\partial}{\partial x}(\overline{u_{f_x}^2}) - \tilde{\rho}_f \frac{\partial}{\partial y}(\overline{u_{f_x} u_{f_y}})$$

$$- \tilde{\rho}_f \frac{\partial}{\partial z}(\overline{u_{f_x} u_{f_z}}) \qquad (I.2)$$

$$y: \quad \tilde{\rho}_f \frac{D\overline{U}_{f_y}}{Dt} = -\frac{\tilde{\rho}_p \overline{\alpha}}{\tau_m}\left(\overline{U}_{f_y} - \overline{U}_{p_x}\right) - \frac{\partial \overline{P}}{\partial y}$$

$$+ \mu \nabla^2 \overline{U}_{f_y} - \tilde{\rho}_f \frac{\partial}{\partial x}\left(\overline{u_{f_x} u_{f_y}}\right) - \tilde{\rho}_f \frac{\partial}{\partial y}\left(\overline{u_{f_y}^2}\right)$$

$$- \tilde{\rho}_f \frac{\partial}{\partial z}\left(\overline{u_{f_z} u_{f_y}}\right) \qquad (I.3)$$

$$z: \quad \tilde{\rho}_f \frac{D\overline{U}_{f_z}}{Dt} = -\frac{\tilde{\rho}_p \overline{\alpha}}{\tau_m}\left(\overline{U}_{f_z} - \overline{U}_{p_z}\right) - \frac{\partial \overline{P}}{\partial z}$$

$$+ \mu \nabla^2 U_{f_z} - \tilde{\rho}_f \frac{\partial}{\partial x}\left(\overline{u_{f_z} u_{f_x}}\right) - \tilde{\rho}_f\left(\overline{u_{f_y} u_{f_z}}\right)$$

$$- \tilde{\rho}_f \frac{\partial}{\partial z}\left(\overline{u_{f_z}^2}\right) \qquad (I.4)$$

In above equations the expressions for Reynolds stresses are given by:

$$-\tilde{\rho}_f \overline{u_{f_x}^2} = 2\mu_{t_f} \frac{\partial \overline{U}_{f_x}}{\partial x} - \frac{2}{3}\tilde{\rho}_f k$$

$$-\tilde{\rho}_f \overline{u_{f_y}^2} = 2\mu_{t_f} \frac{\partial \overline{U}_{f_y}}{\partial y} - \frac{2}{3}\tilde{\rho}_f k$$

$$-\tilde{\rho}_f \overline{u_{f_z}^2} = 2\mu_{t_f} \frac{\partial \overline{U}_{f_z}}{\partial z} - \frac{2}{3}\tilde{\rho}_f k$$

$$-\tilde{\rho}_f \overline{u_{f_x} u_{f_y}} = \mu_{t_f} \left(\frac{\partial \overline{U}_{f_x}}{\partial y} + \frac{\partial \overline{U}_{f_y}}{\partial x} \right)$$

$$-\tilde{\rho}_f \overline{u_{f_x} u_{f_z}} = \mu_{t_f} \left(\frac{\partial \overline{U}_{f_x}}{\partial z} + \frac{\partial \overline{U}_{f_z}}{\partial x} \right)$$

$$-\tilde{\rho}_f \overline{u_{f_x} u_{f_z}} = \mu_{t_f} \left(\frac{\partial \overline{U}_{f_y}}{\partial z} + \frac{\partial \overline{U}_{f_z}}{\partial y} \right)$$

kinetic energy:

$$\frac{Dk}{Dt} = -\frac{\tilde{\rho}_p}{\tilde{\rho}_f \tau_m}\left[\bar{\alpha}(2k)\frac{\tau_m}{\tau_m+T_L} + \overline{\alpha' u_{f_x}}\,(\bar{U}_{f_x}-\bar{U}_{p_x}) + \overline{\alpha' u_{f_y}}\,(\bar{U}_{f_y}-\bar{U}_{p_y})\right.$$

$$\left. + \overline{\alpha' u_{f_z}}\,(U_{f_z}-U_{p_z})\right] + \frac{\partial}{\partial x}\left(\frac{\nu_{t_f}}{\sigma_k}\frac{\partial k}{\partial x}\right) + \frac{\partial}{\partial y}\left(\frac{\nu_{t_f}}{\sigma_k}\frac{\partial k}{\partial y}\right) + \frac{\partial}{\partial z}\left(\frac{\nu_{t_f}}{\sigma_k}\frac{\partial k}{\partial z}\right)$$

$$+ G - \varepsilon \qquad \text{(I.5)}$$

In above equation the expression for Lagrangian integral time scale, T_L, the particle dispersion correlation, $\overline{\alpha' u_{f_i}}$, and the generation of turbulent kinetic energy, G, are given by:

$$T_L = C_T\, k/\varepsilon$$

$$\overline{\alpha' u_{f_x}} = -\nu_{t_p}\frac{\partial \bar{\alpha}}{\partial x}$$

$$\overline{\alpha' u_{f_y}} = -\nu_{t_p}\frac{\partial \bar{\alpha}}{\partial y}$$

$$\overline{\alpha' u_{f_z}} = -\nu_{t_p}\frac{\partial \bar{\alpha}}{\partial z}$$

$$G = \nu_{t_f} \left\{ 2\left[\left(\frac{\partial \overline{U}_{f_z}}{\partial x}\right)^2 + \left(\frac{\partial \overline{U}_{f_y}}{\partial y}\right)^2 + \left(\frac{\partial \overline{U}_{f_z}}{\partial z}\right)^2 + \frac{\partial \overline{U}_{f_x}}{\partial y}\,\frac{\partial \overline{U}_{f_y}}{\partial x} + \frac{\partial \overline{U}_{f_z}}{\partial x}\,\frac{\partial \overline{U}_{f_x}}{\partial z} + \frac{\partial \overline{U}_{f_y}}{\partial z}\,\frac{\partial \overline{U}_{f_z}}{\partial y}\right] + \left(\frac{\partial \overline{U}_{f_z}}{\partial y}\right) + \left(\frac{\partial \overline{U}_{f_x}}{\partial z}\right)^2 + \left(\frac{\partial \overline{U}_{f_y}}{\partial x}\right)^2 + \left(\frac{\partial \overline{U}_{f_y}}{\partial z}\right)^2 + \left(\frac{\partial \overline{U}_{f_z}}{\partial x}\right)^2 + \left(\frac{\partial \overline{U}_{f_z}}{\partial y}\right)^2 \right\}$$

Dissipation of Kinetic Energy

$$\frac{D\epsilon}{Dt} = -\frac{\tilde{\rho}_p}{\tilde{\rho}_f \tau_m}\,\overline{\alpha}\,(\epsilon - I_{fp}) + \frac{\partial}{\partial x}\left(\frac{\nu_{t_f}}{\sigma_\epsilon}\,\frac{\partial \epsilon}{\partial x}\right) + \frac{\partial}{\partial y}\left(\frac{\nu_{t_f}}{\sigma_\epsilon}\,\frac{\partial \epsilon}{\partial y}\right) + \frac{\partial}{\partial z}\left(\frac{\nu_{t_f}}{\sigma_\epsilon}\,\frac{\partial \epsilon}{\partial z}\right) + C_{\epsilon 1}\,\frac{\epsilon}{k}\,G - C_{\epsilon 2}\,\frac{\epsilon^2}{k} \qquad (I.6)$$

With the fluid-particle correlation term given as:

$$I_{fp} = \frac{C_T \nu \tau_m}{\epsilon(\tau_m + T_L)^2}\left[\left(\frac{\partial k}{\partial x}\right)^2 + \left(\frac{\partial k}{\partial y}\right)^2 + \left(\frac{\partial k}{\partial z}\right)^2 - \frac{k}{\epsilon}\left(\frac{\partial k}{\partial x}\right)\left(\frac{\partial \epsilon}{\partial x}\right) - \frac{k}{\epsilon}\left(\frac{\partial k}{\partial y}\right)\left(\frac{\partial \epsilon}{\partial y}\right) - \frac{k}{\epsilon}\left(\frac{\partial k}{\partial z}\right)\left(\frac{\partial \epsilon}{\partial z}\right)\right] + \frac{\epsilon T_L}{\tau_m + T_L}$$

I.1.2 Particulate phase

mass balance:

$$\frac{\partial}{\partial x}\left(\bar{\alpha}\,\bar{U}_{p_x}\right) + \frac{\partial}{\partial y}\left(\bar{\alpha}\,\bar{U}_{p_y}\right) + \frac{\partial}{\partial z}\left(\bar{\alpha}\,\bar{U}_{p_z}\right) + \frac{\partial}{\partial x}\left(\overline{\alpha' u_{p_x}}\right)$$

$$+ \frac{\partial}{\partial y}\left(\overline{\alpha' u_{p_y}}\right) + \frac{\partial}{\partial z}\left(\overline{\alpha' u_{p_z}}\right) = 0 \qquad (I.7)$$

with:

$$\overline{\alpha' u_{p_x}} = - \nu_{t_p} \frac{\partial \bar{\alpha}}{\partial x}$$

$$\overline{\alpha' u_{p_y}} = - \nu_{t_p} \frac{\partial \bar{\alpha}}{\partial y}$$

$$\overline{\alpha' u_{p_z}} = - \nu_{t_p} \frac{\partial \bar{\alpha}}{\partial z}$$

momentum balance:

$$x: \quad \frac{\partial}{\partial x}\left(\bar{\alpha}\,\bar{U}^2_{p_x}\right) + \frac{\partial}{\partial y}\left(\bar{\alpha}\,\bar{U}_{p_x}\bar{U}_{p_y}\right) + \frac{\partial}{\partial z}\left(\bar{\alpha}\,\bar{U}_{p_x}\bar{U}_{p_z}\right) =$$

$$\frac{\bar{\alpha}}{\tau_m}\left(\bar{U}_{f_x} - \bar{U}_{p_x}\right) - \frac{\partial}{\partial x}\left(\bar{\alpha}\,\overline{u^2_{p_x}}\right) - \frac{\partial}{\partial y}\left(\bar{\alpha}\,\overline{u_{p_x}u_{p_y}}\right) - \frac{\partial}{\partial z}\left(\bar{\alpha}\,\overline{u_{p_x}u_{p_z}}\right)$$

$$- \frac{\partial}{\partial x}\left(2\,\bar{U}_{p_x}\,\overline{\alpha' u_{p_x}}\right) - \frac{\partial}{\partial y}\left(\bar{U}_{p_y}\,\overline{\alpha' u_{p_x}} + \bar{U}_{p_x}\,\overline{\alpha' u_{p_y}}\right)$$

$$- \frac{\partial}{\partial z}\left(\bar{U}_{p_z}\overline{\alpha' u_{p_x}} + \bar{U}_{p_x}\,\overline{\alpha' u_{p_z}}\right) \qquad (I.8)$$

$$y: \quad \frac{\partial}{\partial x}\left(\bar{\alpha}\,\bar{U}_{p_x}\bar{U}_{p_y}\right) + \frac{\partial}{\partial y}\left(\bar{\alpha}\,\bar{U}_{p_y}^2\right) + \frac{\partial}{\partial z}\left(\bar{\alpha}\,\bar{U}_{p_y}\bar{U}_{p_z}\right) =$$

$$\frac{\bar{\alpha}}{\tau_m}\left(\bar{U}_{f_y} - \bar{U}_{p_y}\right) - \frac{\partial}{\partial x}\left(\bar{\alpha}\,\overline{u_{p_x}u_{p_y}}\right) - \frac{\partial}{\partial y}\left(\bar{\alpha}\,\overline{u_{p_y}^2}\right) - \frac{\partial}{\partial z}\left(\bar{\alpha}\,\overline{u_{p_y}u_{p_z}}\right)$$

$$- \frac{\partial}{\partial x}\left(\bar{U}_{p_x}\overline{\alpha' u_{p_y}} + \bar{U}_{p_y}\overline{\alpha' u_{p_x}}\right) - \frac{\partial}{\partial y}\left(2\,\bar{U}_{p_y}\overline{\alpha' u_{p_y}}\right)$$

$$- \frac{\partial}{\partial z}\left(\bar{U}_{p_z}\overline{\alpha' u_{p_y}} + \bar{U}_{p_y}\overline{\alpha' u_{p_z}}\right) \qquad \text{(I.9)}$$

$$z: \quad \frac{\partial}{\partial x}\left(\bar{\alpha}\,\bar{U}_{p_z}\bar{U}_{p_y}\right) + \frac{\partial}{\partial y}\left(\bar{\alpha}\,\bar{U}_{p_z}\bar{U}_{p_y}\right) + \frac{\partial}{\partial z}\left(\bar{\alpha}\,\overline{U_{p_z}^2}\right) =$$

$$\frac{\bar{\alpha}}{\tau_m}\left(\bar{U}_{f_z} - \bar{U}_{p_z}\right) - \frac{\partial}{\partial x}\left(\bar{\alpha}\,\overline{u_{p_x}u_{p_z}}\right) - \frac{\partial}{\partial y}\left(\bar{\alpha}\,\overline{u_{p_z}u_{p_y}}\right) - \frac{\partial}{\partial z}\left(\bar{\alpha}\,\overline{u_{p_z}^2}\right)$$

$$- \frac{\partial}{\partial x}\left(\bar{U}_{p_z}\overline{\alpha' u_{p_z}} + \bar{U}_{p_z}\overline{\alpha' u_{p_x}}\right) - \frac{\partial}{\partial y}\left(\bar{U}_{p_y}\overline{\alpha' u_{p_z}} + \bar{U}_{p_z}\overline{\alpha' u_{p_y}}\right)$$

$$- \frac{\partial}{\partial z}\left(2\bar{U}_{p_z}\overline{\alpha' u_{p_z}}\right) \qquad \text{(I.10)}$$

The particulate Reynolds stresses are given by:

$$-\overline{u_{p_x}^2} = 2\,\nu_{t_p}\frac{\partial \overline{U}_{p_x}}{\partial x} - \frac{2}{3}\left[k_p + \nu_{t_p}(\nabla\cdot\overline{U}_p)\right]$$

$$-\overline{u_{p_y}^2} = 2\,\nu_{t_p}\frac{\partial \overline{U}_{p_y}}{\partial y} - \frac{2}{3}\left[k_p + \nu_{t_p}(\nabla\cdot\overline{U}_p)\right]$$

$$-\overline{u_{p_z}^2} = 2\,\nu_{t_p}\frac{\partial \overline{U}_{p_z}}{\partial z} - \frac{2}{3}\left[k_p + \nu_{t_p}(\nabla\cdot\overline{U}_p)\right]$$

$$-\overline{u_{p_x}u_{p_y}} = \nu_{t_p}\left(\frac{\partial \overline{U}_{p_x}}{\partial y} + \frac{\partial \overline{U}_{p_y}}{\partial x}\right)$$

$$-\overline{u_{p_x}u_{p_z}} = \nu_{t_p}\left(\frac{\partial \overline{U}_{p_x}}{\partial z} + \frac{\partial U_{p_z}}{\partial x}\right)$$

$$-\overline{u_{p_y}u_{p_z}} = \nu_{t_p}\left(\frac{\partial \overline{U}_{p_y}}{\partial z} + \frac{\partial U_{p_z}}{\partial y}\right)$$

In above expression the divergence of the mean particle velocity is:

$$\nabla\cdot\overline{U}_p = \frac{\partial \overline{U}_{p_x}}{\partial x} + \frac{\partial \overline{U}_{p_y}}{\partial y} + \frac{\partial \overline{U}_{p_z}}{\partial z}$$

also:

$$\frac{D}{Dt} = \frac{\partial}{\partial t} + \overline{U}_{f_x} \frac{\partial}{\partial x} + \overline{U}_{f_y} \frac{\partial}{\partial y} + \overline{U}_{f_z} \frac{\partial}{\partial x}$$

and:

$$\nabla^2 = \frac{\partial^2}{\partial x^2} + \frac{\partial^2}{\partial y^2} + \frac{\partial^2}{\partial z^2}$$

I.2 Cylindrical Coordinates (r,θ,z):

I.2.1 fluid phase:

mass balance:

$$\frac{\partial \overline{U}_{f_r}}{\partial r} + \frac{1}{r} \frac{\partial \overline{U}_{f_\theta}}{\partial \theta} + \frac{\partial \overline{U}_{f_z}}{\partial z} + \frac{\overline{U}_{f_r}}{r} = 0 \qquad \text{(I.11)}$$

momentum balance:

$$r: \quad \tilde{\rho}_f \left(\frac{D\overline{U}_{f_r}}{Dt} - \frac{\overline{U}_{f_\theta}^2}{r} \right) = - \frac{\tilde{\rho}_p \overline{\alpha}}{\tau_m} (\overline{U}_{f_r} - \overline{U}_{p_r}) - \frac{\partial \overline{P}}{\partial r} + \mu \left(\nabla^2 \overline{U}_{f_r} - \frac{\overline{U}_{f_r}}{r^2} - \frac{2}{r^2} \frac{\partial \overline{U}_{f_\theta}}{\partial \theta} \right)$$

$$- \tilde{\rho}_f \left(\frac{1}{r} \frac{\partial}{\partial r} (\overline{r u_{f_r}^2}) + \frac{1}{r} \frac{\partial}{\partial \theta} \overline{u_{f_r} u_{f_\theta}} + \frac{\partial}{\partial z} \overline{u_{f_r} u_{f_z}} - \frac{\overline{u_{f_\theta}^2}}{r} \right)$$

(I.12)

$$\theta: \tilde{\rho}_f \left(\frac{D\overline{U}_{f_\theta}}{Dt} + \frac{\overline{U}_{f_r} \overline{U}_{f_\theta}}{r} \right) = - \frac{\tilde{\rho}_p \overline{\alpha}}{\tau_m} (\overline{U}_{f_\theta} - \overline{U}_{p_\theta}) - \frac{1}{r} \frac{\partial \overline{P}}{\partial \theta}$$

$$+ \mu \left(\nabla^2 \overline{U}_{f_\theta} - \frac{\overline{U}_{f_\theta}}{r^2} - \frac{2}{r^2} \frac{\partial \overline{U}_{f_r}}{\partial \theta} \right)$$

$$- \tilde{\rho}_f \left(\frac{1}{r} \frac{\partial}{\partial \theta} \overline{U}_{f_\theta}^2 + \frac{\partial}{\partial r} \overline{U_{f_\theta} U_{f_r}} \right.$$

$$\left. + \frac{\partial}{\partial z} \overline{U_{f_\theta} U_{f_z}} + \frac{2}{r} \overline{U_{f_\theta} U_{f_r}} \right) \qquad \text{(I.13)}$$

$$z: \quad \tilde{\rho}_f \frac{D\overline{U}_{f_z}}{Dt} = - \frac{\tilde{\rho}_p \alpha}{\tau_m} (\overline{U_{f_z} - U_{p_z}}) - \frac{\partial P}{\partial z} + \mu \nabla^2 \overline{U}_{f_z}$$

$$- \tilde{\rho}_f \left[\frac{\partial \overline{u_{f_z}^2}}{\partial z} + \frac{1}{r} \frac{\partial}{\partial r} (\overline{r u_{f_r} u_{f_z}}) + \frac{1}{r} \frac{\partial}{\partial \theta} (\overline{u_{f_\theta} u_{f_z}}) \right]$$

(I.14)

In which the Reynolds stresses are expressed as:

$$- \tilde{\rho}_f \overline{u_r^2} = \mu_{t_f} \left(2 \frac{\partial \overline{U}_{f_r}}{\partial r} \right) - \frac{2}{3} \tilde{\rho}_f k$$

$$- \tilde{\rho}_f \overline{u_\theta^2} = \mu_{t_f} \left(\frac{2}{r} \frac{\partial \overline{U}_{f_\theta}}{\partial \theta} + 2 \frac{\overline{U}_{f_r}}{r} \right) - \frac{2}{3} \tilde{\rho}_f k$$

$$- \tilde{\rho}_f \overline{u_z^2} = \mu_{t_f} \left(2 \frac{\partial \overline{U}_{f_z}}{\partial z} \right) - \frac{2}{3} \tilde{\rho}_f k$$

$$- \tilde{\rho}_f \overline{u_{f_r} u_{f_\theta}} = \mu_{t_f} \left(\frac{\partial \overline{U}_{f_\theta}}{\partial r} + \frac{1}{r} \frac{\partial \overline{U}_{f_r}}{\partial \theta} - \frac{\overline{U}_{f_\theta}}{r} \right)$$

$$- \tilde{\rho}_f \overline{u_{f_r} u_{f_z}} = \mu_{t_f} \left(\frac{\partial \overline{U}_{f_z}}{\partial r} + \frac{\partial \overline{U}_{f_r}}{\partial z} \right)$$

$$- \tilde{\rho}_f \overline{u_{f_\theta} u_{f_z}} = \mu_{t_f} \left(\frac{1}{r} \frac{\partial \overline{U}_{f_z}}{\partial \theta} + \frac{\partial \overline{U}_{f_\theta}}{\partial z} \right)$$

and also;

$$\frac{D}{Dt} = \frac{\partial}{\partial t} + \overline{U}_r \frac{\partial}{\partial r} + \frac{\overline{U}_\theta}{r} \frac{\partial}{\partial \theta} + \overline{U}_z \frac{\partial}{\partial z}$$

$$\nabla^2 = \frac{\partial^2}{\partial r^2} + \frac{1}{r} \frac{\partial}{\partial r} + \frac{1}{r^2} \frac{\partial^2}{\partial \theta^2} + \frac{\partial^2}{\partial z^2}$$

kinetic energy:

$$\frac{Dk}{Dt} = - \frac{\tilde{\rho}_p}{\tilde{\rho}_f \tau_m} \left[\frac{2\overline{\alpha}\tau_m k}{\tau_m + T_L} + \overline{\alpha' u_{f_r}} \left(\overline{U}_{f_r} - \overline{U}_{p_r}\right) + \overline{\alpha' u_{f_\theta}} \left(\overline{U}_{f_\theta} - \overline{U}_{p_\theta}\right) \right.$$

$$\left. + \overline{\alpha' u_{f_z}} \left(\overline{U}_{f_z} - \overline{U}_{p_z}\right) \right] + \frac{1}{r} \frac{\partial}{\partial r} \left(\frac{\nu_{t_f}}{\sigma_k} r \frac{\partial k}{\partial r} \right) + \frac{1}{r^2} \frac{\partial}{\partial \theta} \left(\frac{\nu_{t_f}}{\sigma_k} \frac{\partial k}{\partial \theta} \right)$$

$$+ \frac{\partial}{\partial z} \left(\frac{\nu_{t_f}}{\sigma_k} \frac{\partial k}{\partial z} \right) + G - \varepsilon \qquad \text{(I.15)}$$

with:

$$\overline{\alpha' u_{f_r}} = - \nu_{t_p} \frac{\partial \overline{\alpha}}{\partial r}$$

$$\overline{\alpha' u_{f_\theta}} = - \nu_{t_p} \frac{\partial \overline{\alpha}}{r \partial \theta}$$

$$\overline{\alpha' u_{f_z}} = - \nu_{t_p} \frac{\partial \overline{\alpha}}{\partial z}$$

and for production of kinetic energy:

$$G = \nu_{t_f} \left\{ 2 \left[\left(\frac{\partial \bar{U}_{f_r}}{\partial r} \right)^2 + \left(\frac{\partial \bar{U}_{f_\theta}}{r \partial \theta} \right)^2 + \left(\frac{\partial \bar{U}_{f_z}}{\partial z} \right)^2 - \frac{\bar{U}_{f_\theta}}{r} \left(\frac{1}{r} \frac{\partial \bar{U}_{f_r}}{\partial \theta} + \frac{\partial \bar{U}_{f_\theta}}{\partial r} \right) \right.\right.$$

$$\left. + \frac{\bar{U}_{f_r}}{r} \left(\frac{\bar{U}_{f_r}}{r} + \frac{2}{r} \frac{\partial \bar{U}_{f_\theta}}{\partial \theta} \right) + \frac{1}{r} \left(\frac{\partial \bar{U}_{f_r}}{\partial \theta} \frac{\partial \bar{U}_{f_\theta}}{\partial r} + \frac{\partial \bar{U}_{f_z}}{\partial \theta} \frac{\partial \bar{U}_{f_\theta}}{\partial z} \right) + \frac{\partial \bar{U}_{f_r}}{\partial z} \frac{\partial \bar{U}_{f_z}}{\partial r} \right]$$

$$+ \left(\frac{\bar{U}_{f_\theta}}{r} \right)^2 + \left(\frac{\partial \bar{U}_{f_\theta}}{\partial r} \right)^2 + \left(\frac{\partial \bar{U}_{f_\theta}}{\partial z} \right)^2 + \left(\frac{1}{r} \frac{\partial \bar{U}_{f_r}}{\partial \theta} \right)^2$$

$$\left. + \left(\frac{\partial \bar{U}_{f_r}}{\partial z} \right)^2 + \left(\frac{\partial \bar{U}_{f_z}}{\partial r} \right)^2 + \left(\frac{1}{r} \frac{\partial \bar{U}_{f_z}}{\partial \theta} \right)^2 \right\}$$

Disspation of turbulent kinetic energy

$$\frac{D\epsilon}{Dt} = - \frac{\tilde{\rho}_p}{\tilde{\rho}_f \tau_m} \bar{\alpha} (\epsilon - II_{fp}) + \frac{1}{r} \frac{\partial}{\partial r} \left(\frac{\nu_{t_f}}{\sigma_\epsilon} r \frac{\partial \epsilon}{\partial r} \right)$$

$$+ \frac{1}{r^2} \frac{\partial}{\partial \theta} \left(\frac{\nu_{t_f}}{\sigma_\epsilon} \frac{\partial \epsilon}{\partial \theta} \right) + \frac{\partial}{\partial z} \left(\frac{\nu_{t_f}}{\sigma_\epsilon} \frac{\partial \epsilon}{\partial z} \right) \qquad (I.16)$$

with the fluid-particle correlation term II_{fp} given by:

$$II_{fp} = \frac{C_T \nu \tau_m}{\epsilon (\tau_m + T_L)^2} \left[\frac{1}{r^2} \left(\frac{\partial k}{\partial \theta} \right)^2 + \left(\frac{\partial k}{\partial r} \right)^2 + \left(\frac{\partial k}{\partial z} \right)^2 - \frac{k}{\epsilon} \left(\frac{\partial k}{\partial r} \right) \left(\frac{\partial \epsilon}{\partial r} \right) \right.$$

$$\left. - \frac{k}{\epsilon} \left(\frac{\partial k}{r \partial \theta} \right) \left(\frac{\partial \epsilon}{r \partial \theta} \right) - \frac{k}{\epsilon} \left(\frac{\partial k}{\partial z} \right) \left(\frac{\partial \epsilon}{\partial z} \right) \right] + \frac{\epsilon T_L}{\tau_m + T_L}$$

A.2.2 Particulate Phase

mass balance:

$$\frac{1}{r}\frac{\partial}{\partial r}\left(r\bar{\alpha}\,\bar{U}_{p_r}\right) + \frac{\partial}{r\partial\theta}\left(\bar{\alpha}\,\bar{U}_{p_\theta}\right) + \frac{\partial}{\partial z}\left(\bar{\alpha}\,\bar{U}_{p_z}\right)$$

$$+ \frac{1}{r}\frac{\partial}{\partial r}\left(r\overline{\alpha' u_{p_r}}\right) + \frac{\partial}{r\partial\theta}\left(\overline{\alpha' u_{p_\theta}}\right) + \frac{\partial}{\partial z}\left(\overline{\alpha' u_{p_z}}\right) = 0 \qquad (I.17)$$

with:

$$\overline{\alpha' u_{p_r}} = -\nu_{t_p}\frac{\partial\bar{\alpha}}{\partial r}$$

$$\overline{\alpha' u_{p_\theta}} = -\nu_{t_p}\frac{\partial\bar{\alpha}}{r\partial\theta}$$

$$\overline{\alpha' u_{p_z}} = -\nu_{t_p}\frac{\partial\bar{\alpha}}{\partial z}$$

momentum balance:

r:
$$\frac{1}{r}\frac{\partial}{\partial r}\left(r\bar{\alpha}\,\bar{U}_{p_r}^2\right) + \frac{1}{r}\frac{\partial}{\partial\theta}\left(\bar{\alpha}\,\bar{U}_{p_r}\bar{U}_{p_\theta}\right) + \frac{\partial}{\partial z}\left(\bar{\alpha}\,\bar{U}_{p_r}\bar{U}_{p_z}\right) - \frac{\bar{\alpha}\,\bar{U}_{p_\theta}^2}{r} =$$

$$\frac{\bar{\alpha}}{\tau_m}\left(\bar{U}_{f_r} - \bar{U}_{p_r}\right) - \frac{1}{r}\frac{\partial}{\partial r}\left(r\bar{\alpha}\,\overline{u_{p_r}^2}\right) - \frac{\partial}{r\partial\theta}\left(\bar{\alpha}\,\overline{u_{p_r}u_{p_\theta}}\right) - \frac{\partial}{\partial z}\left(\bar{\alpha}\,\overline{u_{p_r}u_{p_z}}\right)$$

$$- \frac{1}{r}\frac{\partial}{\partial r}\left(2r\bar{U}_{p_r}\overline{\alpha' u_{p_r}}\right) - \frac{\partial}{r\partial\theta}\left(\bar{U}_{p_r}\overline{\alpha' u_{p_\theta}} + \bar{U}_{p_\theta}\overline{\alpha' u_{p_r}}\right)$$

$$- \frac{\partial}{\partial z}\left(\bar{U}_{p_r}\overline{\alpha' u_{p_z}} + \bar{U}_{p_z}\overline{\alpha' u_{p_r}}\right) + \bar{\alpha}\,\frac{\overline{u_{p_\theta}^2}}{r} + 2\bar{U}_{p_\theta}\frac{\overline{\alpha' u_{p_\theta}}}{r} \qquad (I.18)$$

$$\theta: \quad \frac{1}{r}\frac{\partial}{\partial r}\left(r\bar{\alpha}\,\bar{U}_{p_r}\bar{U}_{p_\theta}\right) + \frac{1}{r}\frac{\partial}{\partial\theta}\left(\bar{\alpha}\,\bar{U}^2_{p_\theta}\right) + \frac{\partial}{\partial z}\left(\bar{\alpha}\,\bar{U}_{p_\theta}\bar{U}_{p_z}\right) + \frac{\bar{\alpha}}{r}\bar{U}_{p_r}\bar{U}_{p_\theta} =$$

$$\frac{\bar{\alpha}}{\tau_m}\left(\bar{U}_{f_\theta}-\bar{U}_{p_\theta}\right) - \frac{1}{r}\frac{\partial}{\partial r}\left(r\bar{\alpha}\,\overline{u_{p_r}u_{p_\theta}}\right) - \frac{\partial}{r\partial\theta}\left(\bar{\alpha}\,\overline{u^2_{p_\theta}}\right) - \frac{\partial}{\partial z}\left(\bar{\alpha}\,\overline{u_{p_\theta}u_{p_z}}\right)$$

$$- \frac{1}{r}\frac{\partial}{\partial r}\left(r\bar{U}_{p_r}\overline{\alpha' u_{p_\theta}} + r\bar{U}_{p_\theta}\overline{\alpha' u_{p_r}}\right) - \frac{\partial}{r\partial\theta}\left(2\bar{U}_{p_\theta}\overline{\alpha' u_{p_\theta}}\right)$$

$$- \frac{\partial}{\partial z}\left(\bar{U}_{p_\theta}\overline{\alpha' u_{p_z}} + \bar{U}_{p_z}\overline{\alpha' u_{p_\theta}}\right) - \frac{\bar{\alpha}}{r}\overline{u_{p_r}u_{p_\theta}} - \frac{\bar{U}_{p_r}}{r}\overline{\alpha' u_{p_\theta}} - \frac{\bar{U}_{p_\theta}}{r}\overline{\alpha' u_{p_r}} \tag{I.19}$$

$$z: \quad \frac{1}{r}\frac{\partial}{\partial r}\left(r\bar{\alpha}\,\bar{U}_{p_r}\bar{U}_{p_z}\right) + \frac{1}{r}\frac{\partial}{\partial\theta}\left(\bar{\alpha}\,\bar{U}_{p_\theta}\bar{U}_{p_z}\right) + \frac{\partial}{\partial z}\left(\bar{\alpha}\,\bar{U}^2_{p_z}\right) =$$

$$\frac{\bar{\alpha}}{\tau_m}\left(\bar{U}_{f_z}-\bar{U}_{p_z}\right) - \frac{1}{r}\frac{\partial}{\partial r}\left(r\bar{\alpha}\,\overline{u_{p_r}u_{p_z}}\right) - \frac{\partial}{r\partial\theta}\left(\bar{\alpha}\,\overline{u_{p_\theta}u_{p_z}}\right) - \frac{\partial}{\partial z}\left(\bar{\alpha}\,\overline{u^2_{p_z}}\right)$$

$$- \frac{1}{r}\frac{\partial}{\partial r}\left(r\bar{U}_{p_r}\overline{\alpha' u_{p_z}} + r\bar{U}_{p_z}\overline{\alpha' u_{p_r}}\right) - \frac{\partial}{r\partial\theta}\left(\bar{U}_{p_\theta}\overline{\alpha' u_{p_z}} + \bar{U}_{p_z}\overline{\alpha' u_{p_\theta}}\right)$$

$$- \frac{\partial}{\partial z}\left(2\bar{U}_{p_\theta}\overline{\alpha' u_{p_z}}\right) \tag{I.20}$$

the Reynolds stresses are:

$$- \overline{u_{p_r}^2} = \nu_{t_p} \left(2 \frac{\partial \overline{U}_{p_r}}{\partial r} \right) - \frac{2}{3} \left(k_p + \nu_{t_p} \nabla \cdot \overline{U}_p \right)$$

$$- \overline{u_{p_\theta}^2} = \nu_{t_p} \left(\frac{2 \partial \overline{U}_{p_\theta}}{r \partial \theta} + \frac{2 \overline{U}_{p_r}}{r} \right) - \frac{2}{3} \left(k_p + \nu_{t_p} \nabla \cdot \overline{U}_p \right)$$

$$- \overline{u_{p_z}^2} = \nu_{t_p} \left(2 \frac{\partial \overline{U}_{p_z}}{\partial z} \right) - \frac{2}{3} \left(k_p + \nu_{t_p} \nabla \cdot \overline{U}_p \right)$$

$$- \overline{u_{p_r} u_{p_\theta}} = \nu_{t_p} \left(\frac{\partial \overline{U}_{p_\theta}}{\partial r} + \frac{\partial \overline{U}_{p_r}}{r \partial \theta} \right) - \frac{\overline{U}_{p_\theta}}{r}$$

$$- \overline{u_{p_r} u_{p_z}} = \nu_{t_p} \left(\frac{\partial \overline{U}_{p_r}}{\partial z} + \frac{\partial \overline{U}_{p_z}}{\partial r} \right)$$

$$- \overline{u_{p_\theta} u_{p_z}} = \nu_{t_p} \left(\frac{\partial \overline{U}_{p_\theta}}{\partial z} + \frac{\partial \overline{U}_{p_z}}{r \partial \theta} \right)$$

and

$$\nabla \cdot \overline{U}_p = \frac{1}{r} \frac{\partial}{\partial r} \left(r \overline{U}_{p_r} \right) + \frac{1}{r} \left(\frac{\partial \overline{U}_{p_\theta}}{\partial \theta} + \frac{\partial \overline{U}_{p_z}}{\partial z} \right)$$

APPENDIX II

PREDICTION OF CURVED CHANNEL FLOW WITH AN EXTENDED k-ε MODEL OF TURBULENCE

ABSTRACT

Using algebraic approximations for the Reynolds stress equations a general expression has been derived for C_μ in $\nu_t = C_\mu k^2/\varepsilon$ which accounts simultaneously for the effects of streamline curvature and pressure-strain in the flow, with the latter including wall-induced effects on velocity fluctuations. The expression derived encompasses similar but more specific formulations proposed in the literature. The present formulation has been used in conjunction with a k-ε model of turbulence to predict developing, two-dimensional, curved channel flows. While, in general, predictions are in good agreement with experimental measurements of mildly and strongly curved flows, the model tends to overpredict the kinetic energy of turbulence in the inner-radius (convex) wall region. This is attributed to a breakdown of the assumption that $\overline{u_i u_j}/k$ is a constant in the derivation of the general expression for C_μ. The present formulation provides a degree of generality not previously available in two-equation modeling of turbulent flows.

CONTENTS

Abstract

Nomenclature

Introduction

- Three-Dimensional Motions in Curved Channel Flows
- The Prediction of Curved Channel Flows
- The Present Contributions

Governing Equations and Boundary Conditions

General Expression for C_μ

- The Reynolds Stress Equations
- The "f" Wall Function
- Derivation of the C_μ Function
- Limiting Expressions for the C_μ Function

The Numerical Scheme

Calculated Results and Discussion

Conclusions

Acknowledgements

References

Tables

Figure Captions

Figures

NOMENCLATURE

C_w	constant in equation (23)
C_μ	modified coefficient in equation (1) (includes curvature and pressure-strain effects)
$C_{\mu o}$	unmodified coefficient in equation (2)
D	channel width
D_{ij}	Reynolds stress diffusive transport term
f	$(\equiv f(\ell/y))$ wall-dampening function
G_T	$(\equiv 43(\frac{\theta}{R_o})^{1/2})$ Görtler parameter
k	kinetic energy of turbulence
ℓ	modified length scale of turbulence (includes curvature and pressure-strain effects)
ℓ_o	unmodified length scale of turbulence
m	experimental coefficient in equation (24)
P	mean pressure
P_{ij}	Reynolds stress production term
R_c	$(\equiv \frac{r_i + r_o}{2})$ channel mean radius of curvature
Re	$(\equiv DU_m/\nu)$ Reynolds number
R_o	concave wall radius of curvature (corresponds to r_o in a curved channel)
r	radial coordinate
r_i	channel inner-wall radius
r_o	channel outer-wall radius
U_m	maximum (streamwise) velocity
U_r	radial component of mean velocity
U_θ	streamwise component of mean velocity

$\overline{u_i u_j}$	components of Reynolds stress tensor
$\overline{u_i u_j u_k}$	triple velocity correlation
v_o	unmodified velocity scale of turbulence
y	distance along normal to a curved wall (into the flow)

Greek symbols

β	empirical constant in equation (3)
δ	$(\equiv \frac{U_\theta}{r} / \frac{\partial U_\theta}{\partial r})$ extra strain in equation (3)
δ_{ij}	Kronecker delta
ε	rate of dissipation of kinetic energy of turbulence
ε_{ij}	Reynolds stress viscous dissipation term
η	$(\equiv \frac{r - r_i}{r_o - r_i})$ normalized radial coordinate
θ	streamwise coordinate; also boundary layer momentum thickness
κ	von Karman universal constant
λ	spacing between Taylor-Görtler vortices
μ	laminar viscosity
μ_{eff}	$(\equiv \mu + \mu_t)$ effective viscosity
μ_t	turbulent viscosity
ν	laminar kinematic viscosity
ν_t	$(\equiv \frac{\mu_t}{\rho})$ turbulent kinematic viscosity
Π_{ij}	Reynolds stress pressure-strain redistribution term
ρ	density
σ_k	Prandtl number for kinetic energy of turbulence
σ_ε	Prandtl number for dissipation
τ_w	wall shear stress

INTRODUCTION

The importance of experimental measurements and theoretical predictions of turbulent flows over convex and concave surfaces and in curved channels is evidenced by the attention which these two topics have and continue to receive in relation to, for example, flow cooling and erosion of turbine blades and rocket nozzles, flows in compressors, turbomachinery, curved diffusers and channel passages. Cases of studies pertaining to flows over convex surfaces are given in [1-7] while similar examples pertaining to flows over concave surfaces are available in [4-7]. Curved channel studies have been reported in [7-16].

In an extensive review of the subject Bradshaw [19] evidences the sensitivity of turbulent flow characteristics to even small amounts of mean streamline curvature. Thus, for example, in the early study by Kreith [20] and in subsequent investigations by Thomann [21] and Mayle et al. [22] it has been shown that the heat flux through the concave wall of a curved channel can be up to 33 percent larger, and through the convex wall 15 percent smaller, relative to that through the walls of a straight channel. A similar experimental heat transfer study by Brinich and Graham [13] (not entirely free of side-wall-driven secondary motion) confirms this result and, in addition, shows that while friction on the inner curved wall of a channel can fall below the values for a straight channel, friction measurements on the outer curved wall yield increases of about 50 percent.

Three-Dimensional Motions in Curved Channel Flows

Hunt and Joubert [14] make a distinction between two types of curved channel flows: a) 'shear-dominated' flows with small curvature effects, ($R_c/D > 20$, approximately), and b) 'inertia-dominated' flows with large curvature effects ($R_c/D < 20$, approximately). In their study the channel mean radius of curvature was large relative to the channel width ($R_c/D = 100$).

Measurements at three Reynolds numbers corresponding to $3 \cdot 10^4$, $6 \cdot 10^4$ and $1.3 \cdot 10^5$ respectively, indicated small variations of about 2% in the longitudinal mean velocity component. Detailed characterization of this velocity component for $Re = 6 \cdot 10^4$ revealed a Taylor-Görtler vortex pattern [23-25] in the central flow region.

The cellular structure found by Hunt and Joubert has been observed in other curved channel flows, both in laminar [4,17,26] and turbulent regime [4,9,18], and in boundary layers developing on concave walls [4,11,25,27]. The onset and subsequent amplification of longitudinal vortices is characterized by the Görtler parameter G_T. Tani [4] shows that for $G_T \leq 0.35$ longitudinal vortices will be dampended in turbulent flow, while for values $G_T \geq 0.35$ amplification depends on the value of the vortex spacing parameter $\lambda\ \theta$ and the curvature parameter $\lambda\ R_c$.

Although not reported by the authors there is evidence in the study by Eskinazi and Yeh [8] ($R_c/D = 9.5$) supporting the notion that their flow contained Taylor-Görtler vortices. As in [14] measurements of shear stress across the channel show good agreement with theoretical prediction in the inner-radius flow region. However, the data for the outer-radius flow region are in disagreement with the distribution expected from the wall shear measurements and, as pointed out in [14], is most likely an indication of the existence of a weak secondary flow.

Ellis and Joubert [9] specifically remark on having observed Taylor-Görtler vortices for a radius ratio $R_c/D = 30$ but not for $R_c/D = 6$. Similarly, Crane and Winoto [18] observed a collapse of these organized structures for $Re \geq 16000$. These findings contradict expectations based on stability considerations and suggest that turbulence diffusion and pressure redistribution in the flow near the outer-radius wall of a strongly curved channel may be responsible for

'smearing out' three-dimensional time averaged structures which otherwise would be observed. The net effect of the structures, then, can be looked upon as contributing to the overall process of turbulent mixing in the outer-radius wall region of the flow.

The Prediction of Curved Channel Flows

Although concavely curved flows are prone to three-dimensional instabilities, for purposes of numerical computation they are commonly presumed to be two-dimensional in their mean structure. Concave wall boundary layer development predictions of longitudinal velocity in [7] based on this assumption show good agreement with experimental measurements. However, similar calculations for friction factors [6] and turbulent shear stress [11] seriously underpredict the values of these parameters in the concave wall flow region. Likewise, while the fully developed curved channel longitudinal velocity predictions of [7] are in good agreement with experimental measurements of [9] for $R_c/D = 6$ over most of the channel width, near the concave wall velocity is underpredicted by approximately 9%. A similar discrepancy does not arise at the inner-radius wall of this flow. One might attribute the above discrepancies to three-dimensional Taylor-Görtler vortices as, for example, suggested in [11]. However, it also seems reasonable to suspect that the influence of streamline curvature and/or wall effects on turbulent mixing may have been underestimated at the concave walls. That, in fact, higher levels of turbulent diffusion should arise than were actually predicted by the models employed.

The Present Contribution

It is argued in, for example, [2,6] that only turbulence modeling approaches based on the calculation of Reynolds stresses directly from their transport

equations can accurately account for streamline curvature, pressure-strain and wall pressure fluctuations in curved channel flows. Simpler approaches such as in [7], based on a two-equation (k-ε) model of turbulence, appear to require an empirical modeling of curvature effects in the equation for dissipation of kinetic energy of turbulence and the corresponding definition of an additional model constant which must be optimized numerically. Even simpler approaches based on the mixing-length concept, such as in [10], are seriously limited by the need to prescribe different mixing-length variations for differently curved flows.

The present work shows how the k-ε model of turbulence can be rigorously extended to predict developing curved channel flows by making C_μ in the expression for turbulent viscosity:

$$\mu_t/\rho = C_\mu \underbrace{(k^{3/2}/\varepsilon)}_{\ell_o} \underbrace{k^{1/2}}_{v_o} \tag{1}$$

an appropriate function of streamline curvature accounting for pressure-strain and wall-induced pressure fluctuation effects. In Eq. (1) the symbols ℓ_o and v_o denote characteristic length and velocity scales of turbulence respectively, and are determined from transport equations for k and ε. The essence of the approach pursued in this study is then, that the product $C_\mu \ell_o$ in Eq. (1) should yield a modified length scale of turbulence (ℓ) which reflects the direct influence of streamline curvature and pressure-strain in the flow. Calling $C_{\mu o}$ the value of C_μ in the absence of these effects it is clear that:

$$\ell = (C_\mu / C_{\mu o})\, \ell_o \tag{2}$$

If the local-equilibrium approximation is made it can be shown [28] that $C_{\mu o} = 0.12$. The recommended experimental value is $C_{\mu o} = 0.09$.

It has been argued by Wilcox and Chambers [1] and by So [15] that it is not ℓ_o but v_o in Eq. (1) which should be modified for the influence of curvature effects. Their arguments are based on the observation that the transport equation for k does not manifest an explicit dependence on Coriolis and centrifugal accelerations and that, as a consequence, $v_o \equiv k^{1/2}$ misrepresents the turbulence velocity scale. The study by So [15], for example, is based entirely on the assumption that the turbulence length scale is unaffected by streamline curvature. However, there is ample experimental evidence in the work by Eskinazi and Yeh [8] showing that both the microscale and the integral scale of turbulence are increased at the concave wall and decreased at the convex wall of curved channel flow. More recently, Prabhu and Sundarasiva Rao [16] have shown that the mean inclination of large scale structures in curved channel flow also depends strongly on curvature. The essence of their finding is that large eddies are 'flattened' more in the convex wall region of a curved channel than in the concave wall region.

For models based on the notion of a turbulent viscosity as defined by Eq. (1) it would seem to be immaterial which of the two scales (ℓ_o or v_o) is modified to include the influence of curvature (and related) effects. However, because it will be consistent with subsequent modifications to be made to the turbulence model, it will be the length scale which is modified in this work. This approach is consistent with that proposed by Bradshaw [19] on heuristic grounds for mildly curved flow, and parallels to some extent various ideas set forth in the studies of Gibson [2], Irwin and Arnot Smith [6], So [15], Ljuboja and Rodi [29] and Leschziner and Rodi [30]*. The general expression

*Reference [30] came to our attention after the present study was completed.

provided here for C_μ includes as subsets the more specific expressions derived in [28-30] and yields as a special limiting case Bradshaw's proposal [17]:

$$\ell = \left(1 \pm \beta \frac{U_\theta/r}{\partial U_\theta/\partial r}\right) \ell_o \tag{3}$$

for the turbulence length scale in mildly curved channel flows. In Eq. (3) β is an empirical constant of order 10, r is the radial coordinate direction (transverse to the flow) and U_θ is the local value of the streamwise component of mean velocity along a streamline of curvature radius r.

The modified form of the k-ε model provided here, with its general formulation for C_μ, offers a compromise between the potentially more accurate but computationally more costly Reynolds stress model closures and the simpler but considerably more restrictive mixing-length calculation approaches. In this study, attention is fixed principally on flows in channels with relatively strong curvature ($R_c/D \leq 20$) in which inertial effects are dominant. However, the extended form of the model has also been applied successfully to channel flows with mild curvature.

GOVERNING EQUATIONS AND BOUNDARY CONDITIONS

Continuity and momentum equations governing steady, two-dimensional, turbulent, incompressible, developing curved channel flow in cylindrical coordinates (Fig. 1) are given by:

Continuity

$$\frac{\partial U_r}{\partial r} + \frac{1}{r}\frac{\partial U_\theta}{\partial \theta} + \frac{U_r}{r} = 0 \tag{4}$$

r-Momentum

$$\rho\left[U_r \frac{\partial U_r}{\partial r} + \frac{U_\theta}{r}\frac{\partial U_r}{\partial \theta} - \frac{U_\theta^2}{r}\right] = -\frac{\partial P}{\partial r} + \frac{1}{r}\frac{\partial}{\partial r}\left(\mu_{eff}\, r \frac{\partial U_r}{\partial r}\right) + \frac{1}{r}\frac{\partial}{\partial \theta}\left(\mu_{eff}\frac{1}{r}\frac{\partial U_r}{\partial \theta}\right) - \mu_{eff}\frac{U_r}{r^2} - \mu_{eff}\frac{2}{r^2}\frac{\partial U_\theta}{\partial \theta} + S_r \tag{5}$$

θ-Momentum

$$\rho\left[U_r \frac{\partial U_\theta}{\partial r} + \frac{U_\theta}{r}\frac{\partial U_\theta}{\partial \theta} + \frac{U_r U_\theta}{r}\right] = -\frac{1}{r}\frac{\partial P}{\partial \theta} + \frac{1}{r}\frac{\partial}{\partial r}\left(\mu_{eff}\, r \frac{\partial U_\theta}{\partial r}\right) + \frac{1}{r}\frac{\partial}{\partial \theta}\left(\frac{\mu_{eff}}{r}\frac{\partial U_\theta}{\partial \theta}\right) - \mu_{eff}\frac{U_\theta}{r^2} + \mu_{eff}\frac{2}{r^2}\frac{\partial U_r}{\partial \theta} + S_\theta \tag{6}$$

In the above equations the Reynolds stresses have been modeled according to the Boussinesq assumption which relates the stresses to velocity gradients through a turbulent viscosity. The terms S_r and S_θ in equations (5) and (6) are given by:

$$S_r = \frac{1}{r}\frac{\partial}{\partial \theta}\left(\mu_t\, r \frac{\partial}{\partial r}\left(\frac{U_\theta}{r}\right)\right) + \frac{1}{r}\frac{\partial}{\partial r}\left(\mu_t\, r \frac{\partial U_r}{\partial r}\right) - \mu_t \frac{U_r}{r^2} \tag{7}$$

$$S_\theta = \frac{1}{r}\frac{\partial}{\partial\theta}\left(\mu_t\left(2\frac{U_r}{r} + \frac{1}{r}\frac{\partial U_\theta}{\partial\theta}\right)\right) + \frac{\partial}{\partial r}\left(\frac{\mu_t}{r}\left(\frac{\partial U_r}{\partial\theta} - U_\theta\right)\right) + \frac{\mu_t}{r}\left(\frac{\partial U_\theta}{\partial r} - \frac{U_\theta}{r}\right) \qquad (8)$$

In order to solve for the spatial variation of μ_t, transport equations are required for k and ε. Following the modeling approach outlined in [31] (based on the earlier work of [32,33]) but restricted here to two-dimensional cylindrical coordinates yields:

Kinetic energy of turbulence, (k)

$$\rho\left[U_r\frac{\partial k}{\partial r} + \frac{U_\theta}{r}\frac{\partial k}{\partial\theta}\right] = \frac{1}{r}\frac{\partial}{\partial r}\left(\frac{\mu_{eff}}{\sigma_k} r \frac{\partial k}{\partial r}\right) + \frac{1}{r^2}\frac{\partial}{\partial\theta}\left(\frac{\mu_{eff}}{\sigma_k}\frac{\partial k}{\partial\theta}\right) + G - \rho\varepsilon \qquad (9)$$

Dissipation of kinetic energy of turbulence, (ε)

$$\rho\left[U_r\frac{\partial \varepsilon}{\partial r} + \frac{U_\theta}{r}\frac{\partial \varepsilon}{\partial\theta}\right] = \frac{1}{r}\frac{\partial}{\partial r}\left(\frac{\mu_{eff}}{\sigma_\varepsilon} r \frac{\partial \varepsilon}{\partial r}\right) + \frac{1}{r^2}\frac{\partial}{\partial\theta}\left(\frac{\mu_{eff}}{\sigma_\varepsilon}\frac{\partial \varepsilon}{\partial\theta}\right) + C_{\varepsilon 1}\frac{\varepsilon}{k} G - C_{\varepsilon 2}\rho\frac{\varepsilon^2}{k} \qquad (10)$$

with the production term "G" given by:

$$G = \mu_t\left\{2\left[\left(\frac{\partial U_r}{\partial r}\right)^2 + \left(\frac{1}{r}\frac{\partial U_\theta}{\partial\theta}\right)^2 - \frac{U_\theta}{r}\left(\frac{1}{r}\frac{\partial U_r}{\partial\theta} + \frac{\partial U_\theta}{\partial r}\right) + \frac{U_r}{r}\left(\frac{U_r}{r} + \frac{2}{r}\frac{\partial U_\theta}{\partial\theta}\right) + \frac{1}{r}\frac{\partial U_r}{\partial\theta}\frac{\partial U_\theta}{\partial r}\right] + \left(\frac{U_\theta}{r}\right)^2 + \left(\frac{\partial U_\theta}{\partial r}\right)^2 + \left(\frac{1}{r}\frac{\partial U_r}{\partial\theta}\right)^2\right\} \qquad (11)$$

Values of the constants in the above equations were set in accordance with

the recommendations of [33]: $C_{\varepsilon 1} = 1.44$, $C_{\varepsilon 2} = 1.92$ and $\sigma_k = 1.0$. However, the value of σ_ε (customarily fixed to 1.3) was allowed to vary with radial location as described further below.

In order to solve Eqs. (4-6,9 and 10) the boundary conditions summarized in Table 1 were used. The region between a curved wall and the node P closest to that wall was bridged by specifying the wall shear stress (τ_w) from the standard logarithmic velocity profile. Assuming local-equilibrium of the flow in near-wall regions, the law of the wall relation yields:

$$\tau_w = \tau_P = \frac{\rho\, C_{\mu o}^{1/4}\, k_P^{1/2}\, [U_\theta]_P}{A\, \ell n\left[\dfrac{y_P\, C_{\mu o}^{1/4}\, k_P^{1/2}}{\nu}\right] + B} \qquad (12)$$

where subscript P denotes the grid node position nearest to the wall, y is the distance from the wall and τ_w is the wall shear stress. Values of the law of the wall constants were set to A = 2.39 and B = 5.45. It should be mentioned that an attempt to include curvature effects in the law of the wall using an equivalent form of Eq. (8) in the paper by Meroney and Bradshaw [11] did not yield a significant improvement in the calculations. The simpler logarithmic relation given by Eq. (12) above was adhered to.

The wall value of kinetic energy of turbulence, k_P, was found from its standard transport equation with the flux from the wall set equal to zero and the production term modified to include the wall shear stress as given by Eq. (12). The wall value of dissipation of kinetic energy, ε_P, was initially determined by requiring that the turbulence length scale vary linearly with distance from the wall. Substituting $(\partial U_\theta/\partial y)_P$ from the law of the wall into the simplified (near-wall region) turbulent kinetic

energy balance yields:

$$\varepsilon_p = \frac{C_{\mu o}^{3/4}\, k_p^{3/2}}{\ell_o} \tag{13}$$

where the turbulence length scale is given by $\ell_o = \kappa y_p$. Following Bradshaw [17], the influence of extra-strain curvature effects on the magnitude of the turbulence length scale near curved walls can be modeled according to Eq. (3) for regions of the flow in which $\delta \equiv |(U_\theta/r)/(\partial U_\theta/\partial r)| \leq 0.05$. An expression for dissipation at the near-wall node P which includes the influence of streamline curvature effects is:

$$\varepsilon_p = \frac{C_{\mu o}^{3/4}\, k_p^{3/2}}{\kappa\, y_p\, (1 \pm \beta \xi_p)} \tag{14}$$

Following Launder and Spalding [33], the equation for dissipation of kinetic energy in the near wall region simplifies to:

$$0 = \frac{1}{r}\frac{\partial}{\partial r}\left(\frac{\nu_t}{\sigma_\varepsilon}\, r\, \frac{\partial \varepsilon}{\partial r}\right) + C_{\varepsilon 1}\frac{\varepsilon}{k}\, P - C_{\varepsilon 2}\frac{\varepsilon^2}{k} \tag{15}$$

Assuming local-equilibrium in the flow and recalling Eqs. (1) and (15) the above expression may be rewritten:

$$0 = \frac{1}{r}\frac{\partial}{\partial r}\left(\frac{C_{\mu o}\, k^2/\varepsilon}{\sigma_\varepsilon}\, r\, \frac{\partial \varepsilon}{\partial r}\right) + (C_{\varepsilon 1} - C_{\varepsilon 2})\, C_{\mu o}^{3/2}\left(\frac{k}{\kappa^{\dagger} y}\right)^2 \tag{16}$$

where $\kappa' = \kappa(1 \pm \beta\delta_p)$. Further assuming that $\frac{\partial k}{\partial r} = 0$ in the near wall region [33] it may be shown that Eq. (16) simplifies to the following curvature-modified expression for σ_ε:

$$\sigma_\varepsilon = \frac{\kappa'^2}{(C_{\varepsilon 2} - C_{\varepsilon 1})\, C_{\mu o}^{1/2}} \tag{17}$$

In the standard form of the k-ε model of turbulence the value of σ_ε is fixed to the wall value of 1.3 throughout the flow [33]. In this study σ_ε at any radial location was linearly interpolated from the near-wall grid node values determined by means of Eq. (17) at the concave and convex walls respectively.

GENERAL EXPRESSION FOR C_μ

Prior to outlining the derivation of the general form of the C_μ coefficient, it is instructive to justify by means of a simple example the advantages of an improved modeling of this coefficient. Combination of Eqs. (1-3) yields the expression:

$$\mu_t/\rho = C_{\mu o}\, \ell_o\, (1 \pm \beta\, \delta)\, v_o \tag{18}$$

This equation is a limiting form of the more general relation sought in this study. While Eq. (18) accounts for the influence of mild curvature effects on the turbulence length scale ℓ_o through the curvature parameter $(1 \pm \beta\, \delta)$, a more general relationship is desirable in which arbitrary streamline curvature, pressure-strain and wall pressure corrections are simultaneously included. The purpose of this section is to outline the derivation of this more general coefficient, which is obtained by substitution of an expression for the turbulent shear stress, determined from an algebraic-stress model, into a Boussinesq approximation for the shear stress in which the turbulent viscosity is given by Eq. (1).

The Reynolds Stress Equations

The starting point for the present analysis is the high-Reynolds number form of the $\overline{u_i u_j}$ transport equation given in [29]. In three-dimensional Cartesian coordinate notation* and neglecting molecular diffusion this equation is:

*The model equations were formulated and used in cylindrical coordinates. Cartesian notation is used here for convenience.

$$U_k \frac{\partial \overline{u_i u_j}}{\partial x_k} = \underbrace{-\left\{\overline{u_j u_k}\frac{\partial U_i}{\partial x_k} + \overline{u_i u_k}\frac{\partial U_j}{\partial x_k}\right\}}_{P_{ij}} \underbrace{- 2\nu \overline{\frac{\partial u_i}{\partial x_k}\frac{\partial u_j}{\partial x_k}}}_{\varepsilon_{ij}}$$

$$\underbrace{+ \overline{\frac{p}{\rho}\left(\frac{\partial u_i}{\partial x_j} + \frac{\partial u_j}{\partial x_i}\right)}}_{\Pi_{ij}} \underbrace{- \frac{\partial}{\partial x_k}\left\{\overline{u_i u_j u_k} + \overline{\frac{p}{\rho}\left(\delta_{jk} u_i + \delta_{ik} u_j\right)}\right\}}_{D_{ij}} \tag{19}$$

In the above equation P_{ij} represents the production of $\overline{u_i u_j}$ and requires no approximation. Viscous dissipation (ε_{ij}) and contributions to the pressure-strain term (Π_{ij}) were modeled as in [29]. The forms of these terms are:

$$\varepsilon_{ij} = \frac{2}{3}\varepsilon\,\delta_{ij} \quad \text{(isotropic dissipation)} \tag{20}$$

and

$$\Pi_{ij} = \Pi_{ij,1} + \Pi_{ij,2} + \Pi'_{ij,1} + \Pi'_{ij,2} \tag{21}$$

In Eq. (21) $\Pi_{ij,1}$ represents contributions to the pressure-strain arising from fluctuating velocities only, while $\Pi_{ij,2}$ accounts for the interaction between the mean strain and fluctuating velocities. The additional contributions $\Pi'_{ij,1}$ and $\Pi'_{ij,2}$ represent pressure-strain corrections due to the effect of walls on the level of turbulent fluctuations in the flow. The terms in Eq. (21) were approximated according to model 2 of [34]. A tabulated summary of their modeling and of the necessary model constants is given by Humphrey and Pourahmadi [35].

The diffusive transport of $\overline{u_i u_j}$ is attributed primarily to turbulent velocity fluctuations [34] for which the simple gradient diffusion hypothesis

of Daly and Harlow [36] yields:

$$-\overline{u_i u_j u_\ell} = C_s' \frac{k}{\varepsilon} \overline{u_\ell u_m} \frac{\partial \overline{u_i u_j}}{\partial x_m} \tag{22}$$

where C_s' is an empirically determined constant (not needed in this study).

The "f" Wall Function

In the approximations for $\Pi_{ij,1}'$ and $\Pi_{ij,2}'$ a wall function, $f(\ell/y)$, must be specified whose role it is to diminish the magnitude of the wall pressure correction to the total pressure-strain with increased distance from the wall (y). The form of the f function depends on the length scale ℓ of the energy-containing eddies and for straight channel flows is given by [34]:

$$f(\frac{\ell}{y}) \equiv f = \frac{k^{3/2}}{C_w \varepsilon} \left[\frac{1}{y} + \frac{1}{D - y}\right] \tag{23}$$

where D is the channel width. Eq. (23) reflects the fact that distance-weighted contributions to f at any point in the flow arise from both walls. In the expression, the constant C_w is chosen such that $f \to 1$ as $y \to 0$. Therefore, setting $\varepsilon = C_{\mu o}^{3/4} k^{3/2}/\kappa y$ (the inertial sublayer value) in Eq. (23) yields $C_w = \kappa/C_{\mu o}^{3/4}$.

For straight channel flows the function f is symmetrical with respect to the symmetry plane, where it possesses a minimum value. This is consistent with the notion that at the symmetry plane the walls of a straight channel should generate equivalent pressure-corrections to the pressure-strain terms. The same will not be the case for channel flows in which an asymmetric condition exists; for example, straight channel flows with one smooth wall

and one rough wall, and curved channel flows. In these cases the position of the minimum value of f in the flow will be shifted towards the wall contributing least to changes in the turbulence by wall pressure fluctuation effects; (i.e., the convex wall in a curved channel or the smooth wall in an asymmetrically roughened channel). In this work the location for the minimum in the f function has been assumed to coincide with the location of zero turbulent shear stress. This is consistent with the notion that the length scale of the energy-containing motion, which also transmits the pressure-fluctuations effects, should be smallest at the zero shear stress position; see, for example, the data in [8], and Eq. (30) and related discussion in [2]. In this way the flow is divided into two regions in either one of which the wall nearest to that region is the major source of wall-induced contributions to the pressure-strain correlation.

A general expression for f which accomodates both the symmetric and assymmetric conditions referred to above is:

$$f = \frac{k^{3/2}}{C_w \varepsilon}\left[\frac{1}{y} + \frac{(y/D)^m}{D - y}\right] \tag{24}$$

In Eq. (24) y is taken as the distance into the flow measured from the wall which induces the largest contributions to the wall-correction terms: i.e., the concave wall in a curved channel. The value of m can be determined exactly from experimental measurement as described in [35], where it is found that $m = 7.95$ for $R_c/D \leq 20$ and $m = 2.56$ for $R_c/D > 20$. For $m = 0$ Eq. (24) reduces to the straight channel result given by Eq. (23).

Derivation of the C_μ Function

Following Rodi [28], algebraic expressions for the Reynolds stresses are obtained from Eq. (19) by assuming that the ratio $\overline{u_i u_j}/k$ is constant throughout the flow field. Although inexact, this assumption allows convection minus diffusion of the Reynolds stresses to be expressed as a function of turbulent kinetic energy production (G) and its rate of dissipation (ε):

$$U_\ell \frac{\partial \overline{u_i u_j}}{\partial x_\ell} - D_{ij} = \frac{\overline{u_i u_j}}{k} [G - \varepsilon] \tag{25}$$

Substitution of Eq. (25) into Eq. (19) yields:

$$\frac{\overline{u_i u_j}}{k} [G - \varepsilon] = P_{ij} - \varepsilon_{ij} + \Pi_{ij} \tag{26}$$

from which algebraic relations for $\overline{u_i u_j}$ are obtained. The general form of C_μ is obtained by combining the algebraic expression for $\overline{u_i u_j}$ with Eq. (1) for μ_t in the Boussinesq approximation for $\overline{u_\theta u_r}$. Because the derivation in cylindrical coordinates is lengthy, the reader is referred to Humphrey and Pourahmadi [35] for details. The final result may be cast into compact notation form and is given by:

$$C_\mu^{1/2} = 2\, Q^{1/2} \cos\left[\frac{1}{3}\cos^{-1}(R\, Q^{-2/3})\right] - \frac{S}{3} \tag{27}$$

where Q, R and S are complex algebraic expressions available in [35] which are functions of velocity gradients, the wall function f, the ratio G/ε and the turbulence model constants.

Limiting Expressions for the C_μ Function

The general expression for C_μ given by Eq. (27) has several interesting limiting forms attesting to its validity. These have been obtained in [35] and correspond to the following cases: a) Variation of C_μ for flow in the presence of a flat wall [29]; b) Variation of C_μ for flow with variable G/ε [28]; c) Variation of C_μ for flow with streamline curvature [30]; and, d) Variation of C_μ for flow with small δ in the presence of a curved wall.

Case d yields:

$$C_\mu = 0.056\ [1 - 12.17\delta + O(\delta^2)] \tag{28}$$

Comparing Eq. (28) with Eq. (2) and recalling Eq. (3) shows that $C_{\mu o} = 0.056$ and $\beta = 12.17$. This value for β is in good agreement with the values recommended in the literature; for example, Eide and Johnston [37] suggest $\beta = 12$ for both concave and convex walls, while Bradshaw [19] recommends $\beta = 9$ at a concave wall and $\beta = 14$ at a convex wall. Similarly, the value for $C_{\mu o}$ obtained here falls in the range of values calculated for turbulent wall jets in [29] where the authors find that $C_\mu = 0.05$ in the near wall region of their jet flow.

THE NUMERICAL SCHEME

It is required to solve the transport equations (4,6,9 and 10) in conjunction with the boundary conditions summarized in Table 1. Finite difference equations are obtained by volume integration of the transport equations over control volumes or "cells" into which the flow domain is discretized. Details concerning the method for deriving the difference equations and the inclusion of boundary conditions are provided in, for example, [38,39], while an exposition and thorough discussion of the philosophy underlying the calculation approach followed here is available in [40].

The velocity components, pressure, kinetic energy of turbulence and dissipation of kinetic energy of turbulence are the dependent variables calculated on staggered, interconnected grids, each of which is associated with a specific variable (all scalar quantities share the same grid node locations). The general form of the finite difference expressions is given by:

$$\phi_p = \frac{\Sigma A_i \phi_i + S_o}{\Sigma A_i + S_p} \qquad (29)$$

where ϕ_p represents any one of the dependent variables solved for at the grid node 'P'. The A_i coefficients are determined at the respective cell surfaces and they represent combined contributions to balance of ϕ arising from diffusion and convection. The terms S_o and S_p represent other contributions arising from sources (or sinks) in the flow [38].

The numerical procedure used to solve the finite difference equations was the Imperial College "TEACH-2E" code [41]. Together with appropriately

differenced boundary conditions, elliptic forms* of the equations are solved by means of a cyclic series of predictor-corrector operations involving the use of the tridiagonal matrix algorithm applied on a line-by-line basis to the calculation domain. From an initial or intermediate value of the pressure field an intermediate velocity field is found. By means of the SIMPLE [40] algorithm, pressure corrections are determined by bringing the intermediate velocity field into conformity with continuity. After corrections to the pressure and velocity fields are applied, the transport equations for kinetic energy of turbulence and its rate of dissipation are solved. Within each iteration various sweeps are made of the entire calculation domain along the main flow direction. The above steps are repeated until a pre-established convergence criterion is satisfied; usually, that the largest of the normalized residuals be less than $5 \ 10^{-3}$.

All the numerical calculations were performed on a 20×40 grid, evenly spaced in the streamwise direction and unevenly spaced in the radial direction, after ascertaining that this degree of refinement was sufficiently accurate for the purposes of this study. The storage required on a CDC 7600 computer was 61 k_8 words, and a typical (converged) run time for 300 iterations (3 sweeps per variable) was 130-150 CPU seconds.

*In principle, for the flows calculated here, parabolic equations should suffice since there are no streamwise-reversed flow regions. However, parabolic procedures have been shown [42] to lead to poor estimates of the pressure fields in strongly curved duct flows and dictated the present choice of the elliptic scheme.

CALCULATED RESULTS AND DISCUSSION

In this section results are reported of two-dimensional numerical calculations performed using the extended turbulence model and the general expression for C_μ given by Eq. (27). The calculations cover both mildly and strongly curved channel flow configurations and include the straight channel flow data of Laufer [43] as a limiting test case. Prior to presenting the calculated cases a discussion is in order regarding the dependence of C_μ on wall curvature and pressure-strain effects. Also, since it is assumed in the derivation of the general expression for C_μ that the ratio $\overline{u_i u_j}/k$ remains constant in the flow, the limitations of this assumption and its effect on the calculations should be assessed.

Figure 2 is a plot of measurements of $\overline{u_\theta u_r}/k$ for three channel flows ranging from strongly curved to straight. In [8] values of k were not provided but could be estimated from the data for $\overline{u_\theta^2}$ and $\overline{u_r^2}$ by assuming that $\overline{u_z^2} = \overline{u_\theta^2}$ in $k = \frac{1}{2}(\overline{u_\theta^2} + \overline{u_r^2} + \overline{u_z^2})$. The straight channel flow shows two regions, corresponding to $n \leq 0.20$ and $n \geq 0.80$ respectively, wherein $|\overline{u_\theta u_r}/k|$ is approximately constant. Similarly, in the inner-radius wall region the curved channel flows also show relatively constant values of this ratio for $n \leq 0.20$. By contrast, in the outer-radius wall region, the constancy of the ratio is extended (relative to the straight channel flow case) to values of $n \geq 0.60$. In the region $0.20 \leq n \leq 0.65$ the assumption of constant $\overline{u_i u_j}/k$ is obviously invalid and curtails the usefulness of the general expression for C_μ.

Figure 3 shows the variation of C_μ as a function of radial position in channels of different curvature. In general C_μ is seen to increase at both walls of a curved channel, at a rate inversely proportional to channel

curvature (defined earlier as R_c/D). At the inner-radius wall C_μ reaches a maximum value at a radial location dictated by the channel curvature. As of this location C_μ diminishes with increased distance from the inner-radius wall. For strong curvatures the general function for C_μ yielded unrealistic values of this parameter in the region $0.30 \leq n \leq 0.65$ due to the lack of constancy in the ratio $\overline{u_i u_j}/k$. However, calculations revealed an insensitivity of the numerical results towards the absolute value of C_μ in this flow region provided that it was contained within the range $0.045 \leq C_\mu \leq 0.140$. This insensitivity is explained, in part, by the small values of $\partial U_\theta/\partial r$ and the respectively counteracting curvature influences which arise in the core region of curved channel flow. In the present study C_μ was set to the value 0.09 in the region $0.30 \leq n \leq 0.65$.

Wall curvature and wall pressure fluctuations contribute jointly to the value of C_μ. In an effort to separate these two effects, and thereby establish their relative importance, two sets of C_μ profiles in Figure 3 ($R_c/D = 10, 20$) have been calculated with a symmetric distribution of the f function imposed ($m = 0$); equivalent to specifying a straight channel flow condition in so far as wall pressure-corrections are concerned, while retaining the direct influences of the respective wall curvatures on C_μ. Inspection of these profiles shows that curvature at the outer-radius wall acts to enhance C_μ while curvature at the inner-radius wall acts to suppress it. The inclusion of wall pressure-corrections in the pressure-strain ($m = 1.58$, $m = 7.94$) further increases C_μ at both walls, but at the inner-radius wall the direct influence of curvature effects ultimately overcomes the wall pressure contribution to C_μ causing a net decrease in its value with increasing distance from the inner-radius wall.

Plots of the f function, given in [35] for various curvature ratios, show decreasing values of f with increased distance from either channel wall, reflecting the decreased influence of wall-corrections to the turbulent flow. These plots also show that at a fixed radial location the f wall-function decreases strongly with increased curvature at the inner-radius wall, while it increases only slightly in the outer-radius wall region bounded by $0.85 \leq \eta \leq 1$. These observations are in agreement with the algebraic stress model predictions in [2] and illustrate the point that convex surfaces are considerably less effective in redistributing wall-pressure contributions to turbulent flows than are concave surfaces. Since C_μ can be shown to be inversely proportional to the f wall-function the above observations suggest that pressure fluctuations will contribute more strongly to C_μ at the inner-radius wall than at the outer-radius wall with increasing channel curvature. That this is the case is confirmed by comparing the relative increases between pairs of inner-radius wall C_μ profiles in Figure 3 (with the different f functions specified) for $R_c/D = 20$ and $R_c/D = 10$. By contrast, relative change in the C_μ profiles at the outer-radius wall are smaller and of comparable magnitude for both curvatures. This suggests that it is principally the direct influence of curvature effects which determines the shape of the C_μ profiles in the outer-radius flow region, with the magnitude of C_μ being changed only slightly by the wall-pressure correction term. It should be noticed that the same cut-off values set for C_μ apply to the f wall-function since in the present model the effects of the latter parameter appear exclusively through the former.

Prior to conducting curved channel flow predictions, the calculation scheme and the turbulence model in its extended form, including the general formulation for C_μ, were tested by reference to the straight channel turbulent

flow measurements of Laufer [43]. The law of the wall constants used in Eq. (12) were those specifically recommended by Laufer: A = 3.0 and B = 5.5. Figure 4 shows predictions using a standard (C_μ = 0.09; f = 0) k-ε model of turbulence with predictions using the extended version of the model offered here. Also included in the figure are predictions based on the full Reynolds stress closure approach proposed by Hanjalic and Launder [44] (the profiles shown were taken from Hanjalic [45]). While all three models yield excellent agreement between calculated and measured velocity profiles, the figure shows that the inclusion of wall pressure-corrections in the general formulation for C_μ leads to an improved prediction of turbulent kinetic energy near the wall. In fact, it is surprising to find that across the whole channel, better predictions of k are given by both the two-equation models than by the Reynolds stress closure.

Predictions of flow velocity, friction factor and kinetic energy of turbulence are presented in Figures 5 to 9 for mildly and strongly curved channel flows. Calculations of mean velocity corresponding to the mildly curved (R_c/D = 100) channel geometry of Hunt and Joubert [14] provided in Figure 5 show very good agreement with the measurements. Minor differences are displayed between measurements and calculations at $R_c\theta/D$ = 36 and 60 in the inner and outer-radius wall regions. These are attributed to the presence of a weak Taylor-Görtler type secondary motion which was observed in the measurements. Mean velocity calculations for the strongly curved channel configuration of Eskinazi and Yeh [8] (R_c/D = 9.5) are plotted in Figure 6. For this case the discrepancies are larger between measurements and calculations near the outer-radius wall. However, differences are reduced slightly when the more general expression for C_μ given by Eq. (27) is

employed. As before the discrepancies are attributed to the presence of Taylor-Görtler vortices, evidenced in the shear stress measurements of this flow [8].

Measurements of the friction coefficient from the study of Honami et al. [10] are compared in Figure 7 with calculations conducted at three levels of turbulence model refinement. The best results correspond to the extended k-ε model with the general C_μ formulation and in which length-scale curvature adjustments are incorporated in the calculation of dissipation and dissipation Prandtl number near the walls. While the agreement between measurements and calculations with the extended model is very good at the inner-radius wall, it is at the outer-wall where inclusion of the above effects produces the largest improvements. Calculations of the friction coefficient for the flow of Eskinazi and Yeh also yielded similar levels of agreement when using the extended version of the k-ε model offered here.

Calculations of the kinetic energy of turbulence for the channel flow of Eskinazi and Yeh are presented in Figure 8. The profiles showing the best overall agreement with the measurements correspond to the extended model, although differences between models are seen to decrease towards the center of the flow. Calculations in the outer-radius wall region are in better agreement with the measurements than at the inner-wall. When contrasted with similar predictions in [35] of kinetic energy of turbulence for the mildly curved flow of Hunt and Joubert, the results suggest that the magnitude of the discrepancy in the inner-radius wall region is inversely proportional to the curvature ratio (R_c/D); for the strongly curved flow of Eskinazi and Yeh the level of k is overpredicted by between 30 to 50% while for the flow of Hunt and Joubert an overprediction of less than 20% is observed.

Calculations corresponding to the mean velocity measurements of Ellis and Joubert [9] are shown in Figure 9 where they are compared with calculations by Launder et al [7] using a k-ε model of turbulence developed along the lines of Jones and Launder [46]. In the model of Launder et al curvature effects on the length scale of the flow are included via an empirical modification to the dissipation equation. This consists in making the coefficient $C_{\varepsilon 2}$ in Eq. (10) a function of a turbulent Richardson number. The approach has been criticized by Gibson [2], and by Rodi [47] who argues that the appropriate place to make such a modification is in the production term of the dissipation equation. Effectively, it is the latter approach which has been developed in this study. The predictions of Launder et al show slightly better agreement with the measurements at the outer-radius wall, but over a large portion of the inner-wall region the present model yields better results. It is difficult to decide on the basis of this comparison which model is more accurate for the prediction of curved channel flows in general. However, in view of the points raised by Gibson [2] and by Rodi [47], and given the fact that the model of Launder et al requires an additional constant (and its numerical optimization), it would appear that the model offered here is of a more general nature.

CONCLUSIONS

By consideration of Reynolds stress equations in algebraically modeled form a general expression has been derived for the coefficient C_μ in the expression for turbulent viscosity $\mu_t/\rho = C_\mu k^2/\varepsilon$. The generalized form of this coefficient includes streamline curvature and pressure-strain effects (including wall corrections) and, hence, their influence on the turbulent length scale ($k^{3/2}/\varepsilon$) in the flow. The expression derived has been shown to reduce to limiting forms of less general formulations obtained in other works. One of these forms corresponds to the proposal by Bradshaw, Eq. (3) in the text, and yields values of the constants $\beta = 12.17$ and $C_{\mu o} = 0.056$ which are in good agreement with values established in the literature.

Predictions of developing two-dimensional curved channel flow have been conducted by incorporating the general expression for C_μ into a k-ε model of turbulence modified to include the direct influence of curvature effects on the length scale in near-wall regions of the flow. In general, agreement between the measurements and calculations is good. The largest discrepancies observed in the calculations of mean velocity arise at the outer-radius wall and are attributed to the existence of cross-stream motions (Taylor-Görtler vortices) in the experiments. The present turbulence model consistently over-predicts the kinetic energy of turbulence in the inner-radius wall region of curved channel flow. The degree of overprediction appears to be inversely proportional to mean channel curvature (R_c/D). The overprediction is attributed to the failing of the model to accomodate fully the stabilizing influences of convex curvature on turbulent flow; due to the breakdown of the assumption underlying the formulation, that $\overline{u_i u_j}/k$ is a constant everywhere in the flow.

It is a noteworthy feature of the extended k-ε model presented here that no previously established model constants have been modified or "retuned" to

yield improved agreement between predictions and measurements. This includes the new parameter m appearing in the f wall-function which is determined exactly from experimental measurement as opposed to numerical optimization. In this sense, the present turbulence model provides a more general formulation than models based on the ad-hoc inclusion of a flux Richardson number in the equation for dissipation of kinetic energy of turbulence.

ACKNOWLEDGEMENTS

This study was made possible by funding received from the following agencies: Office of Naval Research, Contract Number N00014-80-C-0031; Division of Material Sciences, Office of Basic Energy Sciences, U.S. Department of Energy, Contract No. DE-AC03-76SF00098. We welcome the opportunity to express our appreciation to these two agencies for their support.

REFERENCES

1. Wilcox, D.C. and Chambers, T.L., "Streamline Curvature Effects on Turbulent Boundary Layers," AIAA Journal, Vol. 15, No. 4, 1977, pp. 574-580.

2. Gibson, M.M., "An Algebraic Stress and Heat-Flux Model for Turbulent Shear Flow with Streamline Curvature," International Journal of Heat and Mass Transfer, Vol. 21, 1978, pp. 1609-1617.

3. Simon, T.W. and Moffat, R.J., "Heat Transfer Through Turbulent Boundary Layers - The Effects of Introduction of and Recovery From Convex Curvature," Paper No. 79-WA/GT-10, Dec., 1979, Presented at the ASME Winter Annual Meeting, New York, N.Y.

4. Tani, I., "Production of Longitudinal Vortices in the Boundary Layer Along a Concave Wall," Journal of Geophysical Research, Vol. 67, No. 8, 1962, pp. 3075-3080.

5. Rotta, J.C., "Effects of Streamwise Wall Curvature on Compressible Turbulent Boundary Layers," The Physics of Fluids Supplement, 1967, S174-S180.

6. Irwin, H.P.A.H. and Smith, P. Arnot, "Prediction of the Effect of Streamline Curvature on Turbulence," The Physics of Fluids, Vol. 18, No. 6, 1975, pp. 624-630.

7. Launder, B.E., Priddin, C.H., and Sharma, B.I., "The Calculation of Turbulent Boundary Layers on Spinning and Curved Surfaces," Trans. ASME, Journal of Fluids Engineering, 1977, pp. 231-239.

8. Eskinazi, S., and Yeh, H., "An Investigation on Fully Developed Turbulent Flows in a Curved Channel," Journal of Aeronautical Sciences, 1956, pp. 23-34.

9. Ellis, L.B. and Joubert, P.N., "Turbulent Shear Flow in a Curved Duct," Journal of Fluid Mechanics, Vol. 62, Part 1, 1974, pp. 65-84.

10. Honami, S., Ariga, I., Abe, T. and Watanabe, I., "Investigation of Turbulent Flows in Curved Channels," Paper No. 75-FE-32, May 5-7, 1975, Presented at the ASME Joint Fluids Engineering and Lubrication Conference.

11. Meroney, R.N. and Bradshaw, P., "Turbulent Boundary-Layer Growth Over a Longitudinally Curved Surface," AIAA Journal, Vol. 13, No. 11, 1975, pp. 1446-1453.

12. Blottner, F.G., "Entry Flow in Straight and Curved Channels with Slender Channel Approximations," Trans. ASME, Journal of Fluids Engineering, Vol. 99, 1977, pp. 666-674.

13. Brinich, P.F. and Graham, R.W., "Flow and Heat Transfer in a Curved Channel," NASA TN D-8464, 1977.

14. Hunt, I.A. and Joubert, P.N., "Effects of Small Streamline Curvature on Turbulent Duct Flow," Journal of Fluid Mechanics, Vol. 91, Part 4, 1979, pp. 633-659.

15. So, R.M., "A Turbulence Velocity Scale for Curved Shear Flows," J. Fluid Mechanics, Vol. 70, Part 1, 1975, pp. 37-57.

16. Prabhu, A. and Sundarasiva Rao, B.N., "On the Large-Scale Structure in Turbulent Boundary Layers on Curved Surfaces," Paper presented at the Joint ASME/ASCE Mechanics Conference, University of Colorado, Boulder, Colorado, June 22-24, 1981.

17. Winoto, S.H. and Crane, R.I., "Vortex Structure in Laminar Boundary Layers on a Concave Wall," Int. J. Heat and Fluid Flow, 2, 221, 1980.

18. Crane, R.I. and Winoto, S.H., "Longitudinal Vortices in a Concave Surface Boundary Layer," Paper 9, AGARD Conf. Proc. 271 ('Turbulent Boundary Layers - Experiments, Theory and Modeling'), 1980.

19. Bradshaw, P., "Effects of Streamline Curvature on Turbulent Flow," AGARDograph No. 169, 1973.

20. Kreith, F., "The Influence of Curvature on Heat Transfer to Incompressible Fluids," Trans. ASME, Vol. 77, No. 11, 1955, pp. 1247-1256.

21. Thomann, H., "Effect of Streamwise Wall Curvature Heat Transfer in a Turbulent Boundary Layer," Journal of Fluid Mechanics, Vol. 33, Part 2, 1968, pp. 283-292.

22. Mayle, R.E., Blair, M.F. and Kopper, F.C., "Turbulent Boundary Layer Heat Transfer on Curved Surfaces," Journal of Heat Transfer, Vol. 101, No. 3, 1979, pp. 515-523.

23. Taylor, G.I., "Stability of Viscous Liquid Contained Between Two Rotating Cylinders," Philosophical Transactions of the Royal Society (London), Vol. 223, 1923, pp. 289-343.

24. Taylor, G.I., "Distribution of Velocity and Temperature Between Concentric Rotating Cylinders," Proceedings of the Royal Society of London, Series A, Vol. 151, 1935, pp. 494-512.

25. Görtler, H., "Über Eine Dreidimensionale Instabilität Laminarer Grenz-Schichten an Konkaven Wänden," Nachr. Ges. Wiss. Göttingen, Math.-phys. Kl., Vol. 2(1), 1940. Also available as NACA TM 1375, 1942.

26. Kelleher, M.D., Flentil, D.L. and McKeen, R.J., "An Experimental Study of the Secondary Flow in a Curved Rectangular Channel," Paper No. 79-FE-6, Dec., 1979, Presented at the ASME Winter Annual Meeting, New York, N.Y.

27. Patel, V.C., "Measurements of Secondary Flow in the Boundary Layers of a 180 Degree Channel," Aero. Res. Counc. Current Paper No. 1043, 1968.

28. Rodi, W., "A New Algebraic Relation for Calculating the Reynolds Stresses," Mechanics of Fluid, ZAMM, Vol. 56, 1976, pp. T219-T221.

29. Ljuboja, M. and Rodi, W., "Calculation of Turbulent Wall Jets with an Algebraic Reynolds Stress Model," Proceedings of the ASME Symposium on Turbulent Boundary Layers, Niagara Falls, N.Y., June 1979.

30. Leschziner, M.A. and Rodi, W., "Calculation of Annular and Twin Parallel Jets Using Various Discretization Schemes and Turbulence Model Variants," to appear in J. Fluids Eng., Trans. ASME, 1981.

31. Humphrey, J.A.C., Whitelaw, J.H. and Yee, G., "Turbulent Flow in a Square Duct with Strong Curvature," Journal of Fluid Mechanics, Vol. 103, 1981, pp. 443-463.

32. Jones, W.P. and Launder, B.E., "The Prediction of Laminarization With a Two-Equation Model of Turbulence," International Journal of Heat and Mass Transfer, Vol. 15, 1972, pp. 301-314.

33. Launder, B.E. and Spalding, D.B., "The Numerical Computation of Turbulent Flows," Computer Methods in Applied Mechanics and Engineering, Vol. 3, 1974, pp. 269-289.

34. Launder, B.E., Reece, G.J. and Rodi, W., "Progress in the Development of a Reynolds-Stress Turbulence Closure," J. Fluid Mechanics, Vol. 68, Part 3, 1975, pp. 537-566.

35. Humphrey, J.A.C. and Pourahmadi, F., "A Generalized Algebraic Relation for Predicting Developing Curved Channel Flow with a k-ε Model of Turbulence," University of California, LBL Report No. 12009 Rev.

36. Daly, B.J. and Harlow, F.H., "Transport Equations of Turbulence," Phys. Fluids, Vol. 13, 1970, p. 2634.

37. Eide, S.A. and Johnston, J.P., "Prediction of the Effects of Longitudinal Wall Curvature and System Rotation on Turbulent Boundary Layers," Dept. Mech. Eng., Stanford University, Stanford, CA., 1974, Report No. PD-19.

38. Humphrey, J.A.C., "Numerical Calculation of Developing Laminar Flow in Pipes of Arbritrary Curvature Radius," Can. J. Chem. Eng., Vol. 56, 1978. p. 151.

39. Humphrey, J., Taylor, A., and Whitelaw, J.H., "Laminar Flow in a Square Duct of Strong Curvature," J. Fluid Mechanics, Vol. 83, 1977, pp. 509-527.

40. Patankar, S.V., "Numerical Heat Transfer and Fluid Flow," Hemisphere Publishing Corporations, McGraw-Hill Book Company, 1980.

41. Gosman, A.D. and Pun, W.M., "Lecture Notes for Course Entitled: Calculation of Recirculating Flows," Imperial College Report No. HTS/74/2, 1974, London University.

42. Yee, G., Chilukuri, R., and Humphrey, J.A.C., "Developing Flow and Heat Transfer in Strongly Curved Ducts of Rectangular Cross Section," Journal of Heat Transfer, Trans. ASME, Vol. 102, 1980, pp. 285-291.

43. Laufer, J., "Investigation of Turbulent Flow in a Two-Dimensional Channel," NACA Technical Note 2123, 1950.

44. Hanjalic, K. and Launder, B.E., "A Reynolds Stress Model of Turbulence and its Application to Thin Shear Flows," J. Fluid Mech., Vol. 52, Part 4, 1972, pp. 609-638.

45. Hanjalic, K., "Two-Dimensional Asymmetric Turbulent Flow in Ducts," Ph.D. Thesis, 1970, University of London.

46. Jones, W.P. and Launder, B.E., "The Prediction of Laminarization with a 2-Equation Model of Turbulence," Int. J. Heat Mass Transfer, Vol. 15, 1972, p. 301.

47. Rodi, W., "Influence of Buoyancy and Rotation on Equations for the Turbulent Length Scale," Proceedings of the 2nd Symposium on Turbulent Shear Flows, July 1979, Imperial College, London University.

	Inlet Plane	Exit Plane	At Curved Walls
U_θ	Prescribed from experiment	$\frac{\partial U_\theta}{\partial \theta} = 0$ or prescribed from experiment	τ_w specified through Eq. (12)
U_r	0	$\frac{\partial U_r}{\partial \theta} = 0$	0
k	$0.005(U_e^2)_{inlet}$	$\frac{\partial k}{\partial \xi} = 0$	Prescribed from a simplification of the k and ε equations at the walls. See discussion in text.
ε	$\frac{(k^{3/2})_{inlet}}{0.01\ D}$	$\frac{\partial \varepsilon}{\partial \theta} = 0$	

TABLE 1: Boundary Conditions for Curved Channel Flows

FIGURE CAPTIONS

Figure 1 Curved channel configuration and coordinate system.

Figure 2 Transverse variation of $\overline{u_r u_\theta}/k$ ($\overline{uv}/k$) in fully developed curved (and straight) channel flows.

Figure 3 Transverse variation of C_μ in fully developed curved and straight channel flow. For m = 0 wall-function f is symmetric. Calculations based on extended k-ε model.

Figure 4 Transverse variation of normalized streamwise velocity and kinetic energy of turbulence in fully developed straight channel flow. U_{max} and U_τ are maximum and friction velocity, respectively.

Figure 5 Transverse variation of normalized streamwise velocity in developing mildly curved channel flow.

Figure 6 Transverse variation of normalized streamwise velocity in developing strongly curved channel flow.

Figure 7 Streamwise variation of friction factor at the inner and outer walls of strongly curved channel flow.

Figure 8 Transverse variation of normalized kinetic energy of turbulence in strongly curved channel flow.

Figure 9 Transverse variation of normalized angular momentum in strongly curved channel flow.

FIGURE 1

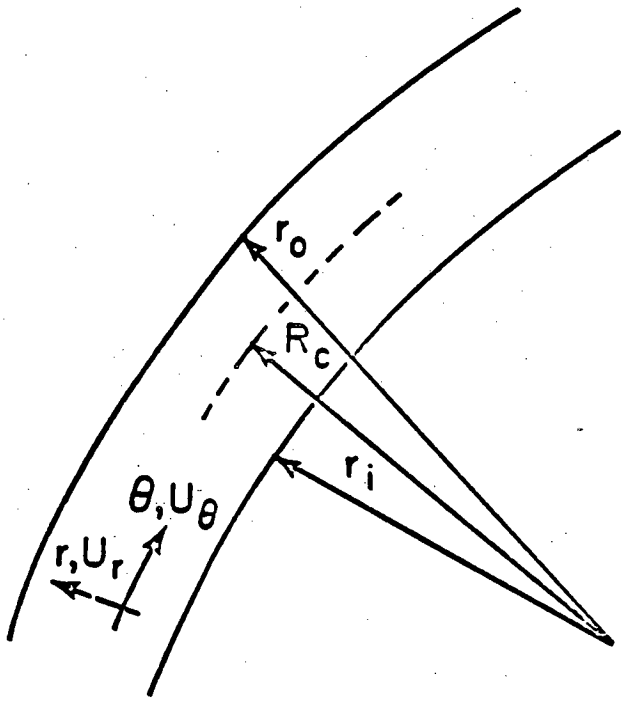

XBL 8111-1594

FIGURE 2

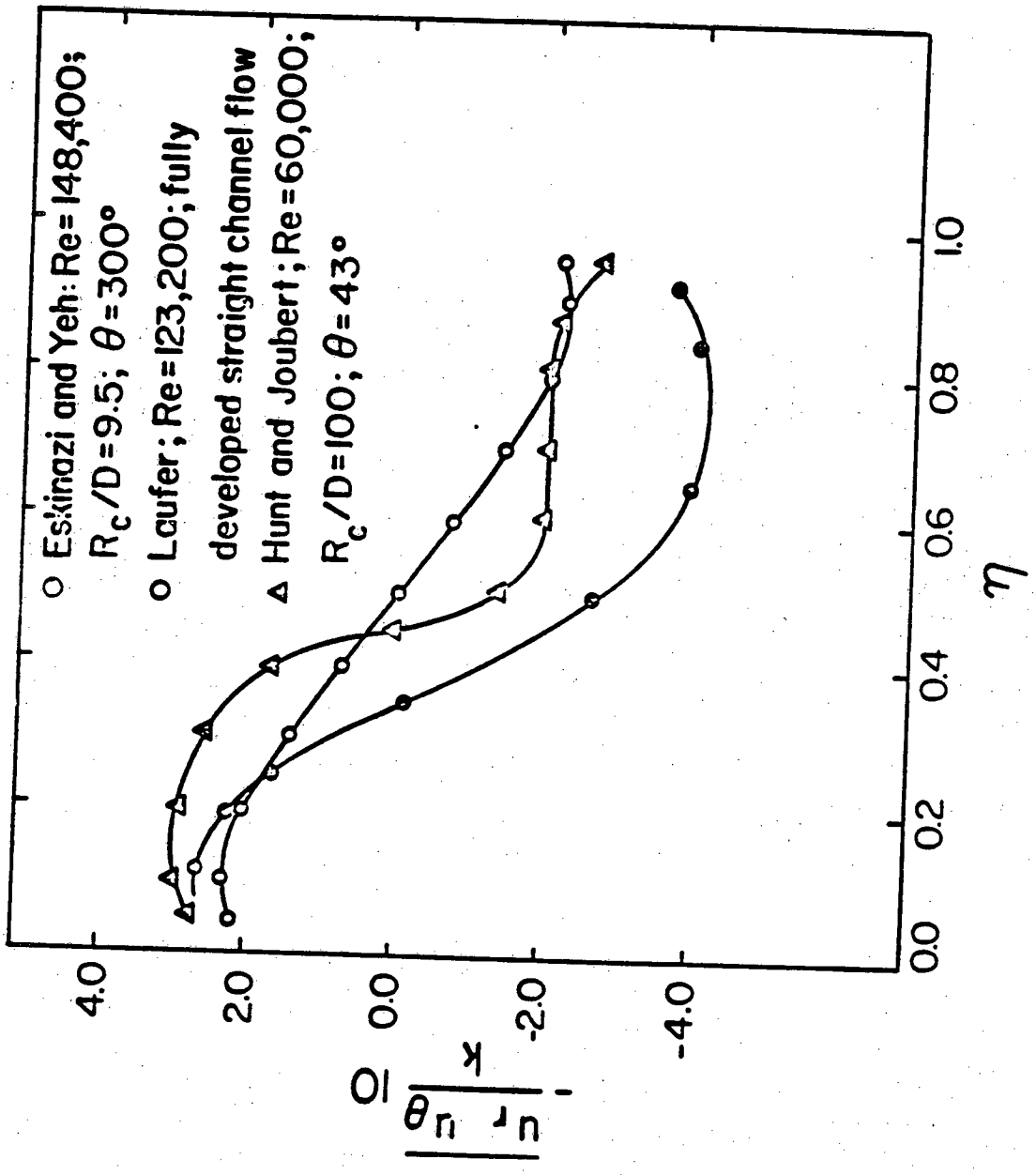

XBL 8111-1595

FIGURE 3

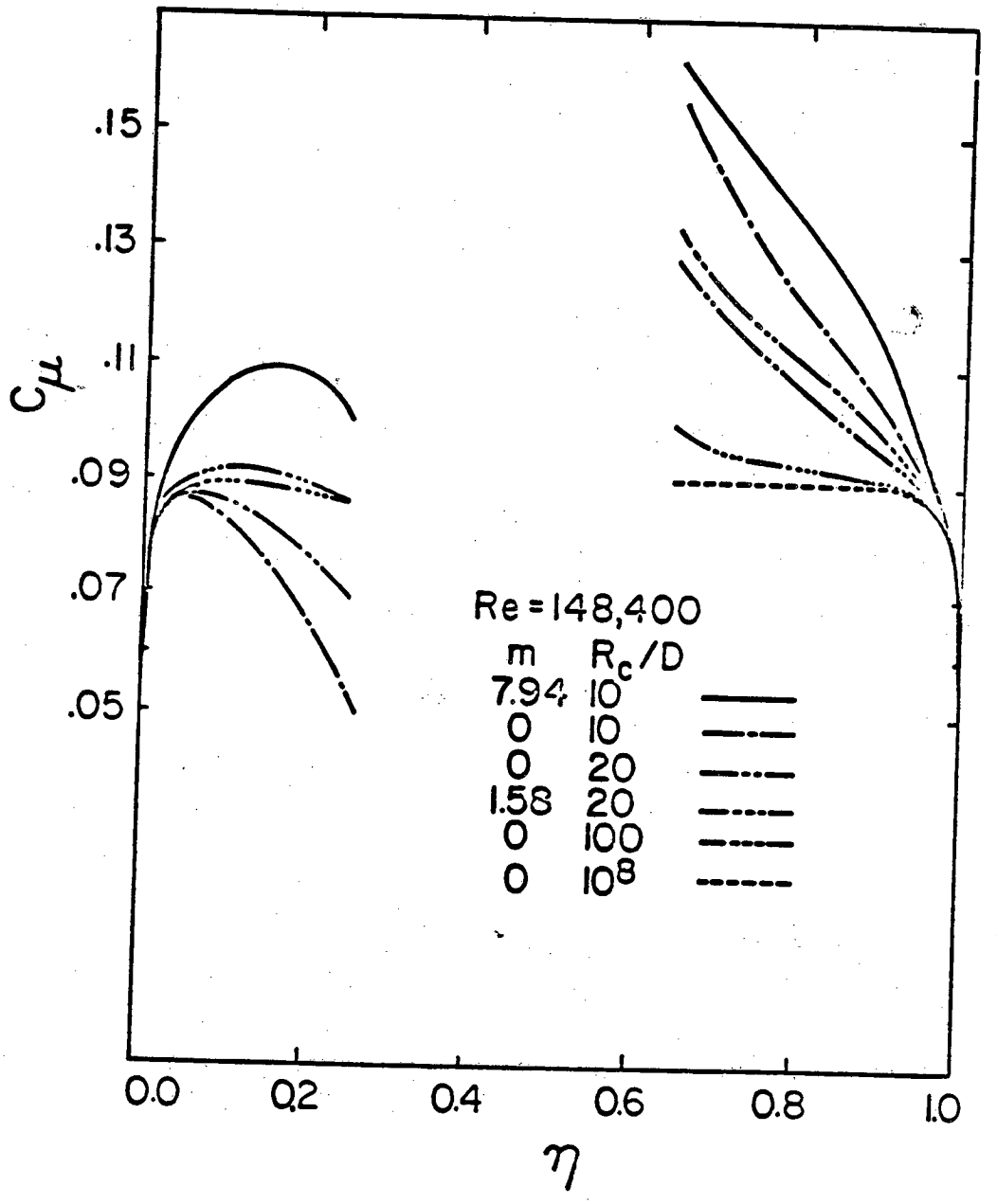

XBL 8111-1595

FIGURE 4

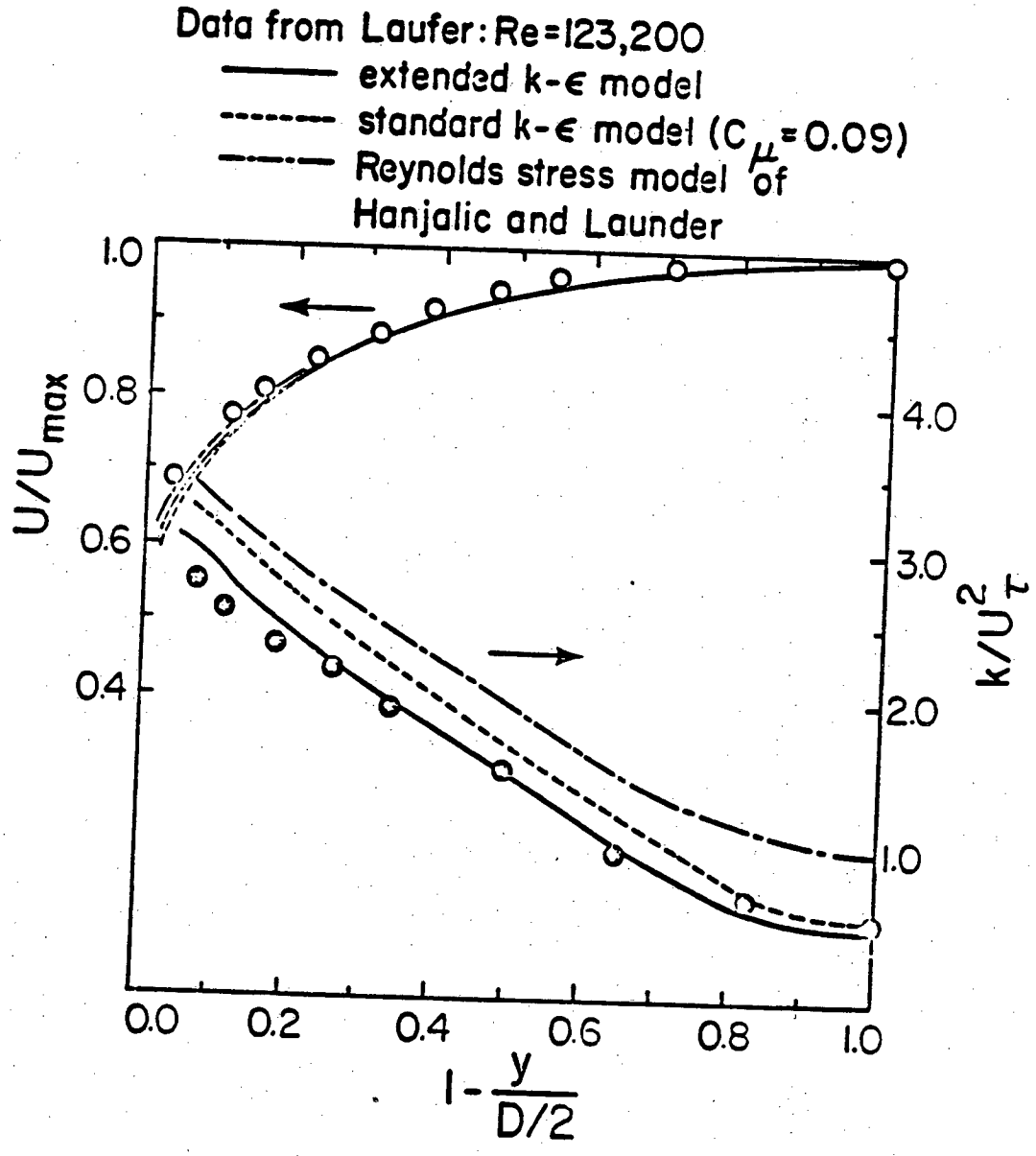

XBL 8111-1597

FIGURE 5

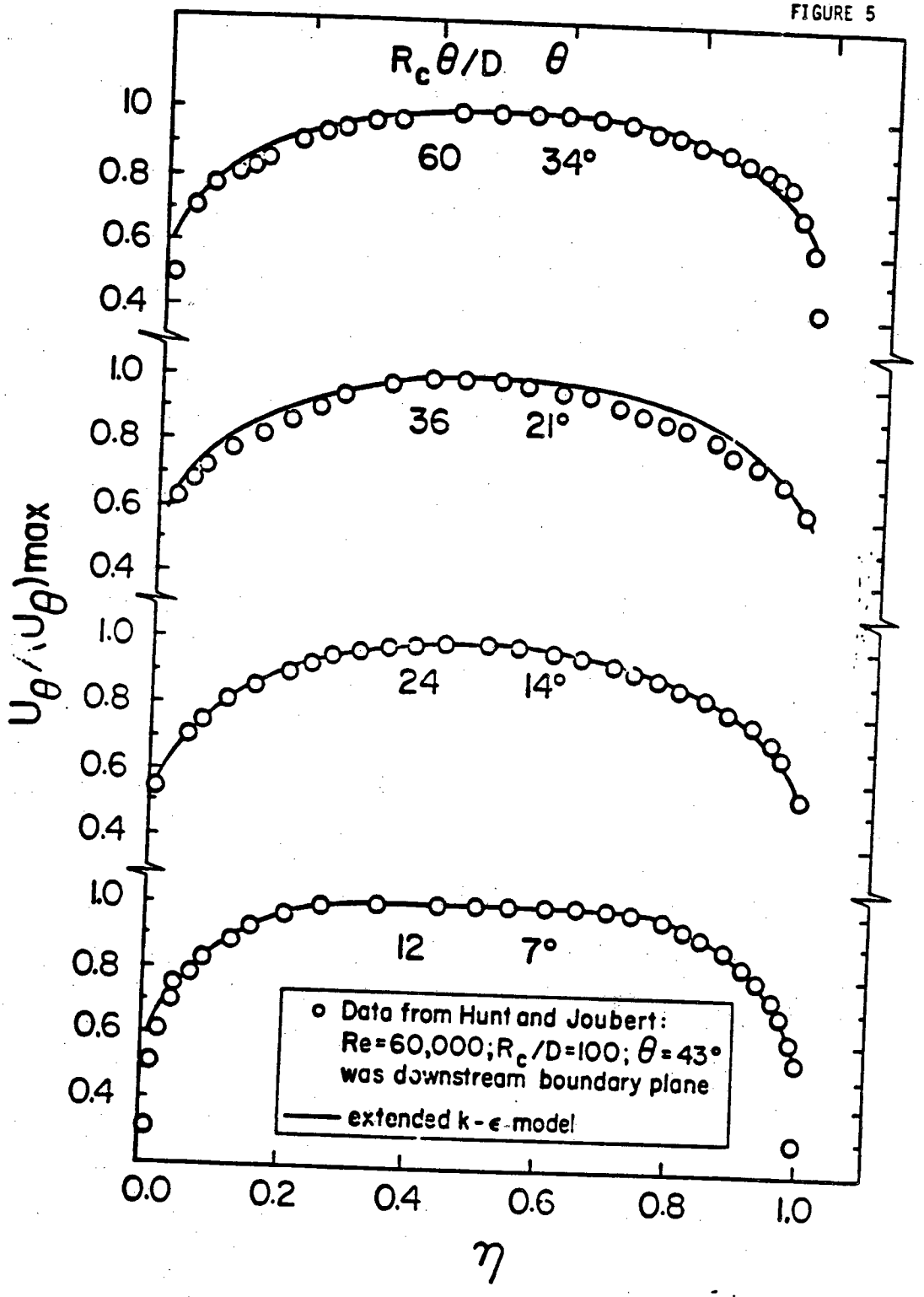

XBL 8111-1593

FIGURE 6

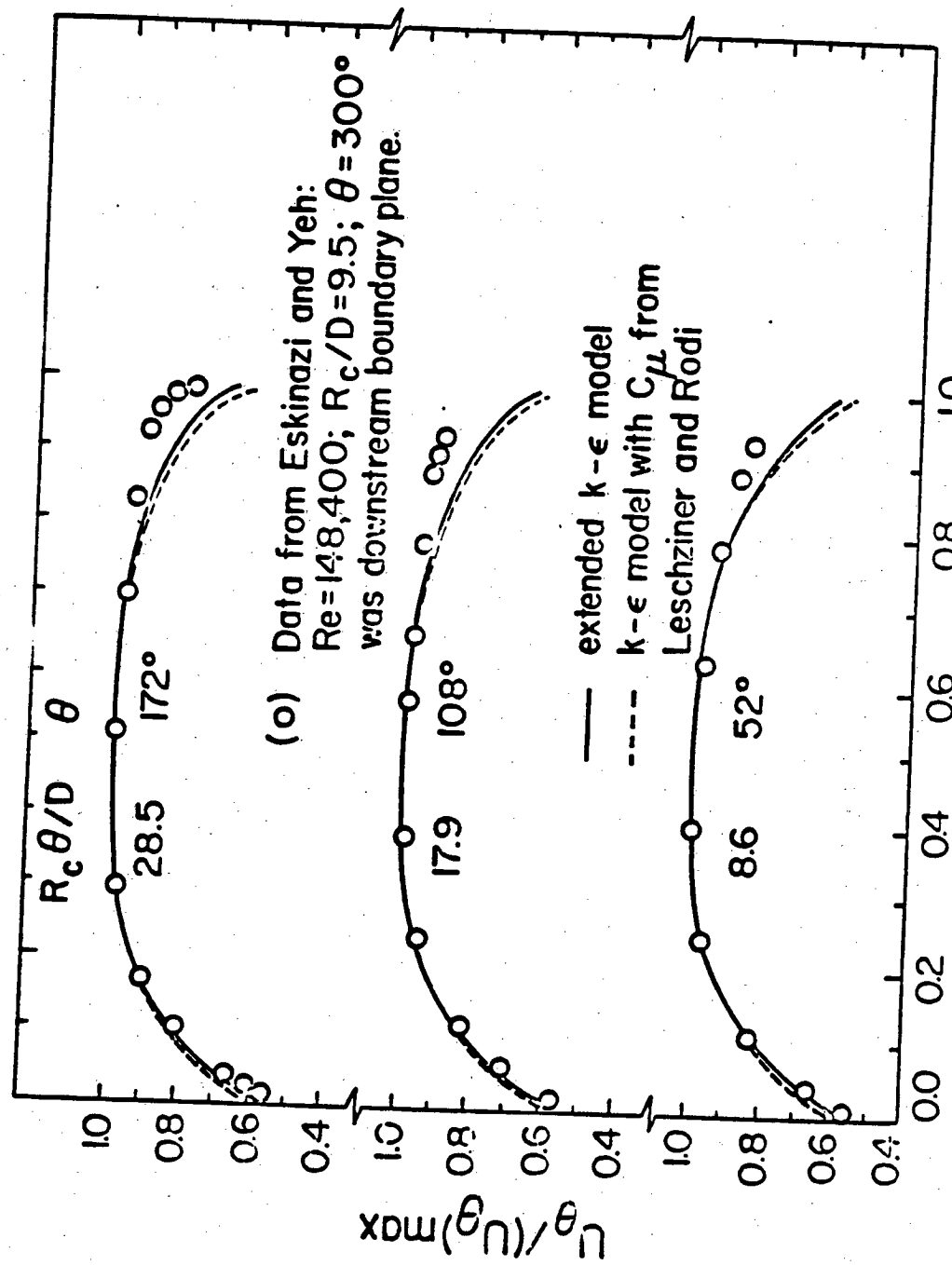

XBL 8111-1602

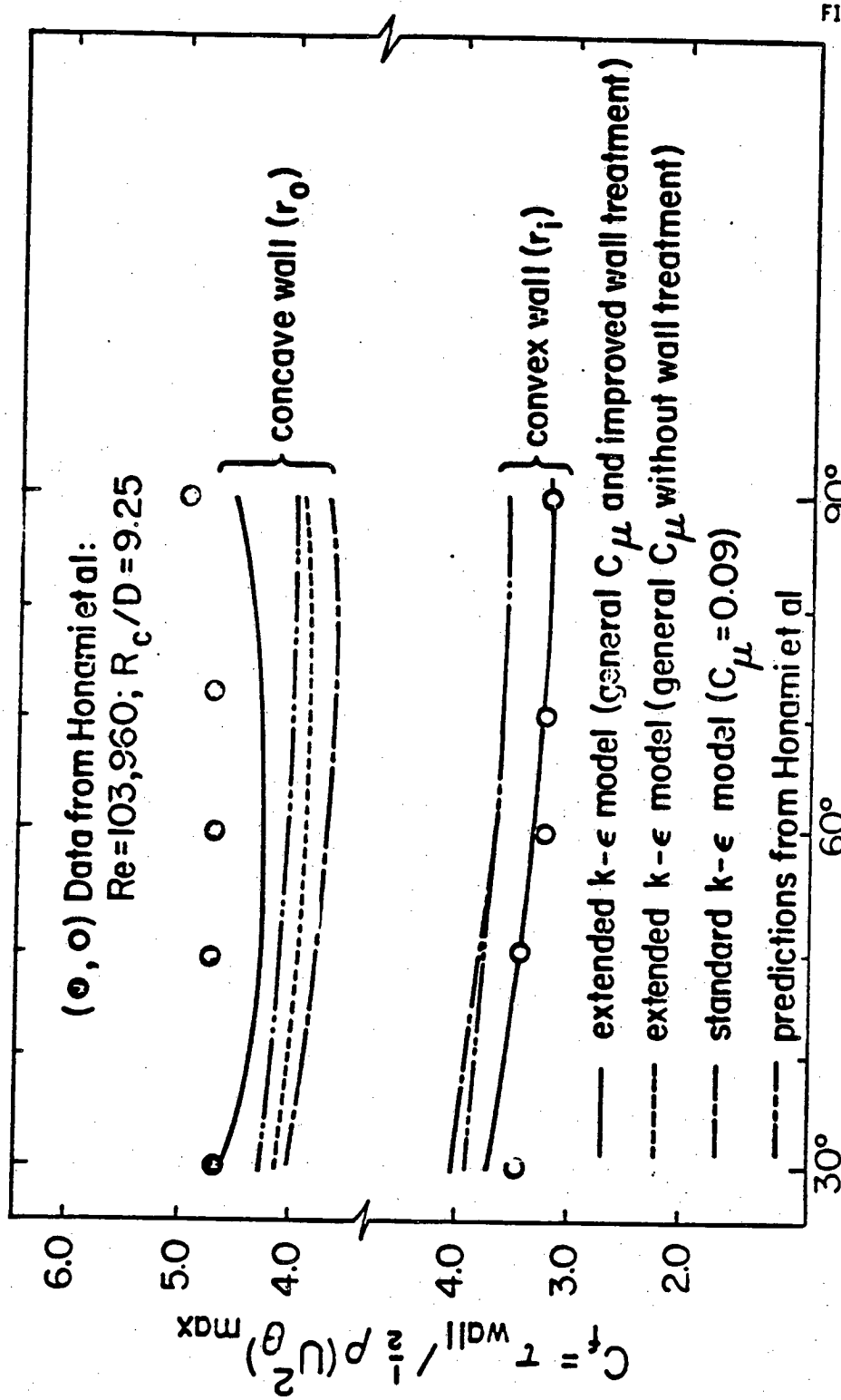

FIGURE 7

XBL 8111-1599

FIGURE 8

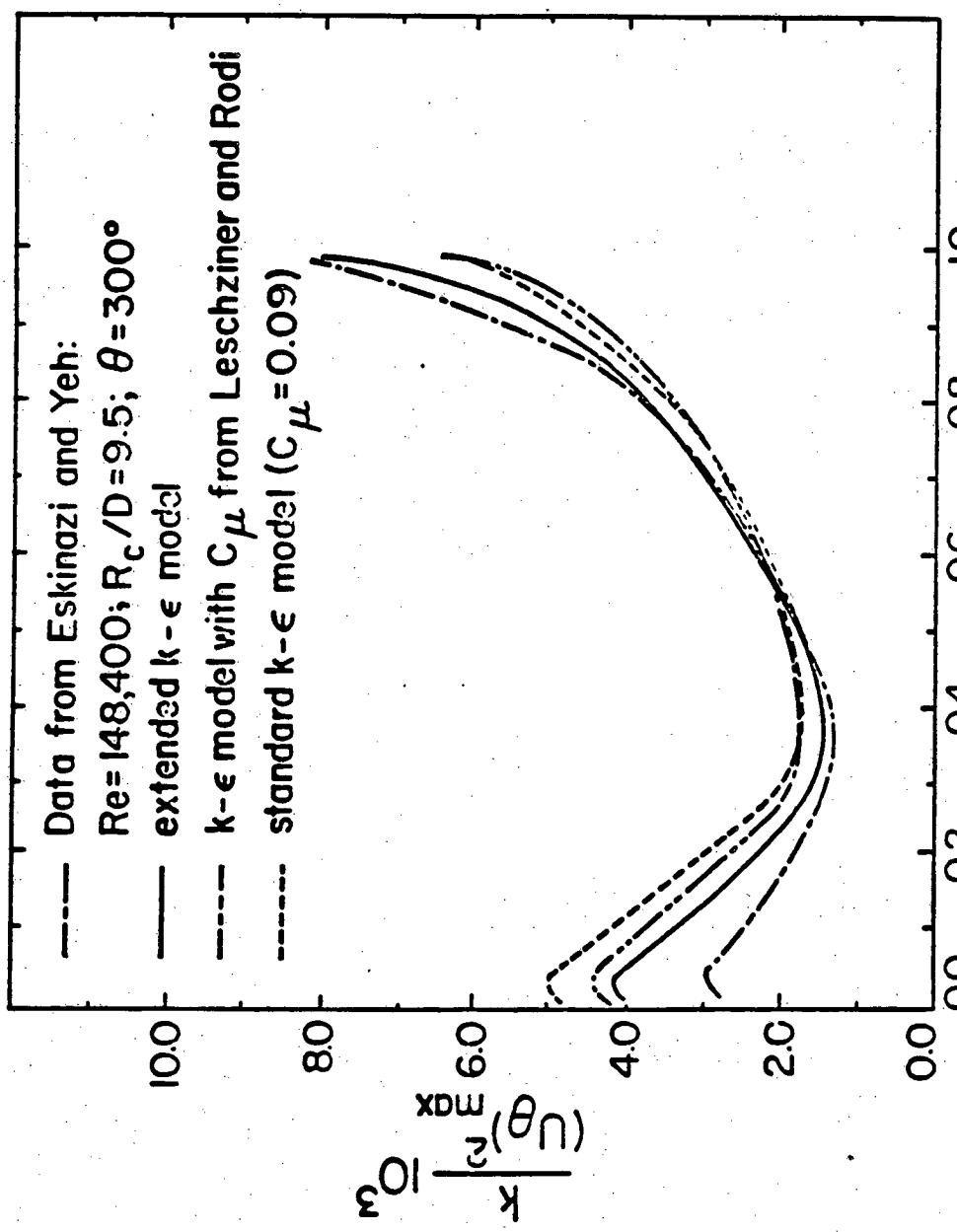

XBL 8111-1601

APPENDIX III

DETAILED DERIVATION OF GENERAL C_μ FUNCTION IN SINGLE-PHASE FLOW

The starting point for the derivation of the C_μ function is Eq. (20) of reference [35] from Appendix II. Noting that the diffusion terms D_{ij} are never actually required in the formulation and that $U_z = 0$ and $\partial/\partial z = 0$, (assumption of 2-D mean flow) Eq. (20) yields the following expressions for $\overline{u_\theta^2}$, $\overline{u_r^2}$ and $\overline{u_\theta u_r}$ in cylindrical coordinates:

$$\frac{D\overline{u_\theta^2}}{Dt} - D_{\theta\theta} = -2\frac{\overline{u_\theta^2}}{r}\frac{\partial \overline{U}_\theta}{\partial \theta} - 2\,\overline{u_\theta u_r}\left(\frac{\partial U_\theta}{\partial r} + \frac{U_\theta}{\partial r}\right) - 2\frac{\overline{U}_r}{r}\,\overline{u_\theta^2} + 2\,\overline{\frac{p}{\rho}\frac{\partial u_\theta}{r\partial\theta}} - \frac{2}{3}\varepsilon \qquad \text{(III.1)}$$

$$\frac{D\overline{u_r^2}}{Dt} - D_{rr} = 4\,\overline{u_\theta u_r}\,\frac{\overline{U}_\theta}{r} - 2\,\overline{u_r^2}\,\frac{\partial \overline{U}_r}{\partial r} - 2\,\overline{u_\theta u_r}\,\frac{\partial \overline{U}_r}{r\partial\theta} + 2\,\overline{\frac{p}{\rho}\frac{\partial u_r}{\partial r}} - \frac{2}{3}\varepsilon \qquad \text{(III.2)}$$

$$\frac{D\overline{u_\theta u_r}}{Dt} - D_{\theta r} = (2\,\overline{u_\theta^2} - \overline{u_r^2})\frac{\overline{U}_\theta}{r} - \overline{u_r^2}\,\frac{\partial \overline{U}_\theta}{\partial r} - \frac{\overline{u_\theta^2}}{r}\frac{\partial \overline{U}_r}{\partial \theta} + \overline{\frac{p}{\rho}\frac{\partial u_\theta}{\partial r}} + \overline{\frac{p}{\rho}\frac{\partial u_r}{r\partial\theta}} \qquad \text{(III.3)}$$

where, for convenience, $D/Dt = \partial/\partial t + \bar{U}_r\,\partial/\partial r + \bar{U}_\theta/r\,\partial/\partial\theta$ has been used even though $\partial/\partial t = 0$. In Eqs. III.1 - III.3 contributes to the pressure strain terms are modeled according to Eq. (22) and Table 2 of ref. [35] from Appendix II. In cylindrical coordinates, these terms are:

$$2\,\overline{\frac{p}{\rho}\frac{\partial u_\theta}{r\partial\theta}} = -C_1\frac{\varepsilon}{k}\left(\overline{u_\theta^2} - \frac{2}{3}k - \frac{C_1'}{C_1}f\,\overline{u_r^2}\right)$$

$$- C_2\left\{-2\,\overline{u_\theta u_r}\left(\frac{\partial\bar{U}_\theta}{\partial r} + \frac{\bar{U}_\theta}{r}\right) - 2\,\overline{u_\theta^2}\,\frac{\partial\bar{U}_\theta}{r\partial\theta} - 2\,\frac{\bar{U}_r}{r}\,\overline{u_\theta^2}\right.$$

$$\left. + C_2'\,f\left[4\,\overline{u_\theta u_r}\,\frac{\bar{U}_\theta}{r} + 2\,\overline{u_r^2}\left(\frac{\partial\bar{U}_\theta}{r\partial\theta} + \frac{\bar{U}_r}{r}\right) - 2\,\overline{u_\theta u_r}\,\frac{\partial\bar{U}_r}{r\partial\theta}\right]\right.$$

$$\left. - \frac{2}{3}P\,(1 + C_2'\,f)\right\} \qquad \text{(III.4)}$$

$$2\,\overline{\frac{p}{\rho}\frac{\partial u_r}{\partial r}} = -C_1\frac{\varepsilon}{k}\left[\left(1 + 2\,\frac{C_1'}{C_1}f\right)\overline{u_r^2} - \frac{2}{3}k\right]$$

$$- C_2\,(1 - 2\,C_2'\,f)\left[\overline{u_\theta u_r}\left(4\,\frac{\bar{U}_\theta}{r} - 2\,\frac{\partial\bar{U}_r}{r\partial\theta}\right)\right.$$

$$\left. + 2\,\overline{u_r^2}\left(\frac{\partial\bar{U}_\theta}{r\partial\theta} + \frac{\bar{U}_r}{r}\right) - \frac{2}{3}P\right] \qquad \text{(III.5)}$$

$$\overline{\frac{p}{\rho}\left(\frac{1}{r}\frac{\partial u_r}{\partial\theta} + \frac{\partial u_\theta}{\partial r}\right)} = -C_1\frac{\varepsilon}{k}\,\overline{u_\theta u_r}\left(1 + \frac{3}{2}\,\frac{C_1'}{C_1}f\right)$$

$$+ C_2\,(1 - \tfrac{3}{2}\,C_2'\,f)\left[\overline{u_r^2}\,\frac{\partial\bar{U}_\theta}{\partial r} - (2\,\overline{u_\theta^2} - \overline{u_r^2})\,\frac{\bar{U}_\theta}{r} + \overline{u_\theta^2}\,\frac{\partial\bar{U}_r}{r\partial\theta}\right]$$

(III.6)

From Eq. (26) of Ref. [35] from Appendix II:

$$\frac{D\,\overline{u_\theta^2}}{Dt} - D_{\theta\theta} = \frac{\overline{u_\theta^2}}{k}(P - \varepsilon) \qquad \text{(III.7)}$$

$$\frac{D\,\overline{u_r^2}}{Dt} - D_{rr} = \frac{\overline{u_r^2}}{k}(P - \varepsilon) \qquad \text{(III.8)}$$

$$\frac{D\,\overline{u_\theta u_r}}{Dt} - D_{\theta r} = \frac{\overline{u_\theta u_r}}{k}(P - \varepsilon) \qquad \text{(III.9)}$$

Eqs. III.1 to III.9 lead to a system of algebraic equations which can be solved the three unknowns $\overline{u_\theta^2}$, $\overline{u_r^2}$ and $\overline{u_\theta u_r}$. The result is:

$$\overline{u_\theta^2} = \frac{d(n\ell-jg) - n(b\ell-cj) + m(bg-cn)}{a(n\ell-gj) - e(b\ell-cj) + i(bg-cn)} \qquad \text{(III.10)}$$

$$\overline{u_r^2} = \frac{a(h\ell-mg) - e(d\ell-mc) + i(dg-hc)}{a(n\ell-gj) - e(b\ell-cj) + i(bg-cn)} \qquad \text{(III.11)}$$

$$\overline{u_\theta u_r} = \frac{a(nm-hj) - e(bm-dj) + i(bh-dn)}{a(n\ell-gj) - e(b\ell-cj) + i(bg-cn)} \qquad \text{(III.12)}$$

with the following values for the coefficients in the above expressions:

$$a = 0 \qquad \text{(III.13)}$$

$$b = \frac{1}{k}\left[P - (1-C_1+2C_1' f)\varepsilon\right] + 2(1-C_2+2C_2C_2'f)\frac{\partial \overline{U}_r}{\partial r} \qquad \text{(III.14)}$$

$$c = 2\,(C_2 - 2C_2'\,C_2\,f - 1)\,\left(2\,\frac{\overline{U}_\theta}{r} - \frac{\partial \overline{U}_r}{r\partial\theta}\right) \qquad \text{(III.15)}$$

$$d = \frac{2}{3}\,\varepsilon\,\left[C_1 - 1 + C_2(1 - 2C_2'\,f)\,\frac{p}{\varepsilon}\right]\,\left(2\,\frac{\overline{U}_\theta}{r} - \frac{1}{r}\,\frac{\partial \overline{U}_r}{\partial\theta}\right) \qquad \text{(III.16)}$$

$$e = \left[1 - C_2\,\left(1 - \frac{3}{2}\,C_2'\,f\right)\right]\,\left(2\,\frac{\overline{U}_\theta}{r} - \frac{1}{r}\,\frac{\partial \overline{U}_r}{\partial\theta}\right) \qquad \text{(III.17)}$$

$$n = -\left[1 - C_2\,\left(1 - \frac{3}{2}\,C_2'\,f\right)\right]\,\left(\frac{\partial \overline{U}_\theta}{\partial r} + \frac{\overline{U}_\theta}{r}\right) \qquad \text{(III.18)}$$

$$g = -\,\frac{1}{k}\,\left[P - \left(1 - C_1 - \frac{3}{2}\,C_1'\,f\right)\,\varepsilon\right] \qquad \text{(III.19)}$$

$$h = 0 \qquad \text{(III.20)}$$

$$i = \frac{1}{k}\,\left[P + (C_1 - 1)\varepsilon\right] - 2\,(1 - C_2)\,\frac{\partial \overline{U}_r}{\partial r} \qquad \text{(III.21)}$$

$$j = -\,C_1'\,f\,\frac{\varepsilon}{k} - 2\,C_2\,C_2'\,f\,\frac{\partial \overline{U}_r}{\partial r} \qquad \text{(III.22)}$$

$$\ell = 2(1 - C_2)\,\frac{\partial \overline{U}_\theta}{\partial r} + \frac{\overline{U}_\theta}{r} + C_2C_2'\,f\,\left(4\,\frac{\overline{U}_\theta}{r} - \frac{2}{r}\,\frac{\partial \overline{U}_r}{\partial\theta}\right) \qquad \text{(III.23)}$$

$$m = \frac{2}{3}\,\left[(C_1 - 1)\varepsilon + C_2\,(1 + C_2'\,f)\,P\right] \qquad \text{(III.24)}$$

Combining the Boussinesq approximation for $u_\theta u_r$, as given by Eq. (28) of ref. [35] from Appendix II, with the algebraically derived expression for $u_\theta u_r$ given above yields a general expression for C_μ of the form:

$$C_\mu = \frac{\alpha_1+\beta_1 \frac{k}{\varepsilon} \frac{\partial \overline{U}_\theta}{\partial r}}{(1-\delta+\delta_c)\left[\alpha_2+\beta_2\left(\frac{k}{\varepsilon}\frac{\partial \overline{U}_\theta}{\partial r}\right)+\gamma_2\left(\frac{k}{\varepsilon}\frac{\partial \overline{U}_\theta}{\partial r}\right)^2+\delta_2\left(\frac{k}{\varepsilon}\frac{\partial \overline{U}_\theta}{\partial r}\right)^3\right]} \quad \text{(III.25)}$$

where α_1, β_1, α_2, β_2, γ_2 and δ_2 are given as:

$$\alpha_1 = E(2\delta-\delta_c)\left[\frac{2}{3}\left(D+H\frac{P}{\varepsilon}\right)\left(\frac{P}{\varepsilon}-1+A\right)+\frac{2}{\varepsilon}\left(D+B\frac{P}{\varepsilon}\right)C_1'f\right]$$
$$- E(1+\delta)\left[\frac{2}{3}\left(D+B\frac{P}{\varepsilon}\right)\right]\left(\frac{P}{\varepsilon}+D\right)$$

$$\beta_1 = E(2\delta-\delta_c)\left[\frac{4}{3}\left(D+H\frac{P}{\varepsilon}\right)(1-B)+\frac{4}{3}\left(D+B\frac{P}{\varepsilon}\right)C_2C_2'f\right]\delta_b$$
$$+\frac{4}{3}E(1+\delta)\left(D+B\frac{P}{\varepsilon}\right)F\,\delta_b$$

$$\alpha_2 = -\left(\frac{P}{\varepsilon}+D\right)\left(\frac{P}{\varepsilon}-1+A\right)\left(\frac{P}{\varepsilon}-1+G\right)$$

$$\beta_2 = -2\left(\frac{P}{\varepsilon}+D\right)(1-B)\left(\frac{P}{\varepsilon}-1+G\right)\delta_b + 2F\left(\frac{P}{\varepsilon}-1+A\right)\left(\frac{P}{\varepsilon}-1+G\right)\delta_b$$

$$\gamma_2 = -E(2\delta-\delta_c)\left\{\left(\frac{P}{\varepsilon}-1+A\right)\left[2F(1+\delta)+2C_2C_2'f(2\delta-\delta_c)\right]+2(1-B)(\delta_c-2\delta)C_1'f\right\}$$
$$+2E(1-B)(\delta_c-2\delta)\left(\frac{P}{\varepsilon}+D\right)(1+\delta)+4F(1-B)\delta_b^2\left(\frac{P}{\varepsilon}-1+G\right)$$

$$\delta_2 = -4E(2\delta-\delta_c)(1-B)\delta_b\,[F(1+\delta)+C_2C_2'f(2\delta-\delta_c) + (\delta_c-2\delta)C_2C_2'f]$$
$$-4EF(1-B)(1+\delta)(\delta_c-2\delta)\delta_b$$

Equation (III.25) does not show the explicit dependence of C_μ on the parameters,

$$\delta_a = \frac{\partial \bar{U}_\theta}{r\partial\theta}\Big/\frac{\partial \bar{U}_\theta}{\partial r}\ ,\quad \delta_b = \frac{\partial \bar{U}_r}{\partial r}\Big/\frac{\partial \bar{U}_\theta}{\partial r}\ ,\quad \delta_c = \frac{\partial \bar{U}_\theta}{r\partial\theta}\Big/\frac{\partial \bar{U}_\theta}{\partial r}\ ,\quad \delta = \frac{\bar{U}_\theta}{r}\Big/\frac{\partial \bar{U}_\theta}{\partial r}\ ,$$

the wall-function f and the ratio P/ε. Using Eq. (11) of reference [35], Appendix II, it is possible to show that:

$$\frac{k}{\varepsilon}\,\frac{\partial \bar{U}_\theta}{\partial r} = \frac{\pm\,(P/\varepsilon)^{1/2}}{C_\mu^{1/2}[(1-\delta+\delta_c)^2 + 4\,\delta_b^2]^{1/2}} \qquad \text{(III.26)}$$

with a positive sign preceding the above expression when $\partial\bar{U}_\theta/\partial r > 0$ and negative when $\partial\bar{U}_\theta/\partial r < 0$. Substitution of Eq. (III.26) into Eq. (III.25) yields (after algebraic manipulation):

$$C_\mu^{3/2} + a_1C_\mu + a_2C_\mu^{1/2} + a_3 = 0 \qquad \text{(III.27)}$$

with:

$$a_1 = \pm\,\frac{2[(D+P/\varepsilon)(1-B) - F(A-1+P/\varepsilon)]\,\delta_b(P/\varepsilon)^{1/2}}{(D+P/\varepsilon)(A-1+P/\varepsilon)[1-\delta+\delta_c)^2 + 4\,\delta_b^2]^{1/2}} \qquad \text{(III.28)}$$

$$
\begin{aligned}
a_2 = & \Big\{ - E(2\delta-\delta_c)\,\{(A-1+P/\varepsilon)\,[2F(1+\delta) + 2\,C_2\,C_2'\,f\,(2\delta-\delta_c)] + 2\,C_1' f (1-B)(\delta_c-2\delta)\} \\
& + 2E(D+P/\varepsilon)(1-B)(\delta_c-2\delta)(1+\delta) + 4F(1-C_2)\delta_b^2(1-B)(G-1+P/\varepsilon)\Big\} \\
& \times P/\varepsilon \Big/ \Big\{[(1-\delta+\delta_c)^2 + 4\delta_b^2]\,[-(D+P/\varepsilon)(A-1+P/\varepsilon)(G-1+P/\varepsilon)]\Big\} \\
& + \Big\{-E(2\delta-\delta_c)\,\{2/3(D+1+P/\varepsilon)(A-1+P/\varepsilon)+2/3(D+B\,P/\varepsilon)\,C_1' f\} \\
& + E(1+\delta)[2/3(D+B\,P/\varepsilon)]\,(D+P/\varepsilon)\Big\} \Big/ \Big\{-(D+P/\varepsilon)(A-1+P/\varepsilon)(G-1+P/\varepsilon)(1-\delta+\delta_c)\Big\}
\end{aligned}
\tag{III.29}
$$

$$
\begin{aligned}
a_3 = & \mp \Big\{E(2\delta-\delta_c)\delta_b\,\{2(1-B)[2F(1+\delta)+2C_2C_2'f(2\delta-\delta_c)]+4(1-B)(\delta_c-2\delta)C_2C_2'f\} \\
& + 4\,E\,F(1-B)(\delta_c-2\delta)\,\delta_b\Big\}\left[\frac{P/\varepsilon}{(1-\delta+\delta_c)^2+4\delta_b^2}\right]^{3/2} \Big/ \Big\{-\,(D+P/\varepsilon)(A-1+P/\varepsilon)(G-1+P/\varepsilon)\Big\} \\
& \mp \Big\{2/3\;E(2\delta-\delta_c)\delta_b\;\;\{2(D+H\,P/\varepsilon)(1-B) + 2(D+B\,P/\varepsilon)\,C_2C_2'f\} \\
& + 4/3\;E(1+\delta)(D+B\,P/\varepsilon)F\delta_b\Big\}\left[\frac{P/\varepsilon}{(1-\delta+\delta_c)^2+4\delta_b^2}\right]^{1/2} \\
& \Big/ \Big\{-\,(D+P/\varepsilon)(A-1+P/\varepsilon)(G-1+P/\varepsilon)(1-\delta+\delta_c)\Big\}
\end{aligned}
\tag{III.30}
$$

In the above expressions:

$$A = C_1(1+2\ f\ C_1'/C_1)$$

$$B = C_2(1-2\ f\ C_2')$$

$$D = C_1 - 1$$

$$E = 1 - C_2\ (1-3/2\ f\ C_2') \qquad \text{(III.31)}$$

$$F = 1 - C_2$$

$$G = C_1\ (1+3/2\ f\ C_1'/C_1)$$

$$H = C_2\ (1+f\ C_2')$$

TECHNICAL INFORMATION DEPARTMENT
LAWRENCE BERKELEY LABORATORY
UNIVERSITY OF CALIFORNIA
BERKELEY, CALIFORNIA 94720